INTERROGATION OF THE FE-S CLUSTER BIOSYNTHETIC MECHANISM USING NATIVE MASS SPECTROMETRIC TECHNIQUES

A Dissertation

by

CHENG-WEI LIN

Submitted to the Graduate and Professional School of
Texas A&M University
in partial fulfillment of the requirements for the degree of

DOCTOR OF PHILOSOPHY

Chair of Committee,	David P. Barondeau
Co-Chair of Committee,	David H. Russell
Committee Members,	Arthur Laganowsky
	Margaret E. Glasner
Head of Department,	Simon W. North

August 2021

Major Subject: Chemistry

ABSTRACT

Iron-sulfur (Fe-S) clusters are ubiquitous protein cofactors that are required for important biological processes including oxidative respiration, nitrogen fixation, and photosynthesis. Defects on Fe-S cluster assembly lead to lethal diseases such as Friedreich's Ataxia. Despite extensive research on Fe-S cluster biogenesis, key molecular mechanisms remain elusive due to the complicated nature of the system. This dissertation contains pioneering works employing advanced mass spectrometry (MS) methods, especially native ion-mobility MS (native IM-MS), to interrogate Fe-S cluster biogenesis. Recent advances in native IM-MS have allowed proteins to be preserved in native-like structures and support applications in the investigation of protein structure, dynamics, ligand interactions, and the identification of protein-associated intermediates. In our mechanistic study of *E. coli* ISC Fe-S cluster assembly, samples were prepared under anaerobic conditions and high-resolution native MS methods were applied to probe the intermediates. This approach was validated by the agreement between native MS and circular dichroism spectroscopic assays. Time-dependent native MS experiments revealed potential iron- and sulfur-based intermediates that decay as the [2Fe–2S] cluster signal developed. Additional experiments establish that Fe(II) ions bind to the scaffold protein IscU active site cysteine residues and promote the intermolecular sulfur transfer reaction from the cysteine desulfurase IscS to the Fe-S scaffold protein IscU. These results together support an iron-first model for Fe-S cluster synthesis. In addition, to elaborate the controversial role of the bacterial frataxin CyaY and its relation to cell antioxidation, acid-

quench denaturing MS and native IM-MS were utilized to respectively monitor sulfur trafficking and protein-protein interactions. A thorough stepwise analysis of CyaY effect on the ISC machinery suggests CyaY specifically inhibits the sulfur transfer step from IscS to IscU. Investigation of sulfur trafficking from IscS to protein acceptors IscU and TusA and glutathione indicates CyaY switches sulfur transfer from protein acceptors to GSH, leading to generation of antioxidant GSSH which helps relieve oxidative stress. Native IM-MS methods were also employed for monitoring the conformation landscape of the human ISC machinery. IM results suggest the NFS1-ISD11-ACP complex is converted from an inactive extended architecture into an active compact architecture upon binding of the allosteric activator FXN in a morpheein-like mechanism. Overall, the crucial insights shown in this dissertation highlight the power and potential of mass spectrometry methods in exploring enzyme mechanisms.

DEDICATION

This dissertation is dedicated to my parents for their unconditional support and guidance towards the path of scientific research career.

ACKNOWLEDGEMENTS

First, I would like to thank my research advisors. Dr. David Barondeau kindly set up this joint appointment position which provides me the opportunity of getting trained on both bioinorganic chemistry and mass spectrometry. He taught me how to analyze a biological topic and identify the key questions, to design experiments that would illustrate physiological-related processes, to write great scientific stories that could be easily understood and catch reader's attention, and most importantly, to be a good person. I am so grateful of him being always supportive and kind to students. Dr. David Russell is also very generous and supportive. He kindly offers me the access and resource of mass spectrometry, invites me to participate in collaborative grants and projects, and provides critical insights on any mass spectrometry-related questions. I am very lucky to learn and cultivate interdisciplinary expertise under the guidance of two fantastic research advisors. I would also like to thank my committee members. Dr. Laganowsky always provides great suggestions and kindly let me borrow instrument or resources when I needed. Dr. Glasner is always engaged and gives insightful perspectives during committee meetings.

I would like to thank Dr. Begley for letting us use the CD and stopped-flow instruments in his laboratory and the support on CysK plasmid. I would also like to thank Dr. Singleton and Kai-Yuan Kuan on their assistance of synthesizing ^{34}S-cysteine.

I am very thankful to the Barondeau and Russell group members for their supports and collaborations. I am especially grateful to former students, Dr. Shachin Patra, Dr. Seth Cory, Dr. Mehdi Shirzadeh, Dr. Michael Poltash, and Dr. Yang Liu for their mentoring

and guidance. I would also like to give special thanks to Jacob McCabe, who is always helpful and has collaborated with me on multiple projects. I also want to thank all former and current lab members, especially those who work closely with me, including Shelby Oney, Seth Van Andel, Amy Spelbring, Elisa Ferrera, Steven Havens, Christopher Mallis, Tom Walker, Dr. Manas Ghosh, and Dr. Klaudia Korcek. I would also like to thank Dr. Deborah Bell-Pedersen and Dr. Teresa Lamb for their collaboration on the ribosome project.

I am grateful to my parents for their guidance, trust and encouragement for pursuing a scientific PhD. I also want to thank my friends in local for the good time we have together. Lastly, I would like to thank my fiancée, Yung-Chun Hsiao for her love, understanding, companion, and for motivating me to finish my PhD.

CONTRIBUTORS AND FUNDING SOURCES

Contributors

This work was supervised by a dissertation committee consisting of Dr. David Barondeau (advisor), Dr. David Russell (co-advisor), and Dr. Arthur Laganowsky from the Department of Chemistry, as well as Dr. Margaret Glasner from the Department of Biochemistry and Biophysics.

The majority of Chapter II is re-printed and modified from a published paper (Lin et. al, *JACS* 2020). The design and manufacturing of vT-ESI source (Figure 2.7) were performed by Jacob McCabe and Benjamin Jones under the supervision of Dr. David Russell and Prof. Vicki Wysocki respectively and was published in 2021. Chapter III is a direct re-print of an unpublished paper which the first author is me. The spectroscopic and activity analysis of the CyaY effect on the ISC pathway was performed by Dr. Shachin Patra (Figure 3.1). The alanine detection assay was performed by Shelby Oney (Figure 3.5A). The majority of Chapter IV is re-printed and modified from an unpublished manuscript. The structural analysis and visualization including Figure 1.11, Figure 4.1, Figure 4.2, Figure 4.11, Figure 4.12, Figure 4.22, Figure 4.23, Figure 4.24 were performed by Dr. Barondeau. The design of Δ1-55NFS1(Q64S, P299H, L300Q) variant and the activity and FXN binding experiments for this variant in the presence of ISD11 and ACP_{ec} were conducted by Dr. Shachin Patra (Figure 4.13). The SAXS (Figure 4.4, Figure 4.5 and Table 4-1, Table 4-2, Table 4-3, Table 4-5, Table 4-6), activity analysis of crystals (Figure 4.3, Figure 4.6, Figure 4.7, and Table 4-7), and cation exchange chromatography (Figure

4.10) were performed by Dr. Seth Cory, who is the co-first author of the manuscript. Steven Havens provided general supports for some material preparation.

All other works done in this dissertation was done by the student independently.

Funding Sources

This work was supported in part by NIH Grants R01GM096100 (D.P.B.), R01GM121751 (D.H.R.), P41GM128577 (D.H.R.), NSF Grant CHE 1508269 (D.P.B.), and the Robert A. Welch Grant A-1647 (D.P.B.).

TABLE OF CONTENTS

Page

LIST OF FIGURES

Page

LIST OF TABLES

Page

1. INTRODUCTION

Fe−S clusters have been proposed to play a critical role in the origin of life on earth. Studies on photosynthetic organisms[1] and nitrogen-fixing bacteria[2] suggest Fe-S proteins were involved in early oxidoreduction reactions. Nowadays, Fe-S clusters have become protein cofactors that are ubiquitous in all life forms and necessary for essential cellular processes such as oxidative respiration, photosynthesis, nitrogen fixation, and DNA replication/repair. Due to the essentialness of Fe-S cofactors, significant effort has been invested in understanding Fe-S cluster biogenesis over the past three decades. The aim of this dissertation is to provide new mechanistic insights into Fe-S cluster biosynthesis using pioneering applications of native ion mobility mass spectrometry, a powerful biophysical technique that reveals binding, structural, and/or sequence information of biomolecules (Figure 1.1).

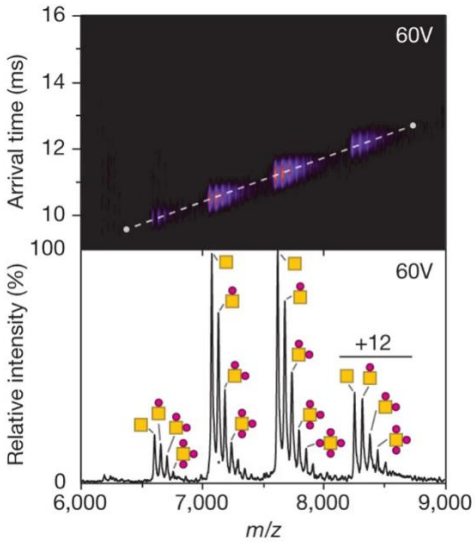

Figure 1.1 An example of native ion mobility mass spectra. The membrane protein (Aqpz) binds with 0-5 lipids (POPC). Different envelopes in the mass spectra correspond to different charge states; the envelope with ~8200-8500 m/z has a charge state of +12. The upper part of the figure shows the arrival time from IM. The collisional cross-section (CCS) calculated from the IM-MS arrival times agree with the CCS calculated from the crystal structure. Reprint with permission from *Nature* **2014**, *510*, 172-175. Copyright 2014 Nature Publication Group.

1.1. Native Ion Mobility Mass Spectrometry

1.1.1. Soft Ionization Enables "Native" Mass Spectrometry

Mass spectrometry (MS) has emerged as a powerful bioanalytical tool. MS measures the mass to charge ratio (m/z) of ions, which can be readily converted to the mass of ions to identify analytes. Recent advancement of MS instrumentation and data processing has extended the application of MS to heterogeneous and/or high molecular weight biomolecules, such as metabolites,[3, 4] peptides,[5, 6] proteins,[7-9] DNAs/RNAs,[10] and non-covalent biological complexes.[11-14] A key factor of successfully transfering these usually large and fragile biomolecules from the solution phase into the gas phase is using soft ionization methods. Electrospray ionization (ESI) has been utilized as one of the most common and robust methods for ionizing non-volatile molecules and is especially useful for the ionization of large biomolecules.[15, 16] While earlier ionization methods often lead to fragmentation or loss of non-covalent interactions, ESI is a "soft" technique that usually generates intact protonated ions including large biomolecules.[15, 17] Larger ions generated from ESI often show multiple charge states, as the protonation sites on the molecules generally increase with molecular weight. To assist desolvation, ESI usually requires a drying gas flow, a heating source capillary, and high desolvation energy. Recently, nanoelectrospray ionization (nanoESI) has emerged as an ultra-soft ionization method. Comparing to conventional ESI, nanoESI follows the same ionization principle but utilizes a capillary with a smaller diameter (100 μm for regular ESI and a few μm for nanoESI). This small orifice size not only allows a very low flow rate and sample consumption but also produces smaller droplets (Figure 1.2). These smaller droplets require limited heating or energy to assist desolvation and thus

non-covalent interactions can be better preserved. Another important aspect of nanoESI is the increased sensitivity, which allows the usage of higher concentrations of salts, such as volatile ammonium acetate solutions, for solubilizing proteins at neutral pH[11]. The successful application of nanoESI on probing the solution properties of large biomolecules is recognized as the new powerful bioanalytical technique "native mass spectrometry" (native MS). The success of native MS on enhanced sensitivity, high salt tolerance, and better preservation of non-covalent interactions have been demonstrated by studies showing comparable binding affinity using ITC, SPR, and native MS.[18-20]

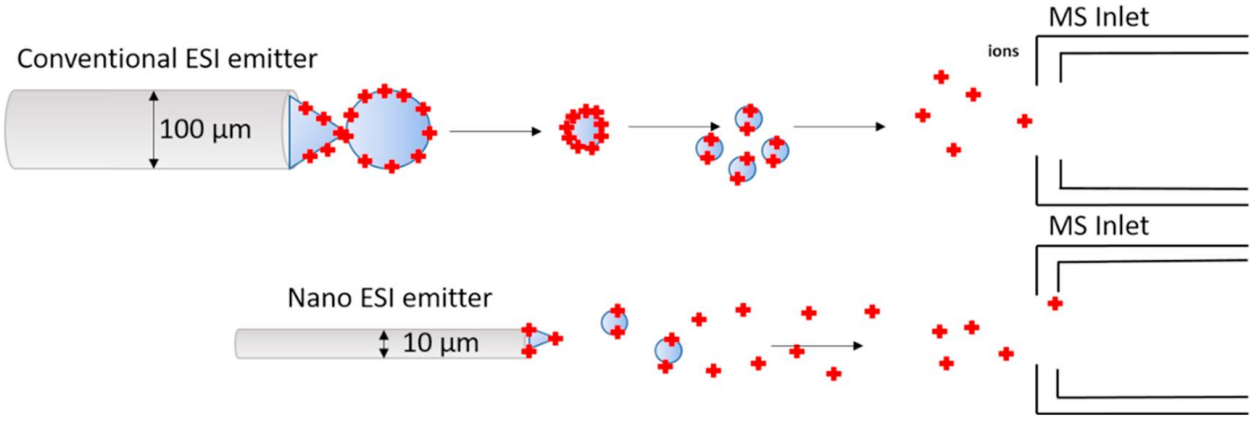

Figure 1.2 Comparison of traditional electrospray ionization and nanoelectrospray ionization. NanoESI produces smaller droplets comparing to traditional ESI. Only a limited amount of activation energy is required for the desolvation of the small droplet, which leads to better-preserved structures of protein ions and non-covalent interactions. Reprint with permission from *Talanta* **2018**, *182*, 380-390. Copyright 2018 Europe PMC Publication Group.

1.1.2. Ion Mobility Spectrometry

Ion mobility (IM) spectrometry is a gas-phase technique that separates ions based on their mass, charge, and shape. The separation is carried out by using a drift tube filled with an inert drift gas and conducted in an electric field. Ions with higher charges fly through the drift tube faster due

to the higher kinetic energy in the electric field. Ions with lower masses fly through the drift tube faster as the square of velocity and mass are inversely proportional at a given kinetic energy. For ions with the same m/z but different shapes, the more compact molecule collides with fewer drift gas molecules and traverses the drift cell more rapidly. The structural information obtained by IM is described as collisional cross-section (CCS), which is an "effective area" that quantifies the likelihood of a scattering event when drift gas molecules strike ions. In most cases, a drift tube is a part of the mass spectrometer for IM-MS analysis. Comparing to only MS analysis, IM-MS analysis provides an extra dimension of separation based on the conformation of the ions. When doing native MS under IM-MS mode, native IM-MS serves as a powerful biophysical technique that reveals thermodynamic, kinetic, and structural information at the same time (Figure 1-3). One important aspect of native IM-MS is the validation of the “native” state of protein ions by IM. Theoretically, the proteins could be transferred into the gas phase in native-like conformations with careful tuning of instrument conditions.[21, 22] A variety of ion mobility and simulation studies have been performed to confirm the preservation of native solution structures of the proteins in the gas phase within the timescale of MS analysis,[11, 23-26] and identify cases in which proteins may have rearranged into non-native conformations after being transferred into the gas phase.[27, 28] In this dissertation, we further utilize solution techniques to validify our native IM-MS results. Native IM-MS is now widely applied to study biological questions that are challenging for traditional techniques such as aggregation mechanism,[29] membrane protein characterization,[30, 31] biomolecule topology,[25] and more recently, Fe-S protein characterization.[32]

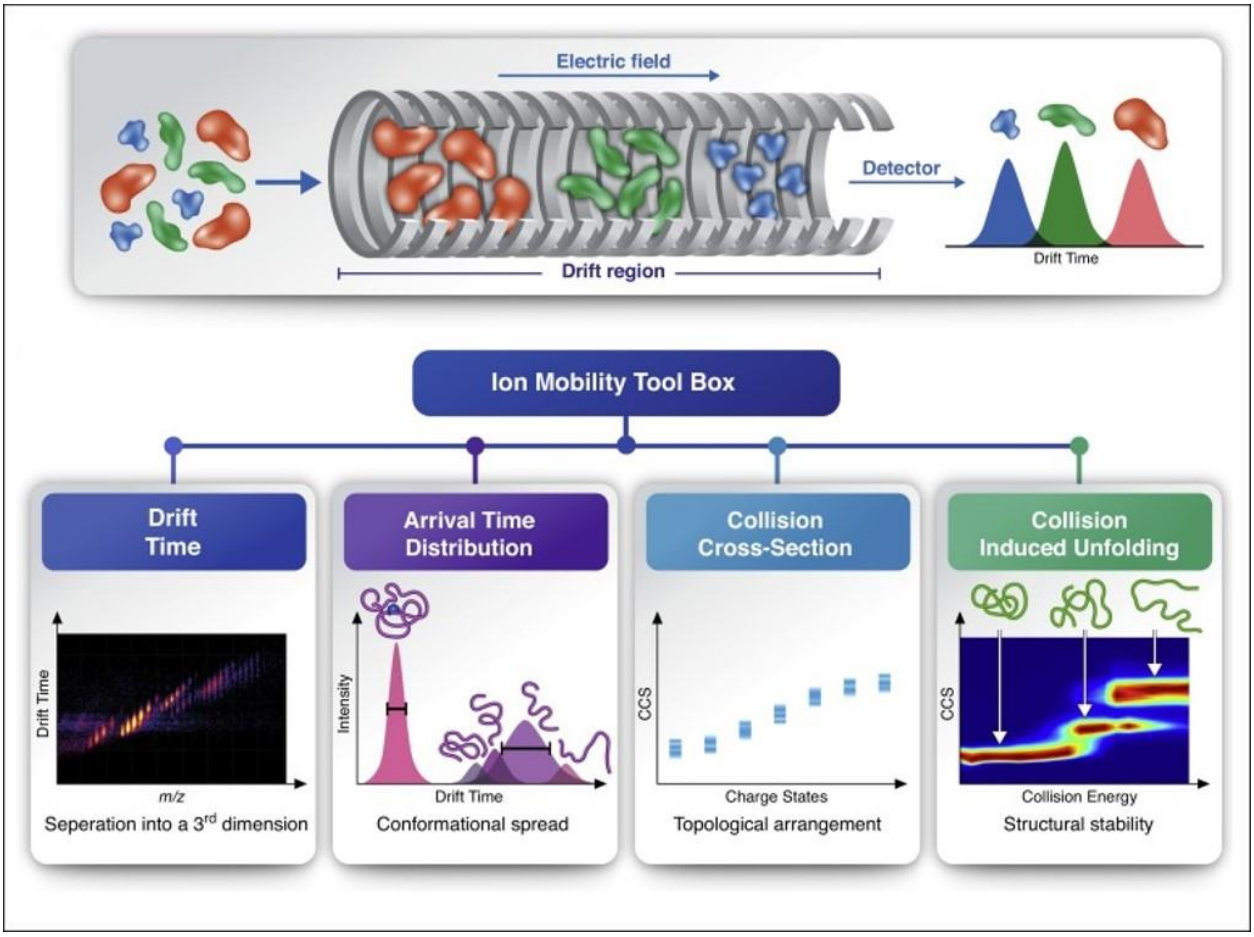

Figure 1.3 Principle and applications of ion mobility. IM- MS experiments include a drift tube inside a mass spectrometer that is filled with drift gas and also under an electric field in the opposite direction. Flying through the drift tube, ions are push by the electric field and collide with drift gas molecules, and the arrival time of the ions to pass through the drift tube is measured. IM-MS measurements give structural properties, adds the third dimension of separation to native MS, and resolves heterogeneous samples that contain closely related species. The arrival time distribution information reveals the conformational range of the ions and can be further converted to CCS. By doing IM-MS experiments over different collision energies, the collisional induced unfolding experiment illustrates the stabilities of ions and the structural information of unfolded intermediates. Reprint with permission from *Current Opinion in Chemical Biology* **2018**, *42*, 25-33. Copyright 2017 Elsevier Ltd.

1.2. *E. coli* ISC Fe-S Cluster Biogenesis Pathway

Fe-S cofactors assist various biological processes by exhibiting a range of functional roles including electron transfer, substrate binding and activation, small molecule sensing, and

controlling activity through regulation at the DNA, RNA, and protein levels.[33, 34] To carry out these diverse functions, Fe-S clusters have a variety of iron-to-sulfur stoichiometries, ligands, and are sometimes coupled to other metal cofactors (Figure 1.4).[35-37] The most common species found in proteins are the rhombic [2Fe−2S] and cubic [4Fe−4S] forms, which may be the building blocks for other Fe-S cofactors. Other forms of Fe-S clusters including [2Fe−2S], [3Fe−4S], [4Fe−4S], [Ni−4Fe−4S], [8Fe−7S], and [7Fe−9S−Mo] complexes have also been discovered.[35] Fe-S clusters are usually ligated to the protein with cysteine residues but can also bind to other amino acids. The most common alternative ligand is histidine, while aspartate, arginine, and threonine have also been revealed.[38]

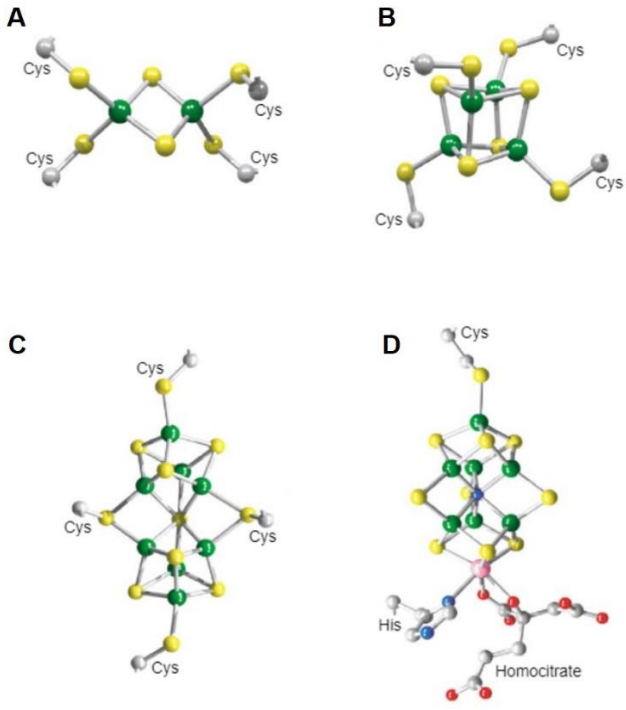

Figure 1.4 Selected Fe–S cluster cofactors found in biological systems. (A) [2Fe–2S] and **(B)** [4Fe–4S] clusters are coordinated to cysteine ligands of their respective protein binding partners. Higher nuclearity clusters such as **(C)** [8Fe-7S] P cluster and **(D)** [Mo-7Fe-9S] FeMo-cofactor have been identified in nitrogenase. (Iron is represented in green, sulfur is yellow, and

molybdenum is magenta) Reprint with permission from *Curr. Opin. Chem. Biol*. **2003**, 7, 166-173. Copyright 2003 Elsevier Science Ltd.

Due to the physiological importance of Fe-S clusters, extensive efforts have been invested in understanding Fe-S cluster biogenesis. While Fe-S clusters normally consist of ferrous ion, ferric ion, and sulfide, their biosynthetic pathways are surprisingly complicated. Without enzymes, iron ions and sulfide combine to form [2Fe–2S] or more complex clusters through a self-assembly process.[37] However, this self-assembly process is problematic for cells due to the toxicity of the substrates. Ferrous ions are prone to Fenton chemistry that generates reactive oxygen species and sulfide is a potent inhibitor of heme enzymes. Therefore, biological systems utilize highly controlled Fe-S cluster biogenesis machinery to control the rate of cluster assembly and sequester reactive ingredients. So far, three independent prokaryotic Fe-S cluster biogenesis systems have been discovered. The nitrogen-fixation (NIF) machinery[39] synthesizes Fe-S clusters for nitrogenase. The sulfur-mobilization (SUF) machinery[40] synthesizes Fe-S clusters using a highly protected molecular machinery that often operates under iron-limiting or oxidative stress conditions.[41] The Iron-Sulfur Cluster (ISC) machinery is considered the "housekeeping" machinery for Fe-S cluster biogenesis under normal physiological conditions for many bacteria such as *E. coli*. This ISC pathway is also present in the eukaryotic mitochondria of organisms such as yeast and humans (Figure 1.5). These different pathways share similar working principles and molecular machinery, which synthesize and then insert Fe-S cofactors into appropriate apoproteins. Here, we will first focus on the prokaryotic ISC machinery (Figure 1-6). The cysteine desulfurase IscS converts the substrate L-cysteine into L-alanine and generates a persulfide intermediate on a mobile S-transfer loop cysteine residue.[40, 41] Sulfur is transferred from IscS to

the scaffold protein IscU for Fe-S cluster assembly.[42] The requirement of an iron donor protein and the source of iron are not clear[43-46]. The IscS-IscU complex can build [2Fe–2S] and, possibly, [4Fe–4S] cluster from ferrous iron, cysteine, and an electron source.[47-49] Ferredoxin is reported to be the electron donor[50, 51] but is not essential and can be substituted with reagents such as DTT or glutathione for *in vitro* Fe-S cluster synthesis assays. To complete the catalytic cycle for the assembly complex, the Fe−S cluster intermediates are transferred intact to the recipient proteins with the assistance of chaperone and/or carrier proteins.[52-55]

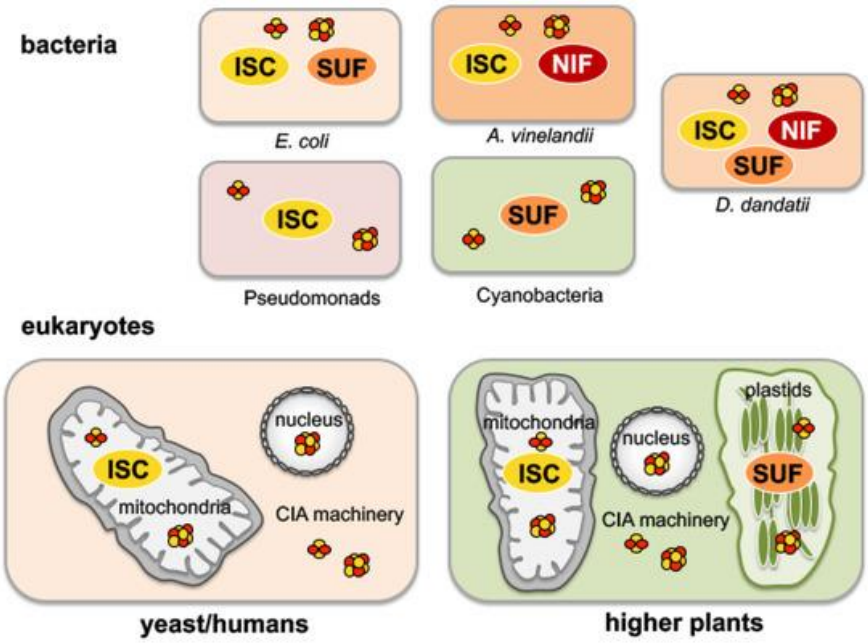

Figure 1.5 Fe-S cluster biogenesis machinery in various organisms. Bacteria have ISC (iron-sulfur cluster), NIF (nitrogen fixation), and SUF (sulfur mobilization) systems. The NIF system synthesizes Fe-S cluster for nitrogenase in azototrophic bacteria. The housekeeping ISC and oxidative stress-resistant SUF systems are distributed in different bacteria and eukaryotes. The ISC machinery in the mitochondria of eukaryotes is likely from an ancestor of α-proteobacteria, the evolutionary origin of the organelles. The SUF machinery in plastids of plants is likely from the endosymbiosis of a photosynthetic bacterium. The cytosolic iron-sulfur protein assembly (CIA) machinery is involved in the maturation of cytosolic and nuclear Fe-S proteins. Reprinted with permission (open access) from *Inorganics* **2020**, *8*(7), 43. Copyright 2020 by the authors. Licensee MDPI, Basel, Switzerland.

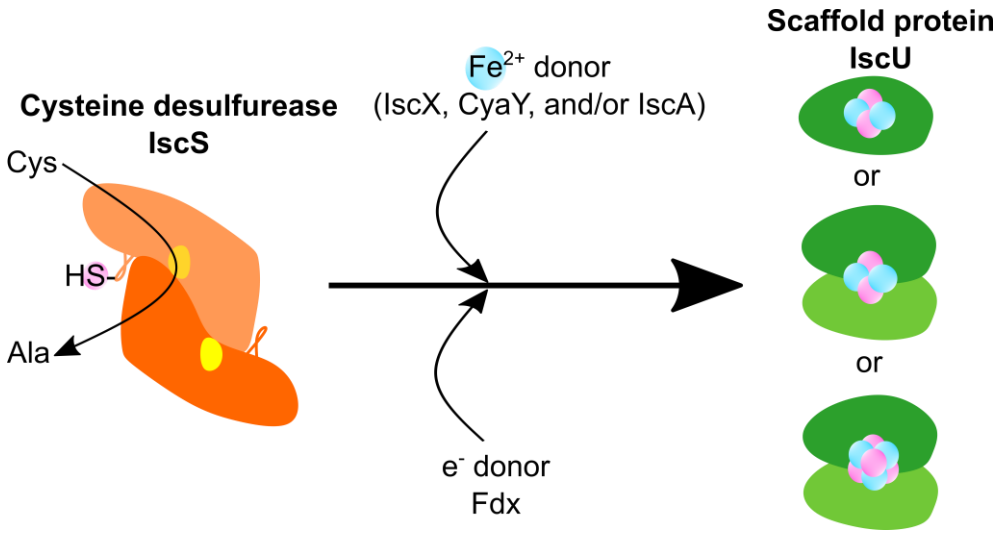

Figure 1.6 *E. coli* ISC Fe-S assembly machinery. The sulfur source is from L-cysteine, which is turned over by the cysteine desulfurase IscS to generate sulfane sulfur. IscS further transfer the sulfane sulfur to the scaffold IscU, where the Fe-S clusters are assembled. The iron source is from proposed carriers IscX, CyaY, and/or IscA. The electron source is from the proposed donor Fdx.

The cluster assembly mechanism on IscU is poorly understood. IscU has three conserved active site cysteine residues, which have been shown to form persulfide or polysulfide species by accepting sulfur from IscS.[56-59] Crystal structures of IscU indicate that both Zn^{2+} and [2Fe–2S] clusters ligate to the three active site cysteine residues, suggesting mutually exclusive binding of these cofactors (Figure 1.7).[60, 61] Metal or cluster binding is important for the overall protein fold of IscU. Studies using multiple biophysical techniques including NMR and SAXS suggest IscU exists in disordered (D) and structured (S) states.[62, 63] Apo-IscU mostly exists in disordered states, which is reported as the binding state with IscS, and the equilibrium shifts toward structured states upon binding of either Zn^{2+} or Fe^{2+}.[64-66] While studies from the Markley group suggest IscU exists primarily in the D state when bound to IscS, results from the Pastore group indicate the opposite.[62, 67] Extra studies are required to further illustrate the conformation landscape of IscU with regard to

cluster assembly. In addition to the conformational ambiguity for IscU, the order in which the sulfur and iron substrates are incorporated into IscU for cluster assembly also remains elusive.

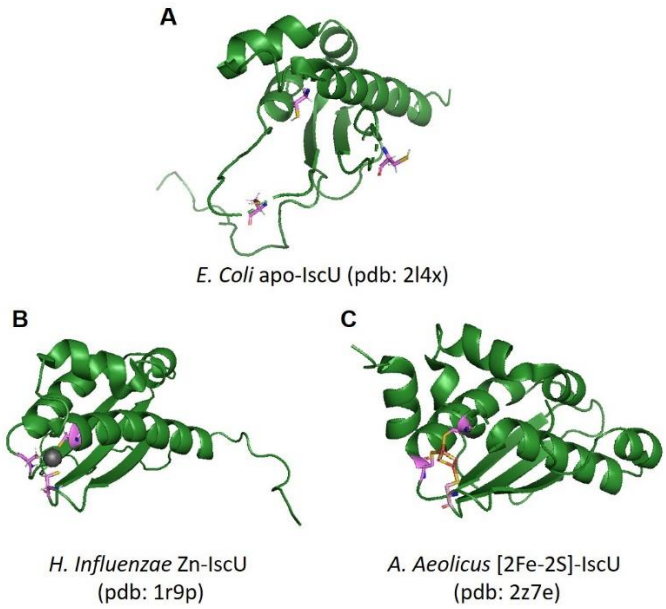

Figure 1.7 Structures of bacterial IscU. (A) Apo- **(B)** Zn bound **(C)** [2Fe–2S] bound IscU are shown in green cartoon images, and the three conserved active site cysteine residues are shown as sticks. The three cysteines are far from each other in apo state and come together to ligate Zn^{2+} or [2Fe–2S] cofactor.

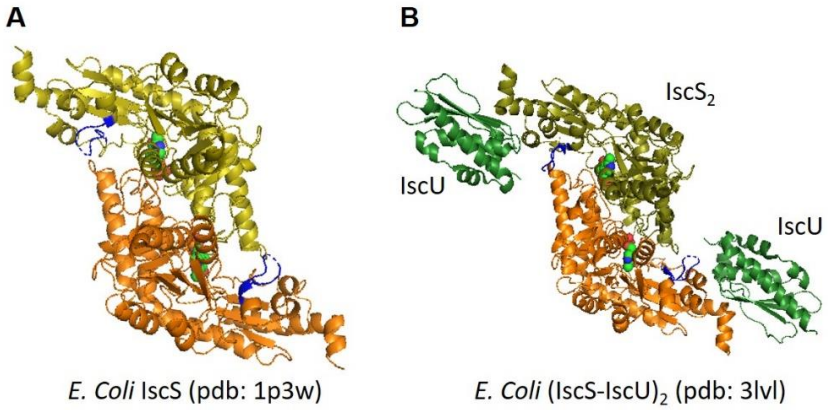

Figure 1.8 Structures of *E. Coli* IscS. Determined structures of **(A)** $IscS_2$ and **(B) (**$IscS\text{-}IscU)_2$. IscS monomers are shown in yellow and orange, PLP as green spheres (buried in IscS monomers), the mobile sulfur transfer loops in blue, and IscU in green.

The cysteine desulfurase IscS exists as a stable homodimer. The C-terminus of each IscS subunit binds IscU with a 5'-pyridoxal phosphate (PLP) cofactor and a mobile S-transfer loop cysteine residue near the IscU active site (Figure 1.8). Studies using site-directed mutation, X-ray crystallographic structures, hydrogen-deuterium exchange, and stopped-flow spectroscopy have established a detailed mechanism of PLP-dependent conversion from cysteine to alanine (Figure 1.9).[68-73]

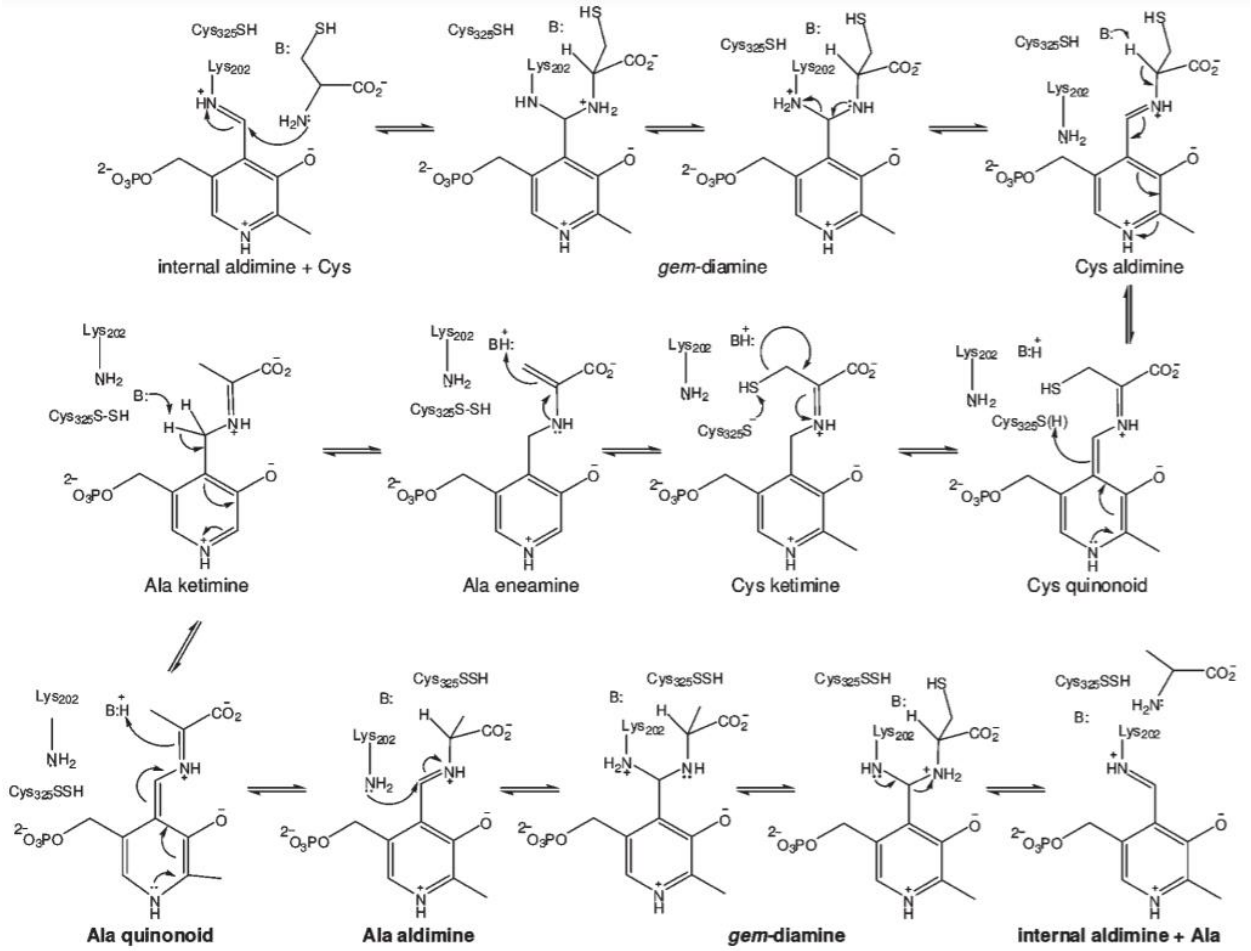

Figure 1.9 Cysteine desulfurase mechanism. Reprint with permission from *Biochemistry* **2009**, 48, 12014-12023. Copyright 2009 American Chemical Society. This figure was adapted from Zheng et al. and requires additional permission. Reprinted (adapted) with permission from *Biochemistry* **1994**, 33, 4714-4720. Copyright 1994 American Chemical Society.

Key insights into the Fe-S cluster biosynthetic mechanism were provided fromcrystal structures. The IscS-IscU complex with and without a [2Fe–2S] cluster reveal protein-protein interactions and provide insight into the intermolecular sulfur transfer reaction.[60, 74] Although different models for the Fe-S cluster biosynthesis mechanism have been proposed,[51, 75-79] the lack of characterized Fe-S enzyme-associated intermediates limits mechanistic insight. One major difference in these proposed mechanisms is the order of sulfur and iron incorporation events (Figure 1-10). In the iron-first model, the first step of [2Fe–2S] assembly is ligation of Fe^{2+} to cysteine residues on the scaffold protein, after iron binds, sulfane sulfur is transferred from the cysteine desulfurase. Four electrons are required to reduce the two sulfane sulfurs to sulfides; two electrons come from oxidation of the two Fe^{2+} to Fe^{3+}, and the other two electrons come from an external source. In comparison, the first step of the sulfur-first mechanism is the sulfane sulfur transfer. Earlier studies are more consistent with the sulfur-first model,[75-77] as scaffold proteins can accept sulfane sulfur from cysteine desulfurases without Fe^{2+}. However, these persulfide species on the scaffold protein have not been shown to form at kinetically competent rates or be viable in generating a Fe-S cluster. The argument in support of an iron-first model was mainly from the iron-binding affinity of the scaffold protein.[80] Recently, a study on the human ISC system revealed the stimulation of sulfur transfer to the scaffold protein in the presence of Fe^{2+}, which is consistent with the iron-first model.[51] Overall, the characterization of intermediates is still necessary to establish the the order of events during Fe-S cluster biogenesis.

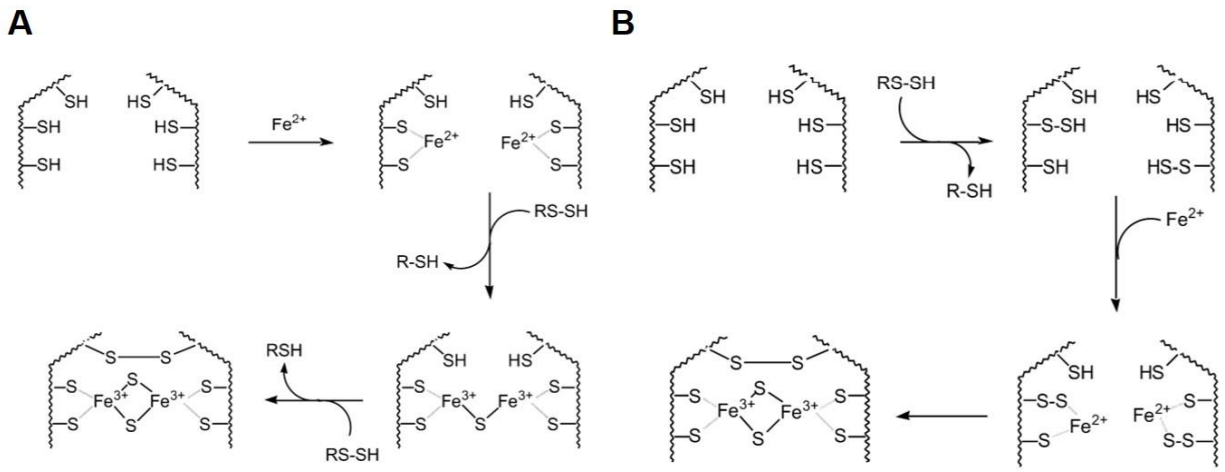

Figure 1.10 Models for Fe-S cluster biogenesis. (A) Iron-first and **(B)** Sulfur-first model for Fe-S cluster assembly. Reprinted with permission from *J. Biol, Inorg. Chem.* **2005**, 276 (25): 22604-22607. Copyright 2005 Springer/Heidelberg.

1.3. Human ISC Fe-S Cluster Biogenesis Pathway

The ISC Fe-S cluster assembly machinery in eukaryotes is located in the matrix of mitochondria. The understanding of the eukaryotic ISC pathway was supplemented by the studies on the prokaryotic system introduced above. Similar to the prokaryotic ISC machinery, the human ISC machinery contains proteins with analogous roles in the controlled assembly of Fe-S clusters and subsequent transfer of the clusters to target apo-proteins. Parallel experiments on the eukaryotic and prokaryotic ISC pathways have provided valuable insights into the similarities and differences in functions of the respective proteins in the pathways.[81]

Here, we focus on the essential eukaryotic cysteine desulfurase NFS1, which has been identified in both the cytosol and mitochondria.[82] The primary function of NFS1 is to convert cysteine into alanine and provide sulfur for the biosynthesis of sulfur-containing biomolecules. Interestingly, although NFS1 has been identified in the cytosol it appears to only function in Fe-S

cluster biogenesis in the mitochondria.[83] Despite a common PLP-based mechanism for all characterized cysteine desulfurases, the eukaryotic cysteine desulfurase complex is substantially different from its prokaryotic homologs. The comparison between *E. coli* IscS and human NFS1 suggests significant differences that may be related to a regulatory mechanism. IscS and NFS1 share a 60 % sequence identity but different complex topologies. IscS is a strong homodimer[84, 85] and in $\alpha_2\beta_2$ complex when binding IscU.[74, 86] The oligomeric state of NFS1 is more dynamic. Early analytical SEC studies suggest NFS1 as a homodimer,[87] while more recent experiments on *S. cerevisiae* NFS1 and human NFS1 indicate that NFS1 also have monomeric fractions.[88-90] Additionally, the activity profiles of IscS and NFS1 complexes are significantly different. The most common method of measuring cysteine desulfurase activity is the methylene blue assay. Persulfide species are cleaved by dithiothreitol (DTT) to generate sulfide, which is then used to synthesizes methylene blue by adding *N*,*N*-dimethyl-*p*-phenylenediamine (DPD) and ferric chloride. The product methylene blue is quantitated by its absorbance at 670 nm. While *E. coli* IscS shows a k_{cat} of 7.5 ± 0.1 min^{-1} and a K_M for cysteine of 17 ± 2 μM, human NFS1 could only perform single turnover and easily precipitates.[81 87] In short, NFS1 itself is unstable and inactive.

ISD11, an LYRM superfamily protein containing the conserved Leu-Tyr-Arg motif, was discovered as an adaptor protein for NFS1. All of the LYRM proteins bind acyl-carrier protein (ACP), which is introduced below.[91-97] ISD11 seems to be incorporated into the complex with the α-proteobacteria endosymbiotic event, which is consistent with the acquisition of ISC proteins in the mitochondria.[98] *In vivo* knockout and siRNA suppression of ISD11 in yeast lead to growth defects and low aconitase activity, which is a Fe-S enzyme typically used for reporting the cellular Fe-S cluster level.[88, 99, 100] *In vitro* characterization using pull-down and SEC indicates that ISD11

binds with NFS1 tightly and forms a stable $\alpha_2\beta_2$ complex.[87, 88, 100] Recently, crystal structures of NFS1 in complex with ISD11 further shed light on how structurally ISD11 together with another adaptor protein ACP stablizes NFS1.[101, 102] Despite higher stability, NFS1-ISD11 complex still exhibits low activity (a k_{cat} of 1.9 ± 0.1 min^{-1} and a K_M for cysteine of 340 ± 60 μM) comparing to *E. coli* IscS (a k_{cat} of 7.5 ± 0.1 min^{-1} and a K_M for cysteine of 17 ± 2 μM).[87, 103] Specific residues, including a clinical R68L mutation, on ISD11 have been shown to be required for the activity.[89, 104]

Another adaptor protein, the mitochondrial ACP, has also been discovered. Mitochondrial ACP conjugates with its 4'-phosphopantetheine cofactor through a thioester bond, which reacts with acetyl-CoA for lipoic acid biosynthesis.[105, 106] The *in vivo* evidence of ACP playing a direct role in Fe-S cluster biosynthesis is demonstrated by *S. cerevisiae* studies. ACP knockdown of *S. cerevisiae* resulted in the loss of the NFS1-ISD11 complex and diminished aconitase activity. Further structural studies demonstrated ACP directly binds and stablizes the NFS1-ISD11 complex.[101, 102, 107] When recombinantly co-expressing NFS1 and ISD11 in *E. coli*, *E. coli* ACP is incorporated to form the NFS1-ISD11-ACP_{ec} complex. Herein, the NFS1-ISD11-ACP human cysteine desulfurase complex is noted as SDA_{ec}. SDA_{ec} has been widely used for *in vitro* studies in the field, as ACP_{ec} appears to have no functional difference to the complex with human ACP.[108] In all the determined structures of SDA_{ec}, the NFS1 fold is highly similar to *E. coli* IscS.[86]

ISD11 forms two different interfaces with NFS1 that stabilize SDA_{ec}. A hydrophobic pocket between specific residues on ISD11 and NFS1 is formed, which helps prevent self-aggregation of NFS1 through intermolecular NFS1 hydrophobic interaction. The ACP-Lipid-ISD11 motif is also revealed, which includes a 3-helix bundle fold for ISD11 that contains most

of the highly conserved residues. A lipid-bound 4′-PPT inserts into the hydrophobic core of ISD11. ACP_{ec} binds ISD11 using interactions with the LYR motif and electrostatic contacts. ACP_{ec} structure in the complex is similar to both uncomplexed bacterial ACP[109] and human ACP.[110] While the incorporation of ISD11 and ACP significantly increases the stability of NFS1, SDA_{ec} still exhibits low activities (a k_{cat} of 0.6 ± 0.04 in^1 and a K_M for cysteine of 1.3 ± 0.3 μM).

Similar to other ISC machinery, the human ISC machinery also contains the scaffold protein for cluster assembly. The human scaffold ISCU2 is similar to *E. coli* IscU in terms of function and structure. Like IscU, ISCU2 also requires two Fe^{2+}, two sulfane sulfur from the cysteine desulfurase, and two electrons likely from the human ferredoxin FDX1/FDX2 to synthesize a [2Fe–2S] cluster. ISCU2 also possesses the three conserved active site cysteine residues that bind either Zn^{2+} or a Fe-S cluster, as well as accept sulfur from the cysteine desulfurase. Both IscU and ISCU2 interact with the C-terminus of their respective cysteine desulfurase. ISCU2 binding to the SDA_{ec} complex generates the $SDA_{ec}U$ complex.

Another essential protein in the human ISC machinery is frataxin (FXN). FXN locates in the mitochondria with the major function of activating the human cysteine desulfurase complex. Mutations on the frataxin gene lead to lethal neurodegenerative disease Friedreich's Ataxia (FDRA). FRDA results primarily from the GAA triplet nucleotide expansions in the first intron of the FXN gene, which produce lower levels of the protein.[111] Given the prevalence of this disease, extensive efforts have been invested to understand the function of FXN. In this dissertation, we focus on the mature functional form of FXN in mitochondria (81-210).[112, 113] *In vivo* studies suggest that FXN levels directly correlate with Fe-S cluster biosynthesis.[114, 115] FXN and its bacterial homolog CyaY have been proposed as the iron donor due to their iron-binding

properties.[116, 117] As recent studies show the iron-binding acidic patch on FXN discretely binds an arginine-rich region at the dimer interface of NFS1 that is far from the cluster synthesis site of ISCU2.[107, 118] Thus, the iron-binding properties of FXN are likely unrelated to iron donation for Fe-S cluster synthesis. Extensive studies on FXN illustrate the role of FXN in the ISC pathway. FXN binds to the complex of SDA_{ec} and ISCU and promotes cluster synthesis by enhancing the cysteine desulfurase activity.[51, 56, 119] Recent studies from the Barondeau group shows that FXN stimulates the activity of the complex not only by promoting the PLP and sulfur transfer chemistry [119], but also by functioning as an allosteric modulator and driving a structural rearrangement.[120] Interestingly, the human ISC system has some key functional differences compared to the bacterial ISC machinery. The human system requires FXN binding to the $SDA_{ec}U$ complex to generate the $SDA_{ec}UF$ complex for a comparable activity to the stand-alone bacterial IscS enzyme. Surprisingly, CyaY does not affect IscS activity but can activate $SDA_{ec}U$ complex similar to FXN.[81, 121] Vice versa, FXN fails to activate IscS. Together, the exchangeable role of FXN and CyaY suggests the difference between human and bacterial ISC systems primarily originate from differences in the cysteine desulfurases. So far, two different structures of the SDA complex,[101, 102] one additional structure of SDAU,[102] and one structure of the SDAUF complex[107] have been determined. Notably, these solved structures exist in vastly different "architectures" that potentially regulate the activity of the human ISC machinery (Figure 1.11). Findings regarding these different architectures and their implications will be discussed in Chapter IV.

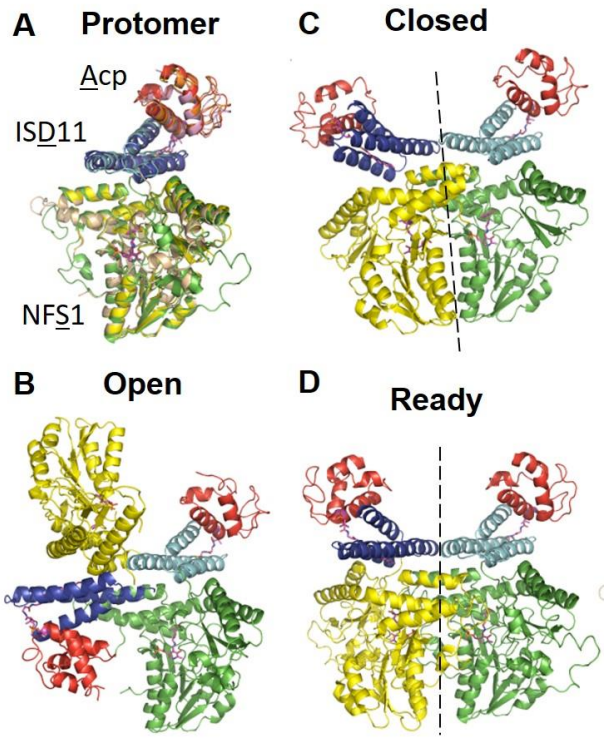

Figure 1.11 Comparison of different SDA_{ec} architectures. (A) Overlay of the subunits from one protomer for NFS1 (green, yellow, and wheat), ISD11 (cyan, blue, and purple), and ACP (red, orange, and pink) of the ready, closed, and open forms, respectfully. Protein cofactors are shown in magenta. Structure of the SDA_{ec} complex in the **(B)** open, **(C)** closed, and **(D)** ready forms. NFS1 is shown in yellow and green, ISD11 in blue and cyan, and ACP_{ec} in red. The green/cyan/red protomer is shown in the same orientation for the different architectures.

1.4. The Putative Roles of Bacterial Frataxin CyaY

Bacterial frataxin CyaY is a small (~14 kDa) monomeric protein. Similar to FXN, structures of CyaY show an acidic ridge, which can bind iron.[79, 122-124] Interaction of CyaY with IscS was first characterized by ITC, showing a 1:1 stoichiometry complex with medium affinity (K_d: 18.5 μM).[125] Site-directed mutagenesis and NMR studies suggested that the IscS residues R220, R223, and R225 interact with the CyaY acidic ridge.[126] While IscU monomer binds at the periphery site of IscS, CyaY monomer binds at a site near the IscS dimer interface.[126] Chemical

cross-linking experiments capture an IscS-IscU-CyaY complex[50], and a model of the 1:1:1 ternary complex was built using SAXS, X-ray structures of the single proteins, and NMR data[126] (Figure 1.12). Further *in vitro* experiments demonstrated that CyaY promotes IscU-IscS binding, changing the K_d for IscS–IscU interaction from low μM to hundreds of nM. Additionally, the K_d of IscS-CyaY interaction changes from 35 nM to 23 μM with the presence of IscU. Together, IscU and CyaY enhance their mutual binding to IscS, forming a tight ternary complex.

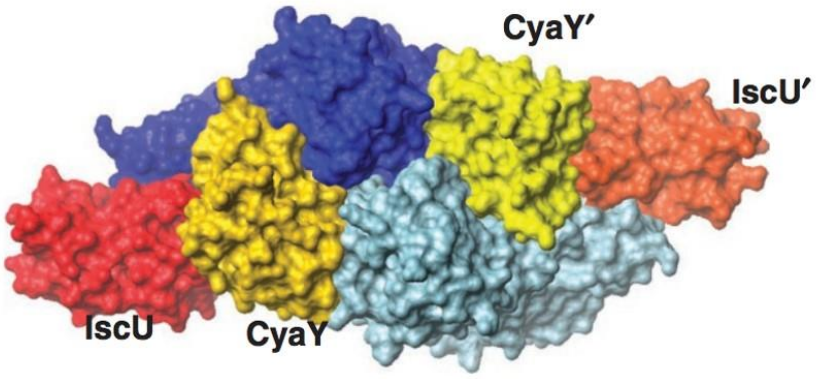

Figure 1.12 Model of (IscS-IscU-CyaY)$_2$ complex. Model built from combined NMR and small-angle X-ray scattering studies shown as a surface representation. IscS protomers are shown in blue and cyan, IscU in red and orange, CyaY in gold and yellow. Reprinted with permission from *Nat. Commun.* **2010**, *1*, 95. Copyright 2010 Nature Publication Group.

The physiological role of CyaY is unclear. While genetic and bioinformatic information suggests a direct role for FXN in the human ISC pathway,[114, 127, 128] the genetic studies of CyaY showed *cyaY* does not belong to the *isc* operon. As mentioned above, mutations in the *fxn* gene lead to a fatal neurodegenerative disease FRDA [129] in human, as well as compromised Fe-S protein activity and survival in other eukaryotic systems.[130] To understand the pathology role of FXN in FRDA, the role of FXN in activating the ISC pathway has been intensively characterized. These studies show enhanced cysteine desulfurase activity, persulfide formation and transfer, and Fe-S

cluster formation on ISCU2, which support the positive role of FXN in the early stages of the human ISC pathway.[56, 57, 103, 118, 131-136] Contrastingly, the role of CyaY on the bacterial ISC system is unclear. Neither *E. coli* nor *Salmonella enterica* single *cyaY* mutants showed a significant loss in Fe-S enzyme activities.[123, 137, 138] Interestingly, while mutated *Salmonella enterica* lacking both CyaY and Yggx show no phenotypic change under normal physiological conditions, major growth defects and impaired survival is observed under oxidative stress conditions.[139, 140] *Salmonella enterica* CyaY and Yggx are also reported to be involved in Fe-S cluster repair.[140] Also, direct evidence of the involvement of bacterial frataxin in Fe-S metabolism was found in *Bacillus subtilis*, in which inactivation of the frataxin homologue gene leads to a decrease in Fe-S enzyme activity.[141] Early *in vitro* studies lead to the proposal that CyaY functions as an iron donor due to its ability to bind Fe^{2+} with moderate affinity and Fe^{3+} with high affinity.[142, 143] FXN has similar iron binding affinities, and both FXN and CyaY oligomerize in an iron-dependent fashion, consistent with the iron donor role.[79, 144, 145] Nevertheless, no evidence of the iron carried by FXN or CyaY being incorporated into the cluster has been shown. Later studies are against this iron donor role, as the deletion of yeast FXN gene could be compensated for by a frataxin variant with defects in iron-induced oligomerization.[146] Also, CyaY exhibits an inhibitory effect on Fe-S cluster biogenesis.[81, 138] Due to this inhibitory effect, CyaY has also been proposed as a "gatekeeper" of Fe-S cluster assembly, preventing excess Fe-S assembly under iron overload conditions.[122] However, the mechanism of CyaY inhibition on the prokaryotic ISC pathway has not been fully elucidated. While FXN clearly benefits Fe-S cluster assembly, the seemingly contradictory effects and roles of CyaY have yet to be resolved.

1.5. Oxidative Stress, Sulfur Trafficking, and CyaY

Since CyaY has been implicated in oxidative stress response (see above), the fundamentals of oxidative stress and the relationship to sulfur metabolism will be discussed in this section. Oxidative stress is a phenomenon caused by an imbalance between the production and accumulation of reactive oxygen species (ROS) in cells and the ability of a biological system to detoxify these reactive products.[147] ROS are highly reactive and toxic species that disrupt cellular functions by damaging essential protein cofactors including Fe-S clusters and oxidizing functional groups such as thiols. Therefore, limiting the amount of ROS such as H_2O_2 is crucial for cells to maintain normal function. Bacteria use many enzymes and systems to scavenge H_2O_2 including catalases, NADH peroxidase, the thioredoxin (Trx) antioxidant system, and the glutathione (GSH) antioxidant system.[148] In *E. coli*, the Trx and GSH systems are the major cellular redox regulation systems that maintain a reduced redox environment by catalyzing electron flux from NADPH (Figure 1.13).[149-151] These two systems both utilize thiols to carry out their function and thus are central to the regulation of the cysteine proteome (Figure 1.14). The oxidation state of biological active thiol groups affects their function; therefore, cysteines act as redox molecular switches and targets of disease.[150, 152, 153] For example, glutathione (GSH), comprising of glutamine, glycine, and cysteine, is the most common antioxidant in cells and often exists in low mM concentrations.[150, 152, 154, 155] The thiol group of GSH has a pKa ~8[156, 157] and can reduce oxidized thiol groups or directly quench ROS. When the cell is under high ROS concentration, GSH will also be oxidized and fail to maintain its function. Thus, the ratio of reduced to oxidized GSH is an index of whether the cell is under oxidative stress. GSH has also been proposed as one of the substrates of sulfide quinone reductase, which catalyzes the generation of glutathione persulfide

(GSSH). GSSH is a stronger antioxidant than GSH due to the low pKa (~6.2) of persulfide and usually exists in low μM in cell.[156, 157] Reactive persulfide species such as GSSH have been proposed to protect *E. coli* from H_2O_2.[158] Due to the toxic nature of ferrous iron and sulfide, Fe-S clusters have a close relationship to oxidative stress.[159-161] For example, labile [4Fe–4S] clusters and $[2Fe–2S]^{2+}$ clusters could be easily damaged by ROS and release labile iron and sulfide ions upon degradation, which subsequently leads to the propagation of ROS.[32, 162-164] To avoid this vicious cycle, bacteria utilize strategies such as sequestering labile irons, repairing [4Fe–4S] clusters, and switch the assembly pathway to the protected SUF pathway.[139, 140, 142, 148, 164, 165] Interestingly, CyaY has been reported to involve in sequestering iron and repairing [4Fe–4S].[123, 139, 140, 142]

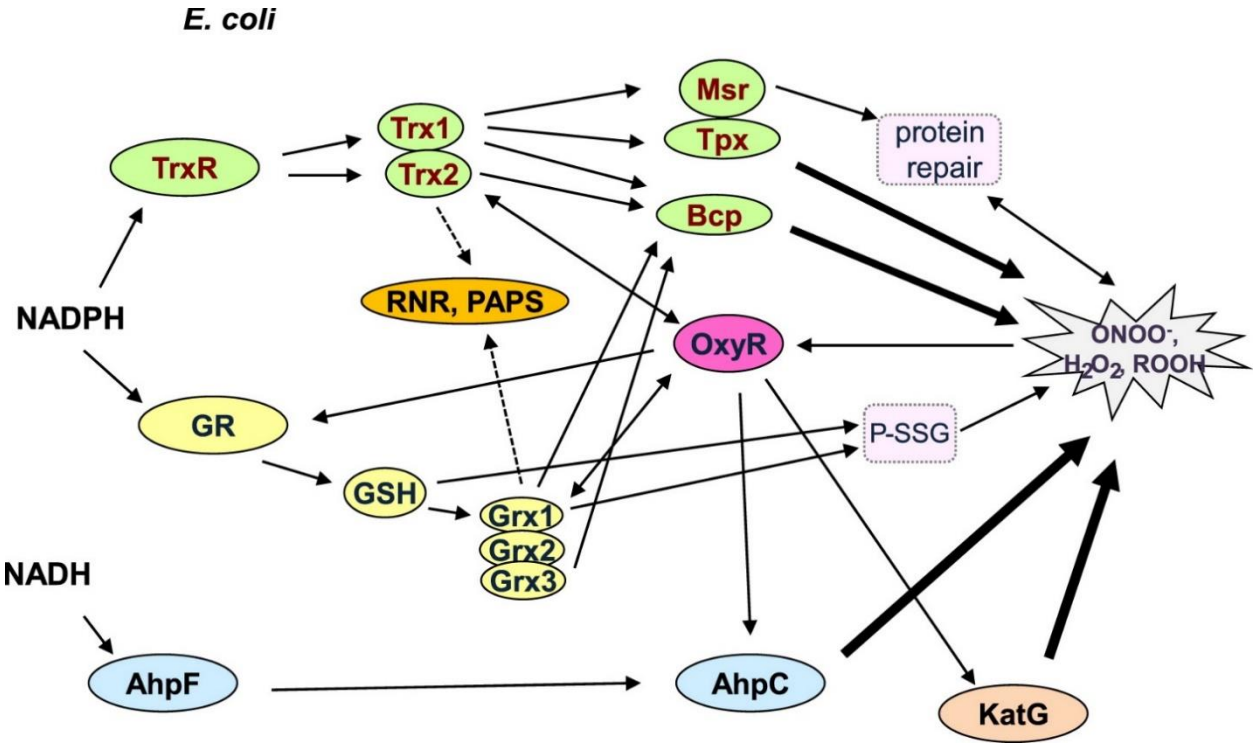

Figure 1.13 Antioxidant systems in *E. coli*. In *E. coli*, GSH, Trx antioxidant systems, and catalase are present. The Trx system is consists of TrxR, Trxs (Trx1 and Trx2), and three major peroxidases (BCP, Tpx, and AhpC). OxyR acts as the transcription factor which regulates the expression of

antioxidant enzymes including catalase, GR, AhpC, Trx2, and Grx1. Reprinted with permission from *Free Radic Biol Med* **2014**, *66*, 75-87. Copyright 2013 Elsevier Inc.

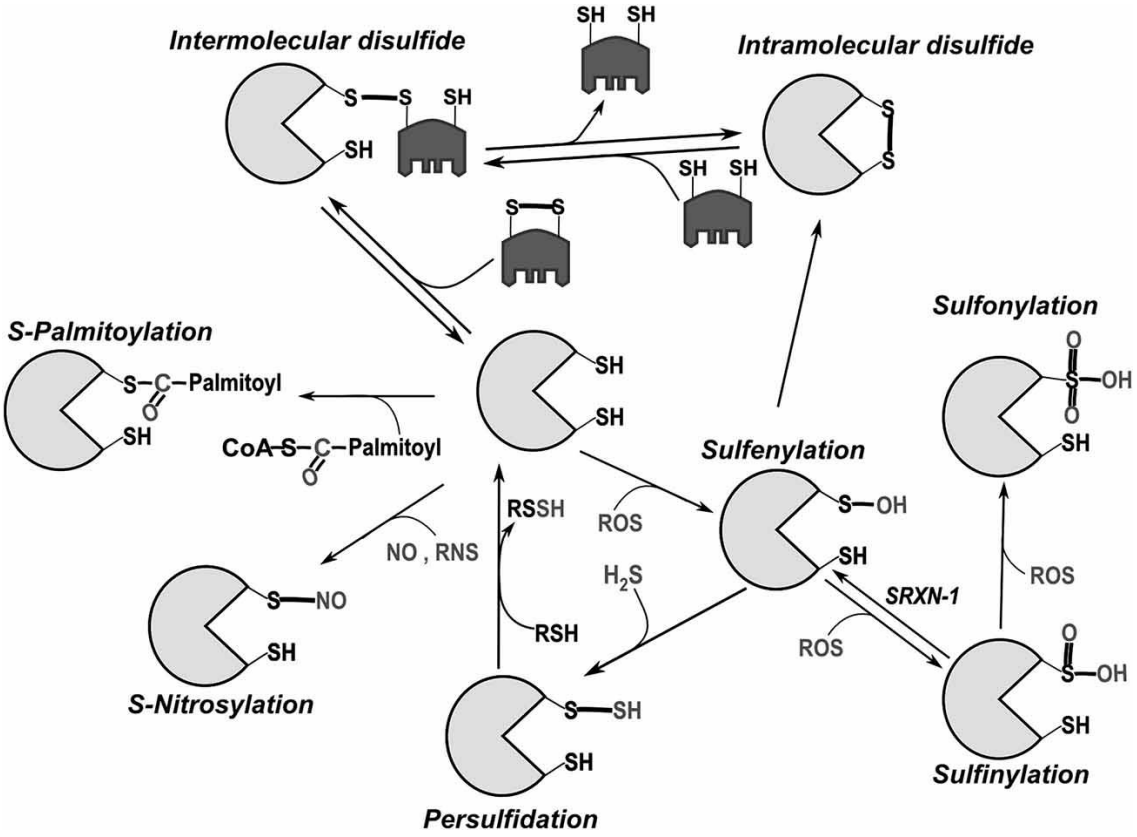

Figure 1.14 Major modifications of cysteine residues. In general, disulfide bonds are caused by oxidation events. Intermolecular disulfide bonds could be formed with another protein or small molecule such as GSH. Intramolecular disulfide bonds could be inserted into a reduced protein by disulfide exchanges. The disulfide bonds would be reduced by GSH under a reduced environment. Under oxidative stress, ROS reaction would first produce reversible sulfenylation and sulfinylation and finally to irreversible sulfonylation. Reprinted with permission (open access) from *Front Mol Neurosci* **2017**, *10, 167*. Copyright 2017 Fra, Yoboue and Sitia.

The effects of CyaY on benefiting Fe-S level and relieve oxidative stress are demonstrated in cell studies described above in Section 1.4. Aside from participating in Fe-S cluster assembly, CyaY has also been proposed to influence IscS-based sulfur trafficking.[123] As mentioned, the cysteine desulfurase converts cysteine into alanine and generates a persulfide on its mobile transfer

loop cysteine residue. This sulfane sulfur is further transferred to the scaffold protein for Fe-S cluster assembly.[42] However, the scaffold protein is often not the only sulfur acceptor of the cysteine desulfurase. The *E. coli* cysteine desulfurase IscS belongs to class I cysteine desulfurase, which contains a longer mobile transfer loop with a twelve-residue sequence insertion following the active site Cys residue.[166] The flexibility of this longer loop has been proposed to allow the enzyme to interact with a variety of sulfur acceptors. For *E.coli* IscS, three sulfur acceptors have been discovered.[74, 167-170] The first one is IscU as discussed above. The second one is ThiI, a dual sulfur acceptor for the biosynthesis of thiamin and 4-thiouridine. The third one is TusA, a dual sulfur acceptor for the biosynthesis of 2-thiouridine tRNA and molybdenum cofactor. The diverse sulfur acceptors and downstream pathways implies the requirement of regulation on sulfur trafficking. The effect of sulfur acceptors and other binding partners on the activity of IscS provide insights into chemical steps of sulfur transfer and the hierarchy of physiological related sulfur trafficking. Recently, the IscS binding footprint for sulfur acceptors and interacting partners including IscU, TusA, ThiI, CyaY, and IscX have been revealed by NMR and site-directed mutagenesis.[74] Different sulfur acceptors have overlaid footprint lines except for IscU and TusA. Nevertheless, additional structural studies suggest the competition between IscU and TusA. The X-ray crystallographic structures of IscS-TusA complex and IscS-IscU complex demonstrate a steric conflict between TusA and IscU on binding IscS. In addition, IscS pulldown experiments suggest IscU and TusA binding on IscS are mutually exclusive.[74] Together, these studies suggest one IscS active site can only accommodate and transfer sulfur to one sulfur acceptor at a time. Notably, CyaY and IscX binds IscS-IscU complex and enhance IscS-IscU binding affinity.[74, 75] Potential CyaY and IscX regulation on sulfur trafficking to different acceptors could be

physiologically important. Overall, *in vivo* studies support a positive effect of CyaY on Fe-S cluster level and antioxidation in the cell. While FXN clearly benefits Fe-S cluster assembly, the seemingly contradictory effects of CyaY *in vivo* and *in vitro* have yet to be resolved.

So far, traditional bioinorganic techniques haven't been successful on answering the questions brought up in this introduction. In this dissertation, examples of employing native IM-MS on providing mechanistic insights on these questions are demonstrated. In Chapter II, enzyme-bound Fe-S intermediates of the ISC pathway are monitored by high-resolution native MS; in Chapter III, the effects of CyaY on competitive sulfur acceptor binding and sulfur trafficking are revealed using native IM-MS; in Chapter IV, the conformation landscape of human ISC machinery is probed by using IM-MS.

2. AN IRON-FRIST MECHANISM OF E. COLI ISC FE-S ASSEMBLY REVEALED BY HIGH-RESOLUTION NATIVE MASS SPECTROMETRY*

2.1. Introduction

Iron-sulfur (Fe−S) clusters are protein cofactors that are necessary for critical cellular processes such as oxidative respiration, photosynthesis, nitrogen fixation, and DNA replication/repair. Fe-S cluster cofactors exhibit a range of functional roles including electron transfer, substrate binding and activation, small molecule sensing, and controlling activity through regulation at the DNA, RNA, and protein levels.[171, 172] Fe-S clusters have a variety of iron-to-sulfur stoichiometries and are sometimes coupled to other metal cofactors.[173-175] The most common species found in proteins are the rhombic [2Fe−2S] and cubic [4Fe−4S] forms, which may be the building blocks for other Fe-S cofactors. Despite their physiological importance, few mechanistic details are known about intermediates in the formation and transformation of these Fe-S species.

The ISC (iron-sulfur cluster) biosynthetic pathway is found in many bacteria and in the mitochondria of eukaryotes.[176-178] In the bacterial pathway, the cysteine desulfurase IscS converts the substrate L-cysteine into L-alanine and provides the sulfur to the scaffold protein IscU for Fe-S cluster assembly.[68, 76, 86] The requirement of an iron donor protein and the source of iron are not clear.[75, 116, 179, 180] The IscU-IscS complex can build [2Fe–2S] and, possibly, [4Fe–4S] cluster intermediates from Fe^{2+}, L-cysteine and an electron source.[181-183] Ferredoxin is reported to be the electron donor[184] but is not essential and can be substituted with reagents such as glutathione

*Reprinted with permission from "Molecular Mechanism of ISC Iron–Sulfur Cluster Biogenesis Revealed by High-Resolution Native Mass Spectrometry" by Lin, C.-W.; McCabe, J. W.; Russell, D. H.; Barondeau, D. P. *Journal of the American Chemical Society* **2020,** *142* (13), 6018-6029. Copyright 2020 American Chemical Society.

(GSH) for *in vitro* Fe-S cluster synthesis assays.[185] To complete the catalytic cycle for the assembly complex, the Fe−S cluster intermediates are transferred intact to the recipient proteins by the assistance of chaperone and/or carrier proteins.[186-191]

Crystal structures of the IscU-IscS complex with and without a [2Fe–2S] cluster reveal key protein-protein interactions and provide insight into the intermolecular sulfur transfer reaction.[60, 74] IscS exists as a stable homodimer with each subunit containing a 5'-pyridoxal phosphate (PLP) cofactor and a mobile S-transfer loop cysteine residue. IscU subunits bind to opposite ends of the IscS dimer to form an overall $\alpha_2\beta_2$ IscU-IscS quaternary structure. Sulfur can be transferred as a persulfide species from IscS to IscU.[76] To transfer sulfur, the mobile loop of IscS oscillates a distance of ~14 Å between the PLP and conserved cysteine residues on IscU.[60, 74] IscU is often referred to as a metamorphic protein and exists as an equilibrium mixture of structured and disordered states.[66] This equilibrium can be shifted toward the structured state upon binding of either Zn^{2+} or Fe^{2+}.[64-66] Structural studies reveal that both Zn^{2+} and [2Fe–2S] clusters are ligated to IscU by its three cysteine residues.[60, 61] Early studies also revealed that IscU can dimerize and undergo a cluster synthesis sequence with one $[2Fe{-}2S]^{2+}$, two $[2Fe{-}2S]^{2+}$, and then one $[4Fe{-}4S]^{2+}$ cluster bound per dimeric protein.[181] Finally, aerobically grown crystals of the IscU-IscS complex revealed an oxidized Fe_2S-S species in which one sulfur both bridges the two iron atoms and also forms a disulfide bond with a second dangling sulfur atom.[60] It is unclear if this species represents an intermediate in cluster formation or is simply an oxidative degradation product. Overall, the lack of characterized intermediates or even the order of sulfur and iron incorporation events have limited our mechanistic understanding of Fe-S cluster biosynthesis.

In this study, we applied time-resolved native mass spectrometry (MS) to probe the formation of intermediate species in the synthesis of Fe-S clusters on the scaffold protein IscU. Visible circular dichroism (CD) spectroscopy is the current state-of-the-art method of monitoring [2Fe–2S] cluster formation in biosynthetic assays.[192-194] However, this technique and other spectroscopic approaches have offered few details into the formation and decay of intermediates in this Fe-S cluster assembly process. Native MS has been used for studying protein structure, dynamics, ligand interactions, and, more recently, the time-dependent tracking of protein-associated Fe-S intermediates for the oxygen sensing protein FNR.[195-204] Native MS takes advantage of soft ionization techniques and careful instrument tuning to minimize collisional activation and preserve proteins in their folded native-like structure.[200, 201, 205] Here, we show that the kinetics of [2Fe–2S]-IscU formation monitored by native MS coincides well with that from a traditional CD spectroscopic assay. In addition, we provide evidence for potential intermediates and a long-sought mechanism for the synthesis of Fe-S clusters by the ISC system.

2.2. Experimental procedures

Preparation of proteins. *Escherichia coli* proteins IscS and IscU were expressed and purified as previously described.[81] A pET-16a plasmid containing the cysteine synthase (*CysK1*) gene from *Mycobacterium tuberculosis* (gift of T. Begley, Texas A&M University) was transformed into *E. coli* BL21 (DE3) cells. The expressed CysK1 contained an N-terminal 6-His affinity tag and a Factor Xa protease site. CysK1 was purified using the same Ni-NTA and size exclusion chromatography columns and procedures used for the IscS purification. An extinction coefficient of 6.6 $mM^{-1}cm^{-1}$ at 388 nm (in 0.1 M NaOH) was used to estimate the concentration of the PLP cofactor,[206] which represents the concentration of active IscS. Extinction coefficients

of 11,460 $M^{-1}cm^{-1}$ at 280 nm was used to estimate the concentrations of both IscU and CysK1. IscS, IscU, and CysK1 were estimated to be >95% pure based on SDS-PAGE analysis. Aliquots of IscS (605 μM; 50 mM HEPES, 250 mM NaCl, pH = 7.5), IscU (301 μM; 50 mM HEPES, 150 mM NaCl, pH = 8.0), and CysK1 (1078 μM; 50 mM HEPES, 150 mM NaCl, pH = 8.0) stock solutions were flash-frozen and stored at -80 °C. All samples were prepared in an anaerobic Mbraun glovebox (<1 ppm O_2 monitored by a Teledyne model 310 analyzer) unless otherwise indicated.

Sample preparation for MS experiments. Protein samples were desalted by two passes through Micro Bio-spin columns with Bio-gel P-6 (Bio-Rad) equilibrated with target MS-compatible ammonium acetate buffers. Under standard conditions, IscU co-purified with Zn^{2+} (Zn-IscU) and was prepared for native MS by desalting the IscU stock solution after purification. Apo-IscU was prepared by treating the IscU stock solution with 10 mM DTPA for 30 mins and then desalting the sample. To minimize potential oxidation during MS analysis, all samples were prepared and incubated in 0.2 mL PCR tubes in the glovebox. The reaction mixtures were then sealed in the PCR tubes, removed from the glovebox, and infused within approximately 1 min into the mass spectrometer.

Monitoring Fe-IscU and [2Fe–2S]-IscU by CD spectroscopy. For CD measurements, the samples were prepared in a 1 cm path length anaerobic cuvette and sealed with a rubber septum and parafilm in the glovebox. The sealed cuvette containing the sample was recorded at ambient conditions and room temperature on a CD spectrometer (Applied Photophysics Chirascan). To evaluate Fe^{2+} binding to IscU, a 50 μM apo-IscU or Zn-IscU sample was mixed with 500 μM ferrous acetate in buffer A (200 mM ammonium acetate, pH = 6.8) at room

temperature for 30 min prior to measuring the CD signal. To monitor [2Fe–2S]-IscU cluster formation, either 100 μM Zn-IscU or apo-IscU was mixed with 3 μM IscS, 200 μM L-cysteine, 100 μM GSH, and 500 μM ferrous acetate in buffer A. The change in ellipticity at 330 nm was measured at room temperature.

Native MS experiments to monitor metal binding to IscU. A titration of IscU with Fe^{2+} was monitored by native MS experiments. Mixtures of either 10 μM apo-IscU or Zn-IscU were mixed with different concentrations of ferrous acetate (50, 100, 200, 400, or 800 μM) in buffer B (900 mM ammonium acetate, 20 mM ammonium bicarbonate, pH = 6.8), incubated for 30 mins, and then analyzed by native MS.

Native MS experiments to monitor IscU dimerization. 10 μM apo-IscU or Zn-IscU were mixed with either 1 mM D,L-DTT, 200 μM GSH, or 1 mM TCEP in buffer B. A sample was immediately removed (labeled initial) for MS analysis. Additional samples were incubated for 36 h at 25 °C in the glovebox or under aerobic conditions prior to MS analysis.

Native MS experiments to monitor IscU-IscS complex formation. To assess the formation and stoichiometry of IscU-IscS complexes, 50 μM IscS was mixed with 50 μM apo-IscU, 50 μM Zn-IscU, 25 μM apo-IscU and 25 μM Zn-IscU, 50 μM apo-IscU and 100 μM Fe^{2+}, or 50 μM Zn-IscU and 100 μM Fe^{2+} in buffer B. The mixtures were incubated for 30 mins before the native MS measurement.

Native MS experiments to monitor Zn^{2+} displacement. To monitor Zn^{2+} removal from IscU, 10 μM Zn-IscU was mixed with 1 mM L-cysteine, 1 mM D,L-DTT, 1 mM GSH, or 800 μM ferrous acetate in buffer A, incubated for 30 mins, and analyzed by native MS. In addition,

40 μM Zn-IscU was mixed with 40 μM IscS, 40 μM IscS and 200 μM Fe^{2+}, or 40 μM IscS and 200 μM L-cysteine in buffer A, incubated for 5 mins, and then diluted 4 fold before analysis by native MS experiments.

Time-dependent acid-quench denaturing MS experiments. To determine whether Fe^{2+} influences sulfur transfer from IscS to IscU, mixtures of 75 μM apo-IscU, 15 μM IscS, and different concentrations (0, 100, or 400 μM) of ferrous acetate were incubated in 200 mM ammonium acetate (pH = 7.5) for 30 mins at 22 °C. The reaction was then initiated by adding 300 μM L-cysteine. At each time point, the assay mixture was quenched by 10-fold dilution into 1% formic acid. The 0.2 mL PCR tubes containing the quenched samples were removed from the glovebox and infused into the mass spectrometer. Linear regression fits were used to determine the initial rates for the sulfur transfer reactions.

Time-dependent native MS monitoring of Fe–S cluster assembly. A mixture (220 μL) of 3 μM IscS and 100 μM IscU in buffer A was first incubated in the glovebox for 30 mins at 22 °C. The reaction was then initiated by adding 200 μM L-cysteine, 100 μM GSH, and 250 μM ferrous acetate. Fe–S cluster formation was monitored by native MS or by CD spectroscopy as a function of time. For time-dependent native MS experiments, the assay mixture was diluted 10-fold by buffer B and placed into 0.2 mL PCR tubes, removed from the glovebox, and immediately infused into an EMR Orbitrap instrument using a commercial nano-ESI source. The MS spectrum was collected for 30 seconds. The entire process from the dilution of the assay mixture to spraying the sample into the MS instrument was completed within approximately 1 min. In addition, the assay sample was transferred to an anaerobic cuvette in the glovebox, sealed with a cap, and brought out of the glovebox for CD measurements.

Isotope labeling to identify sulfur-containing intermediates. An isotope labeling experiment was performed to confirm the identity of the sulfur-containing intermediates. ^{34}S-L-cysteine was synthesized by reacting O-acetyl-L-serine and $^{34}S^{2-}$ with *M. tuberculosis* CysK1 using slight modifications of a previous procedure.[207] $Na_2{}^{34}S$ was prepared by using sodium metal to reduce ^{34}S (CIL Inc) in dry THF with a catalytic amount (7.5 mol%) of naphthalene.[208] ^{34}S-L-cysteine was synthesized by mixing 70 μM CysK1 with 20 mM O-acetyl-L-serine hydrochloride (SigmaAldrich) and ~10 mM $Na_2{}^{34}S$ at 37 °C overnight in the glovebox. A 3 kDa mass spin concentrator was used to separate ^{34}S-L-cysteine from CysK. The ^{34}S-L-cysteine concentration in the flow-through was determined by an acid-ninhydrin assay.[209] The ^{34}S-L-cysteine solution, which contained some unreacted o-acetylserine, was directly used for Fe–S cluster formation assays. For the isotope labeling experiment, mixtures of 100 μM apo-IscU, 3 μM IscS, 200 μM ^{34}S-L-cysteine, 100 μM GSH, and 250 μM ferrous acetate in buffer A were reacted for 40 mins in a glovebox. At the targeted reaction time, the isotope labeling Fe–S cluster formation assay mixture was quenched and cleaned by a Micro Bio-spin column with Bio-gel P-6 previously equilibrated with buffer A. Samples were then removed from the glovebox for native MS measurements. For a peak containing N sulfur atoms, the expected mass shift would be [34(mass of ^{34}S) - 32.1(average mass of natural-abundance sulfur)]*N = 1.9N.

Native MS description and settings. Gold-coated borosilicate glass capillaries were prepared in house for use in the nano-ESI experiments. The sample solution was back-filled into a gold-coated glass capillary tip and sprayed into the mass spectrometer. Native MS experiments were performed by an Exactive Plus with extended mass range (EMR) Orbitrap MS (Thermo Fisher Scientific, San Jose, CA). Instrument parameters were tuned to minimize collisional

activation while retaining reasonable signal to noise. The ion mobility experiments were performed on a homemade instrument, Fourier transform-ion mobility-EMR (FT-IMS-EMR), with previously described experimental conditions.[210, 211] Specifically, the measurements were conducted with a frequency sweep of 5-5005 Hz in 8 mins at approximately 1.725 Torr He in the drift tube.

Reasonable simultaneous transmission for monomeric and dimeric IscU was obtained by tuning the DC voltages on the ion lenses and transport multipoles and using a lower resolution setting (R = 8750). The parameters used for the native MS analysis of IscU include: m/z range 1000–5000, spray voltage 1.5 kV, capillary temperature 50–100 °C, S-Lens RF level 200, source DC offset 25 V, injection flatapole DC 16 V, inter flatapole lens DC 12 V, bent flatapole DC 8 V, transfer multipole DC offset 4 V, C-trap entrance lens tune offset 0 V, trapping gas pressure setting 7, in-source dissociation voltage 0 eV, HCD collision energy 10 eV, FT resolution 8750, positive ion mode, and ion maximum injection time 200 ms.

The acid-quench denaturing MS parameters used for the analysis of the persulfide IscU species include: m/z range 500–5000, spray voltage 1.3 kV, capillary temperature 250 °C, S-Lens RF level 200, source DC offset 25 V, injection flatapole DC 16 V, inter flatapole lens DC 12 V, bent flatapole DC 8 V, transfer multipole DC offset 2 V, C-trap entrance lens tune offset 0 V, trapping gas pressure setting 2, in-source dissociation voltage 0 eV, HCD collision energy 0 eV, FT resolution 70000, positive ion mode, and ion maximum injection time 50 ms.

The native MS parameters used for the analysis of the IscU–IscS complex include: m/z range 4000–9000, spray voltage 1.5 kV, capillary temperature 125 °C, S-Lens RF level 200, source DC offset 25 V, injection flatapole DC 16 V, inter flatapole lens DC 12 V, bent flatapole

DC 8 V, transfer multipole DC offset 9 V, C-trap entrance lens tune offset 0 V, trapping gas pressure setting 7, in-source dissociation voltage 160 eV, HCD collision energy 10 eV, FT resolution 35000, positive ion mode, and ion maximum injection time 200 ms.

MS data processing. The initial MS data were collected using the Thermo Exactive software as RAW format. The Raw data were converted into text files using a Python script making use of Multiplierz. The intensity of the protein and protein–adduct species were deconvoluted and converted into normalized intensity by processing the text files with the software program UniDec.[212] The reported intact mass were obtained from processing native MS spectrum, and the errors were calculated from FWHM of the highest intensity peak with Unidec. Lower charge states (higher m/z) of IscU showed native-like conformations in ion mobility experiments. Ranges that were chosen for further data processing include m/z of 2300–2400 (native monomeric IscU), m/z of 3080–4000 (native dimeric IscU), m/z 1500–4000 (both native monomeric and dimeric IscU), m/z of 800–3500 (denaturing IscU), and m/z of 4000-9000 (native IscU-IscS complexes). For the time-dependent native MS experiments, intensity of individual monomeric/dimeric IscU species per monomeric/dimeric IscU was further converted to the normalized intensity of individual monomeric or dimeric IscU relative to the total amount of IscU.

2.3. Results

Characterization of IscU and IscS. High-resolution native MS was implemented to investigate the sequence of events in the assembly of Fe-S clusters by the ISC biosynthetic pathway. The IscS and IscU proteins were exchanged into a volatile ammonium acetate buffer that is compatible with native MS experiments. The *E. coli* cysteine desulfurase IscS, which is a homodimer with an expected molecular mass of 97,032.3 Da including the His6-tags and PLP

cofactors, was purified to homogeneity. IscS exhibited a mass of 97,029.0 ± 20.3 Da and had typical activity in a sulfide generation assay (8.6 ± 0.2 μM sulfide/min•μM IscS). The *E. coli* scaffold protein IscU had an observed molecular mass of 13,976.0 ± 7.0 Da in the apo form (expected mass of 13,976.7 Da) and could form an $IscU_2IscS_2$ species with IscS (observed molecular mass of 124,972.6 ± 23.6 Da; expected total mass of 124,985.7 Da). Both IscS (cysteine desulfurase activity = 2.0 ± 0.1 μM sulfide /min•μM IscS) and IscU (in a Fe-S cluster assembly assay; see below) were functional under the native MS buffer conditions.

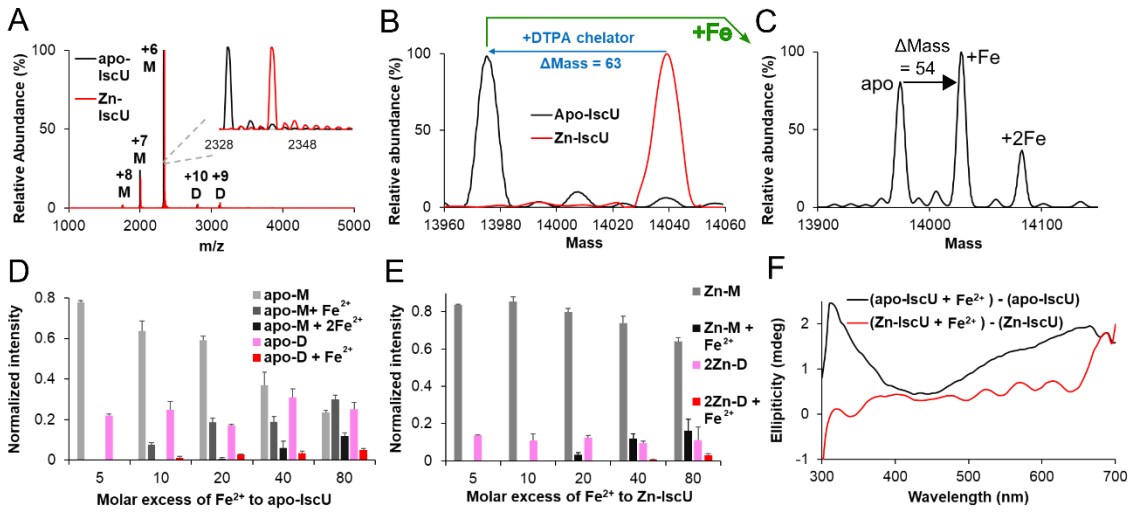

Figure 2.1 The binding of Zn^{2+} and Fe^{2+} ions to IscU. (A) The raw native MS spectrum of apo-IscU (black) overlaid with as-isolated (Zn-bound) IscU (red). The +6, +7, and +8 charge states for monomeric IscU and the +9 and +10 charge states for dimeric IscU are shown (M: monomeric IscU, D: dimeric IscU). The inset shows the raw MS spectrum for the +6 charge state of monomeric IscU. **(B)** Deconvoluted zero charge MS spectrum for the +6 charge state of monomeric IscU. **(C)** Deconvoluted zero charge MS spectrum of 10 μM apo-IscU mixed with 800 μM Fe^{2+}. Titration of Fe^{2+} to 10 μM apo-IscU **(D)** or Zn-IscU **(E)** monitored by native MS revealed up to two metal binding sites per IscU subunit. Both monomeric (apo-M or Zn-M) and dimeric (apo-D or 2Zn-D) forms of IscU were identified. The error bars are replicate errors (n = 3). (F) A CD spectroscopic feature at 315 nm develops upon the addition of 500 μM Fe^{2+} to apo-IscU (50 μM; black) but not to Zn-IscU (50 μM; red).

Zn^{2+} and Fe^{2+} binding to IscU. Native MS analysis of as-isolated IscU revealed a predominantly monomeric form (>95%) with a mass of 14,038.9 ± 7.9 Da, which is consistent with one Zn^{2+} bound to IscU (Figure 2.1A, B; red trace). Moreover, treatment with the DTPA chelator resulted in a mass reduction of 62.9 Da (Zn^{2+} - $2H^{+}$, expected mass reduction of 63.4 Da), indicating conversion to apo-IscU (Figure 2.1A, B; black trace). Mixtures of apo-IscU and Zn-IscU (1:2, 1:1, and 2:1) monitored by native MS showed good match between the relative abundance of peaks and the amount of corresponding species, suggesting that the abundance of species detected by MS could reflect the abundance of species in solution. Ion-mobility MS revealed that apo-IscU exhibited single compact peaks for charge states, which indicates native-like protein folds. Exposure to aerobic conditions slowly converted apo-IscU from a monomeric to a dimeric form (Figure 2.2). Titration of IscU samples exhibiting mixed oligomeric states (approximate monomer-to-dimer ratio of 78:22 for apo-IscU and 86:14 for Zn-IscU) with Fe^{2+} revealed that apo-IscU binds a single Fe^{2+} at lower concentrations and a second Fe^{2+} at higher (≥ 20-fold molar excess) concentrations (Figure 2.1C, D). The relative normalized intensities of unbound and Fe-bound IscU suggests that monomeric IscU has a higher binding affinity for Fe^{2+} than dimeric IscU (Figure 2.1D). Zn-IscU bound one Zn^{2+} per subunit, which was not displaced by the addition of Fe^{2+} (Figure 2.1E), suggesting that Fe^{2+} cannot readily displace IscU-bound Zn^{2+}. The addition of excess iron (≥ 20-fold molar excess) to Zn-IscU generated a species containing both Zn^{2+} and Fe^{2+}. The addition of Fe^{2+} resulted in the development of a positive ellipticity feature at 315 nm in CD spectra when added to apo-IscU, but not Zn-IscU (Figure 1F), consistent with the native MS results (Figure 2.1D, E). Overall, these results indicate that each

IscU molecule is capable of binding up to two metal ions and that Fe^{2+} cannot readily displace the Zn^{2+} under these conditions.

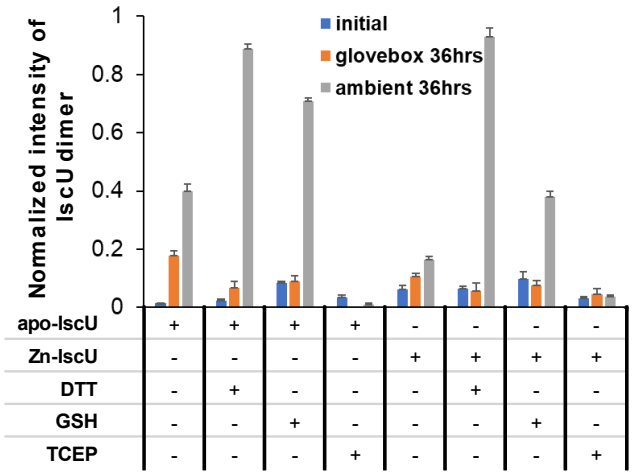

Figure 2.2 Probing IscU dimerization with native MS. Apo/Zn-IscU (10 μM) was mixed with different reducing agents for 36 hrs at 25 °C and then probed by native MS. Reagents included 1 mM D-L-DTT, 200 μM GSH, or 1 mM TCEP.

Dimerization of IscU is promoted by oxidation of the active site cysteine residues.

Next, we used native MS to determine the amount of dimeric IscU after incubation of either apo-IscU or Zn-IscU under anaerobic or aerobic conditions and in the presence or absence of reducing agents (Figure 2.2). Aerobic conditions induced dimerization of both apo-IscU and Zn-IscU, consistent with disulfide formation involving one of the three IscU cysteines located in the [2Fe–2S] cluster assembly active site. Dimerization through intermolecular disulfide formation is supported by the ability of cysteine-ligated Zn^{2+} to reduce the propensity to dimerize under both anaerobic and aerobic conditions and by the ability of the reducing agent TCEP to dramatically lower the formation of dimeric IscU under both anaerobic and aerobic conditions (Figure 2.2). We also observed that both DTT and GSH inhibited the dimerization of apo-IscU and Zn-IscU under anaerobic conditions but promoted dimerization in an aerobic environment. In addition,

non-reducing SDS-PAGE analysis demonstrated that dimeric IscU was diminished after treatment with TCEP. The increase in dimerization under aerobic conditions may be linked to the ability of the oxidized form of these sulfur-containing reagents to facilitate disulfide bond formation. Thus, IscU dimers are mediated by intermolecular disulfide bonds between active site cysteine residues. The formation of disulfide-linked IscU dimers imply the potential physiological role of Zn^{2+} binding on stabilizing IscU.

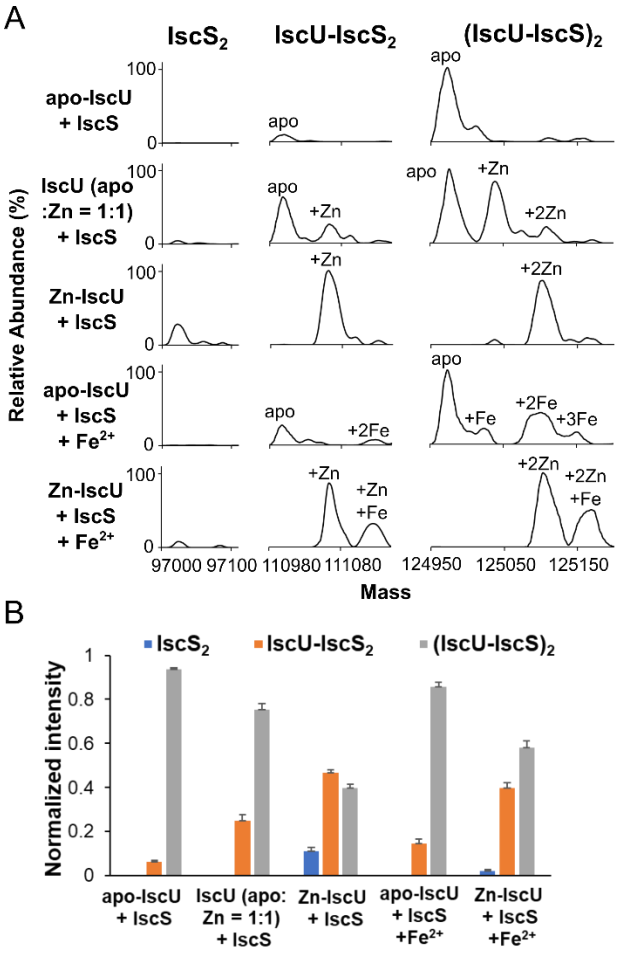

Figure 2.3 Formation of apo and metal bound IscU complexes with IscS. Apo, Zn-bound and a 1:1 mixture of the two forms of IscU (final concentration of 50 μM) were separately combined with IscS (50 μM) in either the presence or absence of Fe^{2+} (100 μM). **(A)** Deconvoluted zero charge MS spectra for mass ranges that correspond to $IscS_2$ (~97,000 Da), IscU-$IscS_2$ (~111,000 Da), and $IscU_2$-$IscS_2$ (~125,000 Da) complexes. **(B)** A comparison of the different protein

complex stoichiometries between IscU and IscS for the five experiments. Protein complexes with apo and metal bound forms of IscU are combined to determine the normalized intensity. The error bars are replicate errors (n = 3).

IscU–IscS binding affinity is influenced by Zn^{2+} and Fe^{2+}. We next investigated the effect of metal binding on the formation of the $IscU_2$-$IscS_2$ complex using native MS (Figure 2.3). Combining apo-IscU with IscS resulted in a predominant fraction (94%) of the $IscU_2$-$IscS_2$ complex and a small fraction (6%) of an IscU-$IscS_2$ species (Figure 2.3B). The addition of a 2-fold molar excess of Fe^{2+} resulted in the binding of two Fe^{2+} per $IscU_2$-$IscS_2$ complex and slightly decreased the fraction (86%) of $IscU_2$-$IscS_2$ species (Figure 2A; apo-IscU + IscS + Fe^{2+}). In contrast, combining Zn-IscU with IscS resulted in a much larger fraction (47%) of incompletely associated IscU-$IscS_2$ complex with a moderate fraction (11%) of $IscS_2$ entirely lacking IscU (Figures 2B, S5). The Zn^{2+} remained bound upon the formation of the complex with IscS (Figure 2A; Zn-IscU + IscS). The addition of Fe^{2+} resulted in the binding of an extra Fe^{2+} per IscU without displacing the Zn^{2+} ion (Figure 2A, Zn-IscU + IscS + Fe^{2+}). Adding a mixture of apo and Zn-bound IscU to IscS generated an intermediate amount of the IscU-$IscS_2$ complex with slightly enhanced binding of Zn-IscU to IscS (Figure 2.3B). Overall, our results reveal that IscU-IscS complexes are capable of uptaking two metal ions per IscU with different affinities, Zn^{2+} binds tighter than Fe^{2+} to IscU, Zn^{2+} decreases the binding affinity of IscU to IscS, and Fe^{2+} has a minor effect on the binding affinity of IscU to IscS.

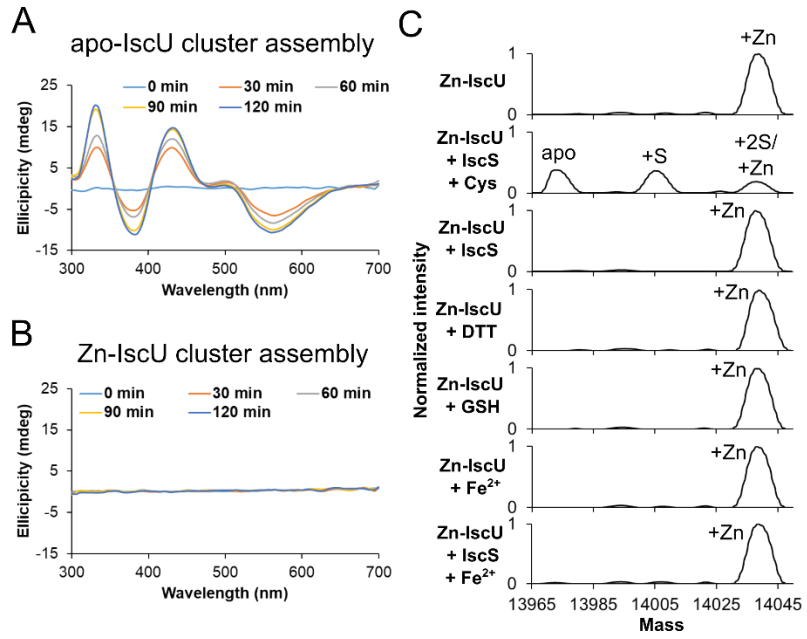

Figure 2.4 Zn^{2+} inhibits Fe-S assembly activity and is removed by IscS-mediated cysteine turnover. Parallel cluster formation reactions using (A) Apo-IscU or **(B)** Zn-IscU were monitored by CD spectroscopy. Experimental conditions: 100 μM IscU, 3 μM IscS, 200 μM L-cysteine, 100 μM GSH, and 500 μM ferrous acetate. **(C)** Deconvoluted zero charge spectra for removal of Zn^{2+} from Zn-IscU (10 μM) monitored by native MS after incubations with L-cysteine (1 mM), D,L-DTT (1 mM), and GSH (200 μM). Similar experiments were performed after incubation of Zn-IscU (40 μM) with IscS (40 μM), ferrous acetate (800 μM), IscS (40 μM) plus Fe^{2+} (200 μM), and IscS (40 μM) plus L-cysteine (200 μM). All reactions were incubated for 30 min at room temperature except for the combination of Zn-IscU with IscS and L-cysteine, which was reacted for 5 min. All experiments were repeated at least twice, and similar results were obtained.

Zn^{2+} binding inhibits cluster formation on IscU. To investigate the effect of Zn^{2+} binding to IscU on [2Fe–2S] cluster formation, cluster assembly under the conditions of low IscS, L-cysteine, and GSH was monitored by CD spectroscopy. A characteristic CD signal for [2Fe–2S]-IscU was observed with apo-IscU (Figure 2.4A), but not Zn-IscU (Figure 2.4B). Consistently, the apo-IscU sample developed a [2Fe−2S]-IscU signal when monitored by native

MS, but the Zn-IscU sample showed neither Zn^{2+} displacement nor simultaneous binding of both Zn^{2+} and a [2Fe–2S] cluster (data not shown; see additional experiments below).

Since Zn^{2+} could function as a physiological inhibitor, we investigated how Zn^{2+} might be displaced from IscU using native MS (Figure 2.4C). The Zn^{2+} ion was not removed by a 30 min incubation of Zn-IscU with L-cysteine, DTT, GSH, IscS, Fe^{2+}, or IscS plus Fe^{2+} (Figure 2.4C). In contrast, a 5 min incubation of Zn-IscU with IscS and L-cysteine resulted in the loss of the Zn^{2+} ion and formation of a persulfide species on IscU. Note that the concentration of IscS (equimolar with IscU) and the resulting cysteine desulfurase activity was much higher in the Zn-removal experiment than in the CD [2Fe–2S] cluster assembly assay (Figure 2.4B). Thus, Zn^{2+} is an inhibitor of Fe-S cluster assembly on IscU and is not readily displaced by Fe^{2+} but can be removed with either a Zn chelator or by cysteine turnover using an equimolar IscS concentration.

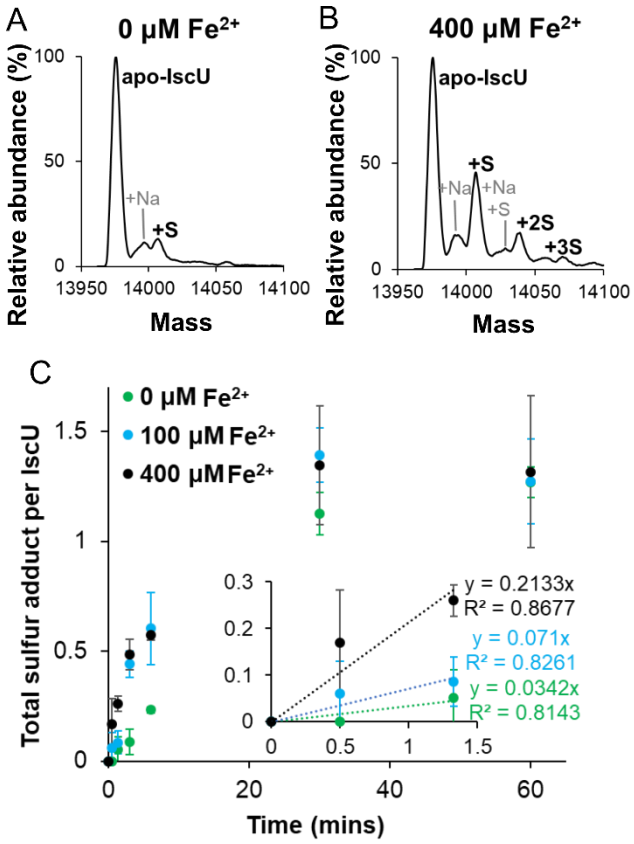

Figure 2.5 Fe^{2+} enhances sulfur transfer from IscS to IscU. Time-resolved acid-quench (1% formic acid) denaturing MS experiments were used to track sulfur accumulation on IscU after mixing apo-IscU (75 μM) with IscS (15 μM), L-cysteine (300 μM) and various concentrations of ferrous acetate. Deconvoluted zero charge MS spectra are shown for monomeric IscU using **(A)** 0 μM and **(B)** 400 μM ferrous acetate after a reaction time of 3 min. **(C)** The total accumulated sulfur adducts per IscU are displayed as a function of time. The inset shows the early time points overlaid with linear regression fits (dashed lines). The error bars represent replicate errors (n = 3).

Fe^{2+} promotes sulfur transfer to IscU. Here, we evaluated the influence of Fe^{2+} on the transfer of sulfur from IscS to IscU using time-dependent acid-quench MS experiments. Previously published studies establish that the addition of acid quenches sulfur transfer reactions and locks the persulfide label in place for subsequent analysis.[213, 214] Apo-IscU, IscS, L-cysteine, and various concentrations of Fe^{2+} were reacted, quenched with acid at different reaction times,

and analyzed by MS. In a 3 min reaction, very little persulfide formation was detected on IscU in the absence of Fe^{2+} (Figure 2.5A), whereas multiple persulfide species were observed upon the addition of Fe^{2+} (Figure 2.5B). After a 1-hour reaction, samples with and without Fe^{2+} had about the same amount of persulfide label (~1.3) per IscU (Figure 2.5C). However, the initial rate of sulfur accumulation on IscU increased by approximately 6-fold in the presence of 400 μM Fe^{2+} ions. These experiments indicate that the addition of Fe^{2+} promotes sulfur transfer from IscS to IscU.

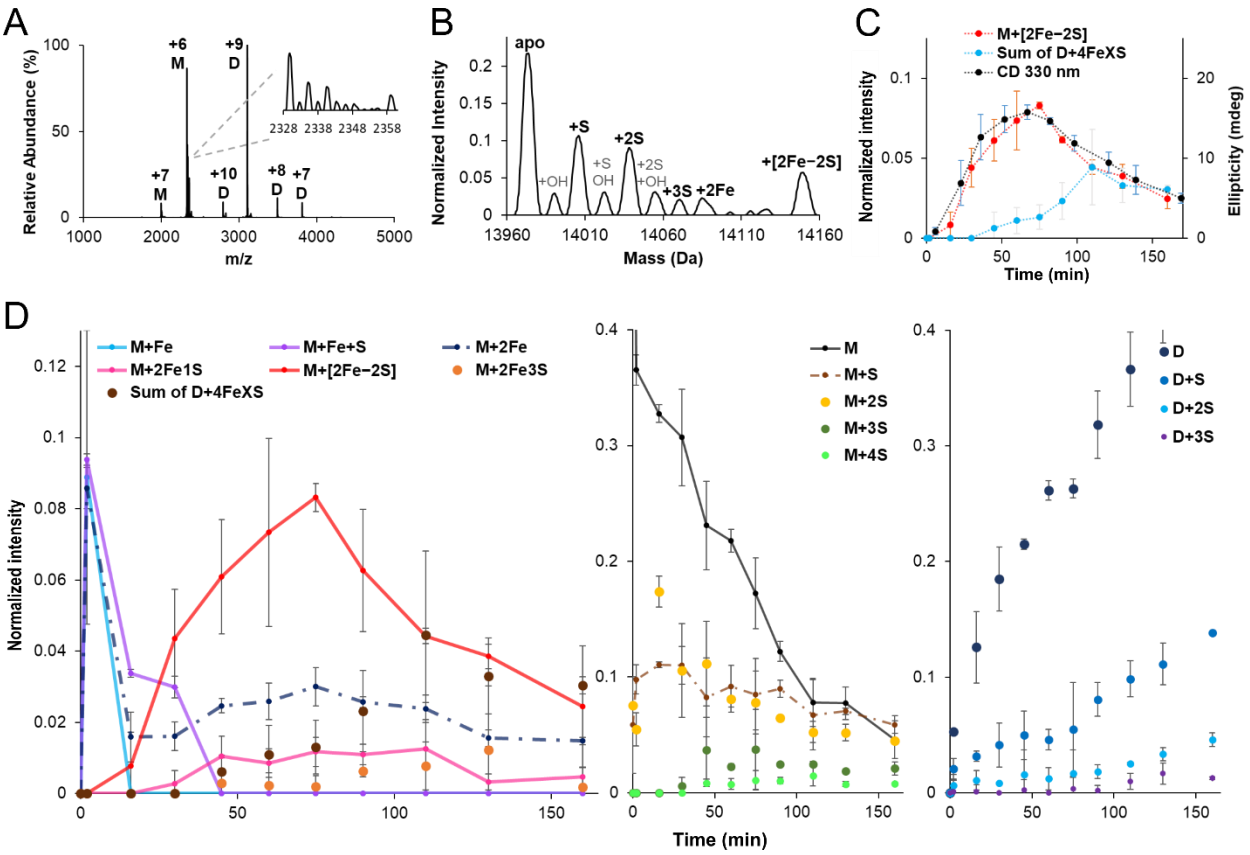

Figure 2.6 Time-dependent tracking of intermediates in Fe-S cluster formation by native MS. (A) Representative raw and **(B)** deconvoluted zero charge MS spectra collected during cluster formation reactions. The inset of (A) shows the raw MS spectrum for the +6 charge state of monomeric IscU (M: monomeric IscU, D: dimeric IscU). Experimental conditions: 100 μM apo-IscU, 3 μM IscS, 200 μM L-cysteine, 100 μM GSH, and 250 μM ferrous acetate. **(C)** Comparison of the kinetics of [2Fe–2S]-IscU formation from native MS (normalized intensity;

orange) and the CD spectroscopic signature at 330 nm (ellipticity; blue). The decay of the native MS [2Fe–2S] cluster signal corresponded to the development of four iron species (gray). The error bars are replicate errors (n = 2). **(D)** Normalized intensity of iron (left panel), non-iron monomeric IscU (middle panel), and non-iron dimeric IscU (right panel) related species displayed as a function of time. Proposed intermediates on the main pathway (see Fig. 6) are shown with connecting solid lines. Additional proposed intermediates for viable secondary pathways are displayed with connecting dotted lines, whereas proposed off pathway species are shown without lines.

Mechanism of cluster formation. Next, we used time-dependent native MS experiments to track the formation and decay of Fe-S cluster assembly intermediates. The Fe-S biosynthetic reaction was initiated in an anaerobic glovebox by combining apo-IscU, IscS, L-cysteine, Fe^{2+}, and GSH. Representative raw MS spectra collected during cluster formation revealed peaks associated with monomeric (1,500–2500 m/z window) and dimeric (2500–4000 m/z window) IscU (Figure 2.6A). The raw MS spectra were deconvoluted to generate normalized intensities and assign intermediates (Figure 2.6B). Well-resolved peaks were observed in all of the collected native MS spectra with low amounts of sodium adducts, which enabled unambiguous assignment. The predicted masses and observed mass shifts matched well for the assigned species (Table 2-1). Further evidence for the assignment of sulfur-based species was provided by repeating the Fe-S assembly reactions with ^{34}S-labeled L-cysteine and comparing the difference in the mass shifts for the normal and isotope-labeled reactions (Table 2-2). A nearly identical time course for the development and decay of the [2Fe–2S] cluster was observed for a reaction monitored by both native MS and CD spectroscopy (Figure 2.6C).

In the first two minutes of the reaction, the amounts of monomeric Fe-IscU, Fe-S-IscU, and 2Fe-IscU species increased dramatically and decreased in concentration at later times as the amount of monomeric [2Fe–2S]-IscU increased (Figure 2.6D, left), consistent with being cluster

assembly intermediates. Similarly, the concentrations of S-IscU and 2S-IscU species also increased rapidly to a concentration that only gradually decreased over the remaining 165 min of the reaction (Figure 2.6D, middle). The lack of rapid decay of these one and two sulfur-bound species either suggests that they are off-pathway products or that they are intermediates that reach a steady state during the reaction. Low levels of IscU containing three and four sulfur atoms were also observed at longer reaction times.

Table 2-1 Predicted and observed mass of IscU intermediates during cluster formation.

Monomeric IscU species	Predicted mass shift from apo (Da)	Average observed mass shift from apo (Da)
M+OH	17.0	17.0 ± 0.4
M+S	32.1[1]	32.2 ± 0.4
M+S+OH	49.1[1]	49.1 ± 0.4
M+Fe	53.8[2]	53.7 ± 0.6
M+2S	64.1[1]	65.0 ± 0.6
M+2S+OH	81.1[1]	81.8 ± 0.7
M+FeS	85.9[1, 2]	85.9 ± 0.6
M+3S	96.2[1]	97.0 ± 0.2
M+2Fe	107.6[2]	110.0 ± 2.3
M+4S	128.3[1]	129.8 ± 0.9
M+2Fe1S	141.7[2, 4]	143.3 ± 0.4
M+Cys+S	151.2[1]	151.0 ± 0.5
M+[2Fe−2S]	173.8[3]	176.0 ± 0.5
M+2Fe3S	209.8[2, 4]	208.6 ± 0.2
M+GSH	305.3	304.8 ± 0.6
M+GSH+S	337.4[1]	337.1 ± 0.7
M+GSH+2S	369.4[1]	370.1 ± 0.4
D+S	32.1[1]	31.2 ± 1.0
D+2S	64.1[1]	64.3 ± 1.0
D+3S	96.2[1]	96.1 ± 1.8
D+2Fe6S	308.0	307.7 ± 0.5
D+4Fe6S	415.6[2, 4]	418.1 ± 0.5
D+4Fe7S	449.7[2, 4]	450.5 ± 0.8
D+4Fe8S	483.8[2, 4]	482.6 ± 0.6

Predicted mass shifts from apo were estimated using the following assumptions: [1]S is annotated as S^0, [2]Fe is annotated as Fe^{2+}; [3][2Fe−2S] is annotated as $[2Fe{-}2S]^{2+}$; [4]S is annotated as S^{2-}. Errors are replicate errors (n = 3). A lower overall charge of the protein-associated small molecule will lead to more protons bound to the protein ion to compensate the overall charge of the protein ion, and these protons are also account for in the mass shifts.

The monomeric [2Fe–2S]-IscU reached a maximum after 75 min and then decreased, and similar kinetics were also observed for the low levels of monomeric 2Fe-IscU and 2Fe1S-IscU species (Figure 2.6D, left). As the [2Fe–2S]-IscU concentration decreased at longer reaction times, we observed the development of monomeric 2Fe3S-IscU and dimeric 4FeXS-IscU (X = 6-8) species (Figure 2.6C, D; Table 2-1, Table 2-2). Interestingly, a separate reaction using excess substrates and the non-physiological reductant DTT generated traditional [4Fe–4S] clusters and not the 4FeXS-IscU species. In general, dimers of IscU both bound to and lacking Fe-S clusters accumulated at later time points (Figure 2.6D, right). Overall, these native MS experiments suggest a iron-first pathway for the development of [2Fe–2S] clusters on IscU with additional conversion chemistry generating clusters with larger stoichiometries at longer reaction times.

Table 2-2 Mass shifts observed for IscU species during cluster formation using ^{34}S-L-cysteine.

Assigned Intermediate	Mass shift from apo (using natural Cys)	Mass shift from apo (using [^{34}S]-Cys)	Number of S (experimental)	Number of S (theoretical)
M+S*	32.2	33.6	0.7	1
M+2S*	64.4	67.0	1.4	2
M+3S*	96.6	100.5	2.1	3
M+4S*	129.2	135.1	3.1	4
M+Cys+S	150.3	154.4	2.2	2
M+[2Fe–2S]	175.6	179.5	2.1	2
D+S*	32.7	34.4	0.9	1
D+2S*	65.3	68.4	1.6	2
D+3S*	96.9	102.0	2.7	3
D+4Fe6S	418.3	429.9	6.1	6
D+4Fe7S	451.1	464.4	7.0	7

*The experimental calculated numbers of sulfur atoms for M+nS (n = 1-4) and D+mS (m = 1-3) are ~70-80 % of that of theoretical values. This might be due to the formation of low abundance sulfinic acid modifications that would have the same mass as persulfide containing species.

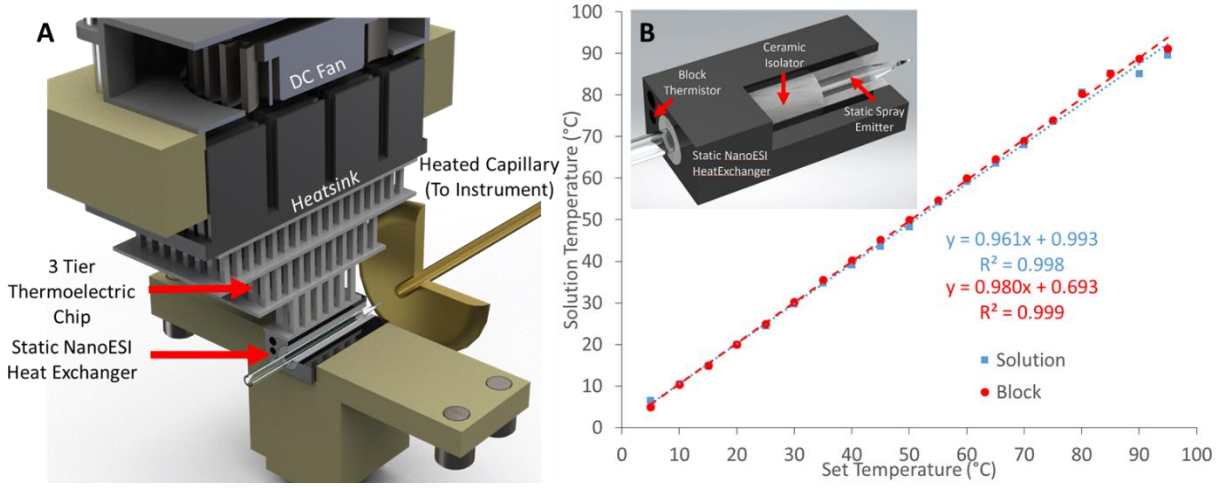

Figure 2.7 vT-ESI source design and performance. (A) Solidworks rendering of the VT-ESI assembly with labels to identify the significant components. The fan mounted to the top of the device prevents overheating and reduces atmospheric moisture condensation for experiments performed below ~15 °C. The top stage of the thermoelectric chip (TEC) makes direct contact with a 40 mm x 40mm x 13mm heatsink (CTS Electronic Components APF40-40-13CB) with the fan; a 40 mm x 15 mm 24 VDC fan with 14.83 CFM rated airflow (Delta Electronics AFB0424SHB). The vT-ESI assembly using custom machined PEEK parts that mount to a commercial Thermo Nanospray Flex source. See supplemental information for additional information about the electronics control system. **(B)** Temperature calibration of the vT-ESI emitter solution is performed using thermocouples inserted into the static spray capillary and the SS heat exchanger (as shown in inset). The temperature variations ranged from ~ +/- 5 °C at the highest and lowest temperature and ~ +/- 2 in the range of 5 – 98 °C. Reprint with permission from *Analytical Chemistry* **2021**. (Articles ASAP) Copyright 2021 ACS Publications.

Pilot structural study of IscU using variable-temperature electrospray ionization (vT-ESI). IscU has been reported to be a metamorphic protein that exists in disordered (D) and structured (S) states.[62, 63, 65, 215] Apo-IscU is more populated in D states, while Zn and Fe binding shifts the equilibrium towards S states.[215] The biological functions of these different states remain elusive and debatable. Results from the Markley group suggest D states to be the binding substrate for IscS[62], while results from the Pastore group indicate the opposite[215]. Additionally, IscU has also been shown to have cold denaturation characteristic by CD spectroscopy and

NMR.[63, 215, 216] To further illustrate the conformation landscape of IscU under different conditions, we employed native MS with a home-built vT-ESI source (Fig).[217] The concept here is that protein ions in relative higher charge states has larger solvent accessible area, which in most cases should also correspond to more disordered and/or extended conformation. The preliminary results first demonstrate the cold denaturation of IscU could be probed by vT-ESI. As the abundance of higher charge state and the overall average charge state of monomer IscU increases in lower temperatures (Figure 2.8A). Apo-IscU has more significant increase in average charge state than Zn-IscU under low teamperature, implying apo-IscU has a higher increase of population in D states in lower temperatures than Zn-IscU. Interestingly, when IscS is also present in the sample, the abundance of higher charge state and the overall average charge state of monomer Zn-IscU under low and high temperatures increases even more significantly (Figure 2.8B) while apo-IscU does not change significantly (Figure 2.8C). This result is consistent with D states being the substrate of binding IscS, as most likely IscS binding shifts the equilibrium of Zn-IscU towards D states, which should be theoretically more susceptible to cold denaturation. In comparison, apo-IscU is already mostly in D states and thus does not change much when IscS is present. Also, under higher temperature, Zn-IscU lost zinc more easily when IscS is present (Figure 2.8D). This again is consistent with IscU binds IscS in D states, which is expected to ligate Zn with lower affinity comparing to S states. One hypothesis of the purpose of D states binding IscS is that this opens the active site to enable sulfur transfer, Zn removal, and Fe incorporation. Further studies on the effect of CyaY and employing ion mobility will provide further insights.

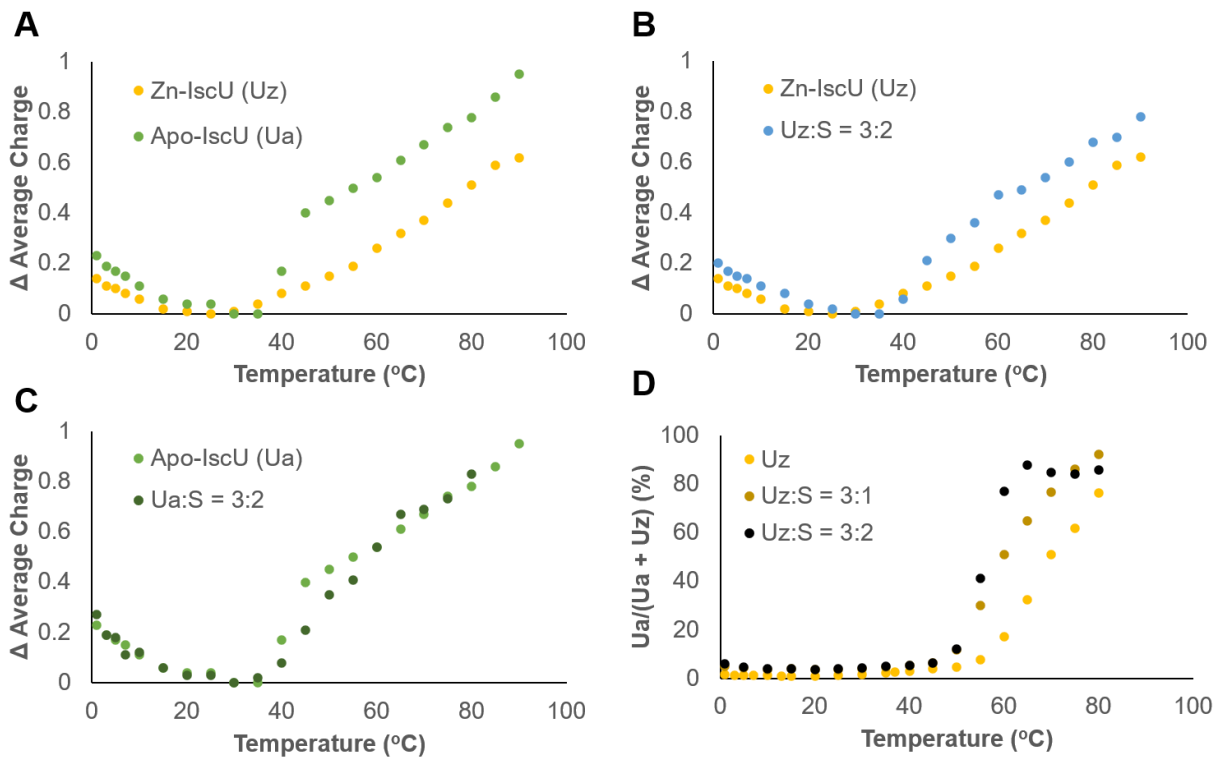

Figure 2.8 vT-ESI experiments of IscU. vT-ESI experiments are done in 3 µM IscU concentration in 200 mM ammonium acetate (pH = 6.8), the temperature is scan from low (1 °C) to high (> 80 °C) temperature with 5 °C increments. MS spectra is collected for 30s with instrument parameters described above. The y-axis is shown in Δ average charge, which is the charge difference with the lowest charge in the experiment. Δ average charge of Zn-IscU vs apo-IscU is shown in **(A)**, Zn-IscU with or without IscS in **(B)**, apo-IscU with or without IscS in **(C)**. **(D)** shows the abundance of Zn-IscU lost zinc over temperature (become apo-IscU).

2.4. Discussion

Elaborate biosynthetic pathways are responsible for assembling Fe-S clusters and delivering the appropriate cluster form to clientele proteins. Although there are decades of excellent studies of the self-assembly of Fe-S clusters and the associated enzymatic process,[218, 219] key mechanistic questions remain. Here, we implemented high-resolution time-dependent

native MS experiments to define intermediates and provide insight into the assembly of Fe–S clusters for the bacterial ISC biosynthetic system.

Native MS experiments separate unreacted substrates from iron and sulfur-based intermediates, which can be identified without relying on model compounds or samples that are chiral, labeled, or paramagnetic. To ensure that the protein ions were not collisionally activated, which might result in the loss of labile intermediates, and that the proteins remained in native-like conformations,[205, 220, 221] ion mobility measurements were performed using a homemade source and a drift tube coupled to an EMR instrument.[210, 211] These experiments revealed protein ions that were in a compact native-like conformation and charge state distributions that were suitable for further data processing. Additional evidence that native MS is appropriate for deciphering solution Fe-S cluster chemistry is provided by the high agreement for the formation and decay of [2Fe–2S]-IscU monitored by native MS and CD spectroscopy (Figure 2.6C-D). The predominant [2Fe–2S]-IscU signal in a cluster reconstitution experiment using excess substrates shows the majority of [2Fe–2S] cluster survives after the sample handling and nano-ESI process (Figure S7). We also provide evidence supporting the correlation of species abundances in solution (mole fraction) with that detected by native MS (normalized intensity). The monomer to dimer ratio of an oxidized IscU sample investigated by native MS (59 ± 5% dimer) or non-reducing SDS-PAGE followed by densitometry (65 ± 6% dimer) are in agreement. Also, different ratios (1:2, 1:1, and 2:1) of apo-IscU and Zn-IscU mixtures match with the relative abundances in the native MS spectrum (Figure S1). Moreover, the highly purified proteins, high mass resolution, and ^{34}S isotope labeling experiments enable unambiguous assignment of the intermediate species associated with IscU (Figure 2.6; Table 2-1, Table 2-2). Collectively, the

data presented in this study highlight the power of native MS in defining protein-associated intermediates and elucidating details of enzymatic reactions.

Native MS experiments revealed that the as-isolated IscU has one Zn^{2+} bound per protein (Figure 2.1B) and is able to form a Zn-bound $IscU_2$-$IscS_2$ complex (Figure 2.3B). Zn^{2+} also inhibited [2Fe–2S] cluster formation on IscU (Figure 2.4), consistent with previous studies that Zn^{2+} stabilizes IscU by binding to the same cysteine residues that are used to ligate [2Fe–2S] cluster intermediates.[60, 61, 102, 107, 222, 223] Zn^{2+} binding stabilizes uncomplexed IscU[223] and, in our experiments, decreases the propensity of the IscU subunits to dimerize (Figure S3). Reductants also decrease IscU dimerization (Figure 2.2) indicating that cysteine residues are being oxidized to form an intermolecular disulfide bond. The ability of Zn^{2+} to protect cysteine residues from oxidation has been reported for other proteins.[224] Although uncomplexed IscU co-purifies with Zn^{2+}, the cellular metal-binding status of IscU under *in vivo* conditions is unclear as *E. coli* is reported to have extremely low free Zn^{2+} concentrations.[225] Moreover, native MS results indicate apo-IscU binds tighter than the Zn-bound form to IscS (Figure 2.3B). Regardless, Zn^{2+} can be removed from Zn-IscU with the chelating agent DTPA (Figure 2.1B)[223, 226] or by reactions that include both L-cysteine and a stoichiometric amount of IscS (Figure 2.4C), which might remove the Zn^{2+} either by generating a persulfide species on IscU that decreases the Zn^{2+} binding affinity or by precipitating the Zn^{2+} with generated sulfide. Overall, the Zn^{2+} stabilizes and protects IscU from oxidation and remains bound until the IscS-dependent turnover of L-cysteine promotes the loss of Zn^{2+} and initiates the Fe-S cluster assembly reaction.

Native MS experiments revealed that apo-IscU can bind two Fe^{2+} ions with different affinities (Figure 1.1D), consistent with recent Mössbauer spectroscopic studies that show two

Fe^{2+} binding sites for human ISCU with distinct chemical environments.[226] Moreover, Fe-IscU exhibited a positive ellipticity peak in the CD spectrum at 315 nm that is characteristic of an S→Fe charge transfer band (Figure 2.1F). Recent studies on human Fe-ISCU describe a similar spectroscopic feature and provide mutagenesis experiments that support cysteine ligation for the Fe^{2+} ion.[226] In addition, we provide evidence that Fe^{2+} is unable to displace the Zn^{2+} (Figures 1C, 3C) but can bind simultaneously with Zn^{2+} to IscU (Figure 1E), likely to the lower affinity site. Notably, the three cysteine residues on IscU are located in the [2Fe–2S] cluster assembly active site. These combined results indicate that IscU has two metal-binding sites: a higher affinity site that binds Zn^{2+} and Fe^{2+} using the active site cysteines and a lower affinity site that binds Fe^{2+}. It is unclear if both iron-binding sites are functionally relevant, but it is important to note that two Fe^{2+} ions are required to synthesize a [2Fe–2S] cluster.

We also found that the addition of Fe^{2+} stimulates the reactivity of the cysteine residues on IscU. Acid-quench denaturing MS experiments revealed that Fe^{2+} accelerates sulfur accumulation on apo-IscU (Figure 2.5), consistent with a recent study for the human assembly system.[226] Previous experiments using the bacterial IscU-IscS complex indicate that Fe^{2+} has no effect on the PLP chemistry or cysteine desulfurase activity,[81] suggesting that Fe^{2+} instead promotes the intermolecular sulfur transfer reaction. The stimulatory role of Fe^{2+} in sulfur transfer might be explained by (*i*) decreasing the pKa of an IscU sulfur-accepting cysteine ligand to increase its nucleophilicity; (*ii*) functioning as a Lewis acid to increase the electrophilicity of the sulfane sulfur of the IscS persulfide; and (*iii*) inducing a local conformational change to properly position the sulfur donor and acceptor residues. Also, native MS experiments revealed that reactions that include Fe^{2+} incorporated oxygen to generate low levels of sulfenic acid

(Table 2-1). Notably, the formation of small amounts of sulfinic acid, which would have the same mass as a persulfide species, might explain the lower than expected mass shifts for reactions with ^{34}S-L-cysteine (Table 2-2). These results are consistent with the ability of redox-active metals such as iron to enhance the reactivity of cysteine ligands.[224, 227, 228]

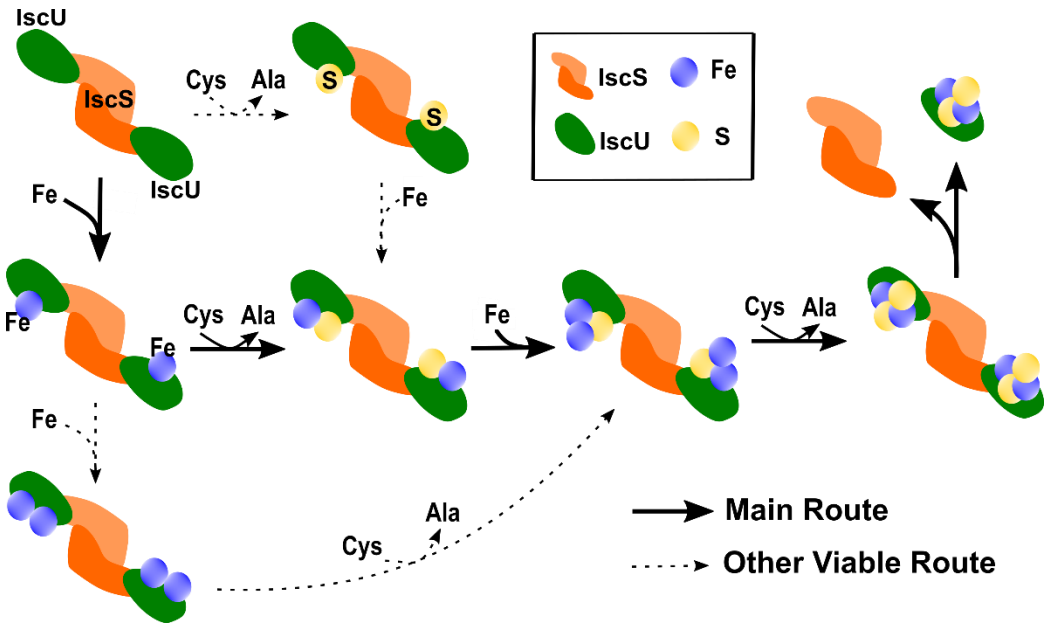

Figure 2.9 Proposed mechanism for iron-sulfur cluster assembly on IscU. The primary route is highlighted in bold with additional secondary pathways shown as dashed lines. The proposed mechanism is based on the assumption that the resulting iron and sulfur bound species of IscU are a readout of intermediates on the IscU-IscS complex.

Model for Fe-S cluster assembly. The Fe-S cluster assembly reaction likely occurs in the context of the IscU-IscS complex. Substrates for the synthesis of Fe-S clusters on IscU are delivered through IscS or proteins that bind with the $IscU_2$-$IscS_2$ complex.[74, 75, 86, 179, 184] One of the challenges in using native MS to investigate intermediates in Fe-S cluster assembly is the $\alpha_2\beta_2$ nature of the IscU-IscS complex; i.e., two Fe-S species bound to separate IscU subunits

would have the same total mass as the $IscU_2$-$IscS_2$ complex with one bound [2Fe–2S] cluster. We, therefore, designed experiments to probe uncomplexed IscU in the reaction with the underlying assumption that the resulting iron and sulfur bound species are a readout of intermediates on the IscU-IscS complex. Fe-S assembly reactions were initiated by mixing apo-IscU, Fe^{2+}, L-cysteine, IscS, and GSH, and the reactions were monitored by measuring changes in the mass of uncomplexed IscU as a function of time.

The MS data suggest an "iron-first" mechanism for [2Fe–2S] cluster synthesis. Our results reveal a [2Fe–2S] cluster bound to monomeric IscU developed, maximized after 75 min, and then decreased in intensity (Figure 2.6D). This trace coincided well with the positive ellipticity at 330 nm associated with [2Fe–2S]-IscU in a parallel assay monitored by CD spectroscopy (Figure 2.6C). Monomeric IscU with shifts in mass consistent with Fe and Fe-S species were observed in the earliest time points that then decayed as the intensity of this [2Fe–2S] cluster peak increased. This behavior is consistent with the Fe-IscU and Fe-S-IscU species being intermediates in the [2Fe–2S] cluster assembly reaction (Figure 2.9). The Fe-IscU peak decayed before the Fe-S-IscU species, suggesting a major route to a [2Fe–2S] cluster is through an iron-first mechanism. This hypothesis is also supported by the acceleration of the intermolecular sulfur transfer reaction from IscS to IscU in the presence of Fe^{2+} (Figure 2.5). As the Fe-S-IscU species decays, signals for both 2Fe-1S-IscU and [2Fe–2S]-IscU develop. Therefore, we propose that an iron atom binds to the Fe-S-IscU species prior to the second intermolecular sulfur transfer reaction. The two iron atoms are likely oxidized from Fe^{2+} to Fe^{3+} to provide the two electrons to break the S-S bond of the persulfide,[229] generate a bridging sulfide intermediate, and freeing the cysteine residue on IscU to accept another persulfide from IscS (Figure 6). We propose an oxidized 2Fe–2S species is then

generated after a second intermolecular sulfur transfer reaction. This species may be reminiscent of the Fe_2S-S oxidized cluster observed in a crystal structure of the IscU-IscS complex[60] and needs to be reduced by two electrons to complete the $[2Fe–2S]^{2+}$ assembly process. These electrons appear to be provided through the oxidation of ferredoxin *in vivo* and glutathione in our *in vitro* assay. We include GSH because it is a physiological reagent that promotes in vitro [2Fe–2S] cluster synthesis and transfer reactions to cluster carrier and target proteins.[185] Although ferredoxin clearly has a role in [2Fe–2S] and/or [4Fe–4S] cluster biogenesis in vivo,[230] the ability of bacterial Fdx to compete with IscU for binding to IscS and also generate a persulfide radical anion on IscS[184] appear counterproductive to a role in [2Fe–2S] cluster synthesis and require further study.

3. REDIRECTION OF SULFUR TRANSFER TO GLUTATHIONE BY CYAY LEADS TO RELIEVAL OF OXIDATIVE STRESS

3.1. Introduction

Iron-sulfur (Fe-S) clusters are essential cofactors for life processes such as oxidative respiration, photosynthesis, DNA modification, etc.[231, 232] These cofactors are ubiquitous for most organisms, from prokaryotes (such as *E. coli*) to eukaryotes (such as human).[233] Fe-S clusters exist in different stoichiometry, for example, rhombic [2Fe–2S] clusters and cubic [4Fe–4S] clusters.[173-175] As essential enzymes bind to various Fe-S clusters to fulfill their functions, a profound understanding of how organisms assemble and transport Fe-S clusters becomes crucial.

In prokaryotes, three Fe-S cluster biosynthesis pathways are known: 1) Nitrogen Fixation (NIF)[234, 235], 2) Iron-Sulfur Cluster (ISC)[236-238] and 3) Sulfur Formation (SUF)[239]. ISC pathway also operates in eukaryotic mitochondria and is highly conserved between the two systems. In *E. coli*, the ISC pathway is the house-keeping pathway under 'normal' growth conditions. In this study, we focus on *E. coli* ISC pathway. The cysteine desulfurase IscS converts its substrate L-cysteine into L-alanine and generate a sulfane sulfur on the mobile loop cysteine residue through persulfide bond.[68, 76, 86] This sulfane sulfur is subsequently transferred to the scaffold protein IscU, where [2Fe–2S] clusters are generated.[181-183] It's generally considered that an iron donor is required due to the toxicity of Fe^{2+}, but the source of Fe^{2+} remains putative.[75, 116, 179, 180] The source of electrons was proposed to be ferredoxin (Fdx).[184] IscU further transfers the cluster to Grx4 in a reaction accelerated by HscA-HscB pair in an ATP dependent manner[240-242] _ENREF_15. Grx4 subsequently transfers the clusters downstream to terminal acceptors.

Despite decades of extensive research on the ISC pathway, certain mechanistic details remain elusive.

The physiological role of bacterial frataxin CyaY is putative. Although CyaY and its eukaryotic homolog frataxin (FXN) share similar sequence, overall structure, and iron binding affinity[243], CyaY behaves differently in the bacterial ISC machinery. In the eukaryotic system, frataxin (FXN) promotes Fe-S assembly as an allosteric activator of the cysteine desulfurase complex.[119, 244] In contrast, *E. coli* CyaY inhibits Fe-S cluster assembly but has no effect on the IscS activity with the presence of IscU.[81, 122, 183, 245] Mutation of human FXN gene causes lethal neurodegenerative disease Friedriech's ataxia. Depletion of FXN results in iron overload, oxidative stress and ultimately cell death.[246-248] On the other hand, *E. coli* CyaY knockout did not directly lead to growth defects under normal aerobic growth conditions.[123, 249] Interestingly, Fe-S enzyme activities were compromised in CyaY knockout strains especially under iron-overload conditions. Also, wildtype *E. coli* strains outcompeted CyaY knockout strains when growing together.[123] Studies of *Salmonella enterica* revealed knockout of CyaY with Fe-S repairing enzyme Yggx further decreased cell viability and Fe-S enzyme activities under oxidative stress.[140] Overall, these *in vivo* studies support positive effect of CyaY on Fe-S cluster level and antioxidation in cell. While FXN clearly benefits Fe-S cluster assembly, the seemingly contradictory effects of CyaY *in vivo* and *in vitro* have yet to be resolved.

We sought to find the missing link between the antioxdative effect and ISC regulation by CyaY. Peroxidases are one of the major H_2O_2 scavenging enzymes. The thioredoxin (Trx) redox system helps transfer electrons from NADPH to thiol-dependent peroxidases for H_2O_2 scavenging.[149] Glutathione (GSH) is the major thiol-containing small molecule involving in

regulation of enzyme activities and redox sensing. GSH assists the glutaredoxin (Grx) redox system, which works similarly as the Trx system.[149] Also, small molecule persulfides such as glutathione persulfide (GSSH) and cysteine persulfdie (Cys-SSH) have been proposed as effective antioxidants.[158] Notably, IscS is effective in generating persulfides and potentially serves as a source of GSSH. Three sulfur protein acceptors of IscS, including IscU, TusA, and Thil, have been reported. IscU utilizes the sulfur for Fe-S assembly as mentioned, TusA transfers sulfur to MoCo biogenesis and tRNA thiolation pathways, and Thil delivers sulfur to thiamine biosynthesis and tRNA thiolation pathways. For *in vitro* assays, small molecules containing thiol groups such as dithiothreitol (DTT) are widely used to accept sulfur from IscS. Thus, GSH (~1-10 mM) likely acts as a small molecule sulfur acceptor for IscS under physiological conditions.

Another interesting study on CyaY and FXN is on a mutant of the scaffold protein. M107I was identified as a spontaneous mutation on Isu1 (yeast homolog of IscU) that could suppress the effect of *FXN* deletion in yeast, thereby making it FXN independent.[250] Recently, the reverse scenario was tested where a single point mutation (I108M) on IscU was shown to make the *E. coli* dependent on CyaY.[251] An *in vitro* study showed that Fe-S cluster biosynthesis is slower for $IscU^{I108M}$ without CyaY.[136] However, a more detailed *in vitro* study interrogating what happens when CyaY is added and these effects explained the *in vivo* observation was not addressed.

In this study, the mechanism of CyaY inhibition on Fe-S cluster assembly and how *in vitro* behavior of CyaY leads to the *in vivo* antioxidation effect are interrogated. Details in sulfur transfer, sulfur trafficking, and protein-protein interactions were obtained through mass spectrometry-based methodologies. The footprint of sulfur was tracked by acid-quench denaturing

MS. Acid-quench has been reported as an effective methodology to stop reactions by denaturing proteins, and lock persulfides in space by preventing disulfide exchanges in low pH. After acid-quench, the current state-of-the-art method in the field is by separating and detecting isotope-labeled sulfur (^{35}S) species using high-performance liquid chromatography (HPLC).[119] Isotope-labeling method has been successful in qualitative assessment between species but not quantitatively accurate due to the instability nature of radioactive elements. Here, we changed the analyzation method into high-resolution nano-electrospray ionization (nano-ESI) MS. The high-resolution of MS clearly resolved sulfur adducts on macromolecules, and the soft nano-ESI method prevents disulfide bond cleavage. Therefore, accurate quantitation of sulfur adducts on proteins was achieved using MS without isotope labeling. The effect of CyaY on the protein interaction network of IscS with sulfur acceptors IscU and TusA was analyzed by native ion mobility mass spectrometry (IM-MS). The protein interaction network and competition of IscS (~91kDa dimer) with IscU (~13kDa), TusA (~9kDa), and CyaY (~12kDa) is challenging for traditional biophysical techniques such as analytical size exclusion, ITC, and SPR due to insufficient resolution. The higher resolution and third dimensional separation of native IM-MS clearly resolved all species formed and enabled quantification of protein interactions in complex protein mixtures. With the soft nano-ESI method and proper instrument tuning, native IM-MS has been shown to preserve protein structure and interactions in the gas phase.[200, 201, 205] Protein ions in native-like folded compacted structure retain smaller and more compact drift time and collisional cross section (CCS) compared to denaturing or activated protein ions. Using drift time and CCS to evaluate whether protein ions are in "native-like" structure preserving non-covalent interactions with other proteins or ligands enhances reliability. Furthermore, we compared metal binding of protein complexes by

performing native MS on a high resolution orbitrap mass spectrometer. Overall, this study highlights the capability of various MS methods in studying challenging biochemical mechanisms, and a mechanism of CyaY inhibition on the ISC pathway and the relation with the antioxidative effect was proposed.

3.2. Experimental procedures

Preparation of proteins. *Escherichia coli* proteins IscS, IscU, CyaY and TusA were expressed and purified as previously described (for TusA ref monomer-dimer).[81] An extinction coefficient of 6.6 $mM^{-1}cm^{-1}$ at 388 nm (in 0.1 M NaOH) was used to estimate the concentration of the PLP cofactor,[206] which represents the concentration of active IscS. Extinction coefficients of 11,460, 28990, and 2560 $M^{-1}cm^{-1}$ at 280 nm was used to estimate the concentrations of IscU, CyaY, and TusA, respectively. IscS, IscU, CyaY, and TusA were estimated to be >95% pure based on SDS-PAGE analysis. Aliquots of IscS (50 mM HEPES, 250 mM NaCl, pH = 7.5), IscU (50 mM HEPES, 150 mM NaCl, pH = 7.5), CyaY (50 mM HEPES, 150 mM NaCl, pH = 7.5), and TusA (50 mM HEPES, 150 mM NaCl, pH = 7.5) stock solutions were flash-frozen and stored at -80 °C. All samples were prepared in an anaerobic Mbraun glovebox (<1 ppm O_2 monitored by a Teledyne model 310 analyzer) unless otherwise indicated.

Methylene blue assay for cysteine desulfurase activity. Cysteine desulfurase activities were measured for each complex (SU and SUC) according to the published procedure.[136] In short, a heating block was used to bring the temperature to 37°C. The proteins were mixed to a final concentration of 0.5 µM IscS, 2.5 µM IscU, 0 or 5 µM CyaY and 4 mM D,L-DTT followed by incubation for 15 minutes on heating block already at 37°C. 1 mM L-cysteine were added,

incubated for 6 min, and quenched with 20 mM N,N'-diphenyl-p-phenylenediamine (DPD) (in 7.2 M HCl) and 30 mM $FeCl_3$ (in 1.2 M HCl) and absorbance at 670 nm was measured. The amount of sulfide produced was determined for each data point using a standard curve.

CD spectroscopy. CD spectra were recorded on a Chirascan CD spectrometer (Applied Photophysics) using a 1 cm path length cuvette. Cuvettes were sealed with a rubber septa and electrical tape in a glove box (O_2 < 1 ppm). The assays were run in 50 mM HEPES and 150 mM NaCl (pH = 7.5) at 22ºC.

Cluster assembly assay on IscU and one-pot cluster synthesis assay on Grx4. The assay mixtures constituted 8 μM IscS, 40 μM IscU, 0 or 50 μM CyaY, 200 μM $Fe(NH_4)_2(SO_4)_2$, and was initiated with addition of 10 mM GSH and 100 μM cysteine using air tight syringes. Cluster assembly rates on IscU were measured for SU, SUC, SU^{I108M}, $SU^{I108M}C$ by monitoring the ellipticity change at 330 nm over time and fitting the initial data points using Kaleidagraph (synergy software) to linear equation ($y=m_1x+m_2$), where m_1 gives the initial rate of cluster synthesis (Figure 1B). [R^2 values: SU (0.99), SUC (0.96)]. For one-pot cluster synthesis on Grx4, 40 μM apo-Grx4 was also added into the assay mixtures then measured for SU, SUC, SU^{I108M}, $SU^{I108M}C$ by monitoring the change of ellipticity at 450 nm over time and fitting the initial time points using Kaleida graph (synergy software) to linear equation ($y=m_1x+m_2$), where m_1 gives the initial rate of cluster formation on Grx4 (Figure 1A). [R^2 values: SU (0.99), SUC (0.94), SU^{I108M} (0.99), $SU^{I108M}C$ (0.62)].

Cluster transfer assay from holo-IscU to apo-Grx4. 20 μM IscU was re-constituted using 1 μM IscS, 40 μM CyaY, 400 μM $Fe(NH_4)_2(SO_4)_2$ and 40 μM L-cysteine with L-cysteine being the limiting reagent to inhibit any further cluster-synthesis. 40 μM Grx4 was then injected

into the cuvette anaerobically using an air-tight syringe and the cluster transfer to the latter was followed by monitoring the ellipticity change at 450 nm over time and fitting the initial data using Kaleidagraph (synergy software) to linear equation ($y=m_1x+m_2$), where m_1 gives the initial rate of cluster transfer from Holo-IscU to apo-Grx4. 450 nm was chosen as the wavelength to monitor the transfer due to minimal contribution from holo-IscU at that wavelength. The rates were compared for SU, SUC (Figure 1C). [R^2 values: SU (0.93), SUC (0.93)].

Sample preparation for MS experiments. Protein samples were treated with 5 mM TCEP, incubated for 30 mins, and desalted by two passes through Micro Bio-spin columns with Bio-gel P-6 (Bio-Rad) equilibrated with target MS-compatible ammonium acetate buffers (buffer A: 200 mM ammonium acetate, pH = 7.5). Under standard conditions, Apo-IscU was prepared by treating the as-isolated IscU stock solution with 10 mM DTPA for 30 mins and then desalting the sample. All the IscU samples used in MS experiments were in apo form, otherwise in Zn bound form. To minimize potential oxidation during MS analysis, samples were prepared and incubated in 0.2 mL PCR tubes in the glovebox. The mixtures were then sealed in the PCR tubes, removed from the glovebox, and infused immediately (< 5 mins) into the mass spectrometer.

Time-dependent acid-quench denaturing MS experiments to determine whether Fe^{2+} and CyaY influences sulfur transfer from IscS to IscU. Mixtures of 15 μM IscS, 75 μM apo-IscU, and different concentrations of ferrous acetate (0 or 400 μM) were incubated in buffer A for 30 mins at 22 °C. The reaction was then initiated by adding 300 μM L-cysteine. At each time point, the assay mixture was quenched by 10-fold dilution into 1% formic acid before MS analysis on EMR. Linear regression fits were used to determine the initial rates for the sulfur transfer reactions.

Native MS experiments to monitor metal binding to IscS-IscU or IscS-IscU-CyaY. Titrations of IscS-apo-IscU or IscS-apo-IscU-CyaY with Fe^{2+} were monitored by high-resolution native MS experiments using EMR. SU (1.5 μM IscS and 4.5 μM apo-IscU) and SUC (1.5 μM IscS, 4.5 μM apo-IscU, and 4.5 μM CyaY) samples were mixed with different concentrations of ferrous acetate (5, 15, or 45 μM) in buffer A, incubated for 30 mins, and then analyzed.

Native IM-MS experiments to assess the effect of Fe^{2+} on formation of CyaY complexes. Mixtures of (*i*) 1.5 μM IscS and 12 μM CyaY (*ii*) 1.5 μM IscS, 1.5 μM apo-IscU and 1.5 μM CyaY (*iii*) 1.5 μM IscS, 1.5 μM apo-IscU, 1.5 μM CyaY and 12 μM TusA were mixed with 0 or 100 μM ferrous acetate in buffer A, incubated for 30 mins, and then analyzed by IM-MS using Synapt G2.

Acid-quench denaturing MS experiments to determine whether Fe^{2+} and CyaY influences sulfur transfer from IscS to IscU and/or TusA. Mixtures of 5 μM IscS, 50 μM apo-IscU and/or TusA, and different concentrations of ferrous acetate (0 or 400 μM) and/or CyaY (0 or 15 μM) were incubated in buffer A for 30 mins at 22 °C. The reaction was then initiated by adding 200 μM L-cysteine. At 10 min time point, the assay mixture was quenched by 10-fold dilution into 1% formic acid before MS analysis on EMR.

Native IM-MS experiments to monitor competition of CyaY and TusA on binding IscS. Titrations of either IscS-TusA complex with CyaY or IscS-CyaY complex with TusA were monitored by IM-MS using Synapt G2. Mixtures of 1.5 μM IscS and 1.5 μM TusA were mixed with different concentrations of CyaY (0, 3, 6, 12 μM), incubated for 30 mins, and then analyzed. On the other hand, mixtures of 1.5 μM IscS and 12 μM CyaY were mixed with

different concentrations of TusA (0, 1.5, 3, 6 μM) incubated for 30 mins, and then analyzed by IM-MS using Synapt G2.

Native IM-MS experiments to monitor competition of IscU and TusA on binding IscS. Titrations of either IscS-TusA complex with apo-IscU or IscS-apo-IscU complex with TusA were monitored by IM-MS using Synapt G2. Mixtures of 1.5 μM IscS and 12 μM TusA were mixed with different concentrations of apo-IscU (0, 1.5, 3, 6 μM), incubated for 30 mins, and then analyzed. On the other hand, mixtures of 1.5 μM IscS and 1.5 μM apo-IscU were mixed with different concentrations of TusA (0, 3, 6, 12 μM) incubated for 30 mins, and then analyzed by IM-MS using Synapt G2.

Native IM-MS experiments to assess the effect of CyaY on formation of IscS-IscU complexes. Mixtures of 1.5 μM IscS and 1.5 μM apo-IscU were mixed with 0 or 1.5 μM CyaY in buffer A, incubated for 30 mins, and then analyzed. To determine the effect of apo-IscU on SC binding as well, mixture of 1.5 μM IscS and 12 μM CyaY were incubated for 30 mins and analyzed using Synapt G2.. Titrations of SUT complex with CyaY were performed to study the effect of CyaY on competition of apo-IscU and TusA on binding IscS. Mixtures of 1.5 μM IscS and 1.5 μM apo-IscU, 12 μM TusA were mixed with different concentrations of CyaY (0, 0.75, 1.5, 3 μM), incubated for 30 mins, and then analyzed by IM-MS using Synapt G2.

Alanine detection assay. In a procedure adapted from Selbach and colleagues, alanine production was observed in terms of its reaction with naphthalene 2,3-dicarboxaldehyde (NDA) to generate a stable fluorescent product.[252] Mixtures of IscS (0.5 μM), IscU (50 μM), L-cysteine (150 μM), Fe^{2+} (250 μM), GSH (2.5 mM), with or without CyaY (0 or 5 μM) were prepared in

50 µL aliquots and quenched after 7 minutes with 70 µL 2.86% trichloroacetic acid (TCA). The samples were then added to 1 mL borate buffer (115 mM sodium borate, 6 mM KCN, 100 µM NDA, pH 9.0) and incubated in darkness for 45 min. Following injection of 100 µL onto a Restek Raptor C18 column, the fluorescence of the mixtures was evaluated at excitation and emission wavelengths 390 and 440 nm, respectively. Samples were separated using an isocratic solvent system of 60% acetonitrile, 40% water, and 0.1% trifluoroacetic acid (TFA) for three min with a flow rate of 1.0 mL/min. The alanine-NDA peaks eluted at 30 s and peak areas integrated. Alanine concentration was determined from peak area by a standard curve using the same procedure and concentration of GSH as samples with corresponding 0, 10, 20, 50, 100, 150, or 200 µM alanine in the initial 50 µL aliquots.

MS experiments to probe generation of GSSH. Mixtures of 20 µM IscS, 50 µM apo-IscU and, 30 µM CyaY, 200 µM ferrous acetate, and 150 µM GSH were incubated in buffer A for 12 mins at 37 °C in the glovebox. The reaction was then initiated by adding 150 µM L-cysteine. At 12 min time point, the assay mixture was quenched by 2-fold dilution into 5 mM NEM. After 10 minutes, the assay mixture was diluted 7.5-folds into 1% formic acid before MS analysis on EMR.

H_2O_2 detection assays to monitor the antioxidation effect of CyaY. Mixtures of 16 µL volume containing 312.5 µM Fe^{2+}, 1.25 mM GSH, and 500 µM L-cysteine with neither IscS, IscU, and CyaY (control), with 25 µM IscS and 100 µM IscU (SU), or with 25 µM IscS, 100 µM IscU, and 100 µM CyaY (SUC) were reacted for 30 seconds, followed by adding 4 µL of 5 mM H_2O_2. Upon adding H_2O_2, the concentrations of present components in the reaction mixtures were 250 µM Fe^{2+}, 1 mM GSH, 400 µM L-cysteine, 20 µM IscS, 80 µM IscU, 80 µM CyaY and

1 mM H_2O_2. Five seconds after adding H_2O_2, 20 μL of 100 mM NEM were added to the reaction mixtures. The concentration of the remained H_2O_2 in the mixtures were analyzed by tracking absorption at 571 nm following manufacturer's protocol of the Amplex™ Red Hydrogen Peroxide/Peroxidase Assay. The NEM-quenched samples reacted with working solution (125 μM 10-Acetyl-3,7-dihydroxyphenoxazine and 0.25 U Horseradish peroxidase) in 1:4 ratio for 30 minutes, and diluted for five folds before measuring absorbance at 571 nm. A linear standard curve with initial concentration of 200 μM, 300 μM, 500 μM, 750 μM, 1.25 mM, 2.5 mM and 5 mM H_2O_2 following the exact same procedure was used ($R^2 > 0.99$) for determining H_2O_2 concentrations.

MS description and settings. Gold-coated borosilicate glass capillaries were prepared in house for use in the nano-ESI experiments. The sample solution was back-filled into a gold-coated glass capillary tip and sprayed into the mass spectrometer.

High-resolution MS experiments were performed by an Exactive Plus with extended mass range (EMR) Orbitrap MS (Thermo Fisher Scientific, San Jose, CA). For native MS experiments using EMR, instrument parameters were tuned to minimize collisional activation while retaining reasonable signal to noise. The parameters used for the native MS analysis of IscS-IscU and IscS-IscU-CyaY complexes include: m/z range 4000–10000, spray voltage 1.2 kV, capillary temperature 350 °C, S-Lens RF level 200, source DC offset 3 V, injection flatapole DC 15 V, inter flatapole lens DC 12 V, bent flatapole DC 13–25 V, transfer multipole DC offset 8 V, C-trap entrance lens tune offset 0 V, trapping gas pressure setting 7, in-source dissociation voltage 98 eV, HCD collision energy 0 eV, FT resolution 35000, positive ion mode, and ion maximum injection time 50 ms. For acid-quench denaturing MS experiments using EMR,

instrument parameters were tuned to prevent cleavage of persulfide bonds while maximizing signal. The parameters used for the acid-quench denaturing MS analysis of IscU and/or TusA include: m/z range 200–4000, spray voltage 1.3 kV, capillary temperature 150 °C, S-Lens RF level 200, source DC offset 3 V, injection flatapole DC 15 V, inter flatapole lens DC 12 V, bent flatapole DC 2 V, transfer multipole DC offset 2 V, C-trap entrance lens tune offset 0 V, trapping gas pressure setting 7, in-source dissociation voltage 0 eV, HCD collision energy 10 eV, FT resolution 8750, positive ion mode, and ion maximum injection time 50 ms. The initial MS data from EMR were collected using the Thermo Exactive software as RAW format. The Raw data were converted into text files using a Python script making use of Multiplierz. The intensity of the protein and protein–adduct species were deconvoluted and converted into normalized intensity by processing the text files with the software program UniDec.[212] The reported intact mass were obtained from processing native MS spectrum, and the errors were calculated from FWHM of the highest intensity peak with Unidec. Ranges that were chosen for further data processing include m/z of 1000–4000 (denaturing IscU and TusA), m/z of 5500–6800 (native IscU-IscS complexes), m/z 5500–8000 (native IscU-IscS-CyaY complexes).

Native ion-mobility mass spectrometry (Native IM-MS) was performed on a Synapt G2 instrument. Instrument parameters were tuned to maximize ion intensity but simultaneously preserve the native-like state of proteins as determined by IM. The instrument was set to a capillary voltage of 1.3 kV, source temperature (30 °C), sampling cone voltage of 20 V, extraction cone voltage of 1 V, trap collision energy 4 V, transfer collision energy off, and backing pressure ~5 mbar, trap flow rate at 8 ml/min, He cell flow rate at 120 ml/min, IMS flow rate at 60 ml/min. The T-wave settings for trap (310 ms^{-1}/6.0 V), IMS (250 ms^{-1}/9–12 V) and

transfer (65 ms^{-1}/2 V), and trap bias (30.0 V). Mass spectra were calibrated externally using a sodium iodide solution. Recorded spectra were deconvoluted using MassLynx 4.1 (Waters). Quantitation of individual species in complex samples was done using Driftscope v2.1 (Waters), Corresponding IMS species were manually recognized through matching m/z and IMS trend line, extracted by the selection tool, and saved as new spectra to obtain total ion current (TIC). Relative TIC of individual species was processed normalized intensities.

MS data processing. The initial MS data from EMR were collected using the Thermo Exactive software as RAW format. The Raw data were converted into text files using a Python script making use of Multiplierz. The intensity of the protein and protein–adduct species were deconvoluted and converted into normalized intensity by processing the text files with the software program UniDec.[212] The reported intact mass were obtained from processing native MS spectrum, and the errors were calculated from FWHM of the highest intensity peak with Unidec. Ranges that were chosen for further data processing include m/z of 1000–4000 (denaturing IscU and TusA), m/z of 5500–6800 (native IscU-IscS complexes), m/z 5500–8000 (native IscU-IscS-CyaY complexes).

3.3. Results

CyaY inhibits cluster assembly on IscU and one-pot cluster synthesis on Grx4. Fe-S cluster formation rates on IscU in the presence and absence of CyaY were determined using CD spectroscopy by monitoring the ellipticity change at 330, respectively. Consistent with previously published results, CyaY was observed to strongly inhibit iron sulfur cluster formation on scaffold protein (Figure 3.1B). We further tested whether the inhibitory effect of CyaY on Fe-S cluster assembly on scaffold protein results in inhibition of holo-Grx4 synthesis in a one-pot

reaction where holo-IscU is not pre-formed. Cluster synthesis on Grx4 was monitored by recording ellipticity change at 450 nm. CyaY strongly inhibited cluster formation on Grx4 (Figure 3.1A).

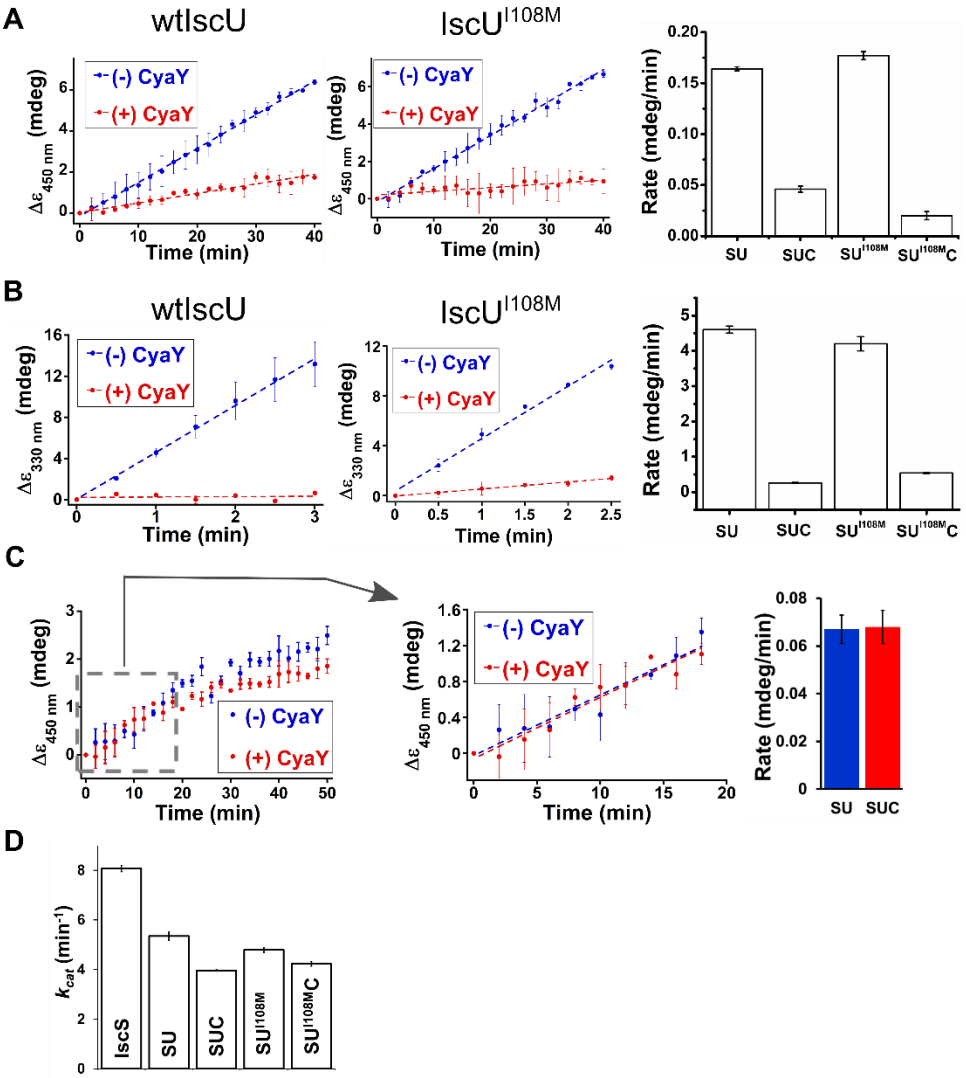

Figure 3.1 CyaY effects on cluster assembly, cluster transfer, and cysteine desulfurase activity. (A) One-pot cluster synthesis on Grx4 started from cluster assembly on IscU or IscU^{I108M}, **(B)** cluster assembly on IscU or IscU^{I108M}, and **(C)** cluster transfer from holo-IscU or holo-IscU^{I108M} to Grx4 was monitored by the change of ellipticity at 450, 330, and 450 nm using CD spectroscopy, respectively. For (A), samples initially consists of 0.5 µM IscS, 20 µM IscU, 0 or 40 µM CyaY, 200 µM $Fe_2(NH4)_2SO_4$ and 40 µM Grx4, and the the reaction was initiated by

adding 100 µM cysteine and 10 mM GSH. For (B), samples initially consist of 8 µM IscS, 40 µM IscU, 0 or 50 µM CyaY, 200 µM $Fe_2(NH_4)_2SO_4$, and the the reaction was initiated by adding 100 µM cysteine and 10 mM GSH. For (C), samples initially consist of 0.5 µM IscS, 20 µM holo-IscU, 10 mM GSH, 0 or 40 µM CyaY, and initiated by adding 40 µM apo-Grx4. The initial rates were obtained by fitting the data to linear equations and plotted. **(D)** The cysteine desulfurase activity were assessed by a sulfide detection assay described in Methods. The reactions contained 0.5 µM IscS, 0 or 2.5 µM IscU/IscU^{I108M}, 0 or 5 µM CyaY, 4 mM D,L-DTT, and initiated by L-cysteine.

CyaY does not affect iron sulfur cluster transfer from IscU to Grx4. Next, we wanted to explore if CyaY has any effect on the cluster transfer step. We reconstituted [2Fe–2S] on the scaffold protein IscU (see methods) followed by addition of apo-Grx4 to initiate the transfer reaction. The cluster transfer reaction was monitored using CD spectroscopy by monitoring ellipticity change at 450 nm (where holo-Grx4 has much larger contribution compared to holo-IscU). The rates were found to be comparable with and without CyaY (Figure 3.1C). This shows that CyaY does not affect cluster transfer from holo-IscU to apo-Grx4.

CyaY does not affect cysteine desulfurase activity. We next investigated whether the inhibition effect of CyaY on cluster assembly was a result of inhibited cysteine desulfurase activity. Cysteine desulfurase activity of IscS with presence of IscU (SU) or presence of both IscU and CyaY (SUC) were measured using a methylene blue assay (Figure 3.1D) or an alanine detection assay. Cysteine desulfurase activities were comparable for SU and SUC complexes in both assays, suggesting CyaY has no effect on IscS activity.

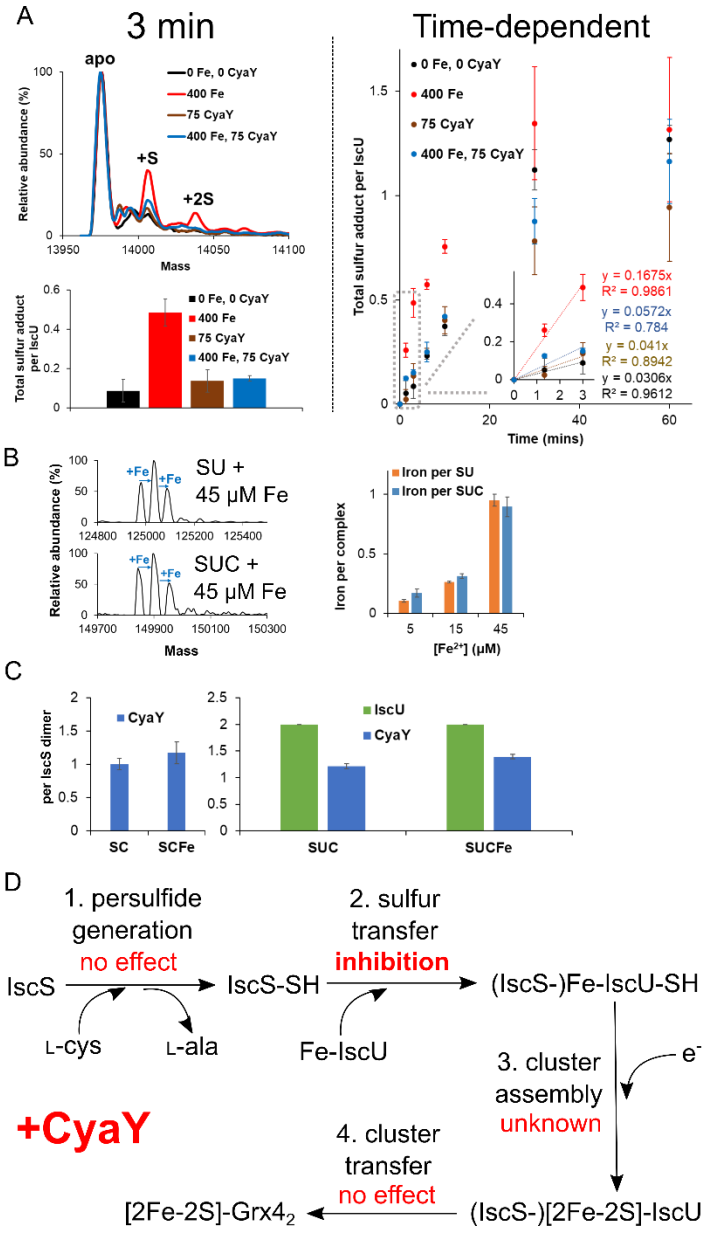

Figure 3.2 CyaY inhibits sulfur transfer from IscS to IscU under the presence of Fe^{2+},while CyaY and Fe have no effect on binding affinity of each other to IscS-IscU complex. Time-dependent acid-quench denaturing MS was utilized to monitor sulfur accumulation on IscU after mixing apo-IscU (75 μM) with IscS (15 μM), L-cysteine (300 μM), ferrous acetate (0 or 400 μM) and CyaY (0 or 75 μM). **(A)** Deconvoluted zero charge MS spectra of monomeric IscU (upper left) and total accumulated sulfur adducts per IscU (lower left) at an initial (3 min) reaction time. Total accumulated sulfur adducts per IscU as a function of time (right panel) revealed an initial rate increase (~6 fold) by adding Fe^{2+} (red) is inhibited when CyaY is also present (blue). The inset shows the early time points overlaid with linear regression fits. The error bars represent replicate errors (n = 3). **(B)** deconvoluted zero charge native MS spectra

(left) of SU (mixture of 1.5 μM IscS and 4.5 μM apo-IscU) or SUC (mixture of 1.5 μM IscS, 4.5 μM apo-IscU and 4.5 μM CyaY) mixed with 45 μM Fe^{2+}. Titration of Fe^{2+} to SU or SUC monitored by native MS (right) indicated similar binding affinity of Fe^{2+} to SU or SUC. **(C)** CyaY binding per IscS dimer of mixtures of C (1.5 μM CyaY) with S (1.5 μM IscS, left panel) or SU (1.5 μM IscS and 1.5 μM IscU, right panel) with 0 or 100 μM Fe^{2+} monitored by native IM-MS revealed that Fe^{2+} has no effect on CyaY binding to S or SU. **(D)** Depiction of CyaY effect on ISC cluster assembly and transfer.

CyaY inhibits sulfur transfer from IscS to apo-IscU under presence of Fe^{2+}.

Notably, as Zn^{2+} binding on active site of IscU inhibits sulfur transfer from IscS, Fe^{2+} binding, and IscS-IscU binding[253], apo-IscU was specifically used in sulfur transfer and protein complex formation experiments in this study (Figure 3.2, 3, 4, and 5B). In these MS-based experiments, apo-IscU was necessary for studying Fe^{2+} interaction with IscU active site. Other non-MS based experiment, such as cysteine desulfurase activity and cluster assembly experiment, were performed with as-isolated IscU (Zn-IscU for Figure 3.1, Figure 3.2, 5A, and 5C-D) since complete removal of zinc contamination in our normal assay environments was not achievable. The outcomes of these experiments should be independent of Zn^{2+} binding on IscU, as Zn^{2+} on IscU could be effectively removed when IscS, L-cysteine and low mM concentrations of GSH are present, which enable efficient cluster assembly on IscU.[253] To evaluate the effect of CyaY on sulfur transfer from IscS to IscU, we monitored the sulfur adducts on IscU using time-dependent acid-quench denaturing MS. Previously published studies establish that the addition of acid quenches sulfur transfer reactions and locks the persulfide in place for subsequent analysis.[213, 214] Apo-IscU, IscS, L-cysteine, and various concentrations of Fe^{2+} and CyaY were reacted, quenched with acid at different reaction times, and analyzed by MS. In a 3 minute reaction (initial time), little persulfide formation was detected on IscU in the absence of Fe^{2+}, whereas multiple persulfide species were observed upon the addition of Fe^{2+}. We already

reported this Fe promotion effect on sulfur transfer from IscS to IscU. Upon adding CyaY, the persulfide formation on IscU without Fe^{2+} was not affected, while the persulfide formation on IscU with Fe^{2+} was inhibited (Figure 3A, left panel). After a 1-hour reaction, samples with and without Fe^{2+} and CyaY had similar amount of sulfur adducts (~0.9-1.3) per IscU (Figure 3A, right panel). The initial rate of sulfur accumulation on IscU was similar upon adding CyaY (~1.3 fold), increased ~6 fold when adding Fe^{2+}, and dropped back when Fe^{2+} and CyaY and both present (~1.9 fold). These experiments indicate that the addition of CyaY inhibits the Fe^{2+} promotion effect on sulfur transfer from IscS to IscU.

CyaY does not affect Fe^{2+} binding to IscS-(apo-IscU) complex, and Fe^{2+} does not affect CyaY binding to IscS-(apo-IscU) complex. We next investigate whether CyaY and Fe^{2+} affect binding of each other to IscS-(apo-IscU) complex. To investigate whether CyaY affect Fe^{2+} binding to SU complex, titration of Fe^{2+} with SU or SUC was analyzed by high-resolution native MS. SU and SUC exhibited comparable binding to Fe^{2+} under different concentrations of Fe^{2+} (Figure 3.2B), suggesting CyaY did not affect Fe^{2+} binding to SU complex . On the other hand, we also evaluated the effect of Fe^{2+} on CyaY binding to S or SU. SC and SUC samples with or without Fe^{2+} were analyzed by native IM-MS. Both SC and SUC showed comparable binding to CyaY with or without Fe^{2+} (Figure 3.2C), indicating that Fe^{2+} did not influence CyaY binding to S or SU complex.

CyaY does not significantly affect sulfur transfer from IscS to TusA. Knowing the inhibitory effect of CyaY on sulfur transfer from IscS to IscU, we wondered if CyaY also affected sulfur transfer from IscS to TusA. Thus, we monitored the sulfur adducts on TusA using time-dependent acid-quench denaturing MS. TusA, IscS, L-cysteine, and various concentrations

of Fe^{2+} and CyaY were reacted, quenched with acid at different reaction times, and analyzed by MS. Sulfur adducts for all the samples after a 10 min reaction are comparable with samples containing CyaY and Fe^{2+} a little lower (difference < 7%, Figure 3.3A), suggesting that CyaY and Fe^{2+} have no significant effect on sulfur transfer from IscS to TusA.

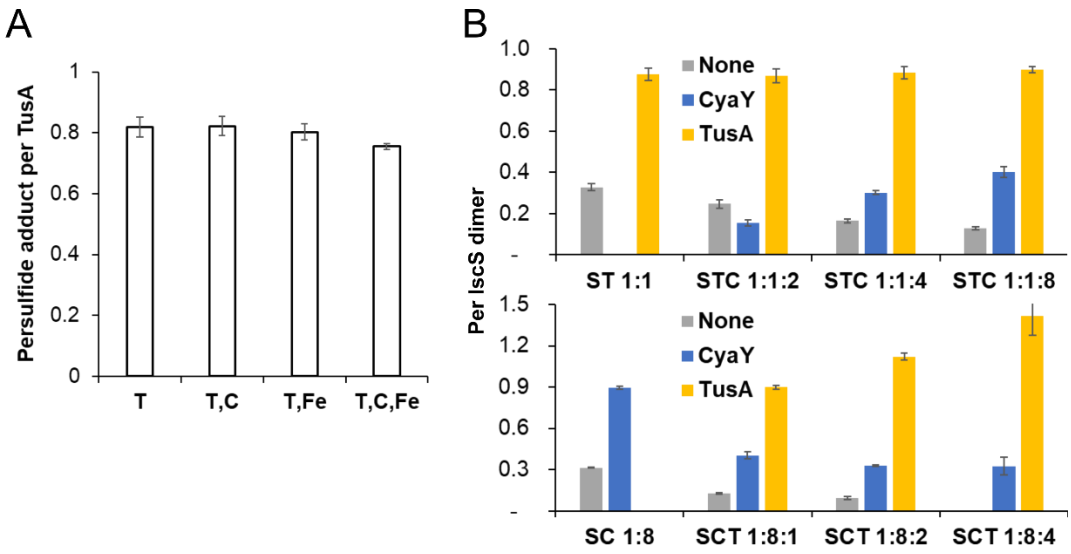

Figure 3.3 Figure 3. CyaY has no effect on sulfur transfer from IscS to TusA and competes against TusA on IscS binding with relative low affinity. Acid-quench denaturing MS was utilized to monitor sulfur accumulation on TusA after mixing TusA (50 µM) with IscS (5 µM), L-cysteine (200 µM), ferrous acetate (0 or 200 µM) and CyaY (0 or 15 µM) at a 10 min time point. **(A)** Total accumulated sulfur adducts per TusA revealed no effect of CyaY and Fe^{2+} on sulfur transfer from IscS to TusA. **(B)** Binding partners per IscS dimer of mixtures of CyaY, TusA and IscS was monitored by native IM-MS. Titration of CyaY to ST (1.5 µM IscS and 1.5 µM TusA, upper panel) indicated that excess CyaY (up to 8 fold) was unable to decrease TusA binding on IscS dimer. In comparison, titration of TusA to SC (1.5 µM IscS and 12 µM TusA, lower panel) revealed that binding of CyaY to IscS decreased as binding of TusA to IscS increased.

CyaY competes with TusA on binding IscS with lower affinity. We next investigate whether CyaY affects binding of TusA to IscS. Titration of CyaY to equimolar of ST mixture showed increasing CyaY binding (up to ~0.4 C per S_2) but no change in TusA binding (remained

~0.9 T per S_2) as CyaY concentration elevated (Figure 3.3B, upper panel). On the other hand, titration of TusA to SC mixture (IscS:CyaY = 1:8) revealed increased TusA binding (up to ~1.5 TusA per S_2) and decreased CyaY binding (from ~0.9 C to ~0.3 C per S_2) as TusA concentration elevated (Figure 3.3B, lower panel). Also, in a SCT mixture (S:C:T = 1:8:1), 1 equivalent of TusA (~0.9 T per S_2) binds IscS better than 8 equivalent of CyaY (~0.4 C per S_2). These results clearly suggest CyaY and TusA binds with IscS competitively, and CyaY has lower affinity than TusA. Notably, the total amount of TusA plus CyaY binding on a IscS dimer was lower than 2 even with excess TusA and CyaY (~1.8 for a SCT mixture of 1:8:4 = S:C:T). In the SCT mixture spectra, IscS dimer could bind up to total two CyaY or TusA (S_2C_2, S_2T_2, and S_2CT were observed). Together, these evidence support that CyaY and TusA have 2 overlapped binding sites on IscS.

CyaY inhibits sulfur trafficking from IscS to protein acceptors. To evaluate the effect of CyaY on sulfur trafficking from IscS to apo-IscU and TusA, we monitored the sulfur adducts on proteins using time-dependent acid-quench denaturing MS (Figure 3.4A, B). Mixtures of IscS (5 μM), L-cysteine (200 μM), apo-IscU (0 or 50 μM), TusA (0 or 50 μM), Fe^{2+} (0 or 200 μM), and CyaY (0 or 15 μM) were reacted, quenched with acid at 10 minutes, and analyzed by MS. First, we performed control experiments of sulfur transfer to individual sulfur acceptors (Figure 4A, left panel). Sulfur adducts on apo-IscU was higher after adding Fe^{2+} (increased from ~0.4 to ~0.6 per IscU) and dropped down when CyaY was also present (~0.2 per IscU), which are similar results as previously shown in Figure 2A. Sulfur adducts on TusA (~0.8 per TusA) were higher than that on IscU under same experimental conditions. Next, we analyzed samples with equimolar apo-IscU and TusA (Figure 4A, right panel). Without CyaY and Fe^{2+}, sulfur adducts

on apo-IscU and TusA are similar (~0.5 per IscU/TusA). After adding Fe^{2+}, sulfur adducts on TusA slightly increased (from ~0.5 to ~0.6 per TusA) and sulfur adducts on apo-IscU apparently elevated (from ~0.5 to ~0.8 per IscU). When both Fe^{2+} and CyaY were present, sulfur adducts on apo-IscU decreased as expected (~0.2 per IscU) while surprisingly sulfur adducts on TusA disappeared.

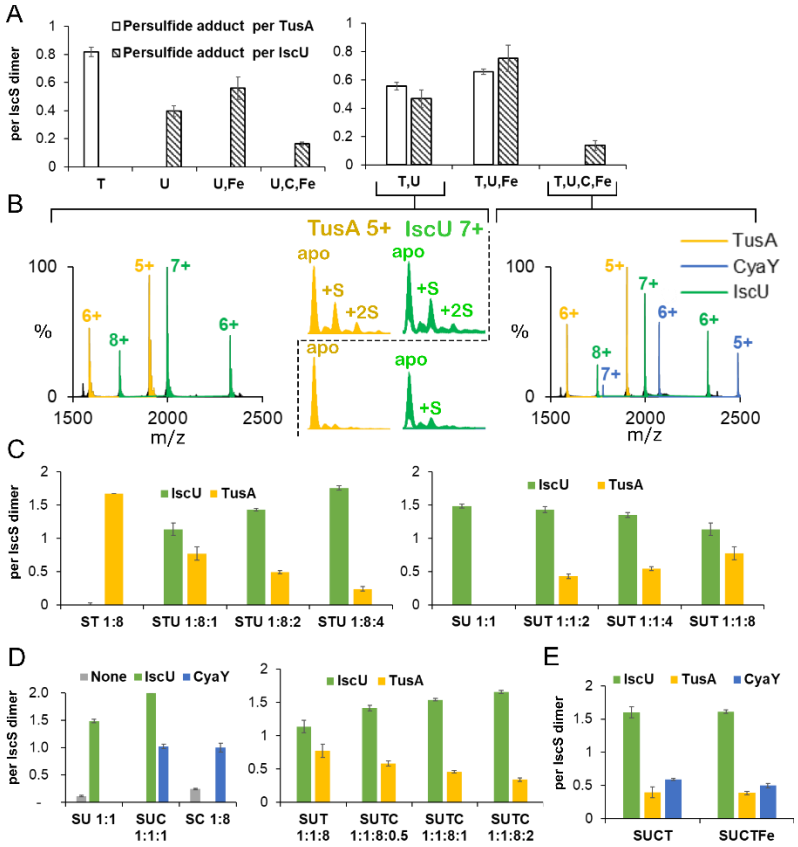

Figure 3.4 CyaY inhibits sulfur transfer from IscS to binding partners under the presence of Fe^{2+}. (A) Acid-quench denaturing MS was utilized to monitor sulfur accumulation on apo-IscU and/or TusA after mixing apo-IscU and/or TusA (50 µM) with IscS (5 µM), L-cysteine (200 µM), Fe^{2+} (0 or 200 µM) and CyaY (0 or 15 µM) at a 10 min time point. Representative spectra and zoom in of TusA 5+ and IscU 7+ of T, U and T, U, C, Fe samples are shown in **(B)**. Relative binding affinities of IscS binding partners were were monitored by native IM-MS. **(C)** Titration of apo-IscU to IscS-TusA (ST) complex (1.5 µM IscS and 12 µM TusA, left panel) indicated that apo-IscU was able to decrease TusA binding on IscS dimer even with lower concentrations. In comparison, titration of TusA to SU (1.5 µM IscS and 1.5 µM apo-IscU, right panel) revealed that binding of apo-IscU to IscS decreased slightly when using excess (8 fold)

TusA. **(D)** The left panel shows mixture of IscS-IscU CyaY (SUC) complex (1.5 µM IscS, 1.5 µM apo-IscU and 1.5 µM CyaY) demonstrated higher IscU binding per IscS than SU (1.5 µM IscS and 1.5 µM apo-IscU), and similar amount of CyaY binding per IscS with SC (1.5 µM IscS and 12 µM CyaY, note that CyaY is in excess in SC compare to SUC). Titration of CyaY to SUT (1.5 µM IscS, 1.5 µM apo-IscU and 12 µM TusA) revealed that CyaY enhanced apo-IscU binding while decreased TusA binding. (E) SUCT complex formation (mixture of 1.5 µM IscS, 1.5 µM apo-IscU, 12 µM TusA and 1.5 µM CyaY) with 0 or 100 µM Fe^{2+} remained the same.

CyaY assists IscU to compete off TusA on binding IscS. To better understand the inhibition effect of CyaY on sulfur trafficking to protein acceptors, we monitored complex formation of apo-IscU, TusA, IscS, Fe^{2+}, and CyaY mixtures by native IM-MS using Synapt G2.

Titration of TusA into SU mixture revealed competition between apo-IscU and TusA on binding IscS. As the concentration of apo-IscU and IscU binding on IscS increased, TusA binding on IscS decreased (Figure 3.4C, left panel). Titration of TusA into SU mixture showed similar results (Figure 3.4C, right panel). IscU binding (~1.1U per S_2) was slightly higher than TusA binding on IscS for SUT mixture with excess TusA (S:U:T = 1:1:8), suggesting apo-IscU has higher affinity than TusA on binding IscS. Notably, the total amount of apo-IscU plus TusA binding on a IscS dimer was equal or lower than 2 even with excess apo-IscU and TusA. In the SUT mixture spectra, IscS dimer could bind up to two apo-IscU or TusA (S_2U_2, S_2T_2, and S_2UT were observed). Together the evidence support that CyaY and TusA have 2 overlapped binding sites on IscS.

Next, we examine the effect of CyaY on apo-IscU binding. Binding of apo-IscU on IscS for a SU sample (S:U = 1:1, ~1.5U per S_2) enhanced after adding CyaY (S:U:C = 1:1:1, ~2.0U per S_2), suggesting the presence of CyaY promoted IscU-IscS binding (Figure 3.4D, left panel). On the other hand, binding of CyaY on IscS were similar (~1.0C per S_2) for a SUC sample (S:U:C = 1:1:1) and a SC sample (S:C = 1:8) (Figure 3.4D, left panel). Much less CyaY was

required to reach the same level CyaY-IscS binding when IscU was present, indicating the presence of IscU enhanced CyaY binding. Titration of CyaY into a SUT mixture revealed increasing apo-IscU binding and decreasing TusA binding as CyaY concentration increased (Figure 3.4D, middle panel). Clearly, CyaY assisted IscU to compete off TusA on binding IscS.

We also investigated if Fe^{2+} affects binding of SUCT mixtures. A SUCT sample (S:U:C:T = 1:1:8:1) showed no difference in complex formation after adding excess Fe^{2+} (Figure 3.4D, right panel), which matches with other results demonstrating Fe^{2+} had no effect on CyaY and apo-IscU binding (Figure 3.2C).

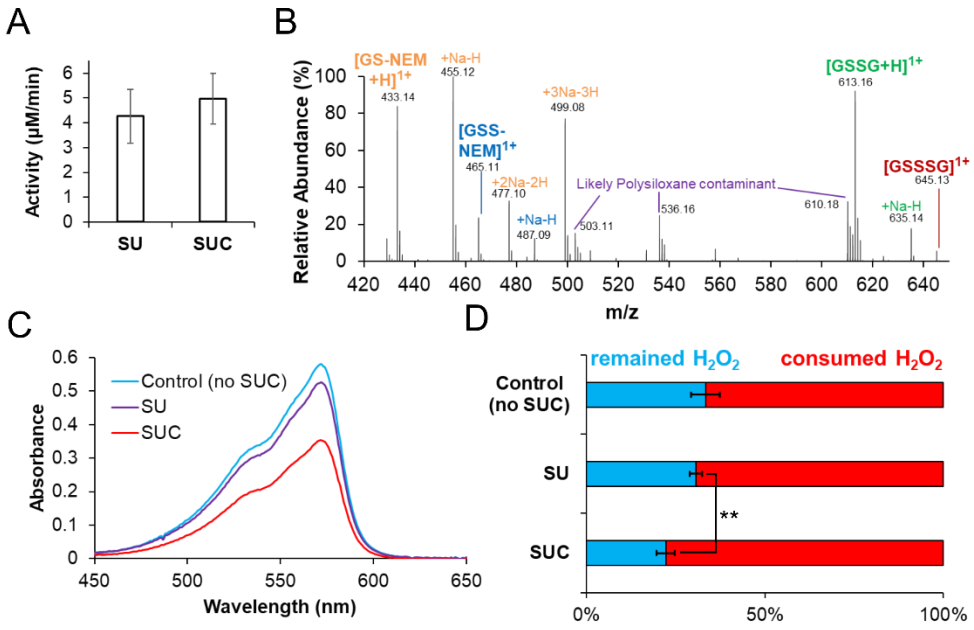

Figure 3.5 Redirection of sulfur trafficking to small molecules by CyaY under the presence of Fe^{2+} results in accelerated consumption of H_2O_2. (A) The effect of CyaY on overall cysteine turnover was further investigated by an alanine detection assay. The reaction mixtures contain IscS (0.5 μM), IscU (50 μM), Fe^{2+} (250 μM), GSH (1 mM), and cysteine (150 μM) with or without CyaY (5 μM). **(B)** Probing the small molecule species accepted sulfur using MS. The assay mixture containing IscS (20 μM), IscU (50 μM), CyaY (30 μM), Fe^{2+} (200 μM), GSH (150 μM), and cysteine (150 μM) were reacted in NaOAc buffer (200 mM, pH = 7.5) for 12 minutes before quenched by 5 mM NEM. The final assay mixture was diluted 15-folds in 1%

formic acid for MS analysis. Consumption of H_2O_2 with or without CyaY was monitored using Amplex™ Red Hydrogen Peroxide/Peroxidase Assay Kit. In Brief, mixtures contain Fe^{2+}, GSH, and cysteine with no IscS, IscU, and CyaY (control), with IscS and IscU (SU), or with IscS, IscU, and CyaY (SUC) reacted with H_2O_2 and were quenched by excess NEM. The concentrations of H_2O_2 remained in the NEM-quenched mixtures were determined by monitoring UV-Vis absorbance at 571 nm from the reaction product of H_2O_2, Amplex Red reagent and HRP with a standard curve. Representative UV-Vis spectra are shown in **(C)** and a bar graph showing enhanced H_2O_2 consumption with presence of CyaY is in (**D**). Student's t test (two-tailed) was used for statistical analysis (**$P < 0.01$) with the remained H_2O_2 percentages used for comparison.

CyaY redirects IscS sulfur transfer from protein acceptors to small molecules under presence of Fe^{2+}. By knowing CyaY inhibits sulfur transfer to protein acceptors under presence of Fe^{2+} and CyaY has no effect on IscS activity using the methylene blue assay, we hypothesized that the sulfur should be instead transferred to small molecules with thiol groups such as GSH in cell. However, the methylene blue assay wouldn't be a proper assay for probing cysteine turnover in physiological conditions as the assay utilizes excess non-physiological reductant DTT to rapidly cleave persulfide on IscS and generate sulfide. To further examine whether cysteine turnover by IscS are similar with or without presence of CyaY in a physiological-like condition containing low mM of GSH, we monitored concentration of the turnover product alanine instead. As one cysteine turns into alanine by IscS, the production rate of alanine represents the turnover rate of cysteine. Mixtures of IscS (0.5 μM), apo-IscU (50 μM), L-cysteine (150 μM), Fe^{2+} (250 μM), GSH (2.5 mM), with or without CyaY (0 or 5 μM) were reacted for 7 minutes before quenching with acid. The production rates of alanine are similar with (~4.96 ± 1.02 μM/min) or without (~4.26 ± 1.09 μM/min) CyaY (Figure 3.5A), suggesting CyaY has no significant effect on the overall cysteine turnover. As CyaY inhibits sulfur trafficking to protein acceptors, the only remain option for sulfur trafficking was GSH. When persulfide is transferred to GSH, the product should be GSSH. We confirmed the production of

GSSH by MS. A mixture of IscS (20 μM), IscU (50 μM), CyaY (30 μM), L-cysteine (150 μM), Fe^{2+} (200 μM), and GSH (150 μM) reacted for 12 minutes before quenching with NEM and analyzed by MS (Figure 3.5B). Aside from GSSH, reaction product of GSSH such as GSSG and GSSSG were also detected.

CyaY promotes antioxidation through generation of small molecule persulfide species. By knowing promotion of sulfur transfer to small molecules by CyaY, we further investigated if higher level of small molecule persulfide species by CyaY results in antioxidation. The effectiveness of antioxidation is dictated by the rate of H_2O_2 consumption. Mixtures contained Fe^{2+}, GSH, and L-cysteine without IscS, IscU, and CyaY (control), with IscS and IscU (SU), or with IscS, IscU, and CyaY (SUC) were incubated for 30 seconds under 37℃, followed by addition of H_2O_2. Upon adding H_2O_2, the concentrations of present components in the reaction mixtures were 250 μM Fe^{2+}, 1 mM GSH, 400 μM L-cysteine, 20 μM IscS, 80 μM IscU, 80 μM CyaY and 1 mM H_2O_2. H_2O_2 rapidly reacted with molecules with free thiols such as L-cysteine, GSH, and GSSH for 5 seconds. To quench the reaction, equal volume of 100 mM NEM were added to the reaction mixtures. The concentration of the remain H_2O_2 in the mixtures were analyzed by using the Amplex™ Red Hydrogen Peroxide/Peroxidase Assay Kit and tracking absorption at 571 nm. The results revealed that the remained H_2O_2 in SUC (222 ± 26 μM) was lower than SU (306 ± 17 μM)(Figure 3.5C-D), consistent with higher level of small molecule persulfide species by CyaY resulting in faster consumption of H_2O_2.

3.4. Discussion

Role of CyaY in Fe-S cluster assembly. Inhibition of Fe-S cluster assembly on IscU by CyaY *in vitro* was shown in literatures[81, 122, 183, 245]. Here, we reconfirmed the CyaY inhibition effect using CD spectroscopy (Figure 3.1). In literature, simultaneous binding of IscU and CyaY on IscS was demonstrated by SAXS and pull-down experiments[74, 126], while the NMR experiment indicated competition between IscU and CyaY on binding IscS[50]. Our native IM-MS results clearly demonstrated simultaneous binding of IscU and CyaY on IscS forming maximum $S_2U_2C_2$ complex. Also, our results are consistent with mutual binding promotion between IscU and CyaY to IscS (Figure 3.4D) and no effect of Fe^{2+} on the binding of $S_2U_2C_2$ (Figure 3.2C, right panel). To understand the molecular basis of CyaY inhibition, stepwise analysis from generation of sulfur adducts on IscS, sulfur transfer from IscS to IscU, [2Fe–2S] formation on IscU, and [2Fe–2S] formation on Grx4 were performed. At first, the sulfide detection cystiene desulfurase activity assay suggest insignificant effect of CyaY on IscS activity with the presence of IscU (Figure 3.1D, Figure 3.5A), consistent with previous reported results[81, 183] Also, stopped-flow spectroscopy results reveal CyaY have no effect on quinonoid decay, the rate limiting step in IscS PLP-chemistry, with the presence of IscU. Together, CyaY has no apparent effect on generation of sulfane sulfur on IscS. For the sulfur transfer step from IscS to IscU, we recently reported accelerated accumulation of sulfur adducts on apo-IscU when Fe^{2+} was present (~6 folds initial rate). Fe^{2+} binding on IscU active site stimulates sulfur transfer towards IscU and Fe-S cluster assembly[253]. When CyaY was added into the mixture of Fe^{2+}, IscS, apo-IscU, and L-cysteine, the sulfur accumulation on IscU significantly dropped (~0.3 fold initial rate, Figure 3.2A). Since CyaY had insignificant effect on generation of sulfur on IscS, the decrease of sulfur

accumulation on IscU should have been the result of decreased sulfur transfer from IscS to IscU. This inhibitory effect of CyaY on iron-stimulated sulfur transfer could be explained by either CyaY blocks Fe^{2+} binding on IscU active site or CyaY interfers sulfur transfer trajectory from IscS mobile loop cysteine to IscU active site. High resolution native MS results reveal similar binding stoichiometries of Fe^{2+} per SU or SUC complex, suggesting CyaY has no effect on Fe^{2+} binding on the IscU active site. Thus, the inhibitory effect was most likely from CyaY interferes the sulfur transfer trajectory. The inhibitory effect of CyaY on iron-stimulated sulfur transfer, which is an early step in an iron-first mechanism model we recently proposed[253], is consistent with literature results revealing CyaY reduced the initial reaction rate of cluster assembly[126].

CyaY was initially proposed as an iron donor due to its low to mid binding affinity for Fe^{2+} (K_d = 3-55 μM) and high binding affinity for Fe^{3+} ($K_{ass} = 10^{17}$ M^{-1}).[46, 143, 254] CyaY has been shown to oligomerize in the presence of iron, especially Fe^{3+}.[79, 142] *In vitro* studies show viable Fe-S cluster assembly when using iron-loaded CyaY.[46, 79] Yet no evidence clearly suggests iron-loaded CyaY directly transfer iron to IscU active site for cluster assembly as iron-loaded CyaY could also release free iron ions to solution for cluster assembly. On the other hand, the inhibition effect of CyaY on cluster assembly is against the iron donor role[81, 122, 183, 245]. *In vivo* studies show deletion of CyaY gene didn't cause major defect on Fe-S proteins under normal physiological conditions[123, 140], implying the major source of iron was not solely from CyaY. In this study, another result arguing against CyaY as the iron donor is provided. Presumably, an iron donor is supposed to enhance iron binding on IscS-IscU complex or deliver iron by binding IscS-IscU complex with higher affinity in iron-loaded form than apo form, but CyaY behaved neither of these characteristics. High resolution native MS analysis demonstrates similar binding

of iron on S_2U_2 and $S_2U_2C_2$ (Figure 3.2B). Native IM-MS analysis shows similar binding of CyaY on S_2 or S_2U_2 with or without iron (Figure 3.C). Overall, our results support CyaY's role in ISC machinery as restraining Fe-S cluster assembly instead of the iron donor.

I108M variant of IscU behaves like wild type. It had been shown by Dancis and co-workers that a single point mutation (M → I) on the scaffold protein ISCU in yeast can rescue all FXN deletion phenotypes via bypassing FXN i.e. M → I mutation on scaffold protein in eukaryotes can make the organism FXN independent[255, 256]. As deletion of CyaY has no effect under normal growth condition, *E. coli* is CyaY independent. This led to study by Roche *et al.* to determine if the reverse mutation I → M would render *E. coli* CyaY-dependent[257]. They showed that cellular iron sulfur cluster level decreased for I → M mutation in *E. coli* and was even worse in absence of CyaY. Recently we determined that $ISCU2^{M106I}$ bypasses FXN by accelerating cluster transfer to GRX5 in human system. Here, we did a similar step-wise analysis to study the effect of $IscU^{I108M}$ on each step in the presence and absence of CyaY. More specifically, we tested if $IscU^{I108M}$ slows down any step and whether CyaY rescues the rate. We found that $IscU^{I108M}$ variant behaved just like wild type in all the steps and the effect of CyaY on cluster assembly of scaffold protein was also similar for $IscU^{I108M}$ and wt-IscU, in other words, inhibitory rather than accelerating. Therefore, at present we still don't have a mechanism that explains the effect of I → M mutation on scaffold protein of *E. coli in vivo*.

The enigma: why CyaY restraining ISC Fe-S cluster assembly turns into increased Fe-S enzyme activities and alleviation of oxidative stress? CyaY benefits Fe-S enzyme activity of *E. coli* in rich media (such as LB) under aerobic conditions and decrease cell susceptibility of *S. enterica* under H_2O_2 stress.[123, 140] The effect of CyaY involves complex

interplay among Fe-S clusters, sulfur metabolism, iron metabolism, and oxidative stress. Here we discuss several major factors.

At first, CyaY redirects sulfur trafficking from IscS to reactive sulfane sulfur molecules. Enzymes utilize cysteine residues to catalyze protein-protein interactions, protein-DNA interactions, protein-lipid interactions, and permit binding of cofactors.[150] Oxidation of cysteine residues in enzymes (e.g., disulfide bond formation) leads to inactivation. Hence, organisms utilize two major redox regulation systems, Trx and GSH, to maintain an overall reduced environment for cysteine residues. Aside from scavenging H_2O_2, GSH also directly rescues oxidized cysteine residues.[150, 153] GSH gradually fails to keep cysteine residues reduced as oxidative stress enhances. Reactive sulfane sulfur on small molecules such as GSSH are proposed as strong antioxidants.[158] GSSH (persulfide thiol pKa ~ 6.2)[258] is significantly more deprotonated and more reactive than GSH (thiol pKa ~8.3)[259] in reducing disulfides and scavenging H_2O_2.[260, 261] Our results demonstrate CyaY redirects sulfur trafficking from protein acceptors to GSH and generates GSSH (Figure 3.5A-B), and thus accelerated the consumption of H_2O_2 (Figure 3.5C-D). Interestingly, the inhibition of sulfur transfer to TusA is consistent with an *in vivo* study on *E. coli* showing deletion of CyaY leads to thiolated-tRNA promoted lambda phage infection.[123]

Next, CyaY prevents generation of toxic labile iron ions from degradation of excess Fe-S clusters. The overall Fe-S cluster amount is determined by Fe-S cluster assembly and degradation. Oxidative stress and Fe-S cluster degradation promote each other as a vicious cycle. [4Fe–4S] clusters, which is often utilized as oxygen-sensing cofactors, are highly reactive to oxygen and reactive oxygen species (ROS).[162, 262] Oxidative degradation of [4Fe–4S] generates

[3Fe–4S] and Fe^{2+}, and [3Fe–4S] can further degrade to generate more free iron ions.[162] Free iron ions generated from cluster degradation catalyze propagation of ROS.[263, 264] To minimize ROS propagation by cluster degradation under oxidative stress, regulation of ISC pathway to prevent excess clusters is required. IscR, the transcription regulator of ISC pathway, suppresses *isc* operon when binding [2Fe–2S].[265, 266] *In vivo* studies demonstrating deletion strain of IscR, the transcription regulator of the ISC pathway which inhibits *isc* translation when binds [2Fe–2S], being hypersensitive to oxidative stress is consistent with the need of restraining ISC pathway to prevent oxidative stress propagation.[159, 267] Notably, the SUF pathway, which assembles Fe-S clusters under a protective mechanism and exists in part of bacteria such as *E. coli* and *S. enterica*, is activated by IscR under oxidative stress.[268] Under iron-replete conditions with oxidative stress, propagation of ROS is catalyzed and inhibition of IscR on *isc* transcription would likely not be as effective if Fe-S clusters degrade before [2Fe–2S] is transferred to IscR. Thus, direct inhibition of the ISC machinery is most likely required for preventing ROS propagation under iron-replete conditions. Our results clearly demonstrate CyaY inhibits ISC pathway from assembly to cluster maturation on Grx4 by blocking iron-induced sulfur transfer from IscS to IscU. As a result, we propose CyaY acts as an allosteric inhibitor of ISC machinery under iron-replete conditions, favoring Fe-S cluster maturation by alleviating cluster degradation and ROS propagation.

CyaY is also proposed to sequester toxic labile iron ions and potentially repair Fe-S clusters. Regulation of iron transportation and storage is crucial for organisms to keep labile iron ions under toxic threshold. The toxic threshold of iron ions decreases as ROS increases under oxidative stress, while essential need of iron still needs to be fulfilled. Thus, proteins store or

sequester iron ions for ROS protection and physiological usage are crucial for cell function under oxidative stress. *In vivo* studies on *S. enterica* suggests CyaY and Yggx bind iron ions and are involve in Fe-S cluster repair.[139, 140] CyaY deletion strain of *S. enterica* inhibited growth under H_2O_2 growth conditions, which was exacerbated when Yggx was also deleted.[140] Also, *E. coli* CyaY prevents the iron-mediated production of hydroxyl free radicals in the presence of H_2O_2 *in vitro*.[142] Notably, as wildtype *E. coli* favors Fe-S cluster maturation under iron-replete and aerobic condition compared to the CyaY deletion strain, a CyaY mutant strain lost interaction with IscS behaved similar to the CyaY deletion strain.[123] The same study also demonstrates that deletion of CyaY as well as iron storage proteins Dps, FtnA, FtnB, and Bfr leads to defect of Fe-S enzyme activities. This activity lost were partially compensated when only the iron storage proteins are deleted (CyaY still present) but compensated when only CyaY is deleted (iron storage protein still present, implying that CyaY partially substitute the function of iron storage proteins but not the other way. Together, literature evidence suggest CyaY sequestering iron ions contributes to part of its *in vivo* role, but the major effect comes from the involvement in ISC pathway.

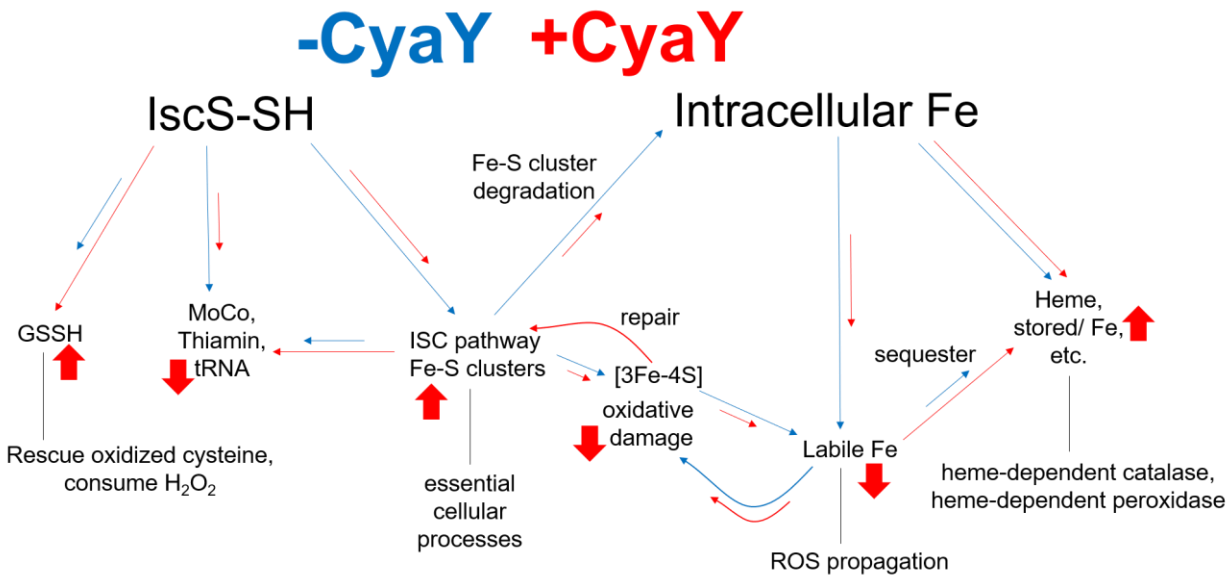

Figure 3.6 Model for the CyaY regulation of iron and sulfur trafficking. Sulfur trafficking (left side) and iron trafficking (right side) with (red thin arrow) or without (blue thin arrow) presence of CyaY are shown. The red wide arrows suggest the effect of CyaY (upwards: increase, downwards: decrease). Overall, CyaY regulation of sulfur and iron trafficking leads to alleviation of oxidative stress, thus benefits Fe-S clusters.

Here, we proposed a model explaining how CyaY regulates iron and sulfur trafficking to overall favor Fe-S clusters and alleviate oxidative stress in iron-replete environments (Figure 3.6). The major function of CyaY is restraining iron and sulfur being utilized by the ISC pathway. For sulfur trafficking from IscS, CyaY inhibited sulfur transfer to IscU and TusA (Figure 3.4A). Sulfur transfer to another acceptor Thil is likely also inhibited as Thil binding site on IscS also overlaps with IscU and CyaY.[170] Instead of transfer to protein acceptors, sulfane sulfur on IscS is transferred to GSH to generate antioxidant GSSH (Figure 3.5A-B). For intracellular iron utilization, CyaY inhibited iron being utilized by ISC pathway. Instead, iron can be stored, utilized by biosynthesis of heme, which is the prosthetic group of antioxidative enzymes such as catalases and peroxidases, or used by SUF pathway under oxidative stress. Interestingly, mitochondria-targeted *E. coli* CyaY

was able to complement the lost of Fe-S cluster enzyme activities and heme deficiencies of a yeast frataxin deletion, implying CyaY might favor heme biosynthesis.[269] Also, *Vibrio cholerae* CyaY binds heme.[270] Whether CyaY actually influences heme biogenesis in *E. coli* is unclear and further investigation is required. The free iron ions are overall decreased by CyaY, since CyaY sequesters iron ions and restrains ISC pathway to prevent generation of iron ions from damage of unprotected Fe-S cluster biosynthesis (ISC pathway) and excess [4Fe–4S]. The outcome of CyaY regulation as an allosteric inhibitor under iron-replete conditions overall increases antioxidants and decreases toxic labile irons, leading to alleviation of oxidative damage and protection of Fe-S clusters.

4. CONFORMATION LANDSCAPE OF HUMAN ISC MACHINERY REVEALED BY ION MOBILITY

4.1. Introduction

Iron-sulfur (Fe-S) clusters are essential inorganic cofactors found in proteins and enzymes amongst all domains of life. These cofactors function in processes such as oxidative respiration, DNA replication and repair, and catalytic transformations of substrates. Pathways for Fe-S cluster synthesis are often found in the cytosol of prokaryotic cells and mitochondria of eukaryotes [219, 271]. Although these cofactors are essential, the substrates required for their synthesis, S^{2-} and Fe^{2+}, contribute to oxidative stress through inhibition of respiratory complex IV [272] and escalation of Fenton chemistry [273], respectively. Consistently, there is emerging evidence that multiple layers of control regulate eukaryotic Fe-S cluster biosynthesis and that defects in this pathway lead to disease [274]. These regulatory mechanisms are still poorly understood and include the use of the allosteric activator protein frataxin (FXN) [56, 103, 136, 214, 226, 275], the metabolite sensing acyl-carrier protein (ACP) [101, 102, 276, 277], and post-translational control [278-280]. Elucidating the details of these mechanisms is critical for a holistic understanding of Fe-S cluster biosynthesis and may provide insights into therapeutic interventions for human disease.

Fe-S cluster synthesis within the eukaryotic mitochondrial matrix is facilitated by a multi-protein assembly complex. The sulfur-hub of the assembly complex exists as a stable subcomplex consisting of the pyridoxal 5'-phosphate (PLP) dependent cysteine desulfurase (NFS1) [281-283], a member of the eukaryotic-specific LYRM superfamily (ISD11) [88, 99, 100], and ACP [101, 102, 276]. This subcomplex generates a persulfide intermediate to transfer sulfane sulfur to the scaffold protein, ISCU2, where it is combined with Fe^{2+} and 2 electrons, provided by FDX1 or FDX2 [131, 284, 285], to

synthesize a $[2Fe–2S]^{2+}$ cluster [286]. The cysteine desulfurase complex is also implicated in sulfur trafficking for molybdenum cofactor biosynthesis and tRNA modifications [169]. A central focus for studies of the eukaryotic Fe-S cluster biosynthetic pathway has been to determine the mechanisms by which the Friedreich's ataxia protein FXN [111] accelerates Fe-S cluster assembly [56, 81, 103, 131, 133, 135, 136, 214, 226, 275, 286]. Although much is now known about the individual chemical steps that are accelerated by FXN, there is still much to learn about the structural basis and physiological purpose for this apparent FXN-based regulation.

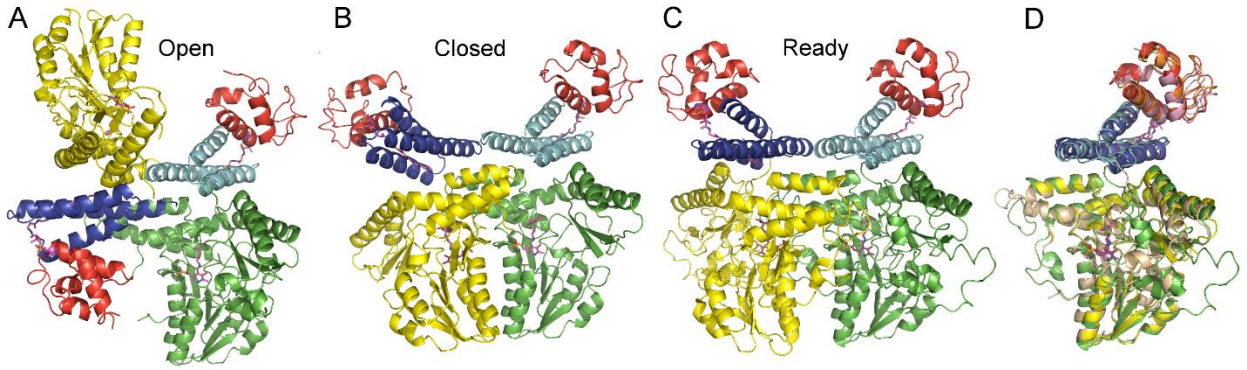

Figure 4.1 Comparison of different SDA_{ec} architectures. Structure of the SDA_{ec} complex in the **(A)** open, **(B)** closed, and **(C)** ready forms. NFS1 is shown in yellow and green, ISD11 in blue and cyan, and ACP_{ec} in red. The green/cyan/red protomer is shown in the same orientation for the different architectures. **(D)** Overlay of the subunits from one protomer for NFS1 (green, yellow, and wheat), ISD11 (cyan, blue, and purple), and ACP (red, orange, and pink) of the ready, closed, and open forms, respectfully. Protein cofactors are shown in magenta.

The first X-ray crystal structure of the human Fe-S cluster assembly subcomplex consisting of NFS1-ISD11 in complex with *E. coli* ACP (ACP_{ec}) revealed an architecture that was unexpected based on the prokaryotic IscS dimer (Figure 4.1A) and a possible explanation for the modest activity and requirement for FXN activation [101]. This "open" NFS1-ISD11-ACP_{ec} (herein called SDA_{ec}) assembly exhibited an $\alpha_2\beta_2\gamma_2$ quaternary structure with ISD11 molecules mediating

interactions between two NFS1-ISD11-ACP protomers (αβγ). Unlike the dimer interface in the prokaryotic IscS structure [74, 86] there were few direct interactions between the NFS1 subunits. A subsequent crystal structure revealed the SDA_{ec} complex can use an NFS1-NFS1 rather than an ISD11-ISD11 interface to generate a second, distinct, $\alpha_2\beta_2\gamma_2$ quaternary structure (Figure 4.1B) [102]. However, the NFS1-NFS1 dimer interface in this "closed" SDA_{ec} architecture differs from the IscS-IscS dimer interface; when the two-fold axes of the dimers are aligned, each NFS1 subunit is rotated by ~10° relative to the corresponding IscS subunit. Additional X-ray crystallography and cryo-electron microscopy (cryo-EM) studies revealed that the SDA_{ec} complex can also form a third "ready" architecture (Figure 4.1C) upon binding of ISCU2 ($SDA_{ec}U$) [102] or both ISCU2 and FXN ($SDA_{ec}UF$) [107]; the ready architecture uses the same interface between NFS1 subunits as is observed in the IscS dimer (Figure 4.2). Overall, the NFS1-ISD11-ACP_{ec} protomers are superimposable for the three forms (Figure 4.1D) but use different protein-protein interactions to generate the open, closed, and ready SDA_{ec} architectures.

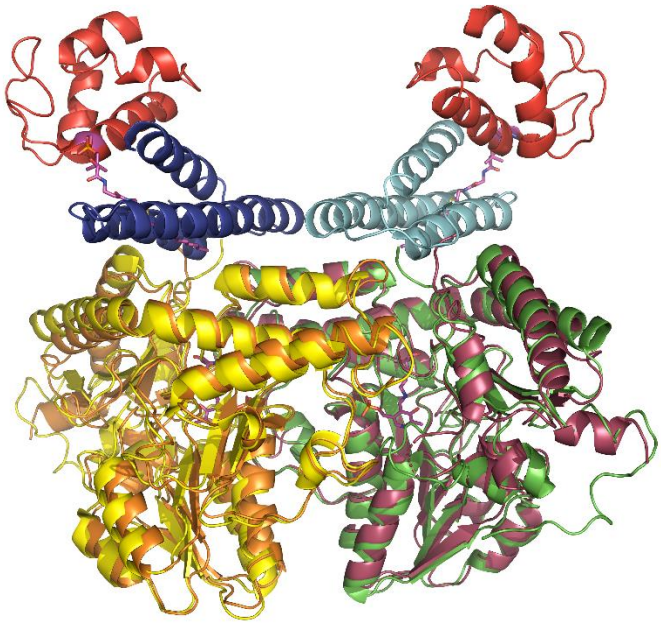

Figure 4.2 Comparison of the ready SDA_{ec} architecture with IscS. Structure of the SDA_{ec} in the ready form (oriented as in Figure 1C; NFS1 colored in green and yellow, ISD11 in blue and cyan, and ACP_{ec} in red) overlaid with IscS (subunits in orange and purple). Protein cofactors shown in magenta.

These different assemblies have raised questions regarding which quaternary structures are physiologically relevant. The similarity of the ready architecture with the prokaryotic system suggests that this may be the functional form for Fe-S cluster biosynthesis [60, 74, 102, 107]. However, the ready architecture provides no clear explanation for the functional requirement of ISD11, unlike the open architecture that depends on ISD11 for its association (Figure 4.1A). Moreover, the ready architecture does not easily explain the low activity and requirement of an activator for the eukaryotic Fe-S assembly system. It also does not explain additional differences from the prokaryotic system such as the distinct binding characteristics of accessory proteins with the respective cysteine desulfurases and opposing activation/inhibition effects of FXN homologs [81, 101, 121, 131, 132, 184, 287]. Interestingly, negative stain electron microscopy studies suggest the open

architecture is the predominant form of the SDA_{ec} complex [101]. In contrast, small-angle X-ray scattering (SAXS) and crosslinking mass spectrometry studies support the closed or ready form as the SDA_{ec} architecture in solution [102, 288]; notably, these studies did not evaluate the presence of the open form in their SDA_{ec} samples.

More recently, stopped-flow and radiolabeling studies revealed that the mobile S-transfer loop of NFS1 is functionally linked to FXN activation [214], which led to the hypothesis that FXN binding activates the complex by inducing a switch between different architectures that are in equilibrium. However, there is currently no evidence that multiple architectures exist simultaneously in solution, that they are in equilibrium, or that this equilibrium can be shifted by FXN binding. The lack of understanding of the conformational landscape for the SDA_{ec} complex warrants additional studies to determine the functional significance and relationship between the open, closed, and ready architectures, which is necessary to provide a clear picture of accessory protein interactions and mechanistic steps in Fe-S cluster biosynthesis. Here we use a variety of functional and biophysical approaches to interrogate solution states of the SDA_{ec} complex and provide key results that point towards architectural swapping as an additional regulatory mechanism that appears to be linked to FXN activation of the human Fe-S cluster biosynthetic complex.

4.2. Experimental procedures

Protein and Purification

Preparation of SDA_{ec}. The NFS1(Δ1-55)-ISD11(S11A)-ACP_{ec} (SDA_{ec}) was prepared following the published procedures describing the open [101] and closed [102] architectures. The two

procedures used identical expression constructs that encode an N-terminal His_6 tag on NFS1, which was not cleaved unless indicated. The two preparation methods differed in expression conditions, using auto-induction (AI conditions) [101] or Terrific broth (TB conditions) [102] media, and slightly different purification procedures. A tobacco etch virus (TEV) protease cleavage site was introduced by mutagenesis into the original NFS1 plasmid to generate material with a cleavable His_6 tag. To generate cleaved SDA_{ec}, the purification was conducted as previously described [101] with a 4 °C overnight TEV cleavage step introduced after the cation exchange column. The digested product, which contained a single glycine residue before residue 56, was loaded onto a Ni-NTA column (5 mL; GE Healthcare) to remove the TEV protease. To generate ^{15}N-labeled SDA_{ec}, 2 – 6 liters of N-5052 auto-induction media [289] were inoculated with 8 mL of an overnight LB starter culture. The ^{15}N-SDA_{ec} complex was purified as previously described [101] except that supplemental pyridoxal 5'-phosphate was not added during the preparation. The QuikChange protocol (Agilent) was used to separately introduce the R68L substitution into the ISD11 plasmid (pACYDuet-1) and the Q64S L299H P300Q substitutions into the NFS1 plasmid (pet-15b) [101]. SDA_{ec} variants were purified using the same protocol as the native enzyme complex. The concentrations for the SDA_{ec} complexes were determined using an extinction coefficient of 10.9 mM^{-1} cm^{-1} at 420 nm.

Preparation of ISCU2. A MEGAWHOP protocol [290] was used to incorporate a TEV protease site and glutathione S-transferase (GST) into a pET-30a(+) vector containing ISCU2 (Δ1-35) and generate the C-terminally tagged construct *ISCU2-TEV-GST*. Further mutagenesis was used to incorporate a C-terminal His_6 tag to generate the *ISCU2-TEV-GST-*His_6 construct. The *ISCU2-TEV-GST* plasmid was transformed into the E. coli strain BL21(DE3) for expression.

Cells were grown at 37 °C to an OD_{600} of 0.5. Protein expression was induced with 0.1 mM isopropyl β-D-1-thiogalactopyranoside (IPTG) at 18 °C. Cells were grown overnight, harvested by centrifugation the following morning, and stored in a -80 °C freezer until use. The cell pellet from a 9 L culture was thawed and resuspended in GST buffer A (50 mM Hepes, 150 mM NaCl, pH = 7.8). Lysozyme (20 mg, Sigma-Aldrich) and protease inhibitor cocktail (20 mg, Sigma-Aldrich) were added to the suspension. The cells were lysed by 2 cycles of French press at 18,500 psi. Cell debris was cleared by centrifugation at 16,420 RCF for 30 min. The clarified lysate was loaded onto a manually packed GST-column (Prometheus) at 4 °C. Bound protein was eluted with GST buffer B (50 mM Hepes, 150 mM NaCl, 10 mM glutathione (GSH), pH = 7.8). The TEV digestion was conducted overnight at 4 °C and the products were loaded onto a Ni-NTA column (5 mL; GE Healthcare) to remove the TEV protease. The flow-through from the Ni-NTA column was concentrated to 20 mL, diluted to 150 mL with cation A buffer (50 mM Hepes, pH = 7.8), and loaded onto a cation exchange column (27 mL; POROS 50HS, Applied Biosystems) and eluted with a linear gradient of NaCl (0 – 1 M). The fractions containing ISCU2 were concentrated, brought into an anaerobic Mbraun glovebox (~12 °C, <1 ppm O_2 as monitored by a Teledyne model 310 analyzer), and supplemented with 5 mM D,L-dithiothreitol (DTT) before loading onto a HiPrep 26/60 Sephacryl S100 HR column (GE Healthcare Life Sciences) equilibrated in size exclusion buffer (50 mM Hepes, 150 mM NaCl, pH = 7.5). The fractions corresponding to monomeric ISCU2 were collected, concentrated, and flash-frozen in liquid nitrogen for storage at -80 °C until use. For the *ISCU2-TEV-GST-His_6* construct, the same procedure was used except that the cation exchange step was skipped. Concentration was

determined using an extinction coefficient of 9970 $M^{-1}cm^{-1}$ at 280 nm as estimated by ExPASy ProtParam [291].

Preparation of FXN. The FXN (Δ1-81) gene was subcloned into a pET-28a(+) vector containing *His_6-GST-TEV-CyaY* [81] using the MEGAWHOP [290] protocol to generate a *His_6-GST-TEV-FXN* construct. Protein expression was conducted similar to that used for the *ISCU2-TEV-GST-His_6* construct. The cell pellet from a 3 L culture was thawed and resuspended in GST buffer A. Cell lysis and the initial GST column, TEV cleavage, and Ni-NTA column clean-up steps were performed similarly to the ISCU2 preparation. The flow-through fractions were collected, concentrated, and loaded onto a HiPrep 26/60 Sephacryl S100 HR column equilibrated in size exclusion buffer. Fractions containing FXN were pooled, concentrated, frozen in liquid nitrogen, and stored at -80 °C until use. Concentration was determined using an extinction coefficient of 26,930 M^{-1} cm^{-1} at 280 nm as estimated by ExPASy ProtParam [291].

Preparation of IscU and IscS. The *E. coli* proteins IscU and IscS were expressed and purified as previously described [81]. The extinction coefficient of 6.6 mM^{-1} cm^{-1} at 388 nm was used to estimate the concentration of the PLP cofactor, which represented the concentration of active IscS, in 0.1 M NaOH. The extinction coefficient of 11,460 M^{-1} cm^{-1} at 280 nm was used to estimate the concentration of IscU.

Activity Measurements of Purified Complexes

To determine the cysteine desulfurase activity, the methylene blue assay was conducted as previously described [101] in assay buffer (50 mM Hepes, 250 mM NaCl, pH = 7.5). Reaction mixtures of 800 µL containing the following components: 0.5 µM SDA_{ec} (or the SHQ variant),

1.5 µM ISCU2, 1.5 µM FXN, 4 mM D,L-DTT, and 5 µM $(NH_4)_2Fe(SO_4)_2$ were incubated at 37 °C for 15 min before the addition of varying amounts of L-cysteine. Reactions were quenched after 6 mins and the sulfide was quantified as previously described. The sulfide formation rate for each L-cysteine concentration was measured at least in triplicate. Data were fit using KaleidaGraph (Synergy Software) to a traditional Michaelis-Menten equation. The errors in the Michaelis-Menten parameters represent errors in the fit to the experimental data. FXN binding was evaluated as previously described [292].

Preparation of the SDA_{ec} Complex for Small-Angle X-ray Scattering

Purified AI-prepared SDA_{ec} was injected onto a Superdex 200 10/300 GL column (S200, GE Healthcare Life Sciences) equilibrated in 50 mM Hepes, 250 mM NaCl, pH = 7.2 to remove any aggregates from the freeze/thaw cycle of the sample. Yellow fractions were collected, pooled, and concentrated to approximately 10 mg/mL. Dialysis buttons (Hampton Research) were loaded with 50 µL of sample and sealed with a 3.5 kDa dialysis membrane disc (Hampton Research, Spectrum) that had been washed thoroughly with Milli-Q H_2O. Samples were then dialyzed in a variety of buffers within 50 mL falcon tubes overnight at 4 ^oC before dilution within a 96-well plate. High salt conditions were defined as 100 mM sodium phosphate, 500 mM NaCl, 2% glycerol, 2 mM TCEP, pH = 8.0. Low salt conditions were defined as 50 mM Hepes, 250 mM NaCl, 2 % glycerol, 2 mM TCEP, pH = 7.5. The 96-well plate containing samples was sealed and shipped wrapped in ice packs to the SIBYLS beamline (12.3.1) at the Advanced Light Source (ALS). The plate was stored at 4 ^oC and was centrifuged at 3700 rpm for 10 minutes before data collection. Data collection parameters can be found in Table 4-1.

Table 4-1 Small-angle X-ray scattering data collection parameters.

	SDA_{ec}
Organism	*H. sapiens* , *E* . coli
Source	Recombinant
Source of Data	This work
Theoretical Mw, excluding cofactors (kDa)	133 kDa
Sample concentrations (mg/mL)	1, 2, 4
Sample buffer	100 mM phosphate 500 mM NaCl 2% glycerol 2 mM TCEP pH = 8.0
Instrument/data processing	SIBYLS ALS 12.3.1
q range ($Å^{-1}$)	0.011-0.565
Wavelength (Å)	1.27
Cell thickness (mm)	1.5
Sample to detector distance (m)	1.5
Temperature (^{o}C)	10
Exposure time (sec)	10
Delta/time slicing	Every 0.3 seconds
Total frames	32

Small-Angle X-ray Scattering Data Collection and Analysis

Individual buffers and frames were analyzed for consistency. Buffers with the same composition and scattering profile were averaged using the ATSAS 2.8.4 [293] package to generate an average buffer scattering curve. Sample frames were then individually subtracted from the averaged buffer in the RAW 1.5.1 package [294, 295]. Subtracted frames were then averaged in RAW at different time points to determine the onset of radiation damage. Exposure times which included the least amount of radiation damage were used for further analysis. The low q region was truncated based on Guinier analysis, and the high q region was truncated to $8/R_g$ prior to the pair distribution analysis. Additional information regarding Guinier analysis, pair-distribution function analysis, and curve fitting can be found in Table 4-2 and Table 4-3. We used the same

procedure for the reanalysis of the Markley and Cygler/Lill SAXS data except that the scattering curve was truncated in the Guinier region due to significant aggregation [102] or interference from the beamstop [288]. Because the crystal structures of the open [101] and closed [102] SDA_{ec} architectures lacked a significant number of non-hydrogen protein scatterers due to disordered regions in crystal structures (17.2% and 31.6%, respectively), we generated more complete models for calculating SAXS profiles by overlaying the NFS1-ISD11-ACP protomers (αβγ) of the cryo-EM ready form [107] onto the open and closed architectures. The model for the ready architecture was generated by removing the ISCU2 and FXN subunits from the cryo-EM $SDA_{ec}UF$ structure [107].

Table 4-2 SAXS parameters for the AI-prepared SDAec under high salt conditions compared to previous data.

	†SDA_{ec}	SDA_{ec}	SDA_{ec}	SDA_{ec}	SDA_{ec}
Data source	This manuscript	This manuscript	This manuscript	This manuscript	Markley (42)
Sample concentration (mg/mL)	1	2	4	Merged	N/A
Exposure time (sec)	1.5	1.5	0.6	0	N/A
Merged regions				1:(0.0109 - 0.07) 2:(0.1001 - 0.3202)	
Guinier analysis:					
I(0)	31.4 ± 0.2	82.1 ± 0.2	194.0 ± 0.4	2	904.6 ± 8.9
q range ($Å^{-1}$)	0.015-0.035	0.018 - 0.034	0.014 - 0.033	0.015-0.035	0.017 - 0.036
R_g (Å)	36.88 ± 0.25	37.71 ± 0.13	39.69 ± 0.12	36.88 ± 0.25	36.27 ± 0.47
qR_g range	0.565 - 1.285	0.662 - 1.293	0.542 - 1.294	0.565 - 1.285	0.619 - 1.290
R^2	0.993	0.998	0.999	0.993	0.995
P(r) analysis:					
I(0)	31.6 ± 0.2	82.3 ± 0.2	194.5 ± 0.4	80.8 ± 0.32	923.9 ± 7.6
R_g (Å)	37.50 ± 0.22	38.17 ± 0.12	40.56 ± 0.12	37.07 ± 0.16	37.63 ± 0.38
d_{max} (Å)	127	129	144	128	124
q range ($Å^{-1}$)	0.0153 - 0.2171	0.0176-0.2121	0.0137-0.2015	0.0153 - 0.2171	0.0171 - 0.2200
χ^2 (total estimate from GNOM)	1.12	1.08	1.15	0.99	0.99
Mw analysis (Vc method, kDa)‡	134	129	139	126	139

†High ionic strength (100 mM sodium phosphate, 500 mM NaCl, 2% glycerol, 2 mM TCEP, pH = 8.0) data
N/A = not available
‡The high-angle data was truncated to 0.320 $Å^{-1}$ to maintain a consistent integration area.

Table 4-3 SAXS parameters for the AI-prepared SDAec under low salt conditions compared to previous data.

	†SDA_{ec}	SDA_{ec}	SDA_{ec}	SDA_{ec}	SDA_{ec}	SDA_{ec}
Data source	This manuscript	This manuscript	This manuscript	Cygler/Lill (15)	Cygler/Lill (15)	Cygler/Lill (15)
Sample concentration (mg/mL)	1.0	2.0	4.0	1.32	2.65	5.29
Guinier analysis:						
q range ($Å^{-1}$)	0.013-0.032	0.014 - 0.028	0.014 - 0.025	0.014 - 0.030	0.012 - 0.028	0.017 - 0.026
R_g (Å)	39.89 ± 0.24	44.86 ± 0.18	51.48 ± 0.13	42.99 ± 0.29	45.65 ± 0.13	50.72 ± 0.18
qR_g range	0.52 - 1.28	0.62 - 1.24	0.73 - 1.28	0.62 - 1.30	0.57 - 1.30	0.87 - 1.30
R^2	0.997	0.998	0.999	0.996	0.999	0.999
P(r) analysis:						
R_g (Å)	40.31 ± 0.19	45.54 ± 0.12	53.30 ± 0.15	44.18 ± 0.27	46.56 ± 0.18	52.15 ± 0.15
d_{max} (Å)	132	154	189	142	158	177
q range ($Å^{-1}$)	0.014 - 0.200	0.014-0.178	0.014-0.155	0.0143 - 0.1863	0.0124 - 0.1754	0.0171 - 0.1575
χ^2 (total estimate from GNOM)	1.04	1.39	1.48	0.90	0.76	1.01
Mw analysis (Vc method, kDa)‡	167	178	220	180	189	233

† Low ionic strength (50 mM Hepes, 250 mM NaCl, 2% glycerol, 2 mM TCEP, pH = 7.5) data

‡ The high-angle data was truncated to 0.320 $Å^{-1}$ to maintain a consistent integration area.

Crystallization of SDA_{ec} from Different Preparation Methods

The open and closed forms of SDA_{ec} were crystallized as previously described [101, 102] using the AI-preparation and TB-preparation methods, respectively. A hanging-drop vapor diffusion method was used that included 500 µL of crystallization solutions in the well and a 4 µL drop (2µL protein: 2µL crystallization solution) on the coverslip. To crystallize AI-prepared SDA_{ec} in the closed form, the protein complex was buffer exchanged into 10 mM BIS-TRIS (pH 5.5), 200 mM NaCl, 20 mM KCl, 2 mM NaH_2PO_4, 2 mM Na_2HPO_4, 5 % (vol/vol) glycerol, 1 mM D,L-DTT, and 75 mM imidazole by multiple rounds of concentration and dilution using a Vivaspin 500 100 kDa spin concentrator (GE Healthcare). To crystallize TB-prepared SDA_{ec} in the open form, the protein complex was either buffer exchanged into 50 mM Hepes, 250 mM NaCl, 10 % glycerol, pH = 7.5 or injected onto a Superdex 200 10/300 GL column (S200, GE Healthcare Life Sciences) equilibrated in 50 mM Hepes, 250 mM NaCl, 10 % glycerol, pH = 7.5. The AI-prepared SDA_{ec} (177 µM) was crystallized in the open architecture at 22 °C with

crystallization conditions generated by adding 5 mL of 40% acetone to 11.25 mL of 0.1 M CBTP (pH = 6.4), 0.3 M CsCl, 0.2 M D,L-allylglycine, 5 mM TCEP, and 8% PEG 3350. The AI-prepared SDA_{ec} (177 μM) without D,L-allylglycine was crystallized in the open architecture at 22 °C with crystallization conditions generated by adding 1.25 mL of 40 % acetone to 11.25 mL of 0.1 M CBTP (pH = 6.4), 0.3 M CsCl, 5 mM TCEP, and 8 % PEG 3350. The AI-prepared SDA_{ec} (220 μM) and the TB-prepared SDA_{ec} (226 μM) were crystallized in the closed architecture at 12 °C using a crystallization solution of 0.1 M MES (pH = 6.5), 0.3 M ammonium acetate, 0.02 M calcium acetate hydrate, 0.02 M calcium chloride dihydrate, and 15% isopropanol. The TB-prepared SDA_{ec} (177 μM) was crystallized in the open architecture at 22 °C using a crystallization solution of 0.1 M CBTP (pH = 6.4), 0.2 M CsCl, 0.2 M D,L-allylglycine, 5 mM TCEP, 10 % PEG 3350, and 4 % acetone.

X-ray Data Collection, Indexing, and Unit Cell Determinations

Single crystals of SDA_{ec} in the open architecture were harvested and cryo-protected as previously described [101] using a final concentration of 20 % (vol/vol) PEG 400. Crystal trays of SDA_{ec} in the closed architecture were transferred to a 17 ^{o}C room where single crystals were harvested and cryo-protected as previously described [102]. Diffraction data were collected using a rotating anode Cu K-α source and a Rigaku R-AXIS IV detector. Specifically, two images for each crystal form were collected at $2\Theta = 0^{o}$ and 90^{o} at a temperature of 120 K with an exposure time of 6 minutes, detector distance ranging from 200 to 250 mm, and an oscillation angle ranging from 0.5^{o} to 0.2^{o} depending on the diffraction quality. Indexing was performed with

iMosflm [296] version 7.2.2 from the CCP4 [297] package. The unit cell parameters were automatically chosen by iMosflm.

Activity Analysis of Single Crystals

Crystals of SDA_{ec}, in either form, were harvested from four separate drops. Wash solution (10 µL of assay buffer) was first added to each drop and then the crystals were transferred to a 200 µL solution of assay buffer. Single crystals from the 200 µL drop were transferred to a seeding tool where the crystals were crushed to generate a slurry. The slurry was brought into an anaerobic glovebox where the activity measurements were conducted. A total of six alternating reactions (150 µL) with and without the additional subunits and Fe^{2+} were performed by mixing 20 µL of crystal slurry, additional subunits (3 µM), Fe^{2+} (10 µM), and D,L-DTT (4 mM) together and incubating at 37 ^{o}C for 15 minutes. The reactions were initiated by the addition of L-cysteine to a final concentration of 1 mM. A quench solution of 37.5 µL of a 1:1 mixture of 20 mM *N*,*N*-dimethyl-p-phenylenediamine in 7.2 N HCl and 30 mM $FeCl_3$ in 1.2 N HCl was added to the mixture after 10 minutes. Sulfide concentration was determined as described above. A total of two independent triplicate runs were conducted totaling six measurements for each sample.

Native Mass Spectrometry Experiments

Native mass spectrometry (Native MS) was performed on two instruments for different purposes: an Exactive Plus with extended mass range (EMR) Orbitrap MS (Thermo Fisher Scientific, San Jose, CA) for high-resolution measurements or a Synapt G2 instrument (Waters

Corporation, U.K.) equipped with an 8k RF generator for ion mobility measurements. Gold-coated tips prepared using a Sutter 1000 were used for nano-electrospray ionization experiments [298]. Fresh protein samples including SDA_{ec}, ISCU2, FXN, IscS, and IscU were buffer exchanged into 200 mM ammonium acetate (pH = 8.5) using Micro Bio-Spin 6 Columns (Bio-Rad). Experimental and expected masses can be found in Table 4-4. All calculated masses excluded the N-terminal methionine (if present in the sequence). The calculated masses of SDA_{ec} and SDA_{ec} complexes included the mass of the covalently attached PLP and the assumed mass of the acyl-4'PPT ACP_{ec} was 523 Da. Masses of SDA_{ec}/SDA_{ec}U/SDA_{ec}UF/ISCU2/FXN were measured under native conditions (200 mM ammonium acetate, pH = 8.5). Masses of SDA_{ec} subunits were also measured under denaturing conditions (1% formic acid). All masses are measured using EMR.

Table 4-4 Calculated and measured masses for SDAec species.

Species	Calculated Mass (Da)	Measured Mass (Da)	Measured Mass range
^{14}N-untagged SDA_{ec}	129097	129265 ± 64	129201−129329
^{15}N-untagged SDA_{ec}	130693	130838 ± 70	130768−130908
^{14}N-untagged SDA_{ec}U	159521	159708 ± 99	159609−159807
^{15}N-untagged SDA_{ec}U	161117	161285 ± 130	161155−161415
^{14}N-untagged SDA_{ec}UF	187997	188175 ± 97	188078−188272
^{15}N-untagged SDA_{ec}UF	189593	189770 ± 124	189646−189894
^{14}N-tagged SDA_{ec}	134135	134235 ± 76	134159−134311
^{15}N-tagged SDA_{ec}	135809	135892 ± 72	135820−135964
^{14}N-tagged SDA_{ec}U	164559	164880 ± 193	164687−165073
^{15}N-tagged SDA_{ec}U	166233	166596 ± 181	166415−166777
^{14}N-tagged SDA_{ec}UF	193035	193329 ± 212	193117−193541
^{15}N-tagged SDA_{ec}UF	194709	195004 ± 155	194849−195159
SDA_{ec}_SHQ	134149	134259 ± 69	15203−15219
ISCU2-Zn	15212	15211 ± 8	14231−14245
FXN	14238	14238 ± 7	134190−134328
Species	**Subunit**		

^{14}N-untagged SDA$_{ec}$	S	44717	44716 ± 17	44700−44734
	D	10611	10610 ± 12	10599−10623
^{15}N-untagged SDA$_{ec}$	S	45273	45262 ± 18	45255−45291
	D	10760	10757 ± 11	10749−10771
^{14}N-tagged SDA$_{ec}$	S	47197	47194 ± 18	47179−47215
	D	10611	10610 ± 12	10599−10623
^{15}N-tagged SDA$_{ec}$	S	47792	47785 ± 18	47774−47810
	D	10760	10758 ± 11	10749−10771
SDA$_{ec}$_SHQ	S	47211	47208 ± 28	47183−47239
	D	10611	10611 ± 13	10598−10624

*Errors of masses are estimated from full width at half maximum.

Protomer Exchange Experiment Using Native Mass Spectrometry

Protomer exchange experiments were performed on an EMR Orbitrap MS. The high resolution of EMR gives resolved peaks between subunit mixtures for quantification purposes. Instrument parameters were tuned to minimize collisional activation while retaining reasonable signal to noise. The mass spectrometer parameters used were set as: m/z range 3000-10000, capillary temperature 200-300 °C, S-Lens RF level 200, source DC offset 25 V, injection flatapole DC 16 V, inter flatapole lens DC 12 V, bent flatapole DC 7-12 V, transfer multipole DC offset 7-10 V, C-trap entrance lens tune offset 0 V, trapping gas pressure setting 7, in-source dissociation voltage 0 eV, HCD collision energy 10 eV, FT resolution 8750–35000, positive ion mode, and ion maximum injection time 50–200 ms. For SDA$_{ec}$ exchange experiments, a 1:1 ratio of ^{15}N-SDA$_{ec}$ and ^{14}N-SDA$_{ec}$ were mixed to initiate the exchange reaction. For subunit exchange of SDA$_{ec}$U, ^{15}N-SDA$_{ec}$ and ^{14}N-SDA$_{ec}$ were incubated with ISCU2 distinctly using a 1:3 ratio for 30 min to form ^{15}N-SDA$_{ec}$U and ^{14}N-SDA$_{ec}$U complexes ($\alpha_2\beta_2\gamma_2\delta_2$). These complexes were mixed in a 1:1 ratio to initiate the exchange reaction. For exchange of SDA$_{ec}$UF, ^{15}N-SDA$_{ec}$ and

^{14}N-SDA$_{ec}$ were incubated with ISCU2 and FXN distinctly using a 1:3:3 ratio for 30 minutes to form ^{15}N-SDA$_{ec}$UF and ^{14}N-SDA$_{ec}$UF complexes ($\alpha_2\beta_2\gamma_2\delta_2\varepsilon_2$). ^{14}N-SDA$_{ec}$UF and ^{15}N-SDA$_{ec}$UF were mixed in a 1:1 ratio to initiate the exchange reactions. Exchange of tagged IscS and untagged IscS was also investigated using a 1:1 ratioFor subunit exchange of IscS-IscU, tagged IscS and untagged IscS were incubated with IscU distinctly using a 1:3 ratio for 30 minutes to form untagged IscS-IscU and tagged IscS-IscU complexes ($\alpha_2\beta_2$). The exchange react90j was initiated by mixing untagged IscS-IscU and tagged IscS-IscU complexes at a 1:1 ratio. At various time points, aliquots (4 uL) were taken for native MS analysis. Each spectrum was taken for 20 seconds. The initial MS data were collected using the Thermo Exactive software under the RAW format. The protein species were deconvoluted using the software program UniDec [212]. All the exchange experiments were performed under room temperature.

Cation Exchange Column Separation of SDA$_{ec}$ Species.

For untreated samples, the protein was thawed rapidly and diluted to 60 µM with 50 mM HEPES, 250 mM NaCl, 10 % glycerol, pH 7.5. The sample was diluted in half with cation buffer A (50 mM HEPES, 20 mM NaCl, 2 % glycerol, pH 8.0) to a final concentration of 30 µM. For samples containing L-cysteine (Sigma-Aldrich), a 100 mM stock solution of L-cysteine was prepared by dilution of 12.1 mg of powder in 1 mL of cation buffer A. A portion of this stock was used to dilute a 60 µM protein sample along with additional buffer A to produce a sample containing 30 µM protein and 10 mM L-cysteine. The substrate treated sample was allowed to incubate for approximately 10 minutes before analysis.

Samples (1 mL) were injected onto a Mono S 5/50 GL (GE Healthcare) column using either a BioRad Quest or an AKTA FPLC (at the BioCAT (18ID) beamline at Advanced Photon Source) and eluted using a step gradient of cation buffer B (50 mM Hepes, 1 M NaCl, 2 % glycerol, pH 8) with steps at 15 %, 30 %, and 100 %. For equilibrium experiments, the peak selected for isolation was concentrated to ~400 – 500 µL using a 100 kDa cutoff Vivaspin 500 (GE Healthcare) by centrifugation at 10,000 RCF. The remaining sample was diluted to 1 mL with cation buffer A and reinjected and eluted using the same procedure. All experiments were performed at room temperature.

Ion-mobility Mass Spectrometry of SDA_{ec}/$SDA_{ec}U$/$SDA_{ec}UF$

Native ion-mobility mass spectrometry (Native IM-MS) was performed on a Synapt G2 instrument. Instrument parameters were tuned to maximize ion intensity but simultaneously preserve the native-like state of proteins as determined by IM. The instrument was set to a capillary voltage of 1-1.5 kV, source temperature of 30 °C, sampling cone voltage of 10 V, extraction cone voltage of 1 V, trap and transfer collision energy off, and backing pressure (5 mbar), trap flow rate at 8 ml/min, He cell flow rate at 200 ml/min, IMS flow rate at 50 ml/min. The T-wave settings for trap (310 ms^{-1}/6.0 V), IMS (250 ms^{-1}/9-12 V) and transfer (65 ms^{-}1/2 V), and trap bias (25.0 V). MassLynx 4.1 (Waters) and Pulsar were used to deconvolute all recorded mass spectra [299]. A sodium iodide solution was used to externally calibrate mass spectra. Experimental collisional cross-section (CCS) of ^{14}N tagged SDA_{ec} (134.2 kDa), ^{14}N untagged SDA_{ec} (129.3 kDa), $SDA_{ec}U$ (using ^{14}N tagged SDA_{ec}, 164.9 kDa), $SDA_{ec}UF$ (using ^{14}N tagged SDA_{ec}, 193.3 kDa) were determined following a well-documented protocol and a CCS database [300, 301]. Calibration curves

(R^2 >0.978) were generated by using solutions of transthyretin (55.6 kDa), concanavalin A (103.0 kDa), and pyruvate kinase (237 kDa). Parameters for calculating the CCS using the online projected superposition approximation (PSA) webserver (psa.chem.fsu.edu) were set as follows: buffer gas of nitrogen, a temperature of 298 K, projection accuracy of 0.01, projection integration accuracy as 0.009, shape accuracy as 0.01, shape maxiter as 25, and shape meshfactor as 1 [302-304]. The models used for calculating the CCS were generated as described above.

4.3. Results

The SDA_{ec} Preparation Method Does Not Affect Activity. We first investigated if different preparation methods for the SDA_{ec} complex affected the activity profile of the enzyme. Identical constructs but slightly different expression and purification conditions were used to produce the SDA_{ec} complex that was previously crystallized in the open and closed forms [101, 102]. The open form was expressed in cells growing in an auto-induction media (herein named AI) [101], whereas the closed-form was induced in cells growing in a rich Terrific broth media (herein named TB) [102]. The purification of the AI-prepared SDA_{ec} complex also includes additional steps. The SDA_{ec} samples prepared by these different methods did not have major differences in catalytic properties when assayed under activated conditions (Figure 4.3). SDA_{ec} prepared under the AI conditions had a k_{cat} of 9.3 ± 0.5 min^{-1} and a K_M for cysteine of 22 ± 5 μM. When prepared under the TB conditions, SDA_{ec} had a k_{cat} of 11 ± 0.4 min^{-1} and a K_M for cysteine of 20 ± 3 μM. These kinetic constants were consistent with each other and with previous reports [81, 101, 103], suggesting that the method of preparation does not influence the activity profile of the SDA_{ec} sample.

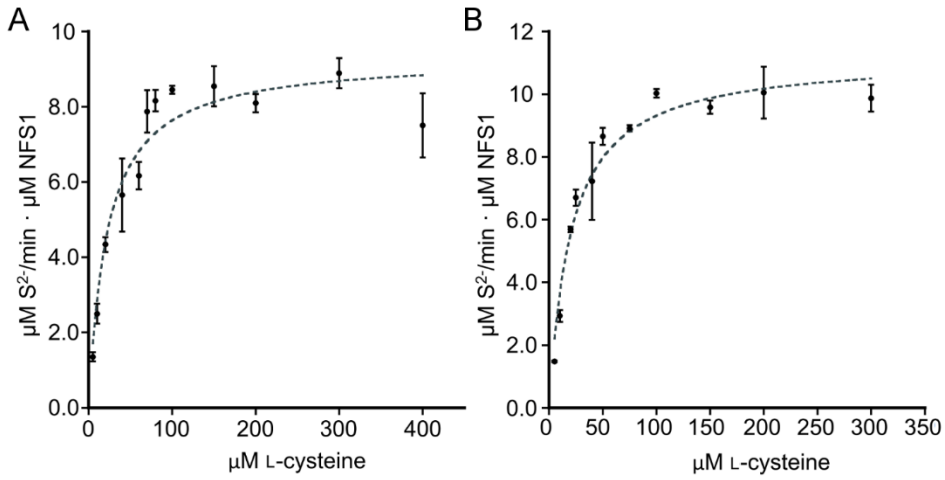

Figure 4.3 SDA_{ec} complexes prepared using different expression conditions exhibit similar kinetics for cysteine turnover. SDA_{ec} (0.5 μM) prepared using the (A) AI and (B) TB conditions was assayed in the presence of ISCU2 (1.5 μM), FXN (1.5 μM), Fe^{2+} (5 μM) and D-L-DTT (4 mM). Error bars are replicate errors (n = 3). The dashed lines through the data are the fits to the Michaelis-Menten equation.

Small-angle X-ray Scattering of SDA_{ec}. We then investigated if the different SDA_{ec} preparation methods affected the solution conformation. SAXS curves of the AI-prepared SDA_{ec} sample were collected, evaluated, and then compared with previously analyzed SAXS samples generated with different preparation methods [102, 288]. We found that a high ionic strength buffer containing glycerol and TCEP maximized the stability of the complex and reduced concentration-dependent aggregation (Figure 4.4A). Kratky plots of the scattering indicated that the samples were folded (Figure 4.4B); however, we still observed minor concentration-dependent aggregation based on the behavior of the low q region of the scattering curve (Figure 4.4A, inset) and the Guinier analysis (Figure 4.4B, inset), as well as a concentration-dependent increase in D_{max} in the pair distribution function (Figure 4.4C). Due to these observations, we analyzed the lowest concentration sample, which provided a smooth pair distribution function, a D_{max} approximately the diameter of all three SDA_{ec} architectures (100-110 Å), and a calculated

[305] molecular weight that matched the expected molecular mass of 134 kDa. Calculated scattering curves from the ready architecture, models of the open and closed forms, and mixtures of the different structures fit the experimental data similarly (Figure 4.4D). Overall, fitting calculated scattering curves or SAXS *ab initio* reconstructions from these and additional models that included limited molecular dynamic simulations failed to be sufficiently deterministic to assign an architecture for the AI-prepared SDA_{ec}.

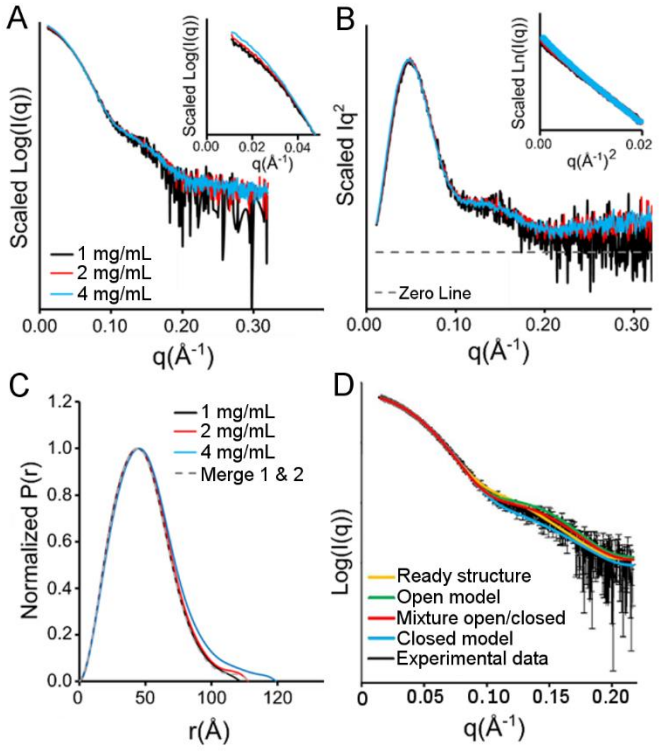

Figure 4.4 Small-angle X-ray scattering data for AI-prepared SDA_{ec}. The SDA_{ec} complex was prepared using the AI method and examined under high salt conditions. **(A)** Overlay of buffer-subtracted scattering curves. Inset: concentration dependent aggregation revealed by overlay of low q region. Negative intensities are not shown. **(B)** Kratky plots for SDA_{ec} at multiple concentrations. Inset: concentration dependent aggregation shown by Guinier plot analysis. **(C)** Pair distribution functions for SDA_{ec} samples. **(D)** Fits to the experimental data for the calculated scattering curves from the ready SDA_{ec} structure (yellow; $\chi^2 = 1.2$), open model (green; $\chi^2 = 2.1$) and closed model (blue; $\chi^2 = 2.1$). The best two state model included the open (68%) and closed (32%) forms but did not improve the fit (red; $\chi^2 = 2.0$).

To compare our SAXS data with data from other preparation methods, we reprocessed the scattering curves published by the Markley group [288], obtained from SASBDB [306], and the Cygler/Lill groups [102], which were kindly provided. The data collected by the Markley group [288] closely resembled the data for our AI-prepared SDA_{ec} complex (Figure 4.5A); the R_g from Guinier analysis was 36.3 Å and 36.9 Å (Table 4-5), respectively. The data collected by the Cygler/Lill groups [102] exhibited some concentration-dependent aggregation in the low q region (Figure 4.5). Our reanalysis of the Cygler/Lill data (Table 4-5) is consistent with their reported R_g of 54.7 Å and D_{max} of approximately 180 Å [102]. Interestingly, when we collected SAXS data with a lower ionic strength buffer comparable to that used by the Cygler/Lill groups, we obtained very similar scattering curves for our AI-prepared SDA_{ec} sample, an R_g of 51.5 Å and a D_{max} of approximately 189 Å (Figure 4.5 and Table S2). Overall, the matching activity profiles and SAXS curves (Figure 4.5, Table S1, and Table S2) [85, 102, 288] suggest that SDA_{ec} complexes prepared by the different methods have very similar structure-function and solution properties.

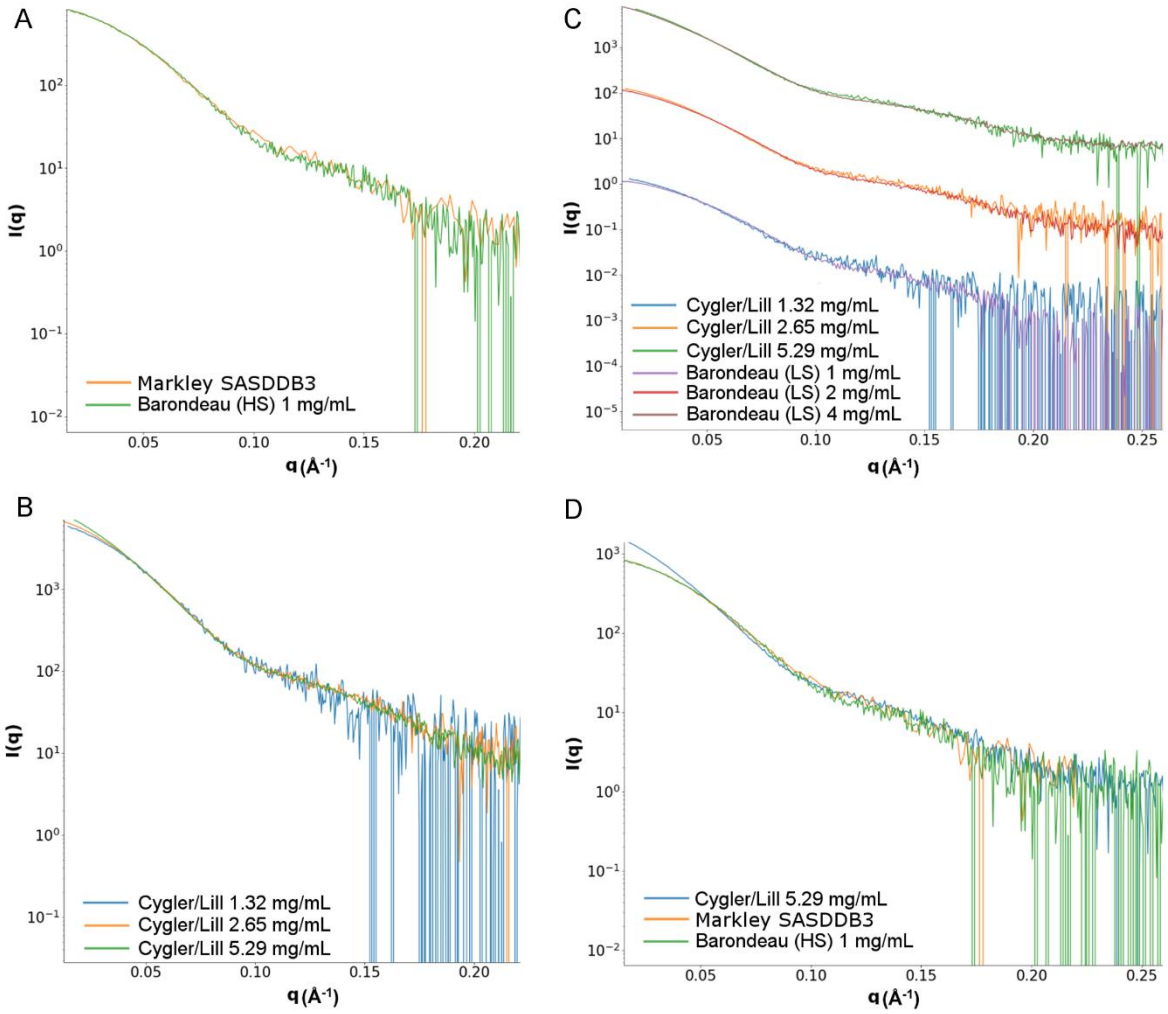

Figure 4.5 Comparisons of scattering curves for AI-prepared SDA_{ec} and previously published data. Intensities are plotted on a logarithmic scale. (A) Scattering curves for the AI-prepared SDA_{ec} complex under high salt conditions (100 mM sodium phosphate, 500 mM NaCl, 2 % glycerol, 2 mM TCEP, pH = 8.0) and the SASDDB3 data from the Markley group (B) Scattering curves from the Cygler/Lill groups at different protein concentrations. The highest concentration sample appears to have been utilized in their manuscript. (C) Scattering curves from the AI-prepared SDA_{ec} complex under low salt conditions (250 mM NaCl, 2 % glycerol, 2 mM TCEP, pH = 7.5) compared to those from the Cygler/Lill groups. (D) Overlay of the scattering curve for the AI-prepared SDA_{ec} sample under high ionic strength conditions with the scattering curves from the Cygler/Lill and Markley data.

Table 4-5 SAXS parameters for the AI-prepared SDA_{ec} under high salt conditions compared to previous data.

	†SDA_{ec}	SDA_{ec}	SDA_{ec}	SDA_{ec}	SDA_{ec}
Data source	This manuscript	This manuscript	This manuscript	This manuscript	Markley (42)
Sample concentration (mg/mL)	1	2	4	Merged	N/A
Exposure time (sec)	1.5	1.5	0.6	0	N/A
Merged regions				1:(0.0109 - 0.07) 2:(0.1001 - 0.3202)	
Guinier analysis:					
I(0)	31.4 ± 0.2	82.1 ± 0.2	194.0 ± 0.4	2	904.6 ± 8.9
q range ($Å^{-1}$)	0.015-0.035	0.018 - 0.034	0.014 - 0.033	0.015-0.035	0.017 - 0.036
R_g (Å)	36.88 ± 0.25	37.71 ± 0.13	39.69 ± 0.12	36.88 ± 0.25	36.27 ± 0.47
qR_g range	0.565 - 1.285	0.662 - 1.293	0.542 - 1.294	0.565 - 1.285	0.619 - 1.290
R^2	0.993	0.998	0.999	0.993	0.995
P(r) analysis:					
I(0)	31.6 ± 0.2	82.3 ± 0.2	194.5 ± 0.4	80.8 ± 0.32	923.9 ± 7.6
R_g (Å)	37.50 ± 0.22	38.17 ± 0.12	40.56 ± 0.12	37.07 ± 0.16	37.63 ± 0.38
d_{max} (Å)	127	129	144	128	124
q range ($Å^{-1}$)	0.0153 - 0.2171	0.0176-0.2121	0.0137-0.2015	0.0153 - 0.2171	0.0171 - 0.2200
χ^2 (total estimate from GNOM)	1.12	1.08	1.15	0.99	0.99
Mw analysis (Vc method, kDa)‡	134	129	139	126	139

†High ionic strength (100 mM sodium phosphate, 500 mM NaCl, 2% glycerol, 2 mM TCEP, pH = 8.0) data
N/A = not available
‡The high-angle data was truncated to 0.320 $Å^{-1}$ to maintain a consistent integration area.

Table 4-6 SAXS parameters for the AI-prepared SDA_{ec} under low salt conditions compared to previous data.

	†SDA_{ec}	SDA_{ec}	SDA_{ec}	SDA_{ec}	SDA_{ec}	SDA_{ec}
Data source	This manuscript	This manuscript	This manuscript	Cygler/Lill (15)	Cygler/Lill (15)	Cygler/Lill (15)
Sample concentration (mg/mL)	1.0	2.0	4.0	1.32	2.65	5.29
Guinier analysis:						
q range ($Å^{-1}$)	0.013-0.032	0.014 - 0.028	0.014 - 0.025	0.014 - 0.030	0.012 - 0.028	0.017 - 0.026
R_g (Å)	39.89 ± 0.24	44.86 ± 0.18	51.48 ± 0.13	42.99 ± 0.29	45.65 ± 0.13	50.72 ± 0.18
qR_g range	0.52 - 1.28	0.62 - 1.24	0.73 - 1.28	0.62 - 1.30	0.57 - 1.30	0.87 - 1.30
R^2	0.997	0.998	0.999	0.996	0.999	0.999
P(r) analysis:						
R_g (Å)	40.31 ± 0.19	45.54 ± 0.12	53.30 ± 0.15	44.18 ± 0.27	46.56 ± 0.18	52.15 ± 0.15
d_{max} (Å)	132	154	189	142	158	177
q range ($Å^{-1}$)	0.014 - 0.200	0.014-0.178	0.014-0.155	0.0143 - 0.1863	0.0124 - 0.1754	0.0171 - 0.1575
χ^2 (total estimate from GNOM)	1.04	1.39	1.48	0.90	0.76	1.01
Mw analysis (Vc method, kDa)‡	167	178	220	180	189	233

† Low ionic strength (50 mM Hepes, 250 mM NaCl, 2% glycerol, 2 mM TCEP, pH = 7.5) data
‡ The high-angle data was truncated to 0.320 $Å^{-1}$ to maintain a consistent integration area.

Different SDA_{ec} Preparations can be Crystallized in Both Open and Closed Forms.

X-ray crystallography has provided the strongest evidence for the presence of different SDA_{ec}

architectures. We therefore investigated if the AI-prepared SDA_{ec} samples, used to generate crystals of the open architecture [101], and TB-prepared SDA_{ec} samples, used to generate crystals of the closed architecture [102], could be used to generate both types of crystals. We buffer exchanged SDA_{ec} samples generated by the two methods and determined that each could be crystallized in the conditions for both the open and closed architectures (Figure 4.6). We further verified the presence of both crystal forms by screening the crystals on an X-ray diffractometer. After indexing the screened images (Table 4-7), it was clear that regardless of the preparation method, the SDA_{ec} complex could be crystallized into forms corresponding to both the open and closed architectures, indicating that both architectures exist in solution and/or that the two architectures can interchange. Next, we tested the activity of samples generated from the crystals of the open and closed forms as a mechanism to "freeze-out" the individual architectures. We selected single crystals of each architecture, washed them to remove any residual protein, and then dissolved them in assay buffer to measure activity with and without the activator subunit FXN. Interestingly, samples generated from both open and closed crystals exhibit the characteristic order of magnitude activation by FXN (Figure 4.7). Together, these data indicate that the SDA_{ec} complex can exchange between both open and closed forms and/or that both exist in solution. Moreover, these data suggest that the addition of FXN either activates both forms equally or, more likely, activates a single architecture generated by an exchange reaction.

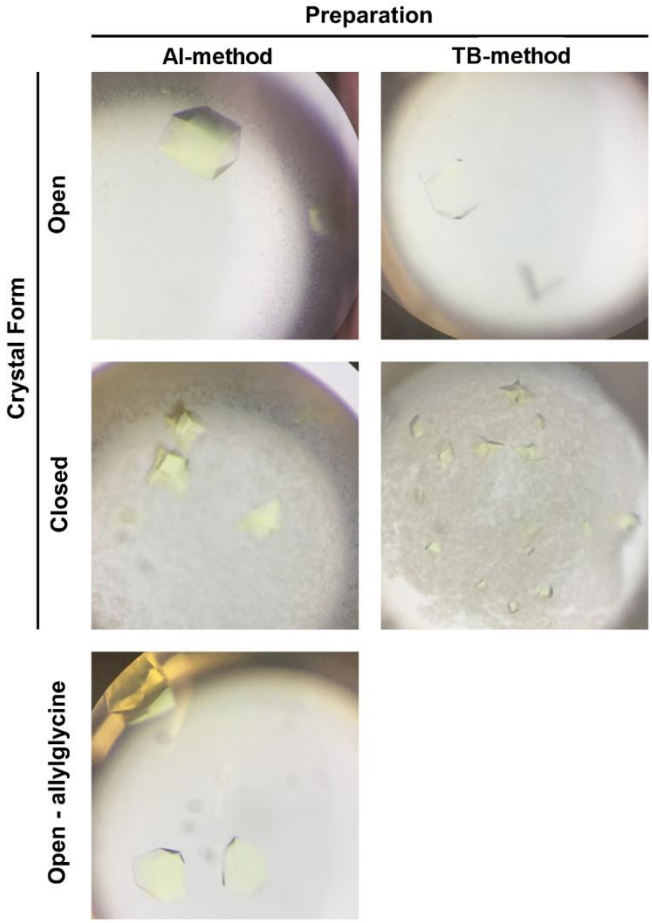

Figure 4.6 AI and TB prepared SDA_{ec} samples form crystals in both open and closed architectures. AI and TB prepared SDA_{ec} samples were crystallized using trials similar to the published conditions. The unit cell parameters were consistent with the open and closed forms.

Table 4-7 Indexing of open (space group $P2_12_12_1$) and closed (space group $H3_2$) crystal forms from AI and TB prepared SDA_{ec} samples.

		Unit Cell Parameters					
Crystal Form	**Preparation**	**a (Å)**	**b (Å)**	**c (Å)**	**α (°)**	**β (°)**	**γ (°)**
Open (5USR)*	AI-method	125.5	147.8	168.5	90	90	90
Open	AI-method	125.8	147.9	168.1	90	90	90
Open (-allylglycine)	AI-method	122.1	144.1	163.6	90	90	90
Open	TB-method	125.2	146.8	166.7	90	90	90
Closed (5WGB)*	TB-method	140.8	140.8	203.3	90	90	120
Closed	TB-method	139.8	139.8	200.6	90	90	120
Closed	AI-method	139.2	139.2	200.5	90	90	120

*Published unit cell parameters.

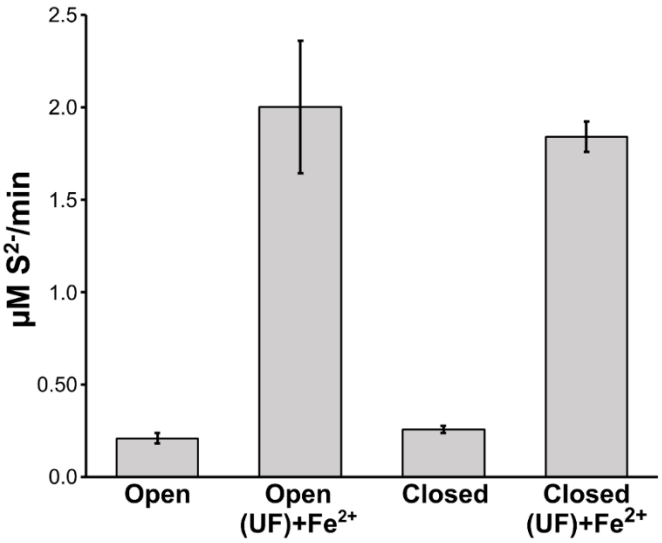

Figure 4.7 Cysteine desulfurase activities from isolated crystals in the open and closed forms. Single crystals of both open and closed architectures were isolated, rinsed, and crystal slurries were dissolved by incubating with assay buffer at 37 °C for 15 min. The cysteine desulfurase activities of the open and closed samples were evaluated in the presence and absence of ISCU2, FXN, and Fe^{2+}. Error bars are replicate errors (n = 6).

The SDA_{ec} Complex Disassembles into Protomers that can Undergo Exchange Reactions.

Based on the ability of SDA_{ec} samples to crystallize into both open and closed architectures, we hypothesized that the distinct SDA_{ec} $\alpha_2\beta_2\gamma_2$ quaternary structures are in equilibrium. Based on the structures of the different architectures, interchange could occur via dissociation and reassociation of αβγ protomers or individual subunits. To test this hypothesis, we separately generated SDA_{ec} samples in which all three subunits were uniformly labeled with either ^{15}N or ^{14}N and used native mass spectrometry to monitor if these complexes underwent exchange reactions when mixed. Upon combining equimolar amounts of ^{15}N- and ^{14}N-labeled SDA_{ec}, an intermediate-mass species consistent with the exchange of entire αβγ protomers to generate a ^{15}N-SDA_{ec}-^{14}N-SDA_{ec} mixed complex was observed (Figure 4.8). In contrast, masses that would suggest the exchange of individual subunits were not observed. The protomer

exchange for SDA_{ec} reached an exchanged-to-unexchanged ratio of 0.83 at 120 min (Figure 4.9); the theoretical maximum for this ratio is 1.0, which corresponds to a completely exchanged equimolar mixture. Similar native MS control experiments using the *E. coli* cysteine desulfurase IscS dimer either with or without a His-tag revealed a somewhat slower exchange process (reaching an exchanged-to-unexchanged ratio of 0.31 at 120 min). Strikingly, the pre-incubation of saturating amounts of ISCU2 or ISCU2 plus FXN with the SDA_{ec} complex or IscU with IscS completely inhibited these exchange reactions (Figure 4.9). Together, these results indicate that the interaction between protomers is dynamic enough for complete protomer dissociation and reassembly, However, the protomer dissociation and reassembly of the SDA_{ec} complex occurs on a slower time course than the FXN activation process and is inhibited by ISCU2/FXN binding. Overall, these experiments indicate that protomers, but not individual subunits, can exchange and that the FXN-activated sample does not undergo a complete protomer dissociation process.

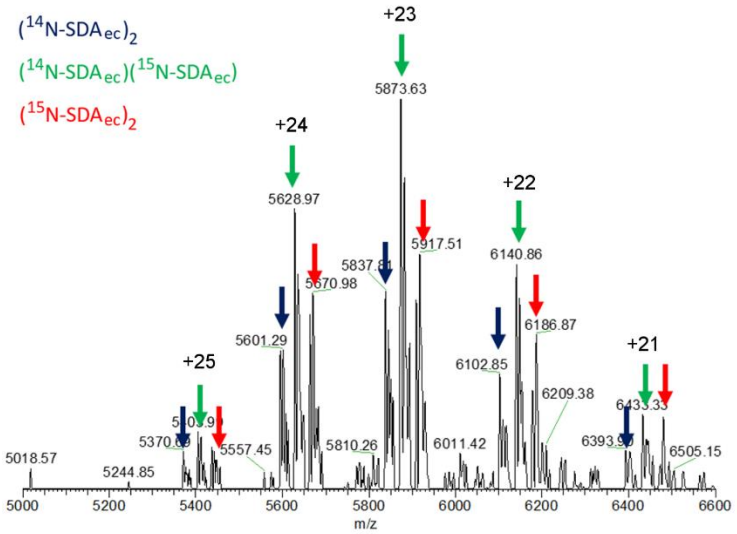

Figure 4.8 Native MS spectra showing protomer exchange for cysteine desulfurase complexes. Representative native MS spectra (2 hr time point from Fig 4) for the reaction of a 1:1 ratio of His-tagged ^{14}N-SDA_{ec} and ^{15}N-SDA_{ec} complexes to form a mixed structure

containing ^{14}N and ^{15}N labeled protomers. The charge states +25 to +21 are shown for the three complexes.

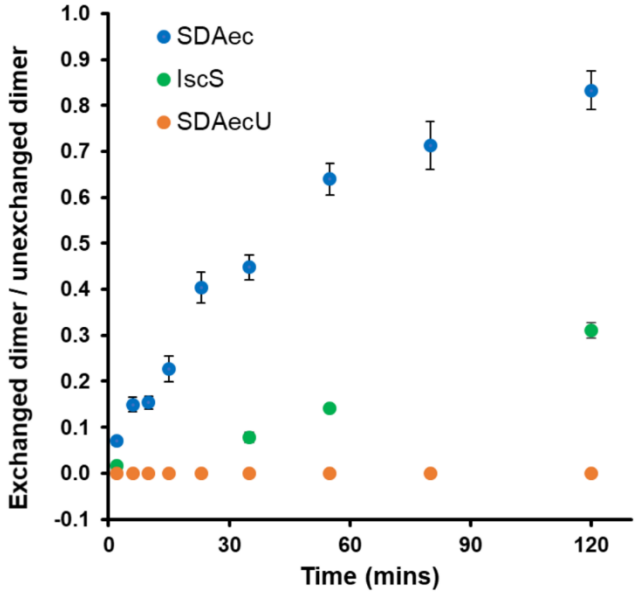

Figure 4.9 Protomer exchange for cysteine desulfurase complexes. Kinetics of an exchange reaction monitored by native mass spectrometry using a 1:1 ratio of His-tagged ^{14}N-SDA_{ec} ($^{14}N^{14}N$) and ^{15}N-SDA_{ec} ($^{15}N^{15}N$) complexes (blue). The Y axis is shown as the ratio of the amount of exchanged dimer ($^{15}N^{14}N$) divided by the sum of unexchanged dimer ($^{14}N^{14}N$ and $^{15}N^{15}N$). His-tagged and untagged versions of IscS undergo a similar exchange reaction monitored by native MS (green). Preincubation of ^{14}N-SDA_{ec} and ^{15}N-SDA_{ec} samples with ISCU2 completely inhibited the subsequent exchange reaction (orange). Error bars are replicate errors (n = 3).

SDA_{ec} Exists in Interconvertible Forms in Solution. . We discovered that different forms of AI-prepared SDA_{ec} could be separated using a high-resolution cation exchange column. Three peaks were observed (Figure 4.10A). Peak 1 is a minor species that may result from the premature elution of peak 2 due to the inability to remove all the salt from the injected sample for stability purposes. Native SDA_{ec} reproducibly separated into a minor species (peak 2) and major species (peak 3). Overall, these results suggest multiple SDA_{ec} species in solution, likely corresponding to different architectures, can be separated by cation exchange chromatography

and undergo interchange through a dynamic equilibrium process that might be linked to activation.

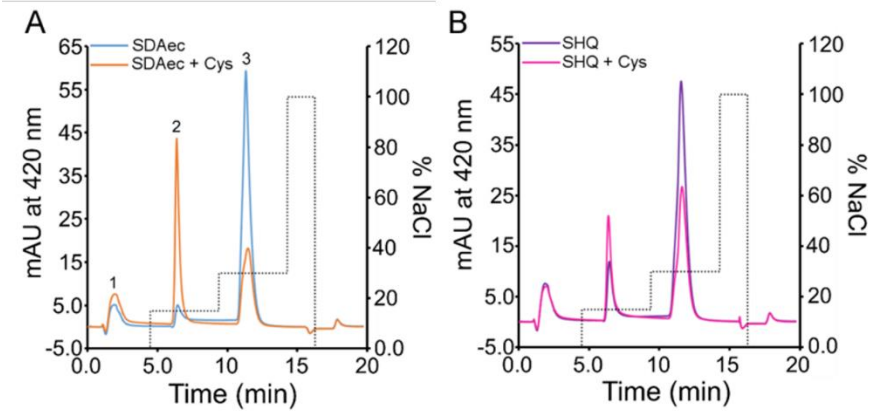

Figure 4.10 Separation of different SDA_{ec} forms. Different species were eluted for cysteine desulfurase samples from a cation exchange column using a step salt gradient. **(A)** SDA_{ec} (30 μM) shows the predominant peak 3 and low abundance peak 2. **(B)** The SHQ (30 μM) variant shows a larger initial population of peak 2 than SDA_{ec}.

A Designed SDA_{ec} Variant that Alters the Distribution of Architectures. We hypothesized that if the multiple species observed in cation exchange chromatography corresponded to the different architectures observed by X-ray crystallography, then variants that stabilized a specific architecture could alter the distribution of species in solution. We therefore generated the Q64S, P299H, L300Q NFS1 variant (herein designated as SHQ) to shift the population from the open to the ready architecture. These introduced SHQ residues are conserved in prokaryotic cysteine desulfurases and were expected to reduce steric clashes near the N-terminus and form new hydrogen bonds across the protein-protein interface of the ready form of the SDA_{ec} complex (Figure 4.11Figure 4.12). The SHQ variant had a 3-fold greater cysteine desulfurase activity than the native SDA_{ec} complex in the absence of FXN ((Figure 4.13). Although the SHQ variant had a 17-fold weaker FXN binding affinity, it still shared a

similar FXN-stimulated activity (8 μM S^{2-}/min · μM NFS1) with the SDA_{ec} complex (Figure 4.13). Moreover, the enhanced amount of peak 2 of the SHQ variant in cation exchange chromatography is consistent with the assignment of peak 2 as the compact form, as the SHQ variant is designed for enriching the ready architecture.

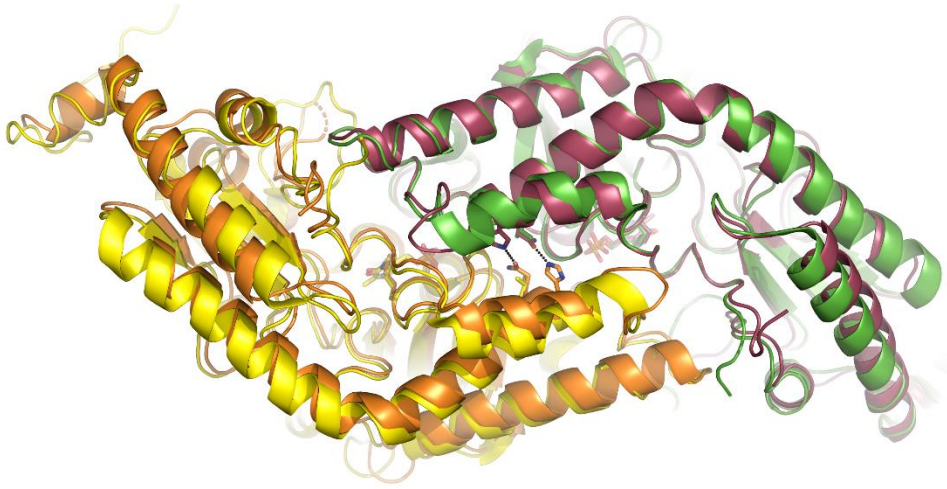

Figure 4.11 Substituting a hydrogen-bonding pair of residues from IscS to stabilize the ready SDA_{ec} architecture. In the IscS structure (subunits in orange and purple), the dimer interface is stabilized by two hydrogen bonds between residues H247 and Q248 of the two subunits. The equivalent residues in human NFS1 are P299 and L300 residues, which can form weaker Vander Waals interactions at the dimer interface. The NFS1 variant P299H L300Q is predicted to stabilize a ready architecture.

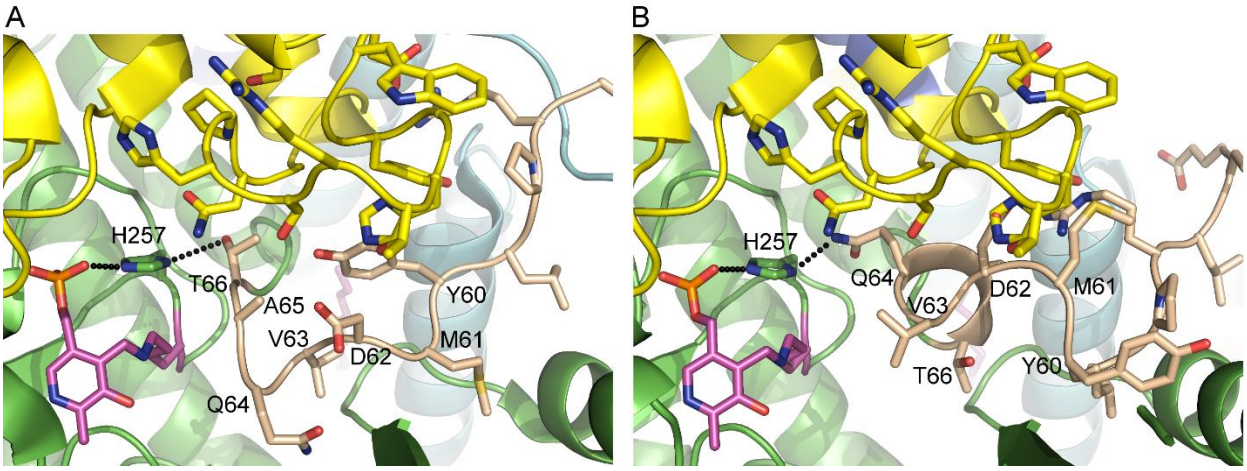

Figure 4.12 N-terminal engineering of SDA_{ec} to favor the ready architecture. (A) In the ready architecture, the NFS1 catalytic subunits (green and yellow) have similar protein interfaces to IscS. T66 from the ready architecture forms a hydrogen bond to H257 that, in turn, hydrogen bonds to the PLP cofactor (magenta). **(B)** In the open architecture, Q64 hydrogen bonds to H257, which results in a structural rearrangement of the N-terminal residues. Residues, especially M61 and D62, from this region of the green NFS1 subunits are shown in wheat and would have steric clashes with the second catalytic subunit from the ready form (docked into structure, shown in yellow).

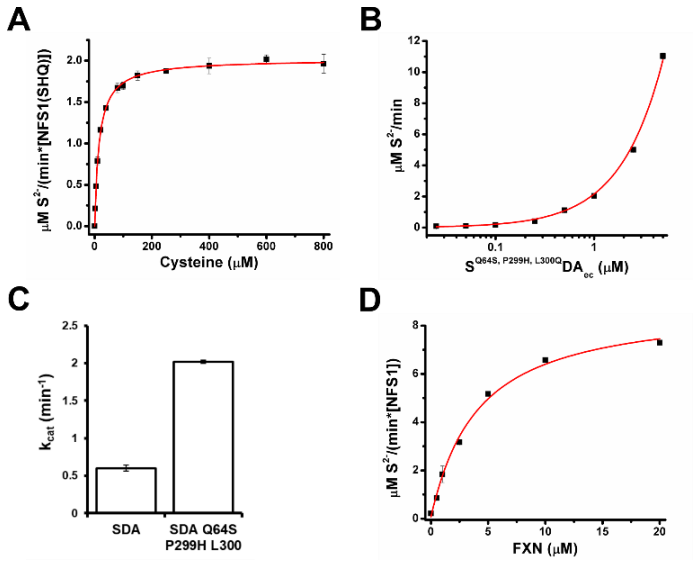

Figure 4.13 The SHQ variant has inherently higher activity than SDA_{ec}. (A) Michaelis-Menten kinetics of the $S^{Q64S\ P99H\ L300Q}DA_{ec}$ (SHQ) variant. **(B)** Variation of the concentration of SHQ while keeping the L-cysteine concentration at 1 mM leads to a linear increase (R^2 - 0.9977) of the activity with a slope of 2.16 ± 0.03, which is very close to the k_{cat} value (2.02 ± 0.02). **(C)** Comparison of k_{cat} of SDA_{ec} and the SHQ variant. **(D)** FXN in the presence of ISCU2 activates

the SHQ variant to the $SDA_{ec}UF$ level but FXN binds weakly (K_D = 3.8 ± 0.6 for SHQ compared to 0.22 ± 0.05 the native enzyme).

The SDA_{ec} and $SDA_{ec}U$ Complex Mainly Exists in the Extended Form and are Driven to the Compact Form by FXN. Next, we used native ion-mobility mass spectrometry (IM-MS) to investigate the conformational landscape and/or different architectures of the SDA_{ec} complex. IM-MS measures the arrival time of ions traveling through a drift tube filled with buffer gases under an electric field. Ions experience the acceleration by an electric field and are slowed by collisions with buffer gases. Therefore, ions with a higher charge, a lower mass, or a compact shape travel faster through the drift cell. IM-MS data for the SHQ variant revealed two species with the same expected *m/z* peaks but different arrival times (Figure 4.15). The species with higher or lower arrival time theoretically have relative extended or compact conformations. Theoretical calculations (Table 4-8) suggested that the ready and closed forms of the SDA_{ec} complex have similar collisional cross-sectional areas and are more compact than the open form [302-304, 307-309]. Therefore, we tentatively assigned the higher arrival time (extended) species in IM-MS as the open architecture and lower arrival time (compact) species as the closed and/or ready forms. While wild type SDA_{ec} and $SDA_{ec}U$ mainly exist in the extended form, the SHQ variant and $S^{SHQ}DA_{ec}U$ exhibit similar amount of the extended and compact forms. The compact form of SDA_{ec} and $SDA_{ec}U$ is observed to vary slightly in different batches (the compact form is always <30%) or incubation temperature, which could be explained by the dynamic interconversion of the different species in solution. The similar extended/compact ratios between SDA_{ec} and $SDA_{ec}U$ or between SHQ and $S^{SHQ}DA_{ec}U$ indicate ISCU2 binds both the extended and the compact forms. In the presence of both ISCU2 and FXN, $SDA_{ec}UF$ and $S^{SHQ}DA_{ec}UF$ strikingly demonstrate a conversion

to a single species following the compact trendline (Fig. 6). With the presence of FXN but not ISCU2, $SDA_{ec}F$ and $S^{SHQ}DA_{ec}F$ also exist in a single compact form (Figure 4.14). These results in combination with the activity, protomer exchange, and cation separation assays suggest a dynamic interconversion between eukaryotic cysteine desulfurase architectures is a critical part of the FXN activation phenomenon.

Table 4-8 Collision cross section (Ω) of tagged SDA_{ec} species.

Sample	Mass (kDa)	z	Form	Ω_{Exp} (Å^2)	Ω_{PA} (Å^2)	Ω_{PSA} (Å^2)
SDA_{ec}	134.2	23	compact*	6928 ± 108	Ready = 7076	Ready = 7721 ± 51
			extended	7203 ± 160	Closed = 6944	Closed = 7692 ± 48
		24	compact*	7021 ± 130	Open = 7287	Open = 8031 ± 39
			extended	7267 ± 111		
$S^{SHQ}DA_{ec}$	134.2	23	compact	7048 ± 20		
			extended	7303 ± 29		
		24	compact	7145 ± 18		
			extended	7389 ± 41		
$SDA_{ec}U$	164.9	26	compact*	8194 ± 140	Closed = 8099	Closed = 8854 ± 44
			extended	8737 ± 48	Ready = 8126	Ready = 8829 ± 51
		27	compact*	8390 ± 81	Open = 8211	Open = 9251 ± 48
			extended	8802 ± 21		
$S^{SHQ}DA_{ec}U$	164.9	26	compact	8108 ± 20		
			extended	8693 ± 20		
		27	compact	8179 ± 19		
			extended	8827 ± 33		
$SDA_{ec}F$	164.1	26	compact	8041 ± 23	Ready = 7868	Ready = 8964 ± 44
		27	compact	8051 ± 37		
$S^{SHQ}DA_{ec}F$	164.1	26	compact	8107 ± 24		
		27	compact	8107 ± 24		
$SDA_{ec}UF$	193.3	27	compact	9333 ± 22	Ready = 8713	Ready = 9758 ± 75
		28	compact	9370 ± 52		
$S^{SHQ}DA_{ec}UF$	193.3	27	compact	9279 ± 25		
		28	compact	9418 ± 30		

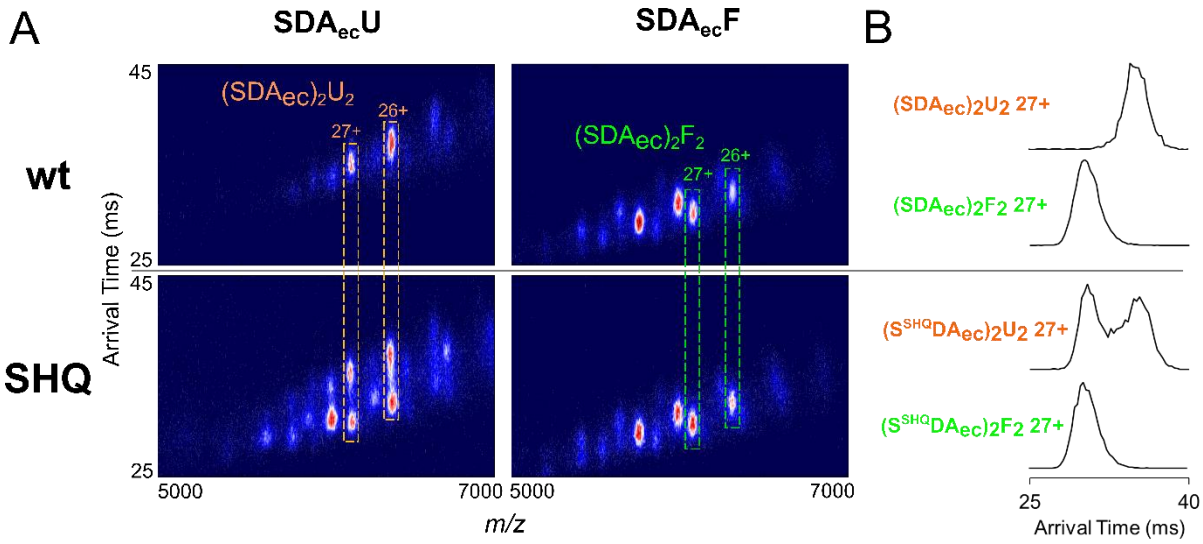

Figure 4.14 Comparison of SDAecU and SDAecF in IM-MS analysis. (A) IM-MS of native and variant SDA$_{ec}$ in the presence of ISCU2 or FXN. **(B)** Arrival time distribution of native and variant SDA$_{ec}$U 27+ and SDA$_{ec}$F 27+.

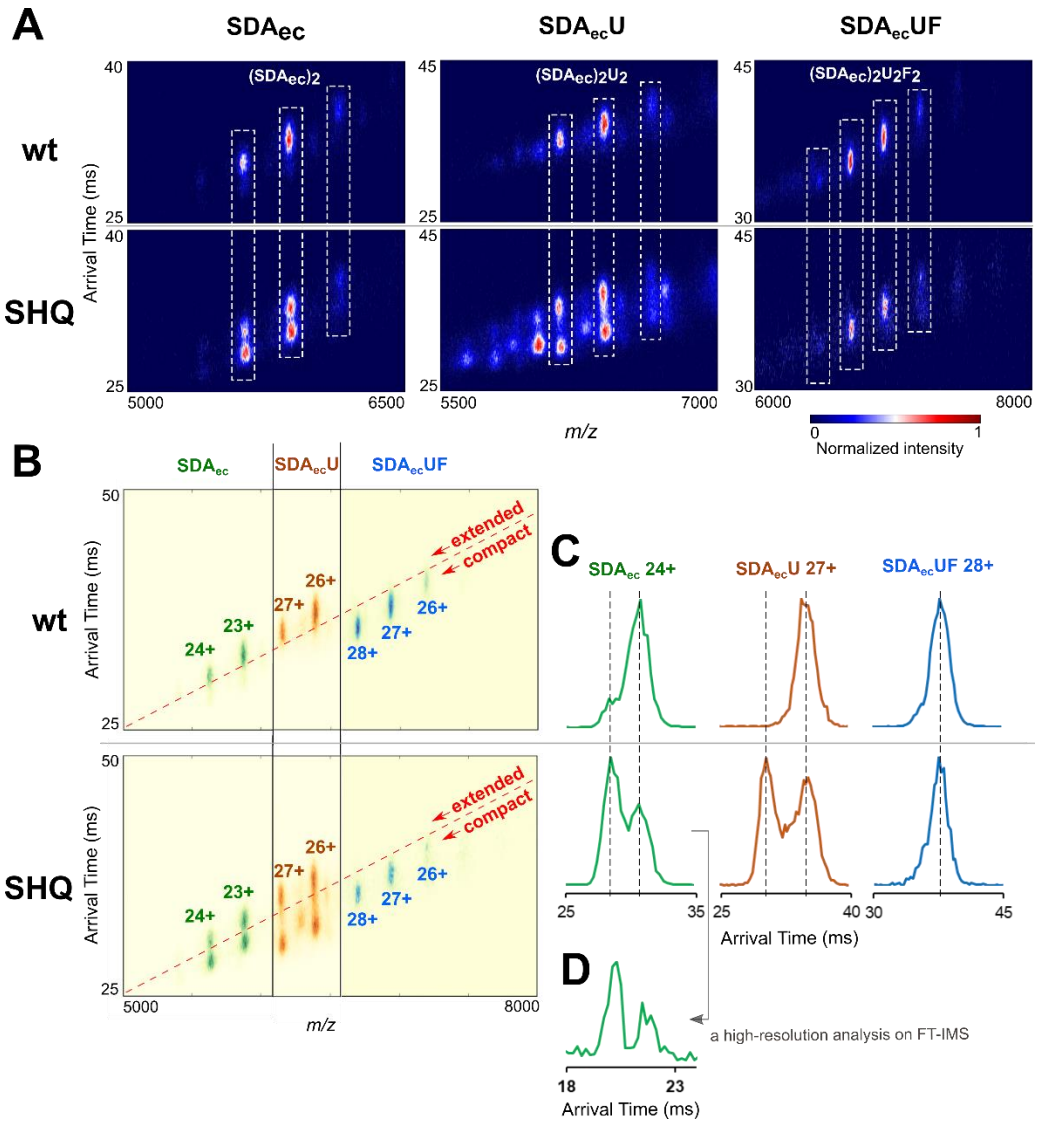

Figure 4.15 IM-MS analysis of different SDA$_{ec}$ forms. (A) IM-MS spectra of native and variant SDA$_{ec}$ as isolated complexes, in the presence of ISCU2, and with both ISCU2 plus FXN. **(B)** Overlaid IM-MS spectra in A. The SDA$_{ec}$ and SDA$_{ec}$U are predominantly in the slower migrating form (extended conformer trend line), whereas the S^{SHQ}DA$_{ec}$ and S^{SHQ}DA$_{ec}$U are enriched in the faster migrating species (compact conformer trend line). SDA$_{ec}$UF and S^{SHQ}DA$_{ec}$UF exist as a single dominant species (compact conformer trend line). **(C)** Arrival time distribution of native and variant SDA$_{ec}$ 24+, SDA$_{ec}$U 27+, and SDA$_{ec}$UF 28+. **(D)** Arrival time distribution of S^{SHQ}DA$_{ec}$ 24+ measured by the high-resolution FT-IMS instrument.

Pilot IM-MS experiments on regulation of SDA$_{ec}$ architectures by different binding partners. Native IM-MS is also applied to SDA$_{ec}$ in presence of ISCU2, wildtype and clinical

variants of FXN (Figure 4.16), proposed electron electron donor FDX1/FDX2, potential sulfur acceptor TUM1, and/or potential sulfur acceptor MOCS3 (only RLD domain) as well as ISD11 variants (Figure 4.17) and a NFS1 clinical variant (Figure 4.18). Overall, aside from ISCU2 can bind both extended and compact forms, other binding partners of SDA all binds with compact forms (Figure 4.19). Further investigation of whether the binding compact form are in closed or ready architectures would illustrate the regulation mechanism of the morpheein-like system, in which binding of substrates leads to conformational changes that affect binding of oligomers (detailed explanation below). In addition, preliminary test on the competition of the binding partners on binding SDA_{ec} have also been performed. Due to the similar mass of FDX1, FDX2, MOCS3 (RLD), ISCU2, and FXN, it is more challenging to get resolved MS spectra and definite information. So far, the preliminary experiments suggest FDX2 competes binding with FXN with higher affinity (Figure 4.20). Interestingly, when ISCU2 is also present, FXN binds stronger than FDX2 (Figure 4.21). Also, MOCS3 (RLD) likely compete binding with ISCU2 + FXN and ISCU2 + FDX2 (data not shown). More investigation is required to illustrate these interactions.

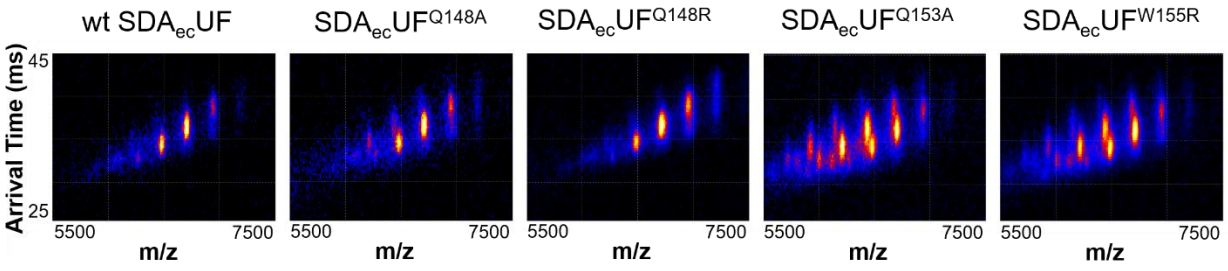

Figure 4.16 IM-MS analysis on $SDA_{ec}UF$ of FXN variants.

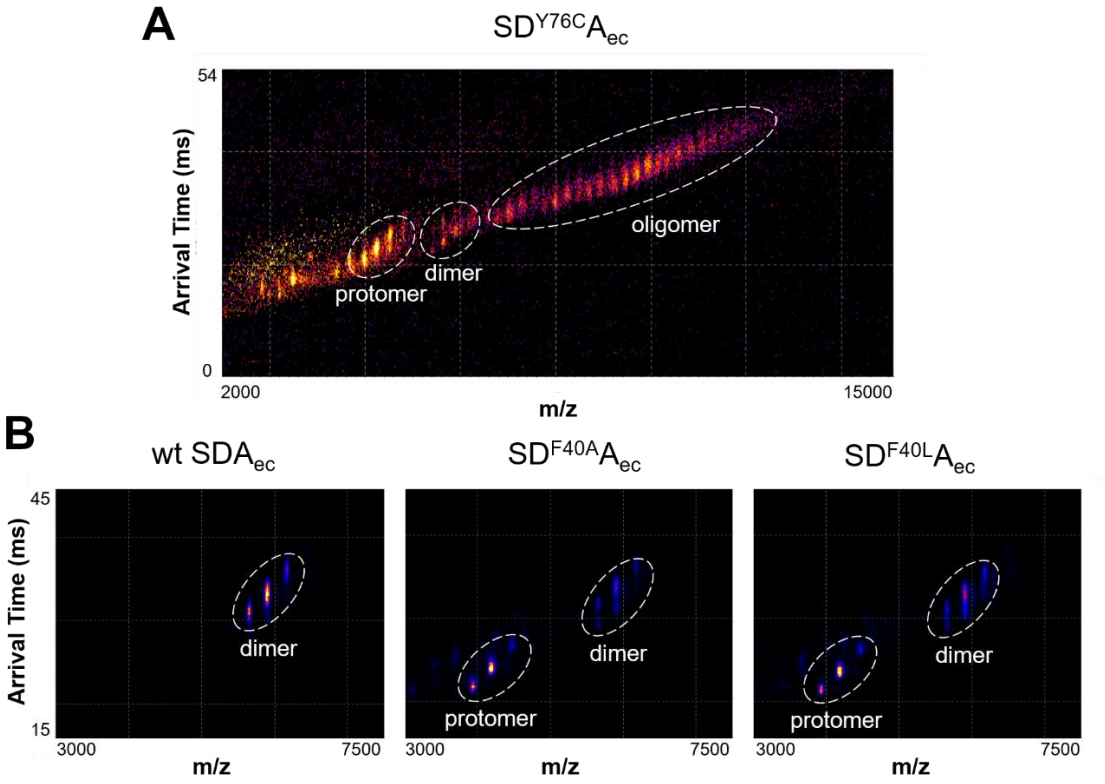

Figure 4.17 IM-MS analysis on SDA_{ec} of ISD11 variants. (A) Y76C variant, which is designed to form a intramolecular disulfide bond between the two ISD11 subunits, and **(B)** F40 variants designed to weaken lipid-ISD11 interaction.

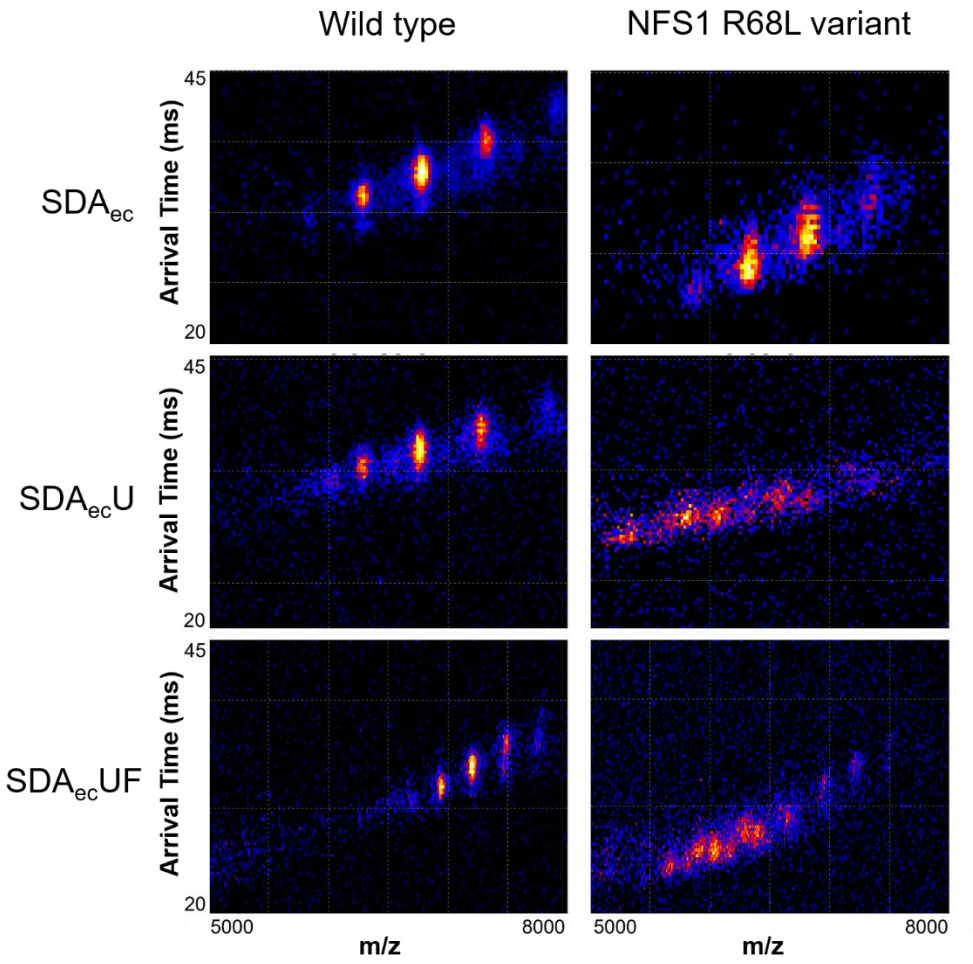

Figure 4.18 IM-MS analysis on SDA_{ec} of a NFS1 variant. The R68L variant is a clinical variant, showing arrival time distribution that is even lower than closed/ready architectures.

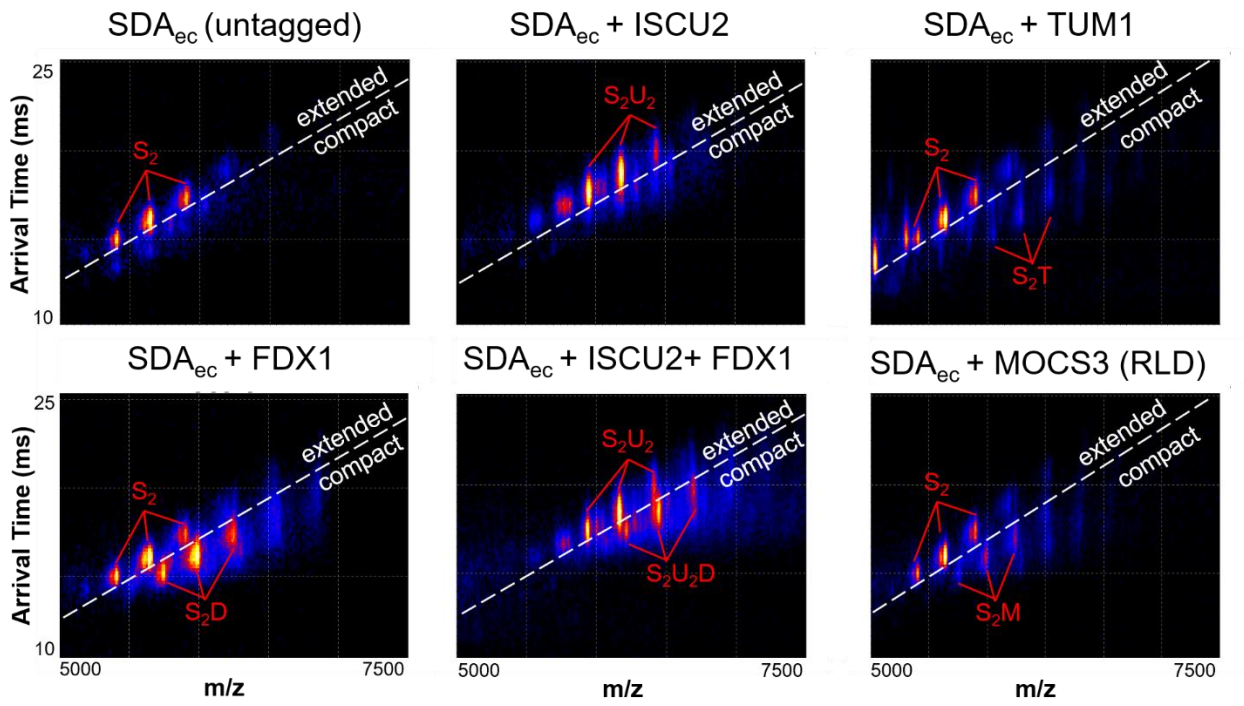

Figure 4.19 IM-MS analysis of SDA$_{ec}$ species binding with different binding partners. All samples are in 200 mM AmA, pH = 8.5. Sample components include 5 μM of SDA$_{ec}$, 15 μM of ISCU2, 40 μM of TUM1, 40 μM of FDX1, and 40 μM of MOCS3 (RLD).

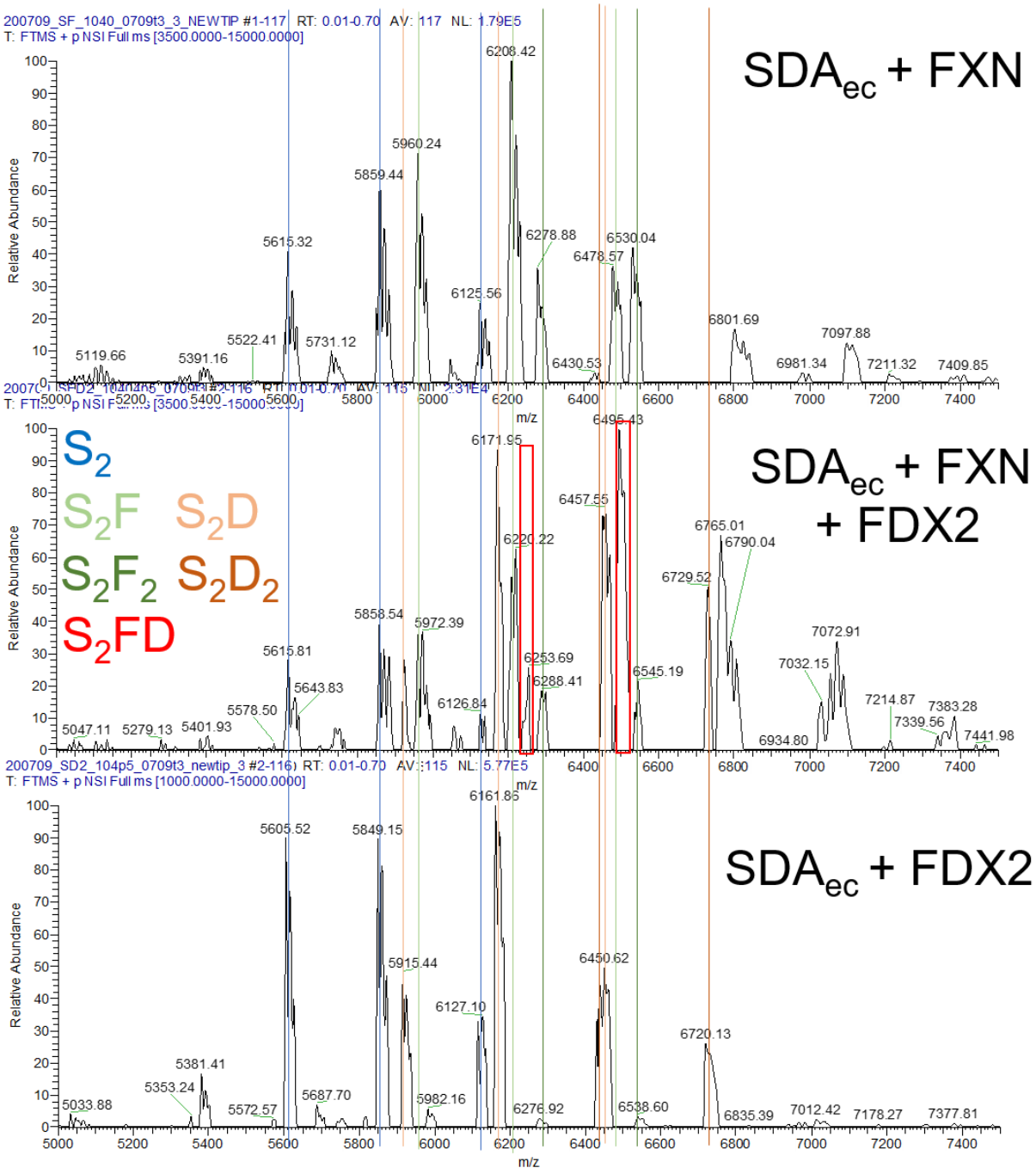

Figure 4.20 Native MS analysis of FDX2 and FXN binding on SDA$_{ec}$. All samples are in 200 mM AmA, pH = 8.5. Sample components include 10 μM of SDA$_{ec}$, 4.5 μM of FDX2, and 40 μM of FXN.

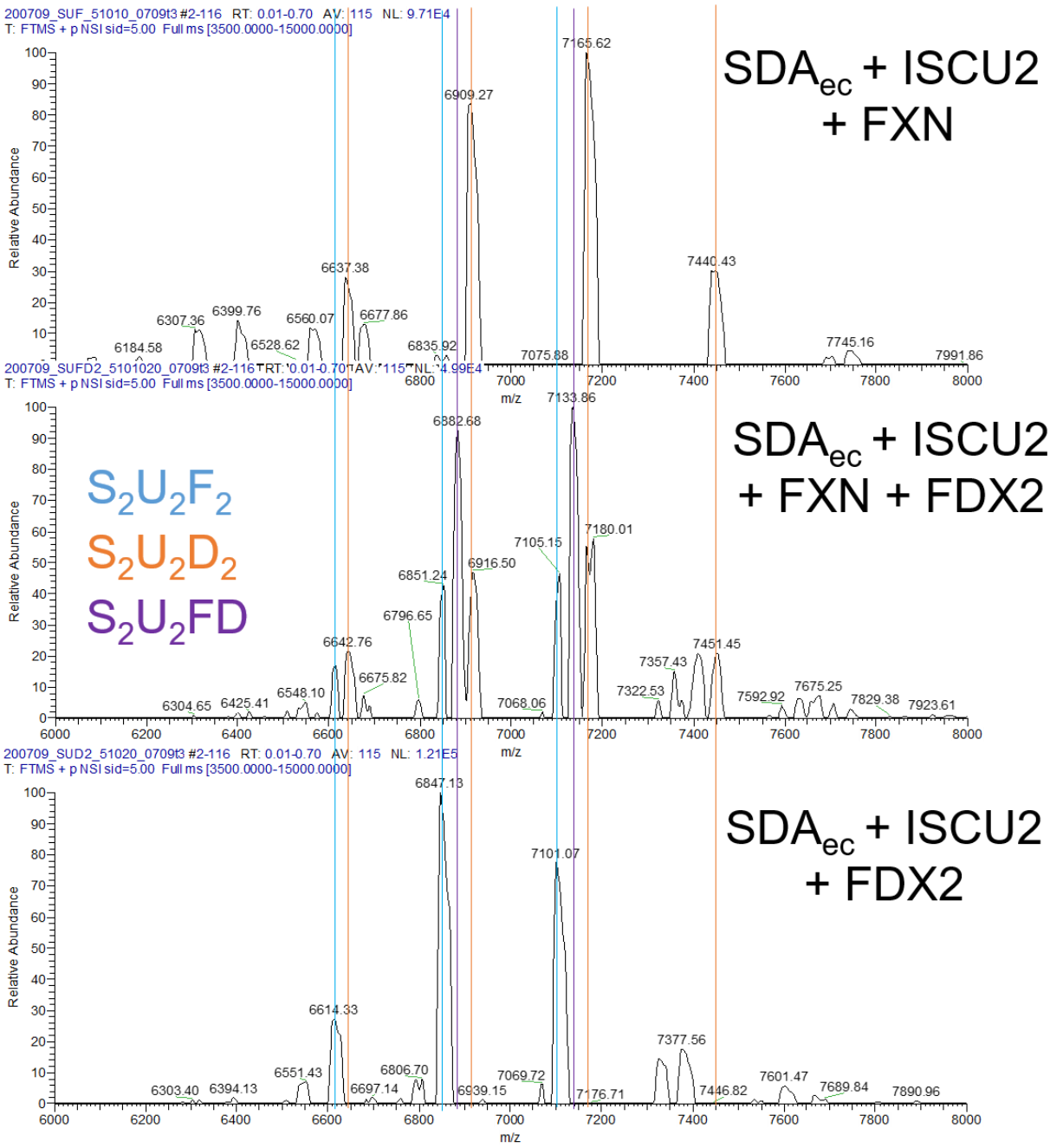

Figure 4.21 Native MS analysis of FDX2 and FXN binding on SDA$_{ec}$U. All samples are in 200 mM AmA, pH = 8.5. Sample components include 5 μM of SDA$_{ec}$, 10 μM of ISCU2, 20 μM of FDX2, and 10 μM of FXN.

4.4. Discussion

Defining the physiological role and mechanistic details of FXN in the eukaryotic Fe-S assembly pathway has received a lot of attention due to its connection to Friedreich's ataxia (FRDA) [111]. About 10 years ago *in vitro* assays revealed a role for FXN in stimulating the activity of the eukaryotic cysteine desulfurase complex [103]. More recent studies show that FXN accelerates chemical steps associated with the mobile S-transfer loop, including the decay of the Cys-quinonoid PLP intermediate, the accumulation of a persulfide species on NFS1, and the sulfur transfer reaction to ISCU2 [214, 226]. The analogous prokaryotic cysteine desulfurases, including the *E. coli* IscS that is 60 % identical to NFS1, does not require the FXN-based activation and is functional without the additional subunits ISD11 and ACP, suggesting fundamental differences between the eukaryotic and prokaryotic cysteine desulfurases.

The first evidence that these differences manifested as dramatic structural changes in the eukaryotic cysteine desulfurases was revealed by the SDA_{ec} crystal structure in the open architecture [101]. The open form features a solvent-exposed PLP, an incomplete substrate binding channel, and a quaternary structure that lacks significant NFS1-NFS1 interactions (Figure 4.1A), which are a hallmark of prokaryotic IscS cysteine desulfurases (Figure 4.2). A crystal structure of the closed architecture soon followed, which revealed a significant NFS1-NFS1 interface [102] but with different protein-protein interactions than IscS [60, 73, 74, 86]. Compared to IscS, the closed structure places the PLP cofactors 5 Å closer to one another and positions structural elements to potentially inhibit the function of the mobile loop cysteine in the sulfur transfer reaction (Figure 4.22). Remarkably, a third form, herein called ready, of SDA_{ec} was revealed in complex with ISCU2 and with ISCU2/FXN [102, 107] that has the same protein interface as IscS (Figure 4.2). The

relationship between these different architectures, their connection to FXN activation, and their functional roles in sulfur transfer reactions remain poorly understood.

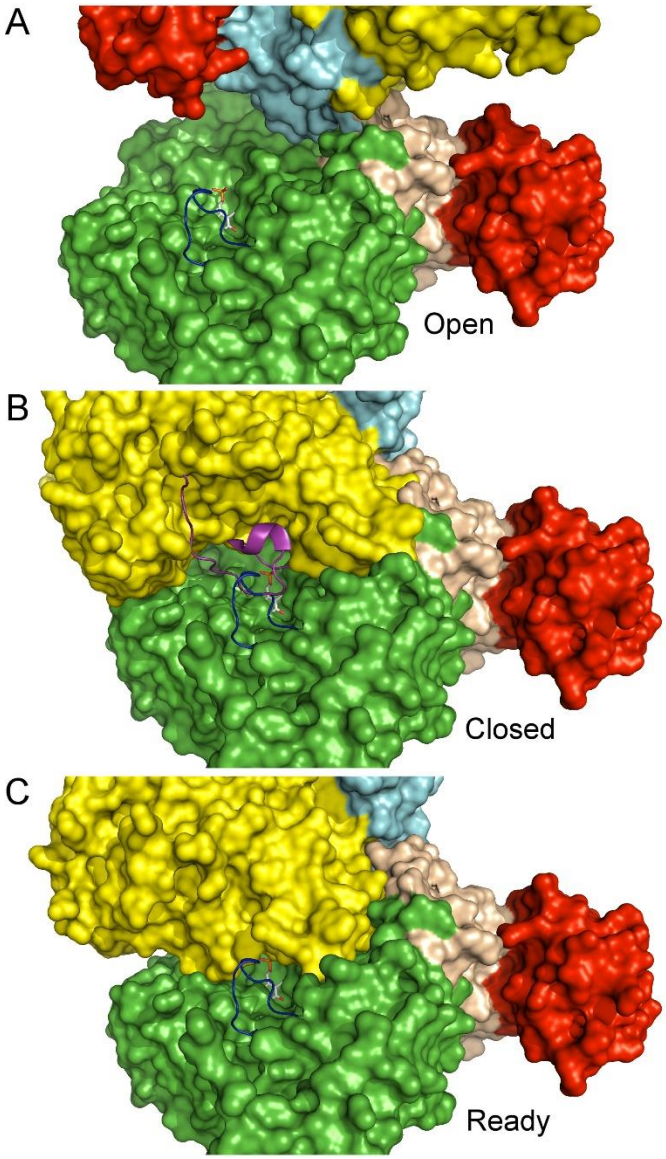

Figure 4.22 Differences in the active sites for the three SDA_{ec} architectures. (A) Surface representation of open SDA_{ec} model highlighting the solvent exposed PLP (white) and the C381-containing mobile S-transfer loop (dark blue). **(B)** Surface representation of the closed SDA_{ec} model that also shows a structural element (purple) from the other subunit that may inhibit the function of the mobile S-transfer loop. Notably, the structural element and mobile loop are

disordered in the closed crystal structure. **(C)** Surface representation of the ready SDA_{ec} model. The NFS1 subunits are colored in green and yellow, the ISD11 in cyan and wheat, and ACP in red.

Here, we establish that the structure-function properties of SDA_{ec} samples are independent of the preparation method, that these samples consist of interconvertible equilibrium mixtures of different species, and that variant complexes or the binding of additional subunits can shift this equilibrium between states. Crystallographic studies reveal SDA_{ec} samples exist as a mixture or can convert between the open and closed forms (Figure 4.6 and Table 4-7). IM-MS and cation exchange chromatography results also indicate multiple components in SDA_{ec} samples with a qualitative correlation between faster (compact) and slower (extended) migrating species in IM-MS with eluting peaks 2 and 3 from the cation exchange column (Figure 4.10). The relative lower abundance of peak 2 in chromatography compared to the compact form in IM-MS is potentially due to the interconvertible nature among architectures shits the equilibrium under different solution conditions, as the effect of solution conditions on the architecture is already demonstrated by the different crystal forms of SDA_{ec}. We assigned the slower migrating species in IM-MS as the open form and the faster migrating species as the closed and/or ready form based on their relative calculated collisional cross-sectional areas (Table 4-8). This assignment is consistent with the enrichment of the open form for SDA_{ec} samples in negative stain electron microscopy studies [101]. IM-MS data also indicates that ISCU2 can bind to both extended and compact species of the SDA_{ec} complex and does not significantly shift the population between forms (Figure 4.15). Although there are no structural snapshots of the open or closed SDA_{ec} forms bound to ISCU2, the ISCU2 binding sites in the ready architecture [102, 107]

are distant from the αβγ protomer interaction sites, suggesting that each architecture can bind ISCU2.

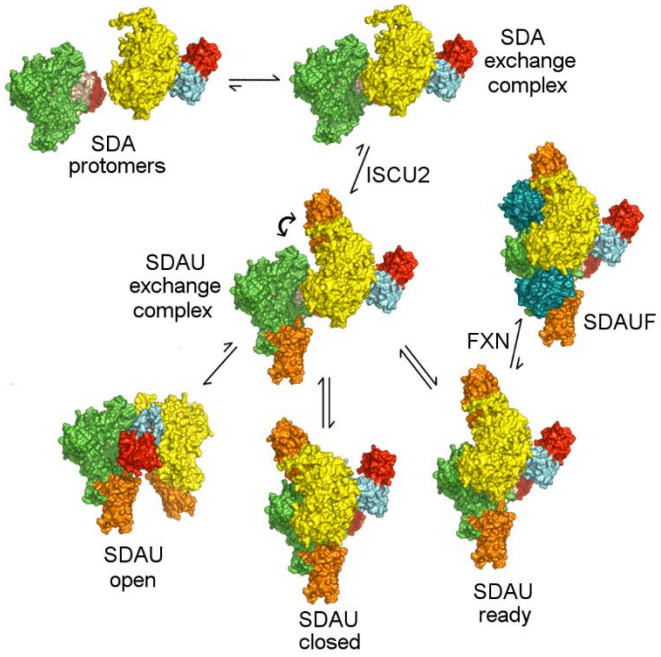

Figure 4.23 Morpheein model for the Fe-S cluster biosynthetic subcomplex. The open, closed, and ready architectures are in equilibrium and interconvert through a tethered exchange complex. FXN binding stabilizes the ready form to activate the complex. The SDA but not SDAU complex undergoes complete protomer dissociation. NFS1 (green and yellow), ISD11 (wheat and cyan), ACP (red), ISCU2 (orange) and FXN (dark teal) subunits shown as surfaces.

Our results provide support and extend an architectural switch model in which FXN drives a change in the quaternary structure to activate the cysteine desulfurase and Fe-S cluster assembly activities [214]. We propose the $SDA_{ec}U$ sample exists as an equilibrium mixture of open, closed, and ready forms (Figure 4.23). These forms likely interconvert through a tethered exchange complex rather than complete protomer dissociation as the $SDA_{ec}U$ sample does not swap protomers in exchange assays (Figure 4.9). Such a tethered exchange complex would require the ability to rotate one protomer relative to the other and sample the different open,

closed, and ready conformations. Our IM-MS data reveals the addition of FXN converts the sample from existing as multiple species to one form, almost certainly the $SDA_{ec}UF$ observed in the cryo-EM structure [107]. Binding at the protomer interface and interact with both NFS1, the FXN subunit acts as a "molecular lock" that stitches the two protomers together in the ready form; whereas, FXN would be expected to be sterically precluded by the relative rotation of the two protomers in the closed architecture and would lose much of its binding interactions in the open form (Figure 4.24). Driving the complex to the ready form would change the mobile S-transfer loop from a primarily disordered (open form) and potentially inhibited (closed form) to a functional trajectory (ready form) that promotes the PLP and sulfur transfer chemistry (Figure 4.22). The inability of the sulfur acceptor protein ISCU2 to shift the population of these different architectures is consistent with its inability to activate the SDA_{ec} complex [103]. The SDA_{ec} complex likely also exists as an equilibrium mixture of open, closed, and ready forms that interchange through a tethered exchange complex (Figure 4.23). However, with the SDA_{ec} complex, there must be occasional complete dissociation into protomers to explain the slow exchange reaction (Figure 4.9).

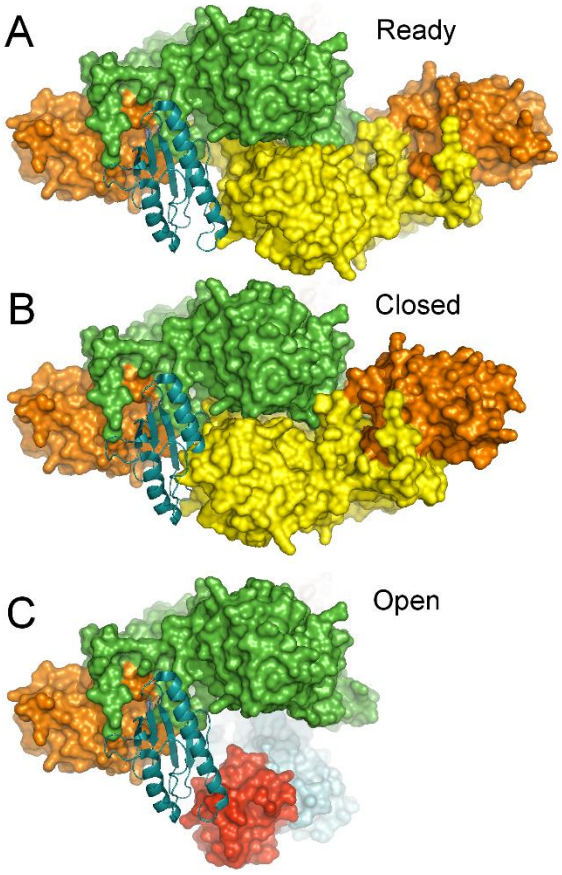

Figure 4.24 Comparison of FXN binding to the different architecture models. (A) Structure of the $SDA_{ec}U$ complex with one FXN bound in the ready (A), closed (B), and open (C) forms. NFS1 surfaces colored in green and yellow, ISD11 in wheat and cyan, ACP_{ec} in red, ISCU2 in orange, and FXN as a teal ribbon diagram. The closed and open forms are based on the binding interaction in the $SDA_{ec}UF$ cryo-EM structure in the ready form. FXN binding has either significant steric clash (closed) or loses interactions (open) with the NFS1 subunit (yellow) from the other protomer.

This type of global structural re-arrangement is, to our knowledge, uncommon. The closest system that describes this process is the morpheein model. Morpheeins are enzymatic systems that are in a dynamic equilibrium with a variety of different oligomeric or architectural states. The equilibrium between states is allosterically regulated, and for one oligomer or architecture to convert to the other, the system must dissociate, undergo a conformational

change, and then re-associate [310]. Similarly, we propose the population of the open, closed, and ready architectures of the $SDA_{ec}U$ complex are determined by conformational differences in the $SDA_{ec}U$ protomers of the exchange complex and then interactions that stabilize the different $\alpha_2\beta_2\gamma_2$ quaternary structures (Figure 4.23). We tested this hypothesis by designing the SHQ variant, which showed enhanced activity and changes in IM-MS and cation exchange results consistent with a shifted population away from the open form and towards a closed or ready form. Examples of human morpheeins are phenylalanine hydroxylase [311], porphobilinogen synthase [312], and cystathionine β-synthase [313]. These systems are typically regulated by small-molecule effectors. In the human Fe-S assembly system, the mechanism of architectural control is through stabilization of the active form by the "molecular lock" FXN. Interestingly, clinical mutations can affect oligomeric distributions and activities for morpheein systems [311, 313, 314]. It will be interesting to evaluate whether clinical variants of NFS1, ISD11, ISCU, and FXN [89, 292, 315-318] alter the equilibrium between different architectures or potentially fail to lock the complex in the active form.

In summary, these and previous studies provide substantial evidence that the eukaryotic cysteine desulfurase is a morpheein-like system that controls activity by its oligomeric form (Table 1). Determining additional details for the mechanistic relationship and functional roles of the different architectures will require thoughtfully designed biochemical probes and high-resolution structural analysis. One possibility is that these architectures are part of a protein assembly based regulatory mechanism that controls sulfur transfer from the SDA_{ec} complex to acceptor proteins for Fe-S cluster assembly, molybdenum cofactor biosynthesis, and tRNA modifications. Overall, we have provided new insights into the relationship between the eukaryotic cysteine desulfurase

architectures and the mechanism of FXN activation that have implications for the regulation of Fe-S cluster assembly. Finally, the ability of the SHQ variant to partially replace FXN function by shifting the population of quaternary structures suggests that molecules that drive a similar architectural switch may have potential applications as FRDA therapeutics.

5. CONCLUSION

Due to the essential functions Fe-S clusters among organisms, significant efforts have been invested to reveal the mechanism of Fe-S cluster biogenesis. Dysfunction of ISC Fe-S cluster biogenesis pathway leads to severe diseases.[274] Mutations on the scaffold protein ISCU leads to hereditary mitochondrial myopathy.[319] Infantile mitochondrial complex II/III deficiency has been reported to be caused by NFS1 deficiency.[320] The most prominent disease, Friedreich's Ataxia, is a result of a GAA triplet repeat expansion or point mutations in the FXN gene.[111] Comprehensive understanding of the Fe-S cluster biogenesis mechanism has been long desired to better understand the pathology of these diseases for therapeutic development. Through extensive genetic, bioinformatic, *in vivo*, and *in vitro* studies, a good overview of how the ISC pathway assembles Fe-S clusters has been provided. While current techniques and methodologies provide wealth information, certain key mechanistic questions remain elusive. To resolve these challenges, new techniques that could go beyond the limitation of current bioinorganic techniques are required.

Native ion-mobility mass spectrometry (IM-MS) has been developed into a new powerful technique for getting binding, structural and sequencing information simultaneously. This unique aspect of getting multi-dimension information in a single analysis leads to increased popularity of native IM-MS in both the biophysical society and the pharmaceutical industry. For example, native IM-MS is arguably the most effective technique for characterization of membrane protein acceptors. The ever improvement on the mass spectrometers is the key for expanding the application of native IM-MS. High resolution orbitrap instruments with optimized ion optics for transmission enable the analysis of mega Dalton large biomolecules such as ribosome. Improved

theoretical calculation of collisional cross section and resolution on ion mobility allow more confidential analysis of small molecule positional isomers and protein structural isomers. Further comprehensive structural information could be obtained when native IM-MS couples with other biophysical mass spectrometry techniques, such as cross-linking mass spectrometry (XL-MS) for identifying adjacent residues, as well as hydrogen-deuterium exchange mass spectrometry (HDX-MS) and hydroxyl radical footprinting-mass spectrometry (HRF-MS) for mapping solvent accessible residues. As the power of native IM-MS on revealing Fe-S cluster biosynthesis mechanism is highlighted in this dissertation, development on the technique and complement with other MS methodologies would further deepen our understanding on these complicated enzyme systems.

Our understanding of how the ISC pathway assemble Fe-S cluster on the scaffold protein has been long limited by the lack of intermediate information. Bioinorganic spectroscopic techniques including Mossbauer spectroscopy, electron paramagnetic spectroscopy (EPR), and CD spectroscopy are unable to resolve the overlapping signals from mixture of Fe-S species. Here, we tracked and resolved these Fe-S intermediates using high-resolution native MS under an experimental condition using a biological relevant reductant GSH. Our pioneer application successfully revealed long-sought intermediates and suggest iron binding on the scaffold protein as the key early step of promoting the sulfur transfer step. Despite this initial success, the current methodology is limited by the low time-resolution for kinetic studies. The low time-resolution requires longer time scale reaction, which was deliberately achieved by using low reductant concentration and high scaffold protein concentration. Also, the current methodology is not strictly anaerobic, which limits our ability of probing potential reduction events by Fdx. Herein,

a tailored nano-electrospray source design is proposed for improving the time-resolution and anaerobicity of the source. A gas-tight syringe containing the sample will be directly connected to the nano-spray source for direct infusion. Two gas-tight syringes will be initially kept in a glove box. One will contain rinsing buffer and the other will contain the sample. The gas-tight syringe will be brought out of the box, and the nano-spray source will be first rinsed by the syringe containing anaerobic buffer before loading the syringe containing the sample. This whole process will help maintain the MS analyzing process to be as anaerobic as possible. Furthermore, this source will also be adaptive to a T-shape connector containing three outlets. Two outlets will be connected to two sample-containing syringes and the other one will be fused into the mass spectrometer. With the ability to probe short time kinetics (second scale) using the T-junction connector, this application enables us to change the assay conditions into overall more physiologically resembled conditions with faster rate and anaerobic-like setup.

The solved structures of the human cysteine desulfurase complexes largely enhanced our understanding on the biophysical characteristics of the human ISC system. By employing native IM-MS, we illustrate the regulation mechanism of the human ISC system on the structural level. Nevertheless, further investigation on this morpheein-like system and its potential regulation on sulfur trafficking to other pathways, including molybdenum cofactor biosynthesis and tRNA thiolation pathways, is desired. Currently, IM-MS is able to resolve open architecture and closed/ready architecture. Closed and ready architecture could not be resolved due to their similar overall conformation and CCS. One way to resolve this challenge is by enhancing the IM resolution. The home-built high-resolution FT-IMS in the Russell group could potentially distinguish closed and ready architectures when both co-exists. In addition, MS-based

biophysical methodologies such as XL-MS, HDX-MS, and HFR-MS could potentially resolve and quantitate these different architectures. A common challenge on using these MS methods to probe the human ISC complexes is the exchange nature among the architectures. The dynamic solvent accessible area and residue interactions could easily lead to unresolvable results. Therefore, methodologies that can "lock" these architectures from exchanging are crucial for these advanced biophysical characterizations. One potential way to achieve this is by designing "clickable" non-canonical amino acids on unique adjacent residues in each architecture. Characterizations on activity, binding, and sulfur trafficking to different pathways of human ISC complex materials with single pure architecture would largely enhance our understanding on the regulation of this perplex system.

The putative roles and the inhibition mechanism of CyaY on the bacterial ISC system were one of the most perplexing enigmas in the Fe-S cluster biogenesis field. By studying complicated competitive binding of sulfur acceptors and sulfur trafficking, we managed to reveal the missing links among CyaY regulation on sulfur trafficking and oxidative stress. Despite our thorough *in vitro* studies, further *in vivo* experiments are desired to validate our model. Comparing the GSSH level of wildtype *E. coli* and CyaY knockout using chemical proteomics, in which maleimide serves as the thiol quenching reagent to compare normal physiological condition with iron rich and/or high H_2O_2 conditions would be good future experiments. In addition, the employment of native IM-MS on resolving and quantitating complicated binding species of sulfur acceptor and cysteine desulfurase mixtures might also arguably be the only techniques that would illustrate the same question on other organisms such as yeast and human. Similar complicated binding and

sulfur trafficking studies on the proposed CyaY equivalence IscX and the proposed electron donor Fdx would also potentially reveal other regulation mechanisms on the ISC system.

Together, there is tremendous potential for application of MS-based biophysical characterization on interrogating the regulation on the ISC machinery and sulfur trafficking. Employment and development of new methods is the key for the interrogation of challenging and detailed fundamental questions on the ISC system, including mechanism of cluster assembly and transfer under physiological-like conditions, regulation and the purpose of different human ISC architectures, as well as the mechanism of action of different effectors on the ISC machinery. This dissertation highlights the implement of advanced MS-based methods in a classic biological field, which would also be beneficial for the investigation on other biological questions.

REFERENCES

1. Chapman, S. K.; White, S. A.; Reid, G. A., Flavocytochrome B2. In *Advances in Inorganic Chemistry*, Sykes, A. G., Ed. Academic Press: 1991; Vol. 36, pp 257-301.
2. Urban, P.; Chirat, I.; Lederer, F., Rat kidney L-2-hydroxyacid oxidase. Structural and mechanistic comparison with flavocytochrome b2 from bakers' yeast. *Biochemistry* **1988,** *27* (19), 7365-7371.
3. Bueschl, C.; Krska, R.; Kluger, B.; Schuhmacher, R., Isotopic labeling-assisted metabolomics using LC-MS. *Anal Bioanal Chem* **2013,** *405* (1), 27-33.
4. Scaraffia, P. Y.; Zhang, Q.; Thorson, K.; Wysocki, V. H.; Miesfeld, R. L., Differential ammonia metabolism in Aedes aegypti fat body and midgut tissues. *Journal of Insect Physiology* **2010,** *56* (9), 1040-1049.
5. Wysocki, V. H.; Cheng, G.; Zhang, Q.; Herrmann, K. A.; Beardsley, R. L.; Hilderbrand, A. E., Peptide Fragmentation Overview. In *Principles of Mass Spectrometry Applied to Biomolecules*, 2006; pp 277-300.
6. Tamvakopoulos, C., Mass spectrometry for the quantification of bioactive peptides in biological fluids. **2007,** *26* (3), 389-402.
7. Han, X.; Aslanian, A.; Yates, J. R., Mass spectrometry for proteomics. *Current Opinion in Chemical Biology* **2008,** *12* (5), 483-490.
8. Halquist, M. S.; Thomas Karnes, H., Quantitative liquid chromatography tandem mass spectrometry analysis of macromolecules using signature peptides in biological fluids. **2011,** *25* (1-2), 47-58.
9. Beveridge, R.; Chappuis, Q.; Macphee, C.; Barran, P., Mass spectrometry methods for intrinsically disordered proteins. *Analyst* **2013,** *138* (1), 32-42.
10. Wetzel, C.; Limbach, P. A., Mass spectrometry of modified RNAs: recent developments. *Analyst* **2016,** *141* (1), 16-23.
11. Hilton, G. R.; Benesch, J. L., Two decades of studying non-covalent biomolecular assemblies by means of electrospray ionization mass spectrometry. *J R Soc Interface* **2012,** *9* (70), 801-16.
12. Heck, A. J. R., Native mass spectrometry: a bridge between interactomics and structural biology. *Nature Methods* **2008,** *5* (11), 927-933.
13. Heuvel, R. H. H. v. d.; Heck, A. J. R., Native protein mass spectrometry: from intact oligomers to functional machineries. *Current Opinion in Chemical Biology* **2004,** *8* (5), 519-526.
14. Sharon, M.; Robinson, C. V., The Role of Mass Spectrometry in Structure Elucidation of Dynamic Protein Complexes. **2007,** *76* (1), 167-193.
15. Fenn, J. B.; Mann, M.; Meng, C. K.; Wong, S. F.; Whitehouse, C. M., Electrospray ionization for mass spectrometry of large biomolecules. *Science* **1989,** *246* (4926), 64.
16. Light-Wahl, K. J.; Schwartz, B. L.; Smith, R. D., Observation of the Noncovalent Quaternary Associations of Proteins by Electrospray Ionization Mass Spectrometry. *Journal of the American Chemical Society* **1994,** *116* (12), 5271-5278.
17. Smith, R. D.; Loo, J. A.; Edmonds, C. G.; Barinaga, C. J.; Udseth, H. R., New developments in biochemical mass spectrometry: electrospray ionization. *Analytical Chemistry* **1990,** *62* (9), 882-899.

18. Chen, X.; Qin, S.; Chen, S.; Li, J.; Li, L.; Wang, Z.; Wang, Q.; Lin, J.; Yang, C.; Shui, W., A Ligand-observed Mass Spectrometry Approach Integrated into the Fragment Based Lead Discovery Pipeline. *Scientific Reports* **2015,** *5* (1), 8361.
19. Beveridge, R.; Kessler, D.; Rumpel, K.; Ettmayer, P.; Meinhart, A.; Clausen, T., Native mass spectrometry can effectively predict PROTAC efficacy. *bioRxiv* **2019**, 851980.
20. Gavriilidou, A. F. M.; Holding, F. P.; Coyle, J. E.; Zenobi, R., Application of Native ESI-MS to Characterize Interactions between Compounds Derived from Fragment-Based Discovery Campaigns and Two Pharmaceutically Relevant Proteins. *SLAS DISCOVERY: Advancing the Science of Drug Discovery* **2018,** *23* (9), 951-959.
21. Hernández, H.; Robinson, C. V., Determining the stoichiometry and interactions of macromolecular assemblies from mass spectrometry. *Nature Protocols* **2007,** *2* (3), 715-726.
22. Benesch, J. L. P.; Ruotolo, B. T.; Simmons, D. A.; Robinson, C. V., Protein Complexes in the Gas Phase: Technology for Structural Genomics and Proteomics. *Chemical Reviews* **2007,** *107* (8), 3544-3567.
23. Benesch, J. L. P.; Ruotolo, B. T., Mass spectrometry: come of age for structural and dynamical biology. *Current Opinion in Structural Biology* **2011,** *21* (5), 641-649.
24. Wyttenbach, T.; Bowers, M. T., Structural Stability from Solution to the Gas Phase: Native Solution Structure of Ubiquitin Survives Analysis in a Solvent-Free Ion Mobility–Mass Spectrometry Environment. *The Journal of Physical Chemistry B* **2011,** *115* (42), 12266-12275.
25. Uetrecht, C.; Rose, R. J.; van Duijn, E.; Lorenzen, K.; Heck, A. J. R., Ion mobility mass spectrometry of proteins and protein assemblies. *Chemical Society Reviews* **2010,** *39* (5), 1633-1655.
26. Valentine, S. J.; Counterman, A. E.; Clemmer, D. E., Conformer-dependent proton-transfer reactions of ubiquitin ions. *Journal of the American Society for Mass Spectrometry* **1997,** *8* (9), 954-961.
27. de la Mora, J. F., Why do GroEL Ions Exhibit Two Gas Phase Conformers? *Journal of The American Society for Mass Spectrometry* **2012,** *23* (12), 2115-2121.
28. Hogan, C. J.; Ruotolo, B. T.; Robinson, C. V.; Fernandez de la Mora, J., Tandem Differential Mobility Analysis-Mass Spectrometry Reveals Partial Gas-Phase Collapse of the GroEL Complex. *The Journal of Physical Chemistry B* **2011,** *115* (13), 3614-3621.
29. Hoffmann, W.; von Helden, G.; Pagel, K., Ion mobility-mass spectrometry and orthogonal gas-phase techniques to study amyloid formation and inhibition. *Current Opinion in Structural Biology* **2017,** *46*, 7-15.
30. Bolla, J. R.; Agasid, M. T.; Mehmood, S.; Robinson, C. V., Membrane Protein–Lipid Interactions Probed Using Mass Spectrometry. **2019,** *88* (1), 85-111.
31. Laganowsky, A.; Reading, E.; Allison, T. M.; Ulmschneider, M. B.; Degiacomi, M. T.; Baldwin, A. J.; Robinson, C. V., Membrane proteins bind lipids selectively to modulate their structure and function. *Nature* **2014,** *510*, 172.
32. Crack, J. C.; Thomson, A. J.; Le Brun, N. E., Mass spectrometric identification of intermediates in the O₂-driven [4Fe–4S] to [2Fe–2S] cluster conversion in FNR. **2017,** *114* (16), E3215-E3223.
33. Arnon, D. I.; Whatley, F. R.; Allen, M. B., Triphosphopyridine Nucleotide as a Catalyst of Photosynthetic Phosphorylation. *Nature* **1957,** *180* (4578), 182-185.

34. Mortenson, L. E.; Valentine, R. C.; Carnahan, J. E., An electron transport factor from Clostridiumpasteurianum. *Biochemical and Biophysical Research Communications* **1962,** *7* (6), 448-452.
35. Rees, D. C.; Howard, J. B., The Interface Between the Biological and Inorganic Worlds: Iron-Sulfur Metalloclusters. *Science* **2003,** *300* (5621), 929.
36. Johnson, D. C.; Dean, D. R.; Smith, A. D.; Johnson, M. K., STRUCTURE, FUNCTION, AND FORMATION OF BIOLOGICAL IRON-SULFUR CLUSTERS. **2005,** *74* (1), 247-281.
37. Beinert, H.; Holm, R. H.; Münck, E., Iron-Sulfur Clusters: Nature's Modular, Multipurpose Structures. *Science* **1997,** *277* (5326), 653.
38. Bak, D. W.; Elliott, S. J., Alternative FeS cluster ligands: tuning redox potentials and chemistry. *Current Opinion in Chemical Biology* **2014,** *19*, 50-58.
39. Jacobson, M. R.; Cash, V. L.; Weiss, M. C.; Laird, N. F.; Newton, W. E.; Dean, D. R., Biochemical and genetic analysis of the nifUSVWZM cluster from Azotobacter vinelandii. *Molecular and General Genetics MGG* **1989,** *219* (1), 49-57.
40. Takahashi, Y.; Tokumoto, U., A Third Bacterial System for the Assembly of Iron-Sulfur Clusters with Homologs in Archaea and Plastids. **2002,** *277* (32), 28380-28383.
41. Outten, F. W.; Djaman, O.; Storz, G., A suf operon requirement for Fe–S cluster assembly during iron starvation in Escherichia coli. **2004,** *52* (3), 861-872.
42. Lill, R.; Mühlenhoff, U., Iron-Sulfur Protein Biogenesis in Eukaryotes: Components and Mechanisms. *Annual Review of Cell and Developmental Biology* **2006,** *22* (1), 457-486.
43. Lill, R., Function and biogenesis of iron–sulphur proteins. *Nature* **2009,** *460* (7257), 831-838.
44. Sheftel, A. D.; Lill, R., The power plant of the cell is also a smithy: The emerging role of mitochondria in cellular iron homeostasis. *Annals of Medicine* **2009,** *41* (2), 82-99.
45. Zheng, L.; White, R. H.; Cash, V. L.; Dean, D. R., Mechanism for the Desulfurization of L-Cysteine Catalyzed by the nifS Gene Product. *Biochemistry* **1994,** *33* (15), 4714-4720.
46. Yoon, T.; Cowan, J. A., Iron−Sulfur Cluster Biosynthesis. Characterization of Frataxin as an Iron Donor for Assembly of [2Fe–2S] Clusters in ISU-Type Proteins. *Journal of the American Chemical Society* **2003,** *125* (20), 6078-6084.
47. Lange, H.; Kaut, A.; Kispal, G.; Lill, R., A mitochondrial ferredoxin is essential for biogenesis of cellular iron-sulfur proteins. *Proceedings of the National Academy of Sciences of the United States of America* **2000,** *97* (3), 1050-1055.
48. Alves, R.; Herrero, E.; Sorribas, A., Predictive reconstruction of the mitochondrial iron-sulfur cluster assembly metabolism. II. Role of glutaredoxin Grx5. **2004,** *57* (3), 481-492.
49. Kim, K.-D.; Chung, W.-H.; Kim, H.-J.; Lee, K.-C.; Roe, J.-H., Monothiol glutaredoxin Grx5 interacts with Fe–S scaffold proteins Isa1 and Isa2 and supports Fe–S assembly and DNA integrity in mitochondria of fission yeast. *Biochemical and Biophysical Research Communications* **2010,** *392* (3), 467-472.
50. Kim, J. H.; Frederick, R. O.; Reinen, N. M.; Troupis, A. T.; Markley, J. L., [2Fe–2S]-Ferredoxin Binds Directly to Cysteine Desulfurase and Supplies an Electron for Iron–Sulfur Cluster Assembly but Is Displaced by the Scaffold Protein or Bacterial Frataxin. *Journal of the American Chemical Society* **2013,** *135* (22), 8117-8120.
51. Gervason, S.; Larkem, D.; Mansour, A. B.; Botzanowski, T.; Müller, C. S.; Pecqueur, L.; Le Pavec, G.; Delaunay-Moisan, A.; Brun, O.; Agramunt, J.; Grandas, A.; Fontecave, M.;

Schünemann, V.; Cianférani, S.; Sizun, C.; Tolédano, M. B.; D'Autréaux, B., Physiologically relevant reconstitution of iron-sulfur cluster biosynthesis uncovers persulfide-processing functions of ferredoxin-2 and frataxin. *Nature Communications* **2019,** *10* (1), 3566.
52. Ding, H.; Clark, R. J.; Ding, B., IscA Mediates Iron Delivery for Assembly of Iron-Sulfur Clusters in IscU under the Limited Accessible Free Iron Conditions*. *Journal of Biological Chemistry* **2004,** *279* (36), 37499-37504.
53. Tong, W.-H.; Jameson, G. N. L.; Huynh, B. H.; Rouault, T. A., Subcellular compartmentalization of human Nfu, an iron–sulfur cluster scaffold protein, and its ability to assemble a [4Fe–4S] cluster. *Proceedings of the National Academy of Sciences* **2003,** *100* (17), 9762.
54. Liu, Y.; Cowan, J. A., Iron sulfur cluster biosynthesis. Human NFU mediates sulfide delivery to ISU in the final step of [2Fe–2S] cluster assembly. *Chemical Communications* **2007,** (30), 3192-3194.
55. Olive, J. A.; Cowan, J. A., Role of the HSPA9/HSC20 chaperone pair in promoting directional human iron-sulfur cluster exchange involving monothiol glutaredoxin 5. *Journal of Inorganic Biochemistry* **2018,** *184*, 100-107.
56. Bridwell-Rabb, J.; Fox, N. G.; Tsai, C. L.; Winn, A. M.; Barondeau, D. P., Human frataxin activates Fe-S cluster biosynthesis by facilitating sulfur transfer chemistry. *Biochemistry* **2014,** *53* (30), 4904-13.
57. Parent, A.; Elduque, X.; Cornu, D.; Belot, L.; Le Caer, J. P.; Grandas, A.; Toledano, M. B.; D'Autreaux, B., Mammalian frataxin directly enhances sulfur transfer of NFS1 persulfide to both ISCU and free thiols. *Nat. Commun.* **2015,** *6*.
58. Smith, A. D.; Frazzon, J.; Dean, D. R.; Johnson, M. K., Role of conserved cysteines in mediating sulfur transfer from IscS to IscU. *FEBS Lett.* **2005,** *579* (23), 5236-40.
59. Kato, S.; Mihara, H.; Kurihara, T.; Takahashi, Y.; Tokumoto, U.; Yoshimura, T.; Esaki, N., Cys-328 of IscS and Cys-63 of IscU are the sites of disulfide bridge formation in a covalently bound IscS/IscU complex: implications for the mechanism of iron-sulfur cluster assembly. *Proc. Natl. Acad. Sci. U.S.A.* **2002,** *99* (9), 5948-52.
60. Marinoni, E. N.; de Oliveira, J. S.; Nicolet, Y.; Raulfs, E. C.; Amara, P.; Dean, D. R.; Fontecilla-Camps, J. C., (IscS-IscU)2 complex structures provide insights into Fe2S2 biogenesis and transfer. *Angew Chem Int Ed Engl* **2012,** *51* (22), 5439-42.
61. Ramelot, T. A.; Cort, J. R.; Goldsmith-Fischman, S.; Kornhaber, G. J.; Xiao, R.; Shastry, R.; Acton, T. B.; Honig, B.; Montelione, G. T.; Kennedy, M. A., Solution NMR structure of the iron-sulfur cluster assembly protein U (IscU) with zinc bound at the active site. *J Mol Biol* **2004,** *344* (2), 567-83.
62. Kim, J. H.; Tonelli, M.; Markley, J. L., Disordered form of the scaffold protein IscU is the substrate for iron-sulfur cluster assembly on cysteine desulfurase. *Proceedings of the National Academy of Sciences* **2012,** *109* (2), 454.
63. Bothe, Jameson R.; Tonelli, M.; Ali, Ibrahim K.; Dai, Z.; Frederick, Ronnie O.; Westler, William M.; Markley, John L., The Complex Energy Landscape of the Protein IscU. *Biophysical Journal* **2015,** *109* (5), 1019-1025.
64. Kim, J. H.; Tonelli, M.; Markley, J. L., Disordered form of the scaffold protein IscU is the substrate for iron-sulfur cluster assembly on cysteine desulfurase. *Proc Natl Acad Sci U S A* **2012,** *109* (2), 454-9.

65. Markley, J. L.; Kim, J. H.; Dai, Z.; Bothe, J. R.; Cai, K.; Frederick, R. O.; Tonelli, M., Metamorphic protein IscU alternates conformations in the course of its role as the scaffold protein for iron-sulfur cluster biosynthesis and delivery. *FEBS Lett* **2013,** *587* (8), 1172-9.
66. Kim, J. H.; Tonelli, M.; Kim, T.; Markley, J. L., Three-dimensional structure and determinants of stability of the iron-sulfur cluster scaffold protein IscU from Escherichia coli. *Biochemistry* **2012,** *51* (28), 5557-63.
67. Adrover, M.; Howes, B. D.; Iannuzzi, C.; Smulevich, G.; Pastore, A., Anatomy of an iron-sulfur cluster scaffold protein: Understanding the determinants of [2Fe–2S] cluster stability on IscU. *Biochimica et Biophysica Acta (BBA) - Molecular Cell Research* **2015,** *1853* (6), 1448-1456.
68. Zheng, L.; White, R. H.; Cash, V. L.; Dean, D. R., Mechanism for the desulfurization of L-cysteine catalyzed by the nifS gene product. *Biochemistry* **1994,** *33* (15), 4714-20.
69. Zheng, L.; White, R. H.; Cash, V. L.; Jack, R. F.; Dean, D. R., Cysteine desulfurase activity indicates a role for NIFS in metallocluster biosynthesis. *Proc. Natl. Acad. Sci. U.S.A.* **1993,** *90* (7), 2754-8.
70. Behshad, E.; Bollinger, J. M., Jr., Kinetic analysis of cysteine desulfurase CD0387 from Synechocystis sp. PCC 6803: formation of the persulfide intermediate. *Biochemistry* **2009,** *48* (50), 12014-23.
71. Tirupati, B.; Vey, J. L.; Drennan, C. L.; Bollinger, J. M., Jr., Kinetic and structural characterization of Slr0077/SufS, the essential cysteine desulfurase from Synechocystis sp. PCC 6803. *Biochemistry* **2004,** *43* (38), 12210-9.
72. Behshad, E.; Parkin, S. E.; Bollinger, J. M., Jr., Mechanism of cysteine desulfurase Slr0387 from Synechocystis sp. PCC 6803: kinetic analysis of cleavage of the persulfide intermediate by chemical reductants. *Biochemistry* **2004,** *43* (38), 12220-6.
73. Kaiser, J. T.; Clausen, T.; Bourenkow, G. P.; Bartunik, H. D.; Steinbacher, S.; Huber, R., Crystal structure of a NifS-like protein from Thermotoga maritima: implications for iron sulphur cluster assembly. *J. Mol. Biol.* **2000,** *297* (2), 451-64.
74. Shi, R.; Proteau, A.; Villarroya, M.; Moukadiri, I.; Zhang, L.; Trempe, J. F.; Matte, A.; Armengod, M. E.; Cygler, M., Structural basis for Fe-S cluster assembly and tRNA thiolation mediated by IscS protein-protein interactions. *PLoS Biol* **2010,** *8* (4), e1000354.
75. Kim, J. H.; Bothe, J. R.; Frederick, R. O.; Holder, J. C.; Markley, J. L., Role of IscX in iron-sulfur cluster biogenesis in Escherichia coli. *J Am Chem Soc* **2014,** *136* (22), 7933-42.
76. Smith, A. D.; Agar, J. N.; Johnson, K. A.; Frazzon, J.; Amster, I. J.; Dean, D. R.; Johnson, M. K., Sulfur transfer from IscS to IscU: the first step in iron-sulfur cluster biosynthesis. *J Am Chem Soc* **2001,** *123* (44), 11103-4.
77. Sendra, M.; Ollagnier de Choudens, S.; Lascoux, D.; Sanakis, Y.; Fontecave, M., The SUF iron–sulfur cluster biosynthetic machinery: Sulfur transfer from the SUFS–SUFE complex to SUFA. *FEBS Letters* **2007,** *581* (7), 1362-1368.
78. Fontecave, M.; Choudens, S. O.; Py, B.; Barras, F., Mechanisms of iron-sulfur cluster assembly: the SUF machinery. *J Biol Inorg Chem* **2005,** *10* (7), 713-21.
79. Layer, G.; Ollagnier-de Choudens, S.; Sanakis, Y.; Fontecave, M., Iron-Sulfur Cluster Biosynthesis: CHARACTERIZATION OF ESCHERICHIA COLI CYaY AS AN IRON DONOR FOR THE ASSEMBLY OF [2Fe–2S] CLUSTERS IN THE SCAFFOLD IscU. **2006,** *281* (24), 16256-16263.

80. Mansy, S. S.; Wu, G.; Surerus, K. K.; Cowan, J. A., Iron-Sulfur Cluster Biosynthesis: THERMATOGA MARITIMA IscU IS A STRUCTURED IRON-SULFUR CLUSTER ASSEMBLY PROTEIN *. *Journal of Biological Chemistry* **2002,** *277* (24), 21397-21404.
81. Bridwell-Rabb, J.; Iannuzzi, C.; Pastore, A.; Barondeau, D. P., Effector role reversal during evolution: the case of frataxin in Fe-S cluster biosynthesis. *Biochemistry* **2012,** *51* (12), 2506-14.
82. Land, T.; Rouault, T. A., Targeting of a human iron-sulfur cluster assembly enzyme, nifs, to different subcellular compartments is regulated through alternative AUG utilization. *Mol Cell* **1998,** *2* (6), 807-15.
83. Biederbick, A.; Stehling, O.; Rosser, R.; Niggemeyer, B.; Nakai, Y.; Elsasser, H. P.; Lill, R., Role of human mitochondrial Nfs1 in cytosolic iron-sulfur protein biogenesis and iron regulation. *Mol Cell Biol* **2006,** *26* (15), 5675-87.
84. Yan, R.; Friemel, M.; Aloisi, C.; Huynen, M.; Taylor, I. A.; Leimkuhler, S.; Pastore, A., The Eukaryotic-Specific ISD11 Is a Complex-Orphan Protein with Ability to Bind the Prokaryotic IscS. *PLoS One* **2016,** *11* (7), e0157895.
85. Cai, K.; Frederick, R. O.; Tonelli, M.; Markley, J. L., Mitochondrial Cysteine Desulfurase and ISD11 Coexpressed in Escherichia coli Yield Complex Containing Acyl Carrier Protein. *ACS Chem. Biol.* **2017,** *12* (4), 918-921.
86. Cupp-Vickery, J. R.; Urbina, H.; Vickery, L. E., Crystal structure of IscS, a cysteine desulfurase from Escherichia coli. *J. Mol. Biol.* **2003,** *330* (5), 1049-59.
87. Marelja, Z.; Stocklein, W.; Nimtz, M.; Leimkuhler, S., A novel role for human Nfs1 in the cytoplasm: Nfs1 acts as a sulfur donor for MOCS3, a protein involved in molybdenum cofactor biosynthesis. *J. Biol. Chem.* **2008,** *283* (37), 25178-85.
88. Adam, A. C.; Bornhovd, C.; Prokisch, H.; Neupert, W.; Hell, K., The Nfs1 interacting protein Isd11 has an essential role in Fe/S cluster biogenesis in mitochondria. *EMBO J.* **2006,** *25* (1), 174-83.
89. Lim, S. C.; Friemel, M.; Marum, J. E.; Tucker, E. J.; Bruno, D. L.; Riley, L. G.; Christodoulou, J.; Kirk, E. P.; Boneh, A.; DeGennaro, C. M.; Springer, M.; Mootha, V. K.; Rouault, T. A.; Leimkuhler, S.; Thorburn, D. R.; Compton, A. G., Mutations in LYRM4, encoding iron-sulfur cluster biogenesis factor ISD11, cause deficiency of multiple respiratory chain complexes. *Hum. Mol. Genet.* **2013,** *22* (22), 4460-73.
90. Friemel, M.; Marelja, Z.; Li, K.; Leimkuhler, S., The N-Terminus of Iron-Sulfur Cluster Assembly Factor ISD11 Is Crucial for Subcellular Targeting and Interaction with l-Cysteine Desulfurase NFS1. *Biochemistry* **2017,** *56* (12), 1797-1808.
91. Huttlin, E. L.; Bruckner, R. J.; Paulo, J. A.; Cannon, J. R.; Ting, L.; Baltier, K.; Colby, G.; Gebreab, F.; Gygi, M. P.; Parzen, H.; Szpyt, J.; Tam, S.; Zarraga, G.; Pontano-Vaites, L.; Swarup, S.; White, A. E.; Schweppe, D. K.; Rad, R.; Erickson, B. K.; Obar, R. A.; Guruharsha, K. G.; Li, K.; Artavanis-Tsakonas, S.; Gygi, S. P.; Harper, J. W., Architecture of the human interactome defines protein communities and disease networks. *Nature* **2017,** *545* (7655), 505-509.
92. Floyd, B. J.; Wilkerson, E. M.; Veling, M. T.; Minogue, C. E.; Xia, C.; Beebe, E. T.; Wrobel, R. L.; Cho, H.; Kremer, L. S.; Alston, C. L.; Gromek, K. A.; Dolan, B. K.; Ulbrich, A.; Stefely, J. A.; Bohl, S. L.; Werner, K. M.; Jochem, A.; Westphall, M. S.; Rensvold, J. W.;

Taylor, R. W.; Prokisch, H.; Kim, J. P.; Coon, J. J.; Pagliarini, D. J., Mitochondrial Protein Interaction Mapping Identifies Regulators of Respiratory Chain Function. *Mol Cell* **2016,** *63* (4), 621-632.
93. Huttlin, E. L.; Ting, L.; Bruckner, R. J.; Gebreab, F.; Gygi, M. P.; Szpyt, J.; Tam, S.; Zarraga, G.; Colby, G.; Baltier, K.; Dong, R.; Guarani, V.; Vaites, L. P.; Ordureau, A.; Rad, R.; Erickson, B. K.; Wuhr, M.; Chick, J.; Zhai, B.; Kolippakkam, D.; Mintseris, J.; Obar, R. A.; Harris, T.; Artavanis-Tsakonas, S.; Sowa, M. E.; De Camilli, P.; Paulo, J. A.; Harper, J. W.; Gygi, S. P., The BioPlex Network: A Systematic Exploration of the Human Interactome. *Cell* **2015,** *162* (2), 425-440.
94. Majmudar, J. D.; Feng, X.; Fox, N. G.; Nabhan, J. F.; Towle, T.; Ma, T.; Gooch, R.; Bulawa, C.; Yue, W. W.; Martelli, A., 4'-Phosphopantetheine and long acyl chain-dependent interactions are integral to human mitochondrial acyl carrier protein function. *Medchemcomm* **2019,** *10* (2), 209-220.
95. Zhu, J.; King, M. S.; Yu, M.; Klipcan, L.; Leslie, A. G.; Hirst, J., Structure of subcomplex Ibeta of mammalian respiratory complex I leads to new supernumerary subunit assignments. *Proc. Natl. Acad. Sci. U.S.A.* **2015,** *112* (39), 12087-92.
96. Angerer, H.; Radermacher, M.; Mankowska, M.; Steger, M.; Zwicker, K.; Heide, H.; Wittig, I.; Brandt, U.; Zickermann, V., The LYR protein subunit NB4M/NDUFA6 of mitochondrial complex I anchors an acyl carrier protein and is essential for catalytic activity. *Proc. Natl. Acad. Sci. U.S.A.* **2014,** *111* (14), 5207-12.
97. Fiedorczuk, K.; Letts, J. A.; Degliesposti, G.; Kaszuba, K.; Skehel, M.; Sazanov, L. A., Atomic structure of the entire mammalian mitochondrial complex I. *Nature* **2016,** *538* (7625), 406-410.
98. Richards, T. A.; van der Giezen, M., Evolution of the Isd11-IscS complex reveals a single alpha-proteobacterial endosymbiosis for all eukaryotes. *Mol Biol Evol* **2006,** *23* (7), 1341-4.
99. Shi, Y.; Ghosh, M. C.; Tong, W. H.; Rouault, T. A., Human ISD11 is essential for both iron-sulfur cluster assembly and maintenance of normal cellular iron homeostasis. *Hum. Mol. Genet.* **2009,** *18* (16), 3014-25.
100. Wiedemann, N.; Urzica, E.; Guiard, B.; Muller, H.; Lohaus, C.; Meyer, H. E.; Ryan, M. T.; Meisinger, C.; Muhlenhoff, U.; Lill, R.; Pfanner, N., Essential role of Isd11 in mitochondrial iron-sulfur cluster synthesis on Isu scaffold proteins. *EMBO J* **2006,** *25* (1), 184-95.
101. Cory, S. A.; Van Vranken, J. G.; Brignole, E. J.; Patra, S.; Winge, D. R.; Drennan, C. L.; Rutter, J.; Barondeau, D. P., Structure of human Fe-S assembly subcomplex reveals unexpected cysteine desulfurase architecture and acyl-ACP-ISD11 interactions. *Proc Natl Acad Sci U S A* **2017,** *114* (27), E5325-E5334.
102. Boniecki, M. T.; Freibert, S. A.; Muhlenhoff, U.; Lill, R.; Cygler, M., Structure and functional dynamics of the mitochondrial Fe/S cluster synthesis complex. *Nat. Commun.* **2017,** *8* (1), 1287.
103. Tsai, C. L.; Barondeau, D. P., Human frataxin is an allosteric switch that activates the Fe-S cluster biosynthetic complex. *Biochemistry* **2010,** *49* (43), 9132-9.
104. Saha, P. P.; Srivastava, S.; Kumar S. K, P.; Sinha, D.; D'Silva, P., Mapping Key Residues of ISD11 Critical for NFS1-ISD11 Subcomplex Stability: IMPLICATIONS IN THE DEVELOPMENT OF MITOCHONDRIAL DISORDER, COXPD19 *. *Journal of Biological Chemistry* **2015,** *290* (43), 25876-25890.

105. Hiltunen, J. K.; Autio, K. J.; Schonauer, M. S.; Kursu, V. A.; Dieckmann, C. L.; Kastaniotis, A. J., Mitochondrial fatty acid synthesis and respiration. *Biochim. Biophys. Acta* **2010,** *1797* (6-7), 1195-202.
106. Brody, S.; Oh, C. K.; Hoja, U.; Schweizer, E., Mitochondrial acyl carrier protein is involved in lipoic acid synthesis in Saccharomyces cerevisiae. *FEBS Lett.* **1997,** *408* (2), 217-220.
107. Fox, N. G.; Yu, X.; Feng, X.; Bailey, H. J.; Martelli, A.; Nabhan, J. F.; Strain-Damerell, C.; Bulawa, C.; Yue, W. W.; Han, S., Structure of the human frataxin-bound iron-sulfur cluster assembly complex provides insight into its activation mechanism. *Nat Commun* **2019,** *10* (1), 2210.
108. Herrera, M. G.; Pignataro, M. F.; Noguera, M. E.; Cruz, K. M.; Santos, J., Rescuing the Rescuer: On the Protein Complex between the Human Mitochondrial Acyl Carrier Protein and ISD11. *ACS Chem. Biol.* **2018,** *13* (6), 1455-1462.
109. Qiu, X.; Janson, C. A., Structure of apo acyl carrier protein and a proposal to engineer protein crystallization through metal ions. *Acta Crystallogr D Biol Crystallogr* **2004,** *60* (Pt 9), 1545-54.
110. Byers, D. M.; Gong, H., Acyl carrier protein: structure-function relationships in a conserved multifunctional protein family. *Biochem. Cell Biol.* **2007,** *85* (6), 649-62.
111. Campuzano, V.; Montermini, L.; Molto, M. D.; Pianese, L.; Cossee, M.; Cavalcanti, F.; Monros, E.; Rodius, F.; Duclos, F.; Monticelli, A.; Zara, F.; Canizares, J.; Koutnikova, H.; Bidichandani, S. I.; Gellera, C.; Brice, A.; Trouillas, P.; De Michele, G.; Filla, A.; De Frutos, R.; Palau, F.; Patel, P. I.; Di Donato, S.; Mandel, J. L.; Cocozza, S.; Koenig, M.; Pandolfo, M., Friedreich's ataxia: autosomal recessive disease caused by an intronic GAA triplet repeat expansion. *Science* **1996,** *271* (5254), 1423-7.
112. Cavadini, P.; Adamec, J.; Taroni, F.; Gakh, O.; Isaya, G., Two-step processing of human frataxin by mitochondrial processing peptidase. Precursor and intermediate forms are cleaved at different rates. *J. Biol. Chem.* **2000,** *275* (52), 41469-75.
113. Schmucker, S.; Argentini, M.; Carelle-Calmels, N.; Martelli, A.; Puccio, H., The in vivo mitochondrial two-step maturation of human frataxin. *Hum. Mol. Genet.* **2008,** *17* (22), 3521-31.
114. Muhlenhoff, U.; Richhardt, N.; Ristow, M.; Kispal, G.; Lill, R., The yeast frataxin homolog Yfh1p plays a specific role in the maturation of cellular Fe/S proteins. *Hum Mol Genet* **2002,** *11* (17), 2025-36.
115. Stehling, O.; Elsasser, H. P.; Bruckel, B.; Muhlenhoff, U.; Lill, R., Iron-sulfur protein maturation in human cells: evidence for a function of frataxin. *Hum. Mol. Genet.* **2004,** *13* (23), 3007-15.
116. Yoon, T.; Cowan, J. A., Iron-sulfur cluster biosynthesis. Characterization of frataxin as an iron donor for assembly of [2Fe–2S] clusters in ISU-type proteins. *J Am Chem Soc* **2003,** *125* (20), 6078-84.
117. Ahlgren, E. C.; Fekry, M.; Wiemann, M.; Soderberg, C. A.; Bernfur, K.; Gakh, O.; Rasmussen, M.; Hojrup, P.; Emanuelsson, C.; Isaya, G.; Al-Karadaghi, S., Iron-induced oligomerization of human FXN81-210 and bacterial CyaY frataxin and the effect of iron chelators. *PLoS One* **2017,** *12* (12), e0188937.
118. Manicki, M.; Majewska, J.; Ciesielski, S.; Schilke, B.; Blenska, A.; Kominek, J.; Marszalek, J.; Craig, E. A.; Dutkiewicz, R., Overlapping binding sites of the frataxin homologue assembly factor and the heat shock protein 70 transfer factor on the Isu iron-sulfur cluster scaffold protein. *J. Biol. Chem.* **2014,** *289* (44), 30268-78.

119. Patra, S.; Barondeau, D. P., Mechanism of activation of the human cysteine desulfurase complex by frataxin. *Proceedings of the National Academy of Sciences* **2019,** *116* (39), 19421.
120. Patra, S.; Lin, C.-W.; Ghosh, M. K.; Havens, S. M.; Cory, S. A.; Russell, D. H.; Barondeau, D. P., Recapitulating the frataxin activation mechanism in an engineered bacterial cysteine desulfurase supports the architectural switch model. *bioRxiv* **2020**, 2020.10.06.326603.
121. Adinolfi, S.; Iannuzzi, C.; Prischi, F.; Pastore, C.; Iametti, S.; Martin, S. R.; Bonomi, F.; Pastore, A., Bacterial frataxin CyaY is the gatekeeper of iron-sulfur cluster formation catalyzed by IscS. *Nat. Struct. Mol. Biol.* **2009,** *16* (4), 390-6.
122. Adinolfi, S.; Iannuzzi, C.; Prischi, F.; Pastore, C.; Iametti, S.; Martin, S. R.; Bonomi, F.; Pastore, A., Bacterial frataxin CyaY is the gatekeeper of iron-sulfur cluster formation catalyzed by IscS. *Nature Structural & Molecular Biology* **2009,** *16* (4), 390-396.
123. Roche, B.; Huguenot, A.; Barras, F.; Py, B., The iron-binding CyaY and IscX proteins assist the ISC-catalyzed Fe-S biogenesis in Escherichia coli. *Mol Microbiol* **2015,** *95* (4), 605-23.
124. Fekry, M.; Alshokry, W.; Grela, P.; Tchórzewski, M.; Ahlgren, E.-C.; Söderberg, C. A.; Gakh, O.; Isaya, G.; Al-Karadaghi, S., SAXS and stability studies of iron-induced oligomers of bacterial frataxin CyaY. *PLOS ONE* **2017,** *12* (9), e0184961.
125. Prischi, F.; Pastore, C.; Carroni, M.; Iannuzzi, C.; Adinolfi, S.; Temussi, P.; Pastore, A., Of the vulnerability of orphan complex proteins: The case study of the E. coli IscU and IscS proteins. *Protein Expression and Purification* **2010,** *73* (2), 161-166.
126. Prischi, F.; Konarev, P. V.; Iannuzzi, C.; Pastore, C.; Adinolfi, S.; Martin, S. R.; Svergun, D. I.; Pastore, A., Structural bases for the interaction of frataxin with the central components of iron-sulphur cluster assembly. *Nat Commun* **2010,** *1*, 95.
127. Huynen, M. A.; Snel, B.; Bork, P.; Gibson, T. J., The phylogenetic distribution of frataxin indicates a role in iron-sulfur cluster protein assembly. *Human Molecular Genetics* **2001,** *10* (21), 2463-2468.
128. Puccio, H.; Simon, D.; Cossée, M.; Criqui-Filipe, P.; Tiziano, F.; Melki, J.; Hindelang, C.; Matyas, R.; Rustin, P.; Koenig, M., Mouse models for Friedreich ataxia exhibit cardiomyopathy, sensory nerve defect and Fe-S enzyme deficiency followed by intramitochondrial iron deposits. *Nature Genetics* **2001,** *27* (2), 181-186.
129. Campuzano, V.; Montermini, L.; Moltò, M. D.; Pianese, L.; Cossée, M.; Cavalcanti, F.; Monros, E.; Rodius, F.; Duclos, F.; Monticelli, A.; Zara, F.; Cañizares, J.; Koutnikova, H.; Bidichandani, S. I.; Gellera, C.; Brice, A.; Trouillas, P.; De Michele, G.; Filla, A.; De Frutos, R.; Palau, F.; Patel, P. I.; Di Donato, S.; Mandel, J.-L.; Cocozza, S.; Koenig, M.; Pandolfo, M., Friedreich's Ataxia: Autosomal Recessive Disease Caused by an Intronic GAA Triplet Repeat Expansion. *Science* **1996,** *271* (5254), 1423.
130. Martelli, A.; Napierala, M.; Puccio, H., Understanding the genetic and molecular pathogenesis of Friedreich's ataxia through animal and cellular models. *Disease Models & Mechanisms* **2012,** *5* (2), 165-176.
131. Webert, H.; Freibert, S. A.; Gallo, A.; Heidenreich, T.; Linne, U.; Amlacher, S.; Hurt, E.; Muhlenhoff, U.; Banci, L.; Lill, R., Functional reconstitution of mitochondrial Fe/S cluster synthesis on Isu1 reveals the involvement of ferredoxin. *Nat Commun* **2014,** *5*, 5013.
132. Fox, N. G.; Das, D.; Chakrabarti, M.; Lindahl, P. A.; Barondeau, D. P., Frataxin Accelerates [2Fe–2S] Cluster Formation on the Human Fe-S Assembly Complex. *Biochemistry* **2015,** *54* (25), 3880-9.

133. Pandey, A.; Gordon, D. M.; Pain, J.; Stemmler, T. L.; Dancis, A.; Pain, D., Frataxin directly stimulates mitochondrial cysteine desulfurase by exposing substrate-binding sites, and a mutant Fe-S cluster scaffold protein with frataxin-bypassing ability acts similarly. *J Biol Chem* **2013,** *288* (52), 36773-86.
134. Turowski, V. R.; Busi, M. V.; Gomez-Casati, D. F., Structural and functional studies of the mitochondrial cysteine desulfurase from Arabidopsis thaliana. *Mol Plant* **2012,** *5* (5), 1001-10.
135. Colin, F.; Martelli, A.; Clemancey, M.; Latour, J. M.; Gambarelli, S.; Zeppieri, L.; Birck, C.; Page, A.; Puccio, H.; Ollagnier de Choudens, S., Mammalian frataxin controls sulfur production and iron entry during de novo Fe4S4 cluster assembly. *J Am Chem Soc* **2013,** *135* (2), 733-40.
136. Das, D.; Patra, S.; Bridwell-Rabb, J.; Barondeau, D. P., Mechanism of frataxin "bypass" in human iron-sulfur cluster biosynthesis with implications for Friedreich's ataxia. *J Biol Chem* **2019,** *294* (23), 9276-9284.
137. Pohl, T.; Walter, J.; Stolpe, S.; Soufo, J. H.; Grauman, P. L.; Friedrich, T., Effects of the deletion of the Escherichia coli frataxin homologue CyaY on the respiratory NADH:ubiquinone oxidoreductase. *BMC Biochem* **2007,** *8*, 13.
138. Li, D. S.; Ohshima, K.; Jiralerspong, S.; Bojanowski, M. W.; Pandolfo, M., Knock-out of the cyaY gene in Escherichia coli does not affect cellular iron content and sensitivity to oxidants. *FEBS Letters* **1999,** *456* (1), 13-16.
139. Thorgersen, M. P.; Downs, D. M., Oxidative stress and disruption of labile iron generate specific auxotrophic requirements in Salmonella enterica. *Microbiology* **2009,** *155* (Pt 1), 295-304.
140. Velayudhan, J.; Karlinsey, J. E.; Frawley, E. R.; Becker, L. A.; Nartea, M.; Fang, F. C., Distinct roles of the Salmonella enterica serovar Typhimurium CyaY and YggX proteins in the biosynthesis and repair of iron-sulfur clusters. *Infect Immun* **2014,** *82* (4), 1390-401.
141. Albrecht, A. G.; Landmann, H.; Nette, D.; Burghaus, O.; Peuckert, F.; Seubert, A.; Miethke, M.; Marahiel, M. A., The Frataxin Homologue Fra Plays a Key Role in Intracellular Iron Channeling in Bacillus subtilis. *ChemBioChem* **2011,** *12* (13), 2052-2061.
142. Ding, H.; Yang, J.; Coleman, L. C.; Yeung, S., Distinct iron binding property of two putative iron donors for the iron-sulfur cluster assembly: IscA and the bacterial frataxin ortholog CyaY under physiological and oxidative stress conditions. *J Biol Chem* **2007,** *282* (11), 7997-8004.
143. Nair, M.; Adinolfi, S.; Pastore, C.; Kelly, G.; Temussi, P.; Pastore, A., Solution structure of the bacterial frataxin ortholog, CyaY: mapping the iron binding sites. *Structure* **2004,** *12* (11), 2037-48.
144. Gakh, O.; Park, S.; Liu, G.; Macomber, L.; Imlay, J. A.; Ferreira, G. C.; Isaya, G., Mitochondrial iron detoxification is a primary function of frataxin that limits oxidative damage and preserves cell longevity. *Human Molecular Genetics* **2006,** *15* (3), 467-479.
145. Adamec, J.; Rusnak, F.; Owen, W. G.; Naylor, S.; Benson, L. M.; Gacy, A. M.; Isaya, G., Iron-Dependent Self-Assembly of Recombinant Yeast Frataxin: Implications for Friedreich Ataxia. *The American Journal of Human Genetics* **2000,** *67* (3), 549-562.
146. Aloria, K.; Schilke, B.; Andrew, A.; Craig, E. A., Iron-induced oligomerization of yeast frataxin homologue Yfh1 is dispensable in vivo. *EMBO reports* **2004,** *5* (11), 1096-1101.
147. Pizzino, G.; Irrera, N.; Cucinotta, M.; Pallio, G.; Mannino, F.; Arcoraci, V.; Squadrito, F.; Altavilla, D.; Bitto, A., Oxidative Stress: Harms and Benefits for Human Health. *Oxidative Medicine and Cellular Longevity* **2017,** *2017*, 8416763.

148. Mishra, S.; Imlay, J., Why do bacteria use so many enzymes to scavenge hydrogen peroxide? *Arch Biochem Biophys* **2012,** *525* (2), 145-60.
149. Lu, J.; Holmgren, A., The thioredoxin antioxidant system. *Free Radic Biol Med* **2014,** *66*, 75-87.
150. Go, Y. M.; Chandler, J. D.; Jones, D. P., The cysteine proteome. *Free Radic Biol Med* **2015,** *84*, 227-245.
151. Fernandes, A. P.; Holmgren, A., Glutaredoxins: Glutathione-Dependent Redox Enzymes with Functions Far Beyond a Simple Thioredoxin Backup System. *Antioxidants & Redox Signaling* **2004,** *6* (1), 63-74.
152. Fra, A.; Yoboue, E. D.; Sitia, R., Cysteines as Redox Molecular Switches and Targets of Disease. *Front Mol Neurosci* **2017,** *10*, 167.
153. Paulsen, C. E.; Carroll, K. S., Cysteine-mediated redox signaling: chemistry, biology, and tools for discovery. *Chem Rev* **2013,** *113* (7), 4633-79.
154. Lu, S. C., Glutathione synthesis. *Biochim Biophys Acta* **2013,** *1830* (5), 3143-53.
155. Forman, H. J.; Zhang, H.; Rinna, A., Glutathione: overview of its protective roles, measurement, and biosynthesis. *Mol Aspects Med* **2009,** *30* (1-2), 1-12.
156. Park, C. M.; Weerasinghe, L.; Day, J. J.; Fukuto, J. M.; Xian, M., Persulfides: current knowledge and challenges in chemistry and chemical biology. *Mol Biosyst* **2015,** *11* (7), 1775-85.
157. Lau, N.; Pluth, M. D., Reactive sulfur species (RSS): persulfides, polysulfides, potential, and problems. *Current Opinion in Chemical Biology* **2019,** *49*, 1-8.
158. Li, K.; Xin, Y.; Xuan, G.; Zhao, R.; Liu, H.; Xia, Y.; Xun, L., Escherichia coli Uses Separate Enzymes to Produce H(2)S and Reactive Sulfane Sulfur From L-cysteine. *Front Microbiol* **2019,** *10*, 298-298.
159. Fuangthong, M.; Jittawuttipoka, T.; Wisitkamol, R.; Romsang, A.; Duang-nkern, J.; Vattanaviboon, P.; Mongkolsuk, S., IscR plays a role in oxidative stress resistance and pathogenicity of a plant pathogen, Xanthomonas campestris. *Microbiol Res* **2015,** *170*, 139-46.
160. Mettert, E. L.; Kiley, P. J., How Is Fe-S Cluster Formation Regulated? *Annu Rev Microbiol* **2015,** *69*, 505-26.
161. Boyd, E. S.; Thomas, K. M.; Dai, Y.; Boyd, J. M.; Outten, F. W., Interplay between oxygen and Fe-S cluster biogenesis: insights from the Suf pathway. *Biochemistry* **2014,** *53* (37), 5834-47.
162. Crack, J. C.; Green, J.; Cheesman, M. R.; Le Brun, N. E.; Thomson, A. J., Superoxide-mediated amplification of the oxygen-induced switch from [4Fe–4S] to [2Fe–2S] clusters in the transcriptional regulator FNR. *Proceedings of the National Academy of Sciences* **2007,** *104* (7), 2092.
163. Jordan, P. A.; Thomson, A. J.; Ralph, E. T.; Guest, J. R.; Green, J., FNR is a direct oxygen sensor having a biphasic response curve. *FEBS Letters* **1997,** *416* (3), 349-352.
164. Imlay, J. A., Iron-sulphur clusters and the problem with oxygen. *Molecular Microbiology* **2006,** *59* (4), 1073-1082.
165. Bai, Y.; Chen, T.; Happe, T.; Lu, Y.; Sawyer, A., Iron-sulphur cluster biogenesis via the SUF pathway. *Metallomics* **2018,** *10* (8), 1038-1052.
166. Mihara, H.; Esaki, N., Bacterial cysteine desulfurases: their function and mechanisms. *Applied Microbiology and Biotechnology* **2002,** *60* (1), 12-23.

167. Cupp-Vickery, J. R.; Urbina, H.; Vickery, L. E., Crystal Structure of IscS, a Cysteine Desulfurase from Escherichia coli. *Journal of Molecular Biology* **2003,** *330* (5), 1049-1059.
168. Dahl, J. U.; Radon, C.; Buhning, M.; Nimtz, M.; Leichert, L. I.; Denis, Y.; Jourlin-Castelli, C.; Iobbi-Nivol, C.; Mejean, V.; Leimkuhler, S., The sulfur carrier protein TusA has a pleiotropic role in Escherichia coli that also affects molybdenum cofactor biosynthesis. *J Biol Chem* **2013,** *288* (8), 5426-42.
169. Leimkuhler, S.; Buhning, M.; Beilschmidt, L., Shared Sulfur Mobilization Routes for tRNA Thiolation and Molybdenum Cofactor Biosynthesis in Prokaryotes and Eukaryotes. *Biomolecules* **2017,** *7* (1).
170. Black, K. A.; Dos Santos, P. C., Shared-intermediates in the biosynthesis of thio-cofactors: Mechanism and functions of cysteine desulfurases and sulfur acceptors. *Biochim Biophys Acta* **2015,** *1853* (6), 1470-80.
171. Johnson, D. C.; Dean, D. R.; Smith, A. D.; Johnson, M. K., Structure, function, and formation of biological iron-sulfur clusters. *Annu Rev Biochem* **2005,** *74*, 247-81.
172. Py, B.; Barras, F., Building Fe-S proteins: bacterial strategies. *Nat Rev Microbiol* **2010,** *8* (6), 436-46.
173. Drennan, C. L.; Peters, J. W., Surprising cofactors in metalloenzymes. *Curr Opin Struct Biol* **2003,** *13* (2), 220-6.
174. Beinert, H., Iron-sulfur proteins: ancient structures, still full of surprises. *J Biol Inorg Chem* **2000,** *5* (1), 2-15.
175. Beinert, H.; Holm, R. H.; Munck, E., Iron-sulfur clusters: nature's modular, multipurpose structures. *Science* **1997,** *277* (5326), 653-9.
176. Frazzon, J.; Dean, D. R., Formation of iron-sulfur clusters in bacteria: an emerging field in bioinorganic chemistry. *Curr Opin Chem Biol* **2003,** *7* (2), 166-73.
177. Zheng, L.; Cash, V. L.; Flint, D. H.; Dean, D. R., Assembly of iron-sulfur clusters. Identification of an iscSUA-hscBA-fdx gene cluster from Azotobacter vinelandii. *J Biol Chem* **1998,** *273* (21), 13264-72.
178. Muhlenhoff, U.; Lill, R., Biogenesis of iron-sulfur proteins in eukaryotes: a novel task of mitochondria that is inherited from bacteria. *Biochim Biophys Acta* **2000,** *1459* (2-3), 370-82.
179. Layer, G.; Ollagnier-de Choudens, S.; Sanakis, Y.; Fontecave, M., Iron-sulfur cluster biosynthesis: characterization of Escherichia coli CYaY as an iron donor for the assembly of [2Fe–2S] clusters in the scaffold IscU. *J Biol Chem* **2006,** *281* (24), 16256-63.
180. Wofford, J. D.; Bolaji, N.; Dziuba, N.; Outten, F. W.; Lindahl, P. A., Evidence that a respiratory shield in Escherichia coli protects a low-molecular-mass Fe(II) pool from O2-dependent oxidation. *J Biol Chem* **2019,** *294* (1), 50-62.
181. Agar, J. N.; Krebs, C.; Frazzon, J.; Huynh, B. H.; Dean, D. R.; Johnson, M. K., IscU as a scaffold for iron-sulfur cluster biosynthesis: sequential assembly of [2Fe–2S] and [4Fe–4S] clusters in IscU. *Biochemistry* **2000,** *39* (27), 7856-62.
182. Agar, J. N.; Zheng, L. M.; Cash, V. L.; Dean, D. R.; Johnson, M. K., Role of the IscU protein in iron-sulfur cluster biosynthesis: IscS-mediated assembly of a [Fe2S2] cluster in IscU. *Journal of the American Chemical Society* **2000,** *122* (9), 2136-2137.
183. Iannuzzi, C.; Adinolfi, S.; Howes, B. D.; Garcia-Serres, R.; Clemancey, M.; Latour, J. M.; Smulevich, G.; Pastore, A., The role of CyaY in iron sulfur cluster assembly on the E. coli IscU scaffold protein. *PLoS One* **2011,** *6* (7), e21992.

184. Kim, J. H.; Frederick, R. O.; Reinen, N. M.; Troupis, A. T.; Markley, J. L., [2Fe–2S]-ferredoxin binds directly to cysteine desulfurase and supplies an electron for iron-sulfur cluster assembly but is displaced by the scaffold protein or bacterial frataxin. *J Am Chem Soc* **2013,** *135* (22), 8117-20.
185. Vranish, J. N.; Das, D.; Barondeau, D. P., Real-Time Kinetic Probes Support Monothiol Glutaredoxins As Intermediate Carriers in Fe-S Cluster Biosynthetic Pathways. *ACS chemical biology* **2016,** *11* (11), 3114-3121.
186. Hoff, K. G.; Silberg, J. J.; Vickery, L. E., Interaction of the iron-sulfur cluster assembly protein IscU with the Hsc66/Hsc20 molecular chaperone system of Escherichia coli. *Proc Natl Acad Sci U S A* **2000,** *97* (14), 7790-5.
187. Hoff, K. G.; Cupp-Vickery, J. R.; Vickery, L. E., Contributions of the LPPVK motif of the iron-sulfur template protein IscU to interactions with the Hsc66-Hsc20 chaperone system. *J Biol Chem* **2003,** *278* (39), 37582-9.
188. Bonomi, F.; Iametti, S.; Morleo, A.; Ta, D.; Vickery, L. E., Facilitated transfer of IscU-[2Fe2S] clusters by chaperone-mediated ligand exchange. *Biochemistry* **2011,** *50* (44), 9641-50.
189. Chandramouli, K.; Johnson, M. K., HscA and HscB stimulate [2Fe–2S] cluster transfer from IscU to apoferredoxin in an ATP-dependent reaction. *Biochemistry* **2006,** *45* (37), 11087-95.
190. Bonomi, F.; Iametti, S.; Morleo, A.; Ta, D.; Vickery, L. E., Studies on the mechanism of catalysis of iron-sulfur cluster transfer from IscU[2Fe2S] by HscA/HscB chaperones. *Biochemistry* **2008,** *47* (48), 12795-801.
191. Shakamuri, P.; Zhang, B.; Johnson, M. K., Monothiol glutaredoxins function in storing and transporting [Fe2S2] clusters assembled on IscU scaffold proteins. *J Am Chem Soc* **2012,** *134* (37), 15213-6.
192. Fidai, I.; Wachnowsky, C.; Cowan, J. A., Glutathione-complexed [2Fe–2S] clusters function in Fe-S cluster storage and trafficking. *J Biol Inorg Chem* **2016,** *21* (7), 887-901.
193. Bonomi, F.; Iametti, S.; Ta, D.; Vickery, L. E., Multiple turnover transfer of [2Fe2S] clusters by the iron-sulfur cluster assembly scaffold proteins IscU and IscA. *J Biol Chem* **2005,** *280* (33), 29513-8.
194. Gao, H.; Subramanian, S.; Couturier, J.; Naik, S. G.; Kim, S. K.; Leustek, T.; Knaff, D. B.; Wu, H. C.; Vignols, F.; Huynh, B. H.; Rouhier, N.; Johnson, M. K., Arabidopsis thaliana Nfu2 accommodates [2Fe–2S] or [4Fe–4S] clusters and is competent for in vitro maturation of chloroplast [2Fe–2S] and [4Fe–4S] cluster-containing proteins. *Biochemistry* **2013,** *52* (38), 6633-45.
195. Dyachenko, A.; Gruber, R.; Shimon, L.; Horovitz, A.; Sharon, M., Allosteric mechanisms can be distinguished using structural mass spectrometry. *Proc Natl Acad Sci U S A* **2013,** *110* (18), 7235-9.
196. Ganem, B.; Li, Y. T.; Henion, J. D., Detection of noncovalent receptor-ligand complexes by mass spectrometry. *Journal of the American Chemical Society* **1991,** *113* (16), 6294-6296.
197. Cubrilovic, D.; Haap, W.; Barylyuk, K.; Ruf, A.; Badertscher, M.; Gubler, M.; Tetaz, T.; Joseph, C.; Benz, J.; Zenobi, R., Determination of protein-ligand binding constants of a cooperatively regulated tetrameric enzyme using electrospray mass spectrometry. *ACS Chem Biol* **2014,** *9* (1), 218-26.
198. Gulbakan, B.; Barylyuk, K.; Zenobi, R., Determination of thermodynamic and kinetic properties of biomolecules by mass spectrometry. *Curr Opin Biotechnol* **2015,** *31*, 65-72.

199. Katta, V.; Chait, B. T., Observation of the Heme Globin Complex in Native Myoglobin by Electrospray-Ionization Mass-Spectrometry. *Journal of the American Chemical Society* **1991,** *113* (22), 8534-8535.
200. Loo, J. A., Studying noncovalent protein complexes by electrospray ionization mass spectrometry. *Mass Spectrom Rev* **1997,** *16* (1), 1-23.
201. Marcoux, J.; Robinson, C. V., Twenty years of gas phase structural biology. *Structure* **2013,** *21* (9), 1541-50.
202. Liu, Y.; Cong, X.; Liu, W.; Laganowsky, A., Characterization of Membrane Protein-Lipid Interactions by Mass Spectrometry Ion Mobility Mass Spectrometry. *J Am Soc Mass Spectrom* **2017,** *28* (4), 579-586.
203. Crack, J. C.; Thomson, A. J.; Le Brun, N. E., Mass spectrometric identification of intermediates in the O2-driven [4Fe–4S] to [2Fe–2S] cluster conversion in FNR. *Proc Natl Acad Sci U S A* **2017,** *114* (16), E3215-E3223.
204. Cong, X.; Liu, Y.; Liu, W.; Liang, X.; Russell, D. H.; Laganowsky, A., Determining Membrane Protein-Lipid Binding Thermodynamics Using Native Mass Spectrometry. *J Am Chem Soc* **2016,** *138* (13), 4346-9.
205. Pacholarz, K. J.; Garlish, R. A.; Taylor, R. J.; Barran, P. E., Mass spectrometry based tools to investigate protein-ligand interactions for drug discovery. *Chem Soc Rev* **2012,** *41* (11), 4335-55.
206. Peterson, E. A.; Sober, H. A., Preparation of Crystalline Phosphorylated Derivatives of Vitamin-B6. *Journal of the American Chemical Society* **1954,** *76* (1), 169-175.
207. Crack, J. C.; Stewart, M. Y. Y.; Le Brun, N. E., Generation of 34S-substituted protein-bound [4Fe–4S] clusters using 34S-L-cysteine. *Biology Methods and Protocols* **2019,** *4* (1).
208. So, J.-H.; Boudjouk, P.; Hong, H. H.; Weber, W. P., Hexamethyldisilathiane. In *Inorganic Syntheses*, 2007; Vol. 29, pp 30-32.
209. Gaitonde, M. K., A spectrophotometric method for the direct determination of cysteine in the presence of other naturally occurring amino acids. *Biochem J* **1967,** *104* (2), 627-33.
210. Poltash, M. L.; McCabe, J. W.; Shirzadeh, M.; Laganowsky, A.; Clowers, B. H.; Russell, D. H., Fourier Transform-Ion Mobility-Orbitrap Mass Spectrometer: A Next-Generation Instrument for Native Mass Spectrometry. *Analytical chemistry* **2018,** *90* (17), 10472-10478.
211. Poltash, M. L.; McCabe, J. W.; Shirzadeh, M.; Laganowsky, A.; Russell, D. H., Native IM-Orbitrap MS: Resolving what was hidden. *TrAC Trends in Analytical Chemistry* **2019**.
212. Marty, M. T.; Baldwin, A. J.; Marklund, E. G.; Hochberg, G. K.; Benesch, J. L.; Robinson, C. V., Bayesian deconvolution of mass and ion mobility spectra: from binary interactions to polydisperse ensembles. *Analytical chemistry* **2015,** *87* (8), 4370-6.
213. Bailey, T. S.; Zakharov, L. N.; Pluth, M. D., Understanding hydrogen sulfide storage: probing conditions for sulfide release from hydrodisulfides. *J Am Chem Soc* **2014,** *136* (30), 10573-6.
214. Patra, S.; Barondeau, D. P., Mechanism of activation of the human cysteine desulfurase complex by frataxin. *Proc Natl Acad Sci U S A* **2019,** *116* (39), 19421-19430.
215. Iannuzzi, C.; Adrover, M.; Puglisi, R.; Yan, R.; Temussi, P. A.; Pastore, A., The role of zinc in the stability of the marginally stable IscU scaffold protein. *Protein Science* **2014,** *23* (9), 1208-1219.

216. Yan, R.; DeLos Rios, P.; Pastore, A.; Temussi, P. A., The cold denaturation of IscU highlights structure–function dualism in marginally stable proteins. *Communications Chemistry* **2018,** *1* (1), 13.
217. McCabe, J. W.; Shirzadeh, M.; Walker, T. E.; Lin, C.-W.; Jones, B. J.; Wysocki, V. H.; Barondeau, D. P.; Clemmer, D. E.; Laganowsky, A.; Russell, D. H., Variable-Temperature Electrospray Ionization for Temperature-Dependent Folding/Refolding Reactions of Proteins and Ligand Binding. *Analytical Chemistry* **2021**.
218. Holm, R. H.; Lo, W., Structural Conversions of Synthetic and Protein-Bound Iron-Sulfur Clusters. *Chem Rev* **2016,** *116* (22), 13685-13713.
219. Braymer, J. J.; Lill, R., Iron-sulfur cluster biogenesis and trafficking in mitochondria. *J Biol Chem* **2017,** *292* (31), 12754-12763.
220. Chen, S. H.; Russell, D. H., How Closely Related Are Conformations of Protein Ions Sampled by IM-MS to Native Solution Structures? *J Am Soc Mass Spectrom* **2015,** *26* (9), 1433-43.
221. Konijnenberg, A.; Butterer, A.; Sobott, F., Native ion mobility-mass spectrometry and related methods in structural biology. *Biochim Biophys Acta* **2013,** *1834* (6), 1239-56.
222. Shimomura, Y.; Wada, K.; Fukuyama, K.; Takahashi, Y., The asymmetric trimeric architecture of [2Fe–2S] IscU: implications for its scaffolding during iron-sulfur cluster biosynthesis. *J Mol Biol* **2008,** *383* (1), 133-43.
223. Fox, N. G.; Martelli, A.; Nabhan, J. F.; Janz, J.; Borkowska, O.; Bulawa, C.; Yue, W. W., Zinc(II) binding on human wild-type ISCU and Met140 variants modulates NFS1 desulfurase activity. *Biochimie* **2018,** *152*, 211-218.
224. Wilcox, D. E.; Schenk, A. D.; Feldman, B. M.; Xu, Y., Oxidation of zinc-binding cysteine residues in transcription factor proteins. *Antioxid Redox Signal* **2001,** *3* (4), 549-64.
225. Outten, C. E.; O'Halloran, T. V., Femtomolar sensitivity of metalloregulatory proteins controlling zinc homeostasis. *Science* **2001,** *292* (5526), 2488-92.
226. Gervason, S.; Larkem, D.; Mansour, A. B.; Botzanowski, T.; Muller, C. S.; Pecqueur, L.; Le Pavec, G.; Delaunay-Moisan, A.; Brun, O.; Agramunt, J.; Grandas, A.; Fontecave, M.; Schunemann, V.; Cianferani, S.; Sizun, C.; Toledano, M. B.; D'Autreaux, B., Physiologically relevant reconstitution of iron-sulfur cluster biosynthesis uncovers persulfide-processing functions of ferredoxin-2 and frataxin. *Nat Commun* **2019,** *10* (1), 3566.
227. Regner, S. R.; Wilcox, N. S.; Friedman, L. S.; Seyer, L. A.; Schadt, K. A.; Brigatti, K. W.; Perlman, S.; Delatycki, M.; Wilmot, G. R.; Gomez, C. M.; Bushara, K. O.; Mathews, K. D.; Subramony, S. H.; Ashizawa, T.; Ravina, B.; Brocht, A.; Farmer, J. M.; Lynch, D. R., Friedreich ataxia clinical outcome measures: natural history evaluation in 410 participants. *Journal of child neurology* **2012,** *27* (9), 1152-8.
228. Poltash, M. L.; Shirzadeh, M.; McCabe, J. W.; Moghadamchargari, Z.; Laganowsky, A.; Russell, D. H., New insights into the metal-induced oxidative degradation pathways of transthyretin. *Chem Commun (Camb)* **2019,** *55* (28), 4091-4094.
229. Krebs, C.; Agar, J. N.; Smith, A. D.; Frazzon, J.; Dean, D. R.; Huynh, B. H.; Johnson, M. K., IscA, an alternate scaffold for Fe-S cluster biosynthesis. *Biochemistry* **2001,** *40* (46), 14069-80.
230. Lange, H.; Kaut, A.; Kispal, G.; Lill, R., A mitochondrial ferredoxin is essential for biogenesis of cellular iron-sulfur proteins. *Proc Natl Acad Sci U S A* **2000,** *97* (3), 1050-5.

231. Brzoska, K.; Meczynska, S.; Kruszewski, M., Iron-sulfur cluster proteins: electron transfer and beyond. *Acta Biochim Pol* **2006,** *53* (4), 685-91.
232. Py, B.; Barras, F., Building Fe-S proteins: bacterial strategies. *Nat Rev Microbiol* **2010,** *8* (6), 436-446.
233. Lill, R., Function and biogenesis of iron-sulphur proteins. *Nature* **2009,** *460* (7257), 831-8.
234. Jacobson, M. R.; Brigle, K. E.; Bennett, L. T.; Setterquist, R. A.; Wilson, M. S.; Cash, V. L.; Beynon, J.; Newton, W. E.; Dean, D. R., Physical and Genetic-Map of the Major Nif Gene-Cluster from Azotobacter-Vinelandii. *J Bacteriol* **1989,** *171* (2), 1017-1027.
235. Jacobson, M. R.; Cash, V. L.; Weiss, M. C.; Laird, N. F.; Newton, W. E.; Dean, D. R., Biochemical and Genetic-Analysis of the Nifusvwzm Cluster from Azotobacter-Vinelandii. *Mol Gen Genet* **1989,** *219* (1-2), 49-57.
236. Zheng, L. M.; Cash, V. L.; Flint, D. H.; Dean, D. R., Assembly of iron-sulfur clusters - Identification of an iscSUA-hscBA-fdx gene cluster from Azotobacter vinelandii. *Journal of Biological Chemistry* **1998,** *273* (21), 13264-13272.
237. Takahashi, Y.; Nakamura, M., Functional assignment of the ORF2-iscS-iscU-iscA-hscB-hscA-fdx-ORF3 gene cluster involved in the assembly of Fe-S clusters in Escherichia coli. *J Biochem-Tokyo* **1999,** *126* (5), 917-926.
238. Tokumoto, U.; Takahashi, Y., Genetic analysis of the isc operon in Escherichia coli involved in the biogenesis of cellular iron-sulfur protein. *J Biochem-Tokyo* **2001,** *130* (1), 63-71.
239. Takahashi, Y.; Tokumoto, U., A third bacterial system for the assembly of iron-sulfur clusters with homologs in archaea and plastids. *Journal of Biological Chemistry* **2002,** *277* (32), 28380-28383.
240. Kim, J. H.; Fuzery, A. K.; Tonelli, M.; Ta, D. T.; Westler, W. M.; Vickery, L. E.; Markley, J. L., Structure and dynamics of the iron-sulfur cluster assembly scaffold protein IscU and its interaction with the cochaperone HscB. *Biochemistry* **2009,** *48* (26), 6062-71.
241. Chandramouli, K.; Johnson, M. K., HscA and HscB stimulate [2Fe–2S] cluster transfer from IscU to apoferredoxin in an ATP-dependent reaction. *Biochemistry* **2006,** *45* (37), 11087-11095.
242. Kim, J. H.; Tonelli, M.; Frederick, R. O.; Chow, D. C.; Markley, J. L., Specialized Hsp70 chaperone (HscA) binds preferentially to the disordered form, whereas J-protein (HscB) binds preferentially to the structured form of the iron-sulfur cluster scaffold protein (IscU). *The Journal of biological chemistry* **2012,** *287* (37), 31406-13.
243. Cho, S.-J.; Lee, M. G.; Yang, J. K.; Lee, J. Y.; Song, H. K.; Suh, S. W., Crystal structure of Escherichia coli CyaY protein reveals a previously unidentified fold for the evolutionarily conserved frataxin family. *Proceedings of the National Academy of Sciences* **2000,** *97* (16), 8932.
244. Tsai, C. L.; Barondeau, D. P., Human Frataxin Is an Allosteric Switch That Activates the Fe-S Cluster Biosynthetic Complex. *Biochemistry* **2010,** *49* (43), 9132-9139.
245. Yan, R.; Adinolfi, S.; Pastore, A., Ferredoxin, in conjunction with NADPH and ferredoxin-NADP reductase, transfers electrons to the IscS/IscU complex to promote iron-sulfur cluster assembly. *Biochim Biophys Acta* **2015,** *1854* (9), 1113-7.

246. Durr, A.; Cossee, M.; Agid, Y.; Campuzano, V.; Mignard, C.; Penet, C.; Mandel, J. L.; Brice, A.; Koenig, M., Clinical and genetic abnormalities in patients with Friedreich's ataxia. *New Engl J Med* **1996,** *335* (16), 1169-1175.
247. Babcock, M.; de Silva, D.; Oaks, R.; Davis-Kaplan, S.; Jiralerspong, S.; Montermini, L.; Pandolfo, M.; Kaplan, J., Regulation of mitochondrial iron accumulation by Yfh1p, a putative homolog of frataxin. *Science* **1997,** *276* (5319), 1709-12.
248. Rotig, A.; deLonlay, P.; Chretien, D.; Foury, F.; Koenig, M.; Sidi, D.; Munnich, A.; Rustin, P., Aconitase and mitochondrial iron-sulphur protein deficiency in Friedreich ataxia. *Nature Genetics* **1997,** *17* (2), 215-217.
249. Li, D. S.; Ohshima, K.; Jiralerspong, S.; Bojanowski, M. W.; Pandolfo, M., Knock-out of the cyaY gene in Escherichia coli does not affect cellular iron content and sensitivity to oxidants. *Febs Lett* **1999,** *456* (1), 13-6.
250. Yoon, H.; Golla, R.; Lesuisse, E.; Pain, J.; Donald, Jason E.; Lyver, Elise R.; Pain, D.; Dancis, A., Mutation in the Fe–S scaffold protein Isu bypasses frataxin deletion. *Biochemical Journal* **2011,** *441* (1), 473-480.
251. Roche, B.; Agrebi, R.; Huguenot, A.; Ollagnier de Choudens, S.; Barras, F.; Py, B., Turning Escherichia coli into a Frataxin-Dependent Organism. *PLoS Genet* **2015,** *11* (5), e1005134.
252. Selbach, B.; Earles, E.; Dos Santos, P. C., Kinetic analysis of the bisubstrate cysteine desulfurase SufS from Bacillus subtilis. *Biochemistry* **2010,** *49* (40), 8794-802.
253. Lin, C.-W.; McCabe, J. W.; Russell, D. H.; Barondeau, D. P., Molecular Mechanism of ISC Iron–Sulfur Cluster Biogenesis Revealed by High-Resolution Native Mass Spectrometry. *Journal of the American Chemical Society* **2020,** *142* (13), 6018-6029.
254. Cook, J. D.; Bencze, K. Z.; Jankovic, A. D.; Crater, A. K.; Busch, C. N.; Bradley, P. B.; Stemmler, A. J.; Spaller, M. R.; Stemmler, T. L., Monomeric Yeast Frataxin Is an Iron-Binding Protein. *Biochemistry* **2006,** *45* (25), 7767-7777.
255. Yoon, H.; Golla, R.; Lesuisse, E.; Pain, J.; Donald, J. E.; Lyver, E. R.; Pain, D.; Dancis, A., Mutation in the Fe-S scaffold protein Isu bypasses frataxin deletion. *The Biochemical journal* **2012,** *441* (1), 473-80.
256. Yoon, H.; Knight, S. A. B.; Pandey, A.; Pain, J.; Turkarslan, S.; Pain, D.; Dancis, A., Turning Saccharomyces cerevisiae into a Frataxin-Independent Organism. *Plos Genet* **2015,** *11* (5).
257. Roche, B.; Agrebi, R.; Huguenot, A.; de Choudens, S. O.; Barras, F.; Py, B., Turning Escherichia coli into a Frataxin-Dependent Organism. *Plos Genet* **2015,** *11* (5).
258. Everett, S. A.; Folkes, L. K.; Wardman, P.; Asmus, K. D., Free-Radical Repair by a Novel Perthiol: Reversible Hydrogen Transfer and Perthiyl Radical Formation. *Free Radical Research* **1994,** *20* (6), 387-400.
259. Tajc, S. G.; Tolbert, B. S.; Basavappa, R.; Miller, B. L., Direct Determination of Thiol pKa by Isothermal Titration Microcalorimetry. *Journal of the American Chemical Society* **2004,** *126* (34), 10508-10509.
260. Massey, V.; Williams, C. H.; Palmer, G., The presence of So-containing impurities in commercial samples of oxidized glutathione and their catalytic effect on the reduction of cytochrome c. *Biochemical and Biophysical Research Communications* **1971,** *42* (4), 730-738.

261. Francoleon, N. E.; Carrington, S. J.; Fukuto, J. M., The reaction of H2S with oxidized thiols: Generation of persulfides and implications to H2S biology. *Archives of Biochemistry and Biophysics* **2011,** *516* (2), 146-153.
262. Crack, J. C.; Green, J.; Le Brun, N. E.; Thomson, A. J., Detection of Sulfide Release from the Oxygen-sensing [4Fe–4S] Cluster of FNR. *Journal of Biological Chemistry* **2006,** *281* (28), 18909-18913.
263. Koskenkorva-Frank, T. S.; Weiss, G.; Koppenol, W. H.; Burckhardt, S., The complex interplay of iron metabolism, reactive oxygen species, and reactive nitrogen species: Insights into the potential of various iron therapies to induce oxidative and nitrosative stress. *Free Radical Biology and Medicine* **2013,** *65*, 1174-1194.
264. Morris, C. J.; Earl, J. R.; Trenam, C. W.; Blake, D. R., Reactive oxygen species and iron—a dangerous partnership in inflammation. *The International Journal of Biochemistry & Cell Biology* **1995,** *27* (2), 109-122.
265. Vinella, D.; Loiseau, L.; de Choudens, S. O.; Fontecave, M.; Barras, F., In vivo [Fe-S] cluster acquisition by IscR and NsrR, two stress regulators in Escherichia coli. *Molecular Microbiology* **2013,** *87* (3), 493-508.
266. Giel, J. L.; Nesbit, A. D.; Mettert, E. L.; Fleischhacker, A. S.; Wanta, B. T.; Kiley, P. J., Regulation of iron–sulphur cluster homeostasis through transcriptional control of the Isc pathway by [2Fe–2S]–IscR in Escherichia coli. *Molecular Microbiology* **2013,** *87* (3), 478-492.
267. Kim, S. H.; Lee, B. Y.; Lau, G. W.; Cho, Y. H., IscR modulates catalase A (KatA) activity, peroxide resistance and full virulence of Pseudomonas aeruginosa PA14. *J Microbiol Biotechnol* **2009,** *19* (12), 1520-6.
268. Mettert, E. L.; Kiley, P. J., Coordinate regulation of the Suf and Isc Fe-S cluster biogenesis pathways by IscR is essential for viability of Escherichia coli. *J Bacteriol* **2014,** *196* (24), 4315-23.
269. Bedekovics, T.; Gajdos, G. B.; Kispal, G.; Isaya, G., Partial conservation of functions between eukaryotic frataxin and the Escherichia coli frataxin homolog CyaY. *FEMS Yeast Research* **2007,** *7* (8), 1276-1284.
270. Uchida, T.; Kobayashi, N.; Muneta, S.; Ishimori, K., The Iron Chaperone Protein CyaY from Vibrio cholerae Is a Heme-Binding Protein. *Biochemistry* **2017,** *56* (18), 2425-2434.
271. Roche, B.; Aussel, L.; Ezraty, B.; Mandin, P.; Py, B.; Barras, F., Iron/sulfur proteins biogenesis in prokaryotes: formation, regulation and diversity. *Biochim Biophys Acta* **2013,** *1827* (3), 455-69.
272. Jiang, J.; Chan, A.; Ali, S.; Saha, A.; Haushalter, K. J.; Lam, W. L.; Glasheen, M.; Parker, J.; Brenner, M.; Mahon, S. B.; Patel, H. H.; Ambasudhan, R.; Lipton, S. A.; Pilz, R. B.; Boss, G. R., Hydrogen Sulfide--Mechanisms of Toxicity and Development of an Antidote. *Sci Rep* **2016,** *6*, 20831.
273. Fenton, H. J. H., LXXIII.—Oxidation of tartaric acid in presence of iron. *J. Chem. Soc., Trans.* **1894,** *65* (0), 899-910.
274. Rouault, T. A.; Tong, W. H., Iron-sulfur cluster biogenesis and human disease. *Trends Genet* **2008,** *24* (8), 398-407.
275. Parent, A.; Elduque, X.; Cornu, D.; Belot, L.; Le Caer, J. P.; Grandas, A.; Toledano, M. B.; D'Autreaux, B., Mammalian frataxin directly enhances sulfur transfer of NFS1 persulfide to both ISCU and free thiols. *Nat Commun* **2015,** *6*, 5686.

276. Van Vranken, J. G.; Jeong, M. Y.; Wei, P.; Chen, Y. C.; Gygi, S. P.; Winge, D. R.; Rutter, J., The mitochondrial acyl carrier protein (ACP) coordinates mitochondrial fatty acid synthesis with iron sulfur cluster biogenesis. *Elife* **2016,** *5*, e17828.
277. Van Vranken, J. G.; Nowinski, S. M.; Clowers, K. J.; Jeong, M. Y.; Ouyang, Y.; Berg, J. A.; Gygi, J. P.; Gygi, S. P.; Winge, D. R.; Rutter, J., ACP Acylation Is an Acetyl-CoA-Dependent Modification Required for Electron Transport Chain Assembly. *Mol Cell* **2018,** *71* (4), 567-580 e4.
278. Rocha, A. G.; Knight, S. A. B.; Pandey, A.; Yoon, H.; Pain, J.; Pain, D.; Dancis, A., Cysteine desulfurase is regulated by phosphorylation of Nfs1 in yeast mitochondria. *Mitochondrion* **2018,** *40*, 29-41.
279. Song, J. Y.; Marszalek, J.; Craig, E. A., Cysteine desulfurase Nfs1 and Pim1 protease control levels of Isu, the Fe-S cluster biogenesis scaffold. *Proc Natl Acad Sci U S A* **2012,** *109* (26), 10370-5.
280. Ciesielski, S. J.; Schilke, B.; Marszalek, J.; Craig, E. A., Protection of scaffold protein Isu from degradation by the Lon protease Pim1 as a component of Fe-S cluster biogenesis regulation. *Mol Biol Cell* **2016,** *27* (7), 1060-8.
281. Li, J.; Kogan, M.; Knight, S. A.; Pain, D.; Dancis, A., Yeast mitochondrial protein, Nfs1p, coordinately regulates iron-sulfur cluster proteins, cellular iron uptake, and iron distribution. *J Biol Chem* **1999,** *274* (46), 33025-34.
282. Kispal, G.; Csere, P.; Prohl, C.; Lill, R., The mitochondrial proteins Atm1p and Nfs1p are essential for biogenesis of cytosolic Fe/S proteins. *EMBO J* **1999,** *18* (14), 3981-9.
283. Nakai, Y.; Umeda, N.; Suzuki, T.; Nakai, M.; Hayashi, H.; Watanabe, K.; Kagamiyama, H., Yeast Nfs1p is involved in thio-modification of both mitochondrial and cytoplasmic tRNAs. *J Biol Chem* **2004,** *279* (13), 12363-8.
284. Cai, K.; Tonelli, M.; Frederick, R. O.; Markley, J. L., Human Mitochondrial Ferredoxin 1 (FDX1) and Ferredoxin 2 (FDX2) Both Bind Cysteine Desulfurase and Donate Electrons for Iron-Sulfur Cluster Biosynthesis. *Biochemistry* **2017,** *56* (3), 487-499.
285. Tsvetkov, P.; Detappe, A.; Cai, K.; Keys, H. R.; Brune, Z.; Ying, W.; Thiru, P.; Reidy, M.; Kugener, G.; Rossen, J.; Kocak, M.; Kory, N.; Tsherniak, A.; Santagata, S.; Whitesell, L.; Ghobrial, I. M.; Markley, J. L.; Lindquist, S.; Golub, T. R., Mitochondrial metabolism promotes adaptation to proteotoxic stress. *Nat Chem Biol* **2019,** *15* (7), 681-689.
286. Fox, N. G.; Chakrabarti, M.; McCormick, S. P.; Lindahl, P. A.; Barondeau, D. P., The Human Iron-Sulfur Assembly Complex Catalyzes the Synthesis of [2Fe–2S] Clusters on ISCU2 That Can Be Transferred to Acceptor Molecules. *Biochemistry* **2015,** *54* (25), 3871-9.
287. Yan, R.; Konarev, P. V.; Iannuzzi, C.; Adinolfi, S.; Roche, B.; Kelly, G.; Simon, L.; Martin, S. R.; Py, B.; Barras, F.; Svergun, D. I.; Pastore, A., Ferredoxin competes with bacterial frataxin in binding to the desulfurase IscS. *J Biol Chem* **2013,** *288* (34), 24777-87.
288. Cai, K.; Frederick, R. O.; Dashti, H.; Markley, J. L., Architectural Features of Human Mitochondrial Cysteine Desulfurase Complexes from Crosslinking Mass Spectrometry and Small-Angle X-Ray Scattering. *Structure* **2018,** *26* (8), 1127-1136 e4.
289. Studier, F. W., Protein production by auto-induction in high density shaking cultures. *Protein Expr Purif* **2005,** *41* (1), 207-34.
290. Miyazaki, K., MEGAWHOP cloning: a method of creating random mutagenesis libraries via megaprimer PCR of whole plasmids. *Methods Enzymol* **2011,** *498*, 399-406.

291. Wilkins, M. R.; Gasteiger, E.; Bairoch, A.; Sanchez, J. C.; Williams, K. L.; Appel, R. D.; Hochstrasser, D. F., Protein identification and analysis tools in the ExPASy server. *Methods Mol Biol* **1999,** *112*, 531-52.
292. Bridwell-Rabb, J.; Winn, A. M.; Barondeau, D. P., Structure-function analysis of Friedreich's ataxia mutants reveals determinants of frataxin binding and activation of the Fe-S assembly complex. *Biochemistry* **2011,** *50* (33), 7265-74.
293. Franke, D.; Petoukhov, M. V.; Konarev, P. V.; Panjkovich, A.; Tuukkanen, A.; Mertens, H. D. T.; Kikhney, A. G.; Hajizadeh, N. R.; Franklin, J. M.; Jeffries, C. M.; Svergun, D. I., ATSAS 2.8: a comprehensive data analysis suite for small-angle scattering from macromolecular solutions. *J Appl Crystallogr* **2017,** *50* (Pt 4), 1212-1225.
294. Nielsen, S. S.; Toft, K. N.; Snakenborg, D.; Jeppesen, M. G.; Jacobsen, J. K.; Vestergaard, B.; Kutter, J. P.; Arleth, L., BioXTAS RAW, a software program for high-throughput automated small-angle X-ray scattering data reduction and preliminary analysis. *J Appl Crystallogr* **2009,** *42* (5), 959-964.
295. Hopkins, J. B.; Gillilan, R. E.; Skou, S., BioXTAS RAW: improvements to a free open-source program for small-angle X-ray scattering data reduction and analysis. *J Appl Crystallogr* **2017,** *50* (Pt 5), 1545-1553.
296. Battye, T. G.; Kontogiannis, L.; Johnson, O.; Powell, H. R.; Leslie, A. G., iMOSFLM: a new graphical interface for diffraction-image processing with MOSFLM. *Acta Crystallogr D Biol Crystallogr* **2011,** *67* (Pt 4), 271-81.
297. Winn, M. D.; Ballard, C. C.; Cowtan, K. D.; Dodson, E. J.; Emsley, P.; Evans, P. R.; Keegan, R. M.; Krissinel, E. B.; Leslie, A. G.; McCoy, A.; McNicholas, S. J.; Murshudov, G. N.; Pannu, N. S.; Potterton, E. A.; Powell, H. R.; Read, R. J.; Vagin, A.; Wilson, K. S., Overview of the CCP4 suite and current developments. *Acta Crystallogr D Biol Crystallogr* **2011,** *67* (Pt 4), 235-42.
298. Laganowsky, A.; Reading, E.; Allison, T. M.; Ulmschneider, M. B.; Degiacomi, M. T.; Baldwin, A. J.; Robinson, C. V., Membrane proteins bind lipids selectively to modulate their structure and function. *Nature* **2014,** *510* (7503), 172-175.
299. Allison, T. M.; Reading, E.; Liko, I.; Baldwin, A. J.; Laganowsky, A.; Robinson, C. V., Quantifying the stabilizing effects of protein-ligand interactions in the gas phase. *Nat Commun* **2015,** *6*, 8551.
300. Ruotolo, B. T.; Benesch, J. L.; Sandercock, A. M.; Hyung, S. J.; Robinson, C. V., Ion mobility-mass spectrometry analysis of large protein complexes. *Nat Protoc* **2008,** *3* (7), 1139-52.
301. Bush, M. F.; Hall, Z.; Giles, K.; Hoyes, J.; Robinson, C. V.; Ruotolo, B. T., Collision cross sections of proteins and their complexes: a calibration framework and database for gas-phase structural biology. *Analytical chemistry* **2010,** *82* (22), 9557-65.
302. Bleiholder, C.; Wyttenbach, T.; Bowers, M. T., A novel projection approximation algorithm for the fast and accurate computation of molecular collision cross sections (I). Method. *Int J Mass Spectrom* **2011,** *308* (1), 1-10.
303. Anderson, S. E.; Bleiholder, C.; Brocker, E. R.; Stang, P. J.; Bowers, M. T., A novel projection approximation algorithm for the fast and accurate computation of molecular collision cross sections (III): Application to supramolecular coordination-driven assemblies with complex shapes. *Int J Mass Spectrom* **2012,** *330-332*, 78-84.

304. Bleiholder, C.; Contreras, S.; Do, T. D.; Bowers, M. T., A novel projection approximation algorithm for the fast and accurate computation of molecular collision cross sections (II). Model parameterization and definition of empirical shape factors for proteins. *Int J Mass Spectrom* **2013,** *345-347*, 89-96.
305. Rambo, R. P.; Tainer, J. A., Accurate assessment of mass, models and resolution by small-angle scattering. *Nature* **2013,** *496* (7446), 477-81.
306. Valentini, E.; Kikhney, A. G.; Previtali, G.; Jeffries, C. M.; Svergun, D. I., SASBDB, a repository for biological small-angle scattering data. *Nucleic Acids Res* **2015,** *43* (Database issue), D357-63.
307. Wyttenbach, T.; Bleiholder, C.; Anderson, S. E.; Bowers, M. T., A new algorithm to characterise the degree of concaveness of a molecular surface relevant in ion mobility spectrometry. *Molecular Physics* **2015,** *113* (15-16), 2344-2349.
308. Wyttenbach, T.; Bleiholder, C.; Bowers, M. T., Factors contributing to the collision cross section of polyatomic ions in the kilodalton to gigadalton range: application to ion mobility measurements. *Analytical chemistry* **2013,** *85* (4), 2191-9.
309. McCabe, J. W.; Mallis, C. S.; Kocurek, K. I.; Poltash, M. L.; Shirzadeh, M.; Hebert, M. J.; Fan, L.; Walker, T. E.; Zheng, X.; Jiang, T.; Dong, S.; Lin, C. W.; Laganowsky, A.; Russell, D. H., First-Principles Collision Cross Section Measurements of Large Proteins and Protein Complexes. *Analytical chemistry* **2020**.
310. Jaffe, E. K.; Lawrence, S. H., The morpheein model of allostery: evaluating proteins as potential morpheeins. *Methods Mol Biol* **2012,** *796*, 217-31.
311. Jaffe, E. K.; Stith, L.; Lawrence, S. H.; Andrake, M.; Dunbrack, R. L., Jr., A new model for allosteric regulation of phenylalanine hydroxylase: implications for disease and therapeutics. *Arch Biochem Biophys* **2013,** *530* (2), 73-82.
312. Jaffe, E. K.; Lawrence, S. H., Allostery and the dynamic oligomerization of porphobilinogen synthase. *Arch Biochem Biophys* **2012,** *519* (2), 144-53.
313. Sen, S.; Banerjee, R., A pathogenic linked mutation in the catalytic core of human cystathionine beta-synthase disrupts allosteric regulation and allows kinetic characterization of a full-length dimer. *Biochemistry* **2007,** *46* (13), 4110-6.
314. Tang, L.; Breinig, S.; Stith, L.; Mischel, A.; Tannir, J.; Kokona, B.; Fairman, R.; Jaffe, E. K., Single amino acid mutations alter the distribution of human porphobilinogen synthase quaternary structure isoforms (morpheeins). *J Biol Chem* **2006,** *281* (10), 6682-90.
315. Farhan, S. M.; Wang, J.; Robinson, J. F.; Lahiry, P.; Siu, V. M.; Prasad, C.; Kronick, J. B.; Ramsay, D. A.; Rupar, C. A.; Hegele, R. A., Exome sequencing identifies NFS1 deficiency in a novel Fe-S cluster disease, infantile mitochondrial complex II/III deficiency. *Mol Genet Genomic Med* **2014,** *2* (1), 73-80.
316. Tsai, C. L.; Bridwell-Rabb, J.; Barondeau, D. P., Friedreich's ataxia variants I154F and W155R diminish frataxin-based activation of the iron-sulfur cluster assembly complex. *Biochemistry* **2011,** *50* (29), 6478-87.
317. Coelho, M. P.; Correia, J.; Dias, A.; Nogueira, C.; Bandeira, A.; Martins, E.; Vilarinho, L., Iron-sulfur cluster ISD11 deficiency (LYRM4 gene) presenting as cardiorespiratory arrest and 3-methylglutaconic aciduria. *JIMD Rep* **2019,** *49* (1), 11-16.

318. Kollberg, G.; Tulinius, M.; Melberg, A.; Darin, N.; Andersen, O.; Holmgren, D.; Oldfors, A.; Holme, E., Clinical manifestation and a new ISCU mutation in iron-sulphur cluster deficiency myopathy. *Brain* **2009,** *132* (Pt 8), 2170-9.
319. Mochel, F.; Knight, M. A.; Tong, W.-H.; Hernandez, D.; Ayyad, K.; Taivassalo, T.; Andersen, P. M.; Singleton, A.; Rouault, T. A.; Fischbeck, K. H.; Haller, R. G., Splice Mutation in the Iron-Sulfur Cluster Scaffold Protein ISCU Causes Myopathy with Exercise Intolerance. *The American Journal of Human Genetics* **2008,** *82* (3), 652-660.
320. Farhan, S. M. K.; Wang, J.; Robinson, J. F.; Lahiry, P.; Siu, V. M.; Prasad, C.; Kronick, J. B.; Ramsay, D. A.; Rupar, C. A.; Hegele, R. A., Exome sequencing identifies NFS1 deficiency in a novel Fe-S cluster disease, infantile mitochondrial complex II/III deficiency. *Molecular Genetics & Genomic Medicine* **2014,** *2* (1), 73-80.